

Oxygenated products from carbon monoxide hydrogenation over supported rhodium and iridium catalysts : a catalytic and characterization study

Citation for published version (APA):

Kip, B. J. (1987). *Oxygenated products from carbon monoxide hydrogenation over supported rhodium and iridium catalysts : a catalytic and characterization study*. [Phd Thesis 1 (Research TU/e / Graduation TU/e), Chemical Engineering and Chemistry]. Technische Universiteit Eindhoven. <https://doi.org/10.6100/IR271485>

DOI:

[10.6100/IR271485](https://doi.org/10.6100/IR271485)

Document status and date:

Published: 01/01/1987

Document Version:

Publisher's PDF, also known as Version of Record (includes final page, issue and volume numbers)

Please check the document version of this publication:

- A submitted manuscript is the version of the article upon submission and before peer-review. There can be important differences between the submitted version and the official published version of record. People interested in the research are advised to contact the author for the final version of the publication, or visit the DOI to the publisher's website.
- The final author version and the galley proof are versions of the publication after peer review.
- The final published version features the final layout of the paper including the volume, issue and page numbers.

[Link to publication](#)

General rights

Copyright and moral rights for the publications made accessible in the public portal are retained by the authors and/or other copyright owners and it is a condition of accessing publications that users recognise and abide by the legal requirements associated with these rights.

- Users may download and print one copy of any publication from the public portal for the purpose of private study or research.
- You may not further distribute the material or use it for any profit-making activity or commercial gain
- You may freely distribute the URL identifying the publication in the public portal.

If the publication is distributed under the terms of Article 25fa of the Dutch Copyright Act, indicated by the "Taverne" license above, please follow below link for the End User Agreement:

www.tue.nl/taverne

Take down policy

If you believe that this document breaches copyright please contact us at:

openaccess@tue.nl

providing details and we will investigate your claim.

OXYGENATED PRODUCTS FROM CO HYDROGENATION

OVER Rh AND Ir CATALYSTS

B.J. KIP

**OXYGENATED PRODUCTS FROM CARBON MONOXIDE
HYDROGENATION OVER SUPPORTED
RHODIUM AND IRIIDIUM CATALYSTS**

A CATALYTIC AND CHARACTERIZATION STUDY

**OXYGENATED PRODUCTS FROM CARBON MONOXIDE
HYDROGENATION OVER SUPPORTED
RHODIUM AND IRIIDIUM CATALYSTS**

A CATALYTIC AND CHARACTERIZATION STUDY

**VORMING VAN ZUURSTOFHOUDENDE PRODUKTEN
BIJ DE HYDROGENERING VAN KOOLMONOXIDE OVER
GEDRAGEN RHODIUM EN IRIIDIUM KATALYSATOREN**

PROEFSCHRIFT

ter verkrijging van de graad van doctor aan de
Technische Universiteit Eindhoven, op gezag van
de rector magnificus, prof. dr. F.N. Hooge, voor
een commissie aangewezen door het college van
dekanen in het openbaar te verdedigen op
dinsdag 6 oktober 1987 te 16.00 uur

door

BEREND JAN KIP
geboren te Dinxperlo

Dit proefschrift is goedgekeurd door de promotoren:

prof. dr. R. Prins

en

prof. dr. R.A. van Santen

The research reported in this thesis was carried out at the Laboratory for Inorganic Chemistry and Catalysis, University of Technology Eindhoven (P.O. Box 513, 5600 MB Eindhoven, the Netherlands) and was supported by the Netherlands Foundation for Chemical Research (SON) with financial aid from the Netherlands Organization for the Advancement of Pure Research (ZWO).

"Men moet weten te twijfelen waar het noodzakelijk is, zich zekerheid verschaffen waar het noodzakelijk is en zich onderwerpen waar het noodzakelijk is. Wie niet zo handelt, miskent de kracht der rede. Er zijn mensen, die in strijd handelen met deze drie grondbeginselen: of ze beweren dat alles bewijsbaar is, omdat zij niets van bewijzen begrijpen; of zij twijfelen aan alles omdat ze niet weten waar zij zich hebben te onderwerpen; of zij onderwerpen zich aan alles omdat zij niet weten waar te oordelen."

Blaise Pascal

aan mijn ouders

aan Anne

CONTENTS

Chapter 1	INTRODUCTION	1
	1.1 Application of synthesis gas	1
	1.2 CO hydrogenation catalysts	3
	1.3 Characterization of catalysts	6
	1.4 Mechanistic aspects of CO hydrogenation	8
	1.4.1 Formation of hydrocarbons	8
	1.4.2 Formation of methanol	9
	1.4.3 Formation of ethanol	11
	1.4.3.1 Product distribution	11
	1.4.3.2 Addition of reactive compounds	14
	1.4.3.3 Labelling experiments	16
	1.4.3.4 IR-spectroscopy	20
	1.4.3.5 General reaction scheme, reaction sites for C ₂ -oxygenates	22
	1.5 Scope and outline of this thesis	23
	1.6 References	25
Chapter 2	EXPERIMENTAL METHODS	29
	2.1 Catalyst preparation	29
	2.2 Catalyst characterization	29
	2.3 CO hydrogenation	31
	2.4 References	37
Chapter 3	PREPARATION AND CHARACTERIZATION OF VERY HIGHLY DISPERSED IRIDIUM ON Al ₂ O ₃ AND SiO ₂	38
	3.1 Introduction	38
	3.2 Experimental	40
	3.2.1 Preparation of the catalysts	40
	3.2.2 Characterization techniques	41
	3.3 Results	42
	3.3.1 Incipient wetness method catalysts	42
	3.3.2 Catalysts prepared by the urea technique	48
	3.4 Discussion	51
	3.5 Conclusions	59
	3.6 References	60

Chapter 4	DETERMINATION OF METAL PARTICLE SIZE OF HIGHLY DISPERSED Rh, Ir AND Pt CATALYSTS BY HYDROGEN CHEMISORPTION AND EXAFS	63
4.1	Introduction	63
4.2	Experimental	65
4.2.1	Preparation of the catalysts	65
4.2.2	Hydrogen chemisorption measurements	65
4.2.3	EXAFS measurements	66
4.3	Results	67
4.3.1	Hydrogen chemisorption measurements	67
4.3.2	EXAFS measurements	69
4.3.3	Model calculations	71
4.4	Discussions	74
4.5	Conclusions	81
4.6	References	82
Chapter 5	THE EFFECT OF CHLORINE IN THE HYDROGENATION OF CARBON MONOXIDE TO OXYGENATED PRODUCTS AT ELEVATED PRESSURE ON Rh AND Ir ON SiO ₂ AND Al ₂ O ₃	86
5.1	Introduction	86
5.2	Experimental	87
5.2.1	Catalyst preparation	87
5.2.2	Characterization techniques	88
5.2.3	The CO-H ₂ reaction	88
5.3	Results and Discussion	88
5.3.1	Characterization	88
5.3.2	The CO-H ₂ reaction	89
5.4	References	95
Chapter 6	PROMOTERS IN SYNTHESIS GAS REACTIONS	97
6.1	Introduction	97
6.2	Possible effects of promoters in syngas reactions	99
6.3	Experimental	102
6.3.1	Catalyst preparation	102
6.3.2	CO hydrogenation	103
6.4	Results and Discussion	103
6.5	Conclusions	106
6.6	References	107

Chapter 7	PREPARATION AND CHARACTERIZATION OF VANADIUM OXIDE-PROMOTED RHODIUM CATALYSTS	110
	7.1 Introduction	111
	7.2 Experimental	112
	7.2.1 Catalyst preparation	112
	7.2.2 Characterization techniques	113
	7.3 Results	114
	7.3.1 Rh/V ₂ O ₃	114
	7.3.2 Rh/V ₂ O ₃ /SiO ₂	116
	7.3.3 Rh/V ₂ O ₃ /Al ₂ O ₃	127
	7.4 Discussion	130
	7.4.1 Temperature programmed reduction	130
	7.4.2 Hydrogen and carbon monoxide chemisorption	133
	7.4.3 Infrared spectroscopy of adsorbed CO	134
	7.4.4 Hydrogen ad- and desorption studies	135
	7.5 Conclusions	136
	7.6 References	137
Chapter 8	HYDROGENATION OF CARBON MONOXIDE OVER VANADIUM OXIDE-PROMOTED RHODIUM CATALYSTS	140
	8.1 Introduction	141
	8.2 Experimental	143
	8.2.1 Catalyst preparation and characterization	143
	8.2.2 CO hydrogenation	143
	8.3 Results	144
	8.3.1 Rh/V ₂ O ₃	144
	8.3.2 Rh/V ₂ O ₃ /SiO ₂	147
	8.3.3 Rh/V ₂ O ₃ /Al ₂ O ₃	155
	8.3.4 Ethylene addition	158
	8.4 Discussion	159
	8.4.1 Rh/V ₂ O ₃ /SiO ₂	159
	8.4.2 Rh/V ₂ O ₃ /Al ₂ O ₃	166
	8.4.3 Rh/V ₂ O ₃	168
	8.5 Conclusions	170
	8.6 References	171

Chapter 9	HYDROGENATION OF CARBON MONOXIDE OVER Rh/SiO ₂ CATALYSTS PROMOTED WITH MOLYBDENUM OXIDE AND THORIUM OXIDE	174
	9.1 Introduction	175
	9.2 Experimental	176
	9.2.1 Catalyst preparation	176
	9.2.2 Characterization techniques	177
	9.2.3 CO hydrogenation	177
	9.3 Results	178
	9.3.1 Temperature programmed reduction	178
	9.3.2 H ₂ and CO chemisorption	183
	9.3.3 Transmission electron microscopy	183
	9.3.4 Infrared spectroscopy of adsorbed CO	184
	9.3.5 Hydrogenation of CO	187
	9.4 Discussion	194
	9.4.1 Temperature programmed reduction	194
	9.4.2 H ₂ and CO chemisorption	196
	9.4.3 Infrared spectroscopy	198
	9.4.4 CO hydrogenation reaction	198
	9.5 Conclusions	204
	9.6 References	205
Chapter 10	CO HYDROGENATION OVER ALKALI-PROMOTED Rh/Al ₂ O ₃ , Rh/V ₂ O ₃ /SiO ₂ AND Rh/ThO ₂ /SiO ₂	209
	10.1 Introduction	209
	10.2 Experimental	211
	10.2.1 Catalyst preparation	211
	10.2.2 CO chemisorption measurements	212
	10.2.3 CO hydrogenation	212
	10.3 Results	212
	10.3.1 Rh/Al ₂ O ₃	212
	10.3.2 Rh/V ₂ O ₃ /SiO ₂	216
	10.3.3 Rh/ThO ₂ /SiO ₂	218
	10.4 Discussion	219
	10.5 Conclusions	220
	10.6 References	220

Chapter 11	CONCLUDING REMARKS	223
	SUMMARY	230
	SAMENVATTING	235
	DANKWOORD	240
	CURRICULUM VITAE	242
	LIST OF PUBLICATIONS	243

Chapter 1

INTRODUCTION

1.1 APPLICATION OF SYNTHESIS GAS

Reliable sources of fuels and chemicals are of vital importance to all countries in the world. The dependence on crude oil became evident in the first and second oil crisis of 1973 and 1979, respectively. Up to now, oil is still the world's major source of energy and feedstock for base chemicals. However, political, economical and strategic considerations have led to a renewed attention for alternative energy sources, like coal, natural gas, nuclear energy and water power, wind and solar energy. From these, coal is undoubtedly the most promising one, since coal reserves are very large. From the proven world fossil energy carriers, approximately 5,000 billion barrels oil-equivalent, about 75% is coal.

Because coal is a solid fuel, which causes problems with transport, handling and removal of pollutants, it has to undergo a number of transformations in order to replace oil as a feedstock for base chemicals or as a source of energy. This can be achieved by coal liquefaction or by gasification with steam resulting in a mixture of carbon monoxide and hydrogen, known as synthesis gas. During the last decade, a lot of research effort has been performed to study the conversion of synthesis gas into base chemicals like methane, short alkenes, alcohols and longer chain hydrocarbons.

From a thermodynamic point of view, products like methane, methanol, longer hydrocarbons and oxygen containing molecules (oxygenates) can be made from synthesis gas if reaction temperatures are not too high (less than about 623 K). However, a catalyst is needed to really make these products at a sufficiently high conversion level using a moderate temperature. A catalyst is a substance which accelerates a chemical reaction without being part of the overall stoichiometric equation by creating a new reaction pathway, often with a lower activation energy than the uncatalyzed pathway. In reactions of synthesis gas, the reactants are in the gas phase, the catalyst is in the solid phase, and we deal with heterogeneous catalysis.

Presently, the price of crude oil has not risen as much as was foreseen in 1980. Then, the crude oil price was predicted to reach Dfl 200 per barrel in 1990. Now, in 1987, the price is only about Dfl 40 per barrel. Because of

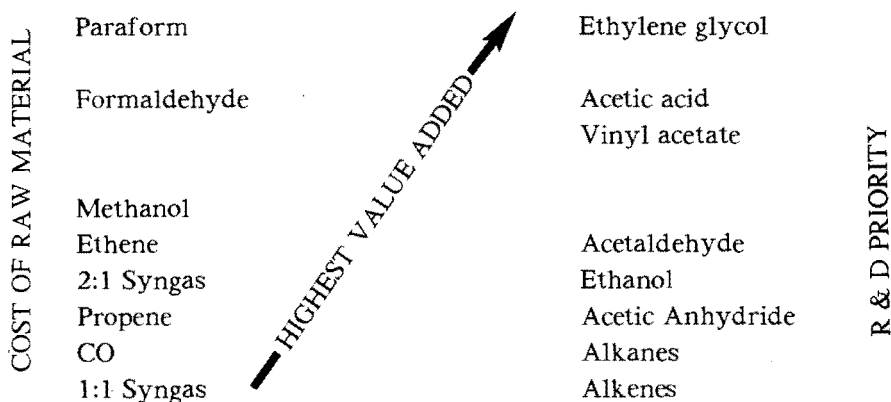


FIGURE 1.1: Direction for R & D in C_1 -chemistry (according to ref. [1]).

this relatively low oil price, the economic feasibility of synthesis gas reactions is low. Aquilo *et al.* [1] made an analysis of the economic and technical factors to decide whether specific C_1 -chemistry projects will pay off (see Figure 1.1). Ethylene glycol is included in the high potential region, because the stoichiometry of its formation from syngas is ideal and the existing ethene based process has a relatively low efficiency. Acetic acid and vinyl acetate fall in the middle category and acetaldehyde and ethanol are placed in the upper part of the lower potential region. The major draw-back for hydrocarbons is the reaction stoichiometry (see Table 1.1). This can be understood if one considers that in the synthesis of syngas from coal, oxygen is introduced into the coal, forming CO. For products like methane, short olefins and longer hydrocarbons, this oxygen has to be removed again. Therefore, it is not surprising that the production of oxygen containing compounds such as methanol and C_2 -oxygenates (ethanol, acetaldehyde and acetic acid) are more interesting from an economic point of view. A new application is the formation of a mixture of methanol, ethanol and longer alcohols that can be used as an additive to gasoline for adjusting the octane number (substitute for tetra-alkyl lead).

Industrial application of synthesis gas is at present rather limited. Methanol is made from CO/H_2 on an industrial scale [2]. It is produced at relatively low pressures (50-100 bars) and at temperatures between 503 and 553 K, using a copper/zinc oxide catalyst [3]. By carbonylation of CO, acetic acid can be made (Monsanto process) [4-6]. Another application is the conversion of methanol into gasoline (MTG) over a zeolite catalyst

TABLE 1.1: Reaction stoichiometries and mass efficiencies for formation of several products from synthesis gas.

Product	H ₂ :CO ratio	efficiency (%)
CH ₄	3	47
C ₂ H ₄	2	44
C ₈ H ₁₈	2.1	43
CH ₃ OH	2	100
CH ₃ COOH	1	100
C ₂ H ₅ OH	2	72
(CH ₃ CHO) ₂ O	1	85

(ZSM-5), developed by Mobil. The first commercialization of the MTG process took place in New Zealand (1985) [7]. For political reasons, in South Africa synthetic fuel is made from coal/synthesis gas in the SASOL Fischer-Tropsch process.

1.2 CO HYDROGENATION CATALYSTS

As already mentioned in the preceding paragraph, it is essential to direct the synthesis gas reaction to products containing oxygen, like methanol and C₂-oxygenates. The choice of the catalyst is an important factor in directing the reaction. As can be seen in Figure 1.2, particular products can be made by using particular catalyst systems.

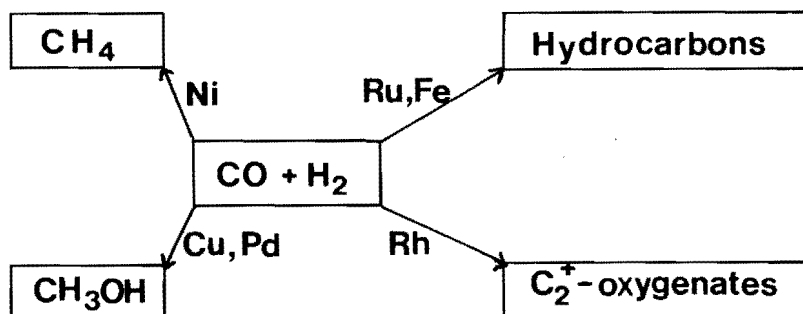


FIGURE 1.2: Catalytic conversion of synthesis gas into several product groups using different catalyst systems.

Methane and longer chain hydrocarbons can be made using Ni/Al₂O₃ and supported Ru, Fe and Co catalysts. It is now generally accepted that these products are made via a dissociative adsorption of CO (see paragraph 1.4.1). Methanol can be made from synthesis gas using Cu/ZnO or supported Pt and Pd catalysts [8-10]. Takeuchi and Katzer showed that methanol is formed via a non-dissociative adsorption of CO [11]. For ethanol formation, both functions, non-dissociative and dissociative adsorption of CO, are required since ethanol is thought to be formed by CO insertion into a CH_x intermediate. It is not surprising that catalysts based on rhodium as the active element can produce C₂-oxygenates [12-18], since rhodium is placed on the line separating metals that adsorb CO dissociatively and metals that adsorb CO non-dissociatively under synthesis gas reaction conditions (see Figure 1.3). Metals left to the heavy line marked "synthesis temperature" dissociate CO at temperatures of 473-573 K.

Mn	Fe	Co	Ni	Cu
Tc	Ru	Rh	Pd	Ag
Re	Os	Ir	Pt	Au

↑ ambient temperatures ↑ synthesis temperatures

FIGURE 1.3: Regions of dissociative and non-dissociative adsorption of CO at room temperature and CO hydrogenation reaction temperature (according to ref. [18]).

The catalytic reactions will take place at the metal surface and therefore it is of interest to create a surface-to volume ratio as large as possible, especially in view of the availability and price of metals like rhodium, platinum and iridium. For instance, the price of rhodium in the form of RhCl₃.xH₂O is about Dfl 75 per gram. However, for a very finely dispersed unsupported metal catalyst, the fraction of metal atoms exposed is too low. For a metal particle 1 μm in size, the fraction exposed is about 0.001. Therefore, metals are deposited on high surface area supports like Al₂O₃ and SiO₂ (100-300 m² g⁻¹) resulting in very small metal particles with a fraction exposed of two or three orders higher and in some cases even approaching unity. The ordinary way to make these catalysts is to dissolve the desired amount of

metal salt in water and impregnate the support with this solution. The solution will be sucked up into the pores of the support by capillary forces. After this step, the water is removed by drying, and subsequently the catalyst is reduced in order to bring the active component in the metallic state. This procedure results in very small particles (about 10 - 100 Å) in the pores of the support and thus a high fraction exposed is obtained.

The catalytic behaviour of a supported metal catalyst may depend on the structure of the crystallites and can be influenced to a great extent by the interaction between the metal particle and the underlying support. A special case of these metal-support interactions is the so-called Strong Metal Support Interaction (SMSI). After reduction at 473 K, well dispersed group VIII metals on oxidic supports like TiO_2 , V_2O_3 , MnO and Nb_2O_5 chemisorb amounts of hydrogen and carbon monoxide, which are in accordance with the metal particle sizes, as determined by transmission electron microscopy. Reduction of the same catalysts at 773 K results in decreased sorption characteristics to near zero [19-21]. Electron Microscopy and X-ray diffraction proved that this loss of chemisorption capacity was not due to the trivial effect of sintering of the supported metal at 773 K. Since the discovery of this SMSI-effect by Tauster et al. [19,20], many investigations have been carried out to explain this anomalous effect. Two models are proposed. The first model is based on charge transfer from the support to the metal [22], and assumes that the adsorption characteristics of the metal are changed (electronic model). The second model assumes the formation of lower oxides of the support material during the high temperature reduction. These lower oxides can diffuse onto the metal and spread over the metal surface (covering model). Strong experimental evidence in favour of the second explanation have been reported by several authors [23-30].

For small metal particles, the choice of the support may be of great importance for the catalytic behaviour, since the number of metal atoms in direct contact with the support is relatively high. Thus, Ichikawa *et al.* have shown that the product distribution of CO hydrogenation over supported rhodium catalysts is highly dependent on the support used [12,13]. Another probability for directing the synthesis gas reaction to desired products is the addition of promoters. A promoter is a substance added to a catalyst in a small amount, which by itself has little or no activity, but which imparts a better activity, stability or selectivity for the desired reaction than is realized without it. In synthesis gas reactions, promoters are widely used. For instance, Ichikawa *et al.* [31] and Van den Berg *et al.* [32] reported high C_2 -oxygenate selectivities for silica-supported rhodium catalysts promoted by

transition metal oxides.

1.3 CHARACTERIZATION OF METAL CATALYSTS

Catalysts can be characterized best by their activity, selectivity and stability. In addition, their structure can be characterized by several chemical and spectroscopic techniques. The general objective of fundamental catalytic research is to obtain insight into the structure of the heterogeneous metal catalysts and the relation between this structure and the catalytic properties, in other words: to transform catalysis from an "art" into a "science". A fundamental understanding can result in well-defined concepts for catalyst design, and might finally result in cheaper catalytic processes due to an improved activity, selectivity and stability of the catalyst.

As we deal with highly dispersed metal catalysts, information about the metal particle size (distribution) and the fraction of exposed metal atoms (dispersion) is indispensable. Simple chemical techniques, like hydrogen and carbon monoxide chemisorption techniques are often used to get information about the metal particle size. However, if one wants to calculate metal surface areas in an absolute way the hydrogen-to-metal and carbon monoxide-to-metal stoichiometry must be known. Often a stoichiometry of one is used, but as early as 1960, data began to appear in the literature about hydrogen-to-metal stoichiometries exceeding unity for supported Pt [33,34], Rh [35] and Ir [36,37] catalysts. Carbon monoxide-to-metal stoichiometries can also exceed unity [35]. Infrared spectroscopy can provide useful information about the ways in which CO is adsorbed on metals. For instance for CO adsorbed on supported rhodium catalysts, Yang and Garland [38] observed infrared bands that could be assigned to CO multiply coordinated to several rhodium atoms (bridge-bonded), or to CO singly coordinated to one rhodium atom (linearly bonded, on top), or to CO adsorbed in the gem-dicarbonyl or twin form (see Figure 1.4). In the twin form two CO molecules are bonded to one rhodium ion.

Transmission Electron Microscopy and X-ray Diffraction can also give information about the metal particle size. However, for very highly dispersed metal catalysts ($d < 10 \text{ \AA}$), it is difficult to establish the degree of dispersion by these techniques. Extended X-ray Absorption Fine Structure (EXAFS) is a very powerful technique to study these highly dispersed supported metal catalysts. It is sensitive to short range order and can provide information about the coordination of metal atoms. From the metal-metal coordination number, the metal particle size and dispersion can be

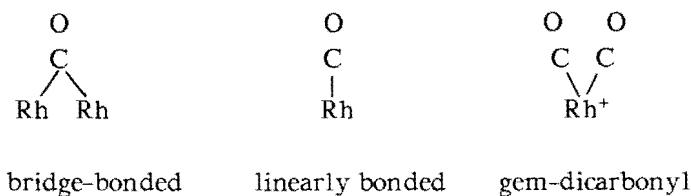


FIGURE 1.4: Adsorption forms of CO bonded to the rhodium surface.

calculated. In addition, the interface between the metal particle and the oxidic support can be studied by EXAFS.

Other often used spectroscopic techniques are X-ray Photo-electron Spectroscopy, Mössbauer Spectroscopy, Electron Spin Resonance, Nuclear Magnetic Resonance and several others. Especially when applied *in situ*, these techniques can be very useful. Moreover, generally each technique gives only details of the structure and several techniques must be combined to complete the characterization of the structure.

Recently, a lot of chemical characterizations are used in a temperature programmed way, i.e. the reaction progress is studied with the temperature increasing according to a, usually linear, temperature program. In this way reactivity patterns as a function of temperature are obtained. In principle, there is no limitation to the type of reaction that can be studied. Applications are known in the study of decomposition, desorption, oxidation and reduction reactions. In this thesis temperature programmed reduction, oxidation and desorption of hydrogen is used. As the catalysts must be brought in the active state by reduction of the metal precursor, temperature programmed reduction can provide useful information about this process. Temperature programmed oxidation can be used to characterize the small metal particles in the catalyst systems, while temperature programmed desorption of hydrogen can be used to study the binding states of hydrogen adsorbed on the metal particles. For a detailed description of the temperature programmed reduction and oxidation experiments we refer to [39-41].

In this thesis, a combination of spectroscopic and chemical techniques is used to obtain detailed information on the structure of the catalysts in order to better understand the differences in catalytic performance of the catalysts.

1.4 MECHANISTIC ASPECTS OF CO HYDROGENATION

1.4.1 Formation of hydrocarbons

Numerous studies have been done to unravel the elementary steps of hydrocarbon synthesis on Fischer-Tropsch catalysts such as Fe, Ni, Co and Ru. At present there appears to be a fair consensus that the following steps are involved [42-50]:

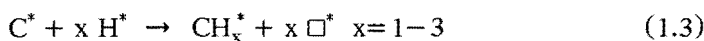
* Dissociation of H₂:



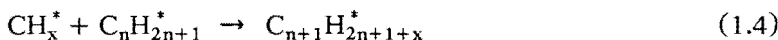
* Adsorption and subsequent dissociation of CO:



* Formation of methyl groups:



* Propagation, formation of longer chain products by insertion of CH_x^{*}:



* Termination reactions by β-hydrogen abstraction, leading to α-olefins:



or by hydrogenation, leading to paraffins:



From results of Ponec *et al.* [47,48], Biloen and Sachtler [51,52] and Tamaru *et al.* [53], using ¹³CO, it became evident that the dissociation of CO (step 2) is essential.

The Fischer-Tropsch product distribution can be described by simple statistics [54-56]. As first shown by Anderson *et al.* [55,56], the formation of hydrocarbons over Fischer-Tropsch catalysts can be described by the chain growth models originally developed by Schulz [57] and Flory [58] for polymerization reactions. For a polymerization reaction in general, a step-wise chain growth mechanism leads to a product distribution which can be described by a single growth probability α. Formally speaking, the

Fischer-Tropsch reaction can be divided into three stages: the initiation, the propagation and the termination. In this model the rate of the reaction is determined by the rate of initiation k_i . The selectivity depends on the rates of propagation and termination, k_p and k_t , respectively. The chain-growth probability factor is defined as $\alpha = k_p/(k_p + k_t)$. The following equation can be derived:

$$\log X_n = \log((1-\alpha)/\alpha) + n \times \log \alpha \quad (1.7)$$

Plotting $\log(X_n)$ versus n should result in a straight line with a slope equal to $\log \alpha$ and an intercept equal to $\log((1-\alpha)/\alpha)$, according to the Flory-Schulz-Anderson equation (X_n is the fraction of products with n C-atoms). This is indeed found to be true for Fischer-Tropsch active metals such as cobalt, iron, nickel, ruthenium and rhodium for $n > 2$. Low molecular weight hydrocarbons (CH_4 , C_2H_4 , C_2H_6) deviate from this line.

1.4.2 Formation of methanol

Methanol is at the moment the most important oxygenated product produced from syngas. The oldest generation of high pressure catalysts was a mixture of oxides (i.e. $\text{ZnO}/\text{Cr}_2\text{O}_3$), the newest generation of low pressure catalysts also contains Cu. In a recent article [59], Klier reviewed probable mechanisms for the formation of methanol from synthesis gas. The active centers for methanol formation are suggested to be unreduced metal ions (Cu^+ , Zn^+ etc.) [60,61].

For a long time Cu has been considered to be the only metal active in the methanol synthesis. Now, several papers report the formation of methanol over Pt, Pd, Rh and Ir catalysts [9,10,62,63]. Poels *et al.* [9,62,63] and Hindermann *et al.* [64] found a proportional relation between the methanol activity and the amount of Pd extractable with acetyl acetone (i.e. Pd^{2+}). They therefore ascribe the activity for methanol formation to Pd ions and they view the role of the support and promoter as the stabilization of Pd^{2+} active centres in the neighbourhood of the Pd^0 metal particles, which in turn supply the H atoms required for the hydrogenation.

Formates, often postulated as key intermediates towards methanol in the reaction of synthesis gas, can indeed be observed by I.R. spectroscopy with certain catalysts, although not with every catalyst active in methanol synthesis [65]. It has been claimed however, that these formates adsorbed on the support are not taking part in the above mentioned reactions on Ru catalysts yielding oxygenates [66]. When adsorbing CO onto a support

producing a formate, one would expect exchange between oxygen of the support and oxygen of the CO molecule. This has only been found after prolonged reaction [65].

Takeuchi and Katzer [11] studied the mechanism of methanol synthesis over a Rh/TiO₂ catalyst using a 50-50 mixture of ¹³C¹⁶O and ¹²C¹⁸O. The major products formed were ¹³CH₃¹⁶OH and ¹²CH₃¹⁸OH, indicating that methanol synthesis occurs by a non-dissociative mechanism and that no scrambling occurs in a reaction intermediate, as is expected for formate. After prolonged reaction (30 % conversion) also ¹²CH₃¹⁶OH is present, caused by exchange of ¹²C¹⁸O with the oxygen of the support resulting in ¹²C¹⁶O. Considering the results of Takeuchi and Katzer, the route from CO to methanol via formates cannot be a general one.

Recently, new and strong support for the importance of formyl species bound to positively charged centres was given. Hindermann *et al.* [64] reported that the activity for methanol, plotted as a function of the amount of MgO added to a Pd/SiO₂ catalyst, runs parallel with the concentration of formyl species on these catalysts (determined by chemical trapping). No correlation was found between methanol activity and the concentration of formates on the catalyst surface. Furthermore, a study of Kiennemann *et al.* [67], using both IR spectroscopy and chemical trapping, confirmed that on ZnO, formyl species were formed from the interaction of CO and H₂. The formyl species were very reactive and their lifetime and their concentration was very low at reaction temperature, so that they could only be seen by IR at 260 K. At reaction temperature adsorption bands of the methoxy group were found, and therefore Kiennemann *et al.* concluded that the formyl species are the main intermediates in the synthesis of the methoxy group.

Kazanskii *et al.* [68] performed a non-empirical quantum chemical study on the insertion of CO into the M-H bond (in the case of Pd) yielding a M-formyl complex, and showed that this insertion proceeded with a monotonically decreasing energy along the reaction coordinate for a model system including a positive Pd ion (HPd⁺CO) and that on the other hand the same process was strongly endothermic for the neutral system (H₂PdCO).

So, taking into account the calculations of Kazanskii *et al.*, the model most in compliance with the data described in the literature is the non-dissociative hydrogenation of CO via the formyl intermediate on a metal ion, as has also been concluded before by Poels [65].

1.4.3 Formation of C₂-oxygenates

The mechanism of C₂-oxygenates formation from syngas has been studied from several angles:

- by comparing the product distribution of hydrocarbons and oxygenates,
- by addition of reaction products (like ethene or propene) to a working catalyst,
- by isotopic tracer studies, and
- by IR spectroscopy studies, studying the synthesis gas reaction *in situ* (reaction intermediates)

In the following paragraphs we will discuss these angles of incidence and the consequences for the mechanism of C₂-oxygenate formation. In § 1.4.3.5 we will describe a generally accepted scheme for syngas reactions and will discuss the sites responsible for the several steps in the reaction scheme.

1.4.3.1 Product distribution of H₂-CO reaction

Van den Berg [69] performed a detailed analysis of the products formed from synthesis gas over a Rh/SiO₂ catalyst promoted by Mn and Mo. (T = 548 K, P = 10 MPa, GHSV = 10000 h⁻¹, H₂/CO = 1). He observed a similar chain growth probability for hydrocarbons, alcohols and aldehydes, 0.34, 0.36 and 0.32 respectively (see Figure 1.5). The fact that separate product distributions for hydrocarbons and oxygenates obeyed a linear Schulz-Flory relation with a similar slope and the fact that only linear hydrocarbons and alcohols were observed indicate that a chain growth mechanism similar to the mechanism of the Fischer-Tropsch reaction is operating and that all products are produced via a single chain growth mechanism.

The C₁- and C₂-products clearly deviate from the Schulz-Flory curves. There is a discrepancy between the maximum yield of C₂-products predicted by the Flory-Schulz equation (28 wt%) and the maximum yield of C₂-products that can be obtained over rhodium catalysts (up to 90 %, mainly C₂-oxygenates). This can be explained by the following:

- As suggested from ethylene addition experiments (see § 1.4.3.2) oxygenates (except methanol) are made by CO insertion into a metal-CH_x bond. Therefore, C₂-oxygenates should be viewed as "C₁-compounds" in Flory-Schulz terminology and can be produced with 100 % selectivity ($\alpha = 0$) [69].

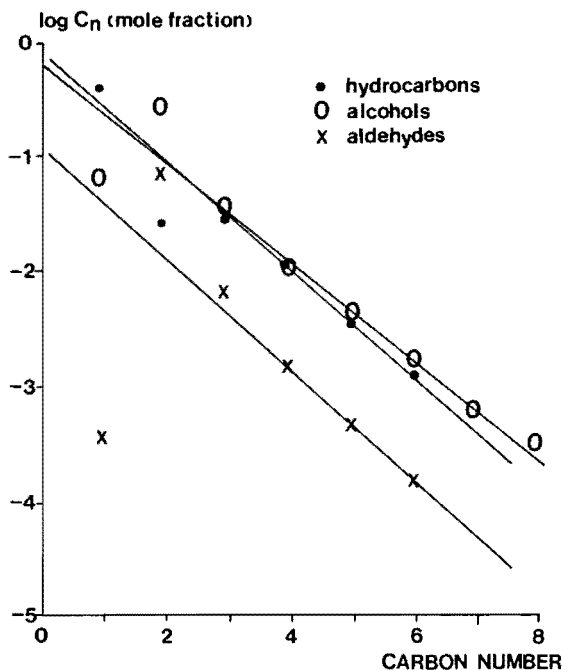


FIGURE 1.5: Schulz-Flory plot of products formed over rhodium catalyst (from ref. [69], with permission).

- In the derivation of the Flory-Schulz equation it is assumed that the rates of propagation and termination are independent of the chain length. However, CO is inserted more rapidly into an M-CH₃-group than into an M-C₂H₅-group [70].

Based on these considerations and ethylene addition experiments, Van den Berg [69] suggested the mechanism as depicted in Figure 1.6.

Takeuchi *et al.* [72] studied the syngas reaction over Rh/TiO₂ reduced at 473 K (3.0 wt% Rh/TiO₂, T = 423 K, P = 0.1 MPa) and observed a large deficit in C₂-hydrocarbons. This type of undershoot of C₂-hydrocarbons has usually been explained by invoking the rapid insertion reaction of the product ethene, leading to higher carbon number products and reduced C₂-product concentration [44] (for Ni, Fe and Co catalysts). If the total products, hydrocarbons and alcohols (C_n + C_nO), are plotted versus n, the product distribution shows Schulz-Flory-Anderson type behaviour (no overnor undershoot of C₂-products) with an increasing α -value when going to higher n ($\alpha = 0.22$ at C₂, $\alpha = 0.54$ above C₄). Furthermore, there were essentially no alkenes, indicating a complete hydrogenation to the

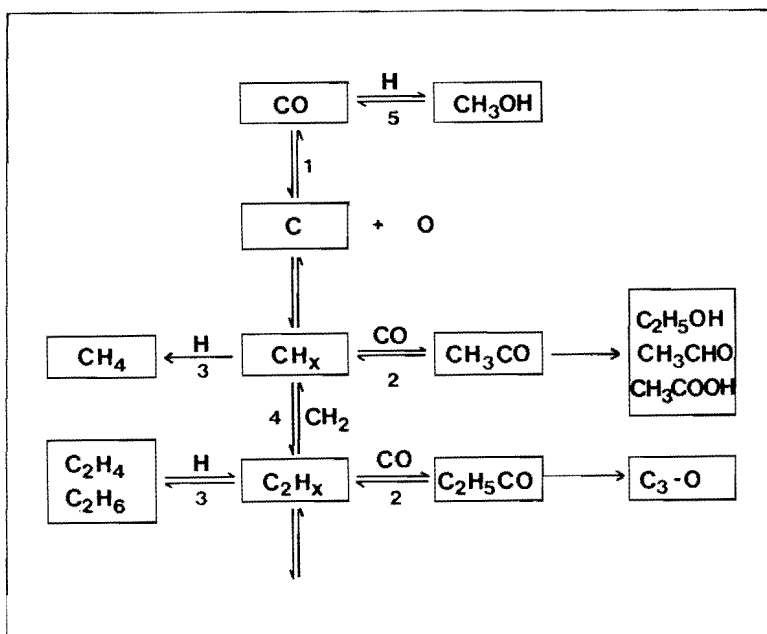


FIGURE 1.6: A model for the reactions of CO/H₂ over rhodium catalysts, as proposed by Van den Berg *et al.* [31,69] and Ichikawa [71].

corresponding alkanes. The same results were reported by Takeuchi *et al.* [73] for Co-Re-Sr/TiO₂ catalysts. Takeuchi *et al.* inferred that the large deficit in C₂-hydrocarbons cannot be attributed to the reaction of ethene, but appears to be due to the formation of ethanol. This suggests that a common intermediate may be involved in the formation of hydrocarbons and oxygenates (see Figure 1.7). According to Takeuchi *et al.*, the intermediate I₂ is an adsorbed ketene or oxirene intermediate, formed by CO insertion into a surface carbene (see paragraph 1.4.3.3). I₁ is assumed to be CHOH_{ad} (formyl), or a non-dissociatively adsorbed CO molecule.

So, the differences between the model proposed by Takeuchi and by Van den Berg are:

- 1) Takeuchi proposed a common intermediate for C₂-oxygenates and C₂-hydrocarbons whereas Van den Berg proposed a common intermediate for C₂-oxygenates and C₁-hydrocarbons.
- 2) The chain growth of all products occurs by CO insertion according to Takeuchi, while Van den Berg suggests that CO insertion only takes place to form oxygenates.

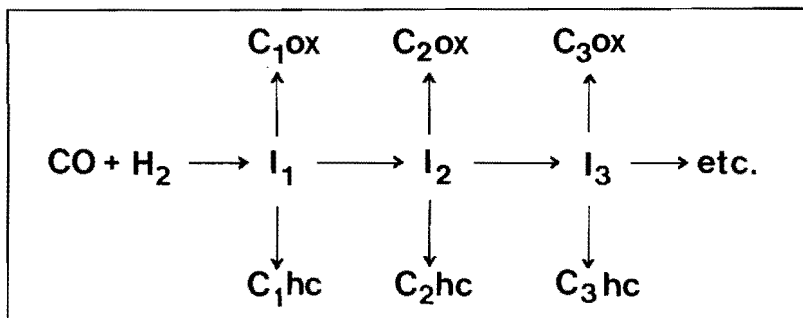


FIGURE 1.7: Model for chain growth and formation of alcohols and hydrocarbons as proposed by Takeuchi *et al.* [72].

1.4.3.2 Addition of reactive compounds

Several authors used the addition of reactive compounds to a working catalyst to study the reaction mechanism. As shown in § 1.4.3.1, the CO insertion mechanism is believed to be an important step in the production of oxygenates and/or chain-growth. Alkene addition is often used to study this hydroformylation reaction. Van den Berg [70], using a Rh/Mo/Mn/SiO₂ catalyst, showed that 50 % of the ethene added was converted into propanol, 30 % to ethane, 10 % to methane and the rest to other products, mainly hydrocarbons. So ethene, formed during the reaction, can undergo a number of secondary reactions, notably hydroformylation, hydrogenation and even hydrogenolysis. Pijolat and Perrichon [74] studying the H₂/CO reaction over Fe/Al₂O₃ catalysts, (0.8 - 3.0 MPa) reported the enhancement of the production of 1-pentanol by adding 1-butene to the H₂/CO mixture and concluded that CO insertion in a metal-alkyl bond must occur during the synthesis and probably constitutes the reaction pathway to alcohols.

Ichikawa *et al.* [75] observed a parallel between the rates of ethylene hydroformylation and the rate of formation of propanol for TiO₂- and ZrO₂-promoted Rh/SiO₂ catalysts using carbonyls as rhodium precursor.

Chuang *et al.* [76] investigated alkali promotion of Rh/TiO₂ by ethene addition (P = 1.0 MPa, T = 473 K, H₂/CO = 2). The methanol, methane and C₂-oxygenates formation rate is not influenced. From the fact that methane formation is not influenced one can conclude that no hydrogenolysis of ethene takes place. The formation rate of propionaldehyde, propanol and

ethane is influenced markedly, while the formation of C_3^+ hydrocarbons is only slightly influenced. These results support the CO insertion mechanism for oxygenates.

However, Chuang *et al.* [76] noted that the ethene produced from CO hydrogenation was not the same as the ethene added until it desorbed from the surface of the catalyst. Specifically, the adsorbed ethene, added to the syngas mixture, was not equivalent to the precursor for ethene formed from the CO hydrogenation reaction. This could be concluded, since the selectivity for the added ethene to enter chain-growth rather than to be hydrogenated to ethane is significantly different from that for the C_2H_x surface intermediate formed during CO hydrogenation. Chuang *et al.* only used the added ethylene to serve as a probe to distinguish hydrogenation and CO insertion activities under synthesis conditions.

Favre *et al.* [77] used CH_2Cl_2 addition to study the synthesis gas reaction over Rh/ V_2O_3 and Pd/ V_2O_3 (473 K, 0.1 MPa, $H_2/CO = 2$) in order to supply extra CH_x fragments to the catalyst. In the case of Pd/ V_2O_3 , for which methanol is the almost exclusively made oxygenate, this results in a significant increase in ethanol selectivity. In the case of Rh/ V_2O_3 , the effect on C_2-OH selectivity was marginal. So, normally on Pd/ V_2O_3 , there is an insufficient number of CH_x fragments. External delivery of CH_x fragments results in an increase of C_2 -oxygenates, indicating that CO insertion can also take place on Pd. Thus, CH_x fragments are necessary for the formation of C_2 -oxygenates by CO insertion.

Van den Berg [70] also studied the influence of the addition of acetaldehyde, acetic acid, ethanol and methanol to a Rh-Mn-Mo/ SiO_2 catalyst. The major part of the added acetaldehyde was hydrogenated to ethanol, indicating that acetaldehyde and ethanol are formed from the same precursor. Acetic acid addition results in an increased amount of ethanol, methyl- and ethylacetate. Ethanol addition had practically no effect on the product distribution. Methanol addition caused an irreversible decrease in the rate of production of oxygenates. Based on the fact that methanol addition does not result in the production of C_2 -oxygenates, Van den Berg concluded that C_2 -oxygenates are not produced via carbonylation of methanol (homogeneous catalysis, Monsanto process) under his reaction conditions.

Summarizing the above described investigations, the addition of several compounds can deliver very useful information. However, one must be very careful, because the added alkene does not necessarily increase the number of intermediates for alkane production, but may react directly.

1.4.3.3 Labelling experiments

Isotopic tracer studies are a powerful tool in mechanistic studies. As already mentioned in paragraph 1.4.2, Takeuchi and Katzer [11] clearly showed, by using $^{13}\text{C}^{16}\text{O}$ and $^{12}\text{C}^{18}\text{O}$, that methanol synthesis over a Rh/TiO₂ catalyst occurs via a non-dissociative mechanism. They also studied the formation of C₂-oxygenates using isotopes [78,79]. ^{13}C -NMR and ^1H -NMR studies of the isotopic composition of ethanol formed after addition of $^{12}\text{CH}_3^{16}\text{OH}$ to a reaction mixture of $^{13}\text{C}^{16}\text{O} + \text{H}_2$ showed that the methanol homologation contribution to ethanol synthesis is only minor (10%) [78]. However, several objections to this conclusions can be made. Their experiments are performed at low pressure (500 Torr) and one cannot exclude that one of the precursors of methanol undergoes homologation to ethanol at high pressure. Even if the results of Takeuchi and Katzer show that there is only a minor contribution to ethanol production by methanol homologation, they cannot exclude the intermediacy of methanol precursors.

Takeuchi and Katzer also performed very important studies of the isotopic composition of ethanol from a mixture of $^{12}\text{C}^{18}\text{O}$ and $^{13}\text{C}^{16}\text{O}$ and H₂ using a gaschromatograph/chemical ionization mass spectrometer combination [79]. We will follow their discussion and the comments made by Deluzarche *et al.* [80]. The experimental isotopic distribution obtained by Takeuchi and Katzer for the ethanol produced is in accordance with the hypothesis of breaking of the C-O bond for all the molecules. However, these results do not prove that the fully dissociative model is operative [79,80]. On the basis of their results Takeuchi and Katzer raised serious doubts (a) on the enolic condensation mechanism of Anderson [81], and (b) on the mechanism of CO insertion into a methyl group. The M-CH₃-group could be obtained from formyl species according to Henrici-Olivé and Olivé [82] (b1), or according to Pichler and Schulz [83](b2), or from a surface carbon obtained by a dissociated CO molecule with subsequent insertion of undissociated CO, as suggested by Biloen and Sachtler [44] (b3) (see Figure 1.8).

None of these mechanisms can explain the formation of $^{12}\text{C}^{12}\text{C}^{16}\text{O}$ and $^{13}\text{C}^{13}\text{C}^{18}\text{O}$ starting from a $^{12}\text{C}^{18}\text{O}$ and $^{13}\text{C}^{16}\text{O}$ mixture. These results led Takeuchi and Katzer to propose a complex mechanism, in which a M=CH₂ species is formed followed by CO insertion resulting in the formation of a (very unstable) ketene/oxirene intermediate (c1). Statistical scrambling of O and C may result from reversibility of (c1) or exchange due to ring

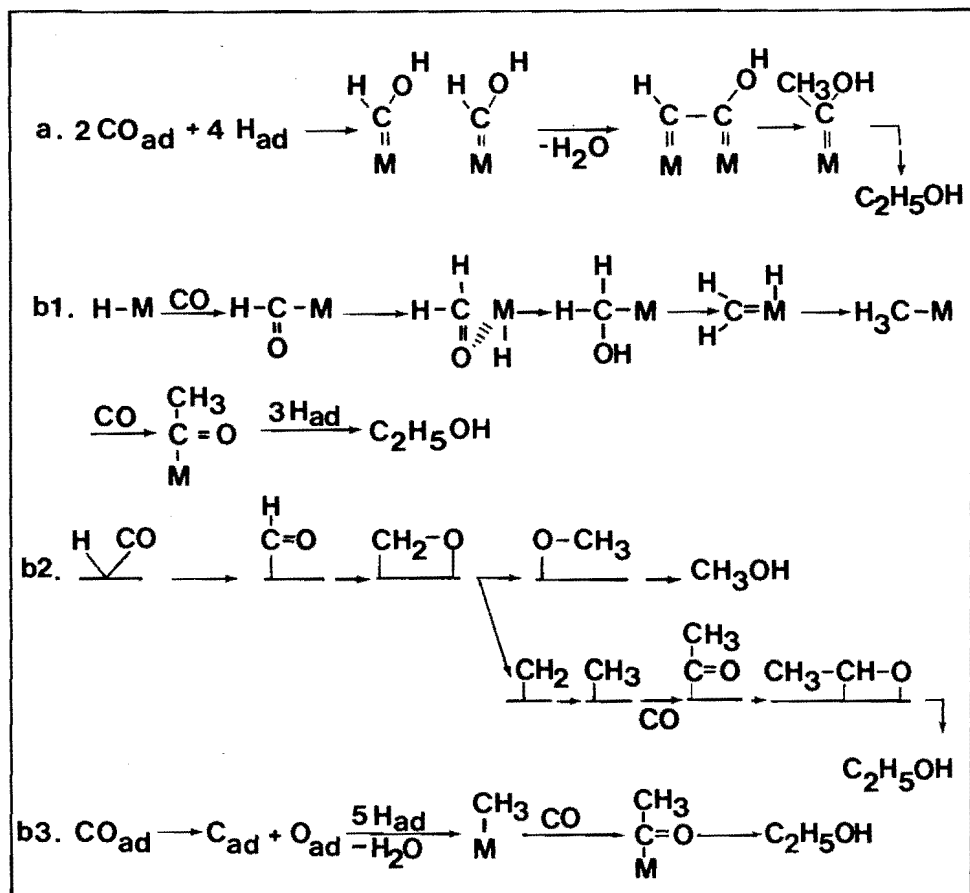


FIGURE 1.8: Formation of C_2 -oxygenates according to a) Anderson [81], b1) Henrici-Olivé and Olivé [82], b2) Pichler and Schulz and b3) Biloen and Sachtler [84].

breaking (c3)(see Figure 1.9).

Deluzarche *et al.* [80] formulated the following objections against this model:

- the mechanism makes use of a ketene species that has been proposed and subsequently abandoned by Blyholder and Emmett [84], and that has not been re-used since,
- ethylene oxide is generally not observed as a product,
- the mechanism cannot explain the fact that the formation of ethylene glycol takes only place at high pressures.

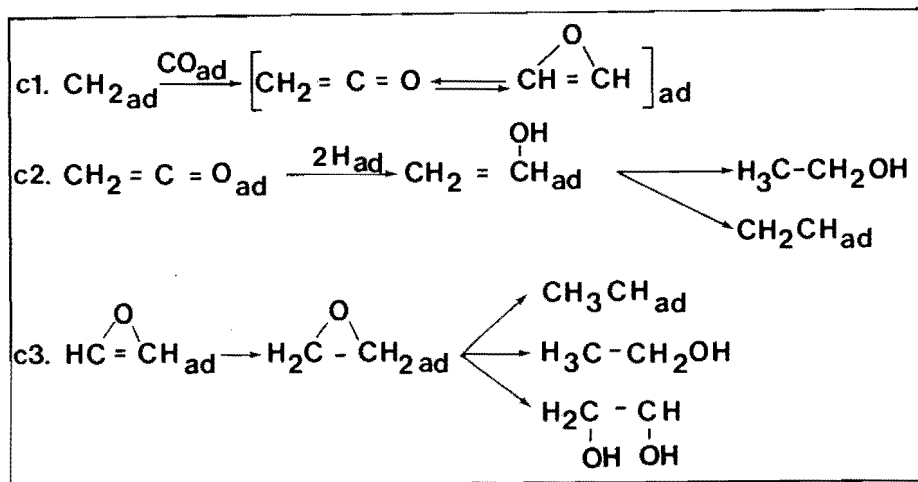


FIGURE 1.9: Mechanism of C_2 -oxygenates according to Takeuchi and Katzer [79].

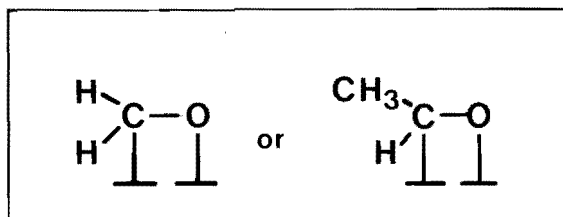


FIGURE 1.10: Intermediates for C_2 -oxygenate formation as proposed by Deluzarche [80].

Deluzarche *et al.* suggest that adsorbed aldehydes (see Figure 1.10) are intermediates (acetaldehyde is one of the possible products [70]) and then it is possible to explain Takeuchi and Katzer's results by a mechanism consisting of CO insertion into a methyl-metal group or via a carboxylate species. Deluzarche *et al.* report that adsorbed aldehyde can react with a water molecule formed during the reaction. The kinetics of this reaction are so fast that it cannot be measured. They conclude that without any water-aldehyde exchange, the statistical isotopic distribution for ethanol is far from the isotopic distribution obtained by Takeuchi and Katzer, but when equilibrium is obtained Deluzarche *et al.* find the same distribution as for

the mechanism of Takeuchi and Katzer. Furthermore, there is also ^{16}O - ^{18}O exchange through the acetate species formation. The results of Takeuchi and Katzer even cannot reject the mechanism in which carboxylate species play a role as proposed by Deluzarche et al. in earlier publications [85]. The already mentioned results of Takeuchi and Katzer about the minor role of methanol homologation in ethanol production [78] also cannot exclude the intermediacy of methanol precursors in the formation of C_2 -oxygenates.

Orita *et al.* [86,87] studied acetaldehyde formation over Rh/SiO_2 and $\text{Rh-Mn}/\text{SiO}_2$ catalysts by the isotopic tracer method. In contrast to Takeuchi and Katzer, they could distinguish between the carbon isotope distribution in the methyl group of acetaldehyde and that of the formyl group. They started with $^{13}\text{CO} + \text{H}_2$ and cooled to room temperature after 3.5 h of reaction, changed to $^{12}\text{CO} + \text{H}_2$ and then heated again to reaction temperature. Isotope distribution in the products as a function of time was measured. The ^{13}C distribution in the methyl group of acetaldehyde exhibited almost the same behaviour as the ^{13}C distribution in the hydrocarbons and could be extrapolated to the purity of the ^{13}CO used at the initial stage of the reaction. In contrast, the ^{13}C distribution in the formyl group of acetaldehyde was markedly different from the distributions in the hydrocarbons and decreased rapidly to the natural abundance of ^{13}C . These results indicate that during steady-state $\text{CO} + \text{H}_2$ reaction, there exist common C_1 -intermediates from which hydrocarbons and the methyl group of acetaldehyde are formed, and acetaldehyde is produced via CO insertion into these C_1 -intermediates. Orita *et al.* also studied the reaction of $\text{C}^{18}\text{O} + \text{H}_2$. They followed the ^{18}O distribution and found that in acetaldehyde, its abundance was nearly 50 % at the initial stage of the reaction and gradually increased. In CO, the ^{18}O abundance was constant at 99%, suggesting that there was no exchange between CO and the support. These results suggest that the intermediates which form acetaldehyde via CO insertion into the C_1 -species have an acetate ion-like structure, in which one oxygen atom is supplied by CO and the other by the support, and that these intermediates are hydrogenated to acetaldehyde before further exchange reactions of oxygen with the support take place. An objection against the experiments of Orita *et al.* is that they measured at a very low reaction temperature (403 K), and therefore used high contact times (consecutive reactions might occur).

Ichikawa and Fukushima [88] studied C_2 -oxygenates formation over $\text{Rh-Ti}/\text{SiO}_2$ catalysts using ^{13}CO and $^{13}\text{CH}_3\text{OH}$. Before $\text{H}_2 + \text{CO}$ reaction they treated the catalyst with ^{13}CO to enrich the surface with carbide (^{13}C) by

the Boudouard reaction at 473-493 K. Subsequently, the catalyst was exposed to ^{12}CO (298 K) to exchange chemisorbed ^{13}CO . The reaction mixture ($^{12}\text{CO} + \text{H}_2$) was introduced and the temperature raised to 473 K. They also reported a significant ^{13}C enrichment only in the methyl carbon of ethanol and acetaldehyde and a negligible enrichment in the carbonyl derived fragments. Methane was formed with parallel enrichment of ^{13}C . In contrast, a trace amount of ^{13}C was detected in methanol. The abundance of ^{13}C in $^{13}\text{CH}_3\text{CH}_2\text{OH}$ and $^{13}\text{CH}_3\text{CHO}$ could be extrapolated to above 80 % at the initial reaction. These results suggest that the methyl group of the C_2 -oxygenates originates from surface carbon, i.e. the CH_3/CH_2 unit is formed by CO dissociation on the Rh metal, and a subsequent insertion reaction of CO provides a common precursor to C_2 -oxygenates, possibly CH_3CO species. Absence of incorporation of surface carbon into the methanol fraction indicates that methanol is formed by hydrogenation of non-dissociated CO. Addition of $^{13}\text{CH}_3\text{OH}$ showed, that only in 20 % of the ethanol formed, incorporation of methanol has occurred. No incorporation was seen in acetaldehyde. In methylacetate, incorporation of $^{13}\text{CH}_3\text{OH}$ at the methyl ester position was found suggesting that acyl and acetate species are accumulated on the catalyst surface, which are transformed to methyl acetate by the transient methanol feed.

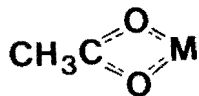
1.4.3.4 IR-spectroscopy

Fukushima *et al.* studied the formation of C_2 -oxygenates using high-pressure *in situ* IR spectroscopy [89,90]. In the first paper, they studied Rh/SiO₂ and Rh-Mn/SiO₂ catalysts during syngas reaction and observed a band at 1672 cm⁻¹, which is sensitive to hydrogen reduction, that could be assigned to $\nu(\text{C}=\text{O})$ of the acetyl species (M-(C=O)-CH₃). The assignment is confirmed by comparison with some related organometallic acetyl compounds. During reaction two other intense bands at 1564 and 1442 cm⁻¹ appeared. These bands were assigned to a bidentate acetate possibly attached to the Mn-oxide as is confirmed by the bands of Mn(MeCO₂)₂·2H₂O (1564, 1434 cm⁻¹). The band around 1735 cm⁻¹ is assigned to physically adsorbed acetaldehyde on the catalyst. In the case of Rh/SiO₂, a much weaker band at 1650 cm⁻¹ was observed than in the case of Rh-Mn/SiO₂. Three other bands at 1749, 1460 and 1381 cm⁻¹ were assigned to a silyl acetate [MeCOO-Si=].

Fukushima also studied Fe-Rh/SiO₂ catalysts using *in situ* high-pressure FT-IR spectroscopy. IR bands of three different surface species, e.g. acyl $\nu(\text{C}=\text{O})$ at 1650 cm⁻¹, and methoxy and ethoxy $\nu(\text{CH}_3/\text{CH}_2)$ deformation

bands at 1444 and 1396 cm^{-1} , respectively, are observed. These surface species were suggested to be the active intermediates related to the formation of methanol and ethanol. The evidence for methoxy and ethoxy species lies in the agreement of the bands of the CH_3/CH_2 deformation modes with analogous bands of known alkoxides. The band shifts (ca. 15 cm^{-1}) in acyl and methoxy species observed in the CO/D_2 reaction could be explained by the stepwise deuteration of their methyl groups. The addition of Fe markedly enhanced the formation of methoxy and ethoxy species and suppressed the formation of acetate species. This was reflected in the product distribution, more methanol and ethanol, and less acetaldehyde and acetic acid was formed.

Orita *et al.* [87,91] studied the mechanism of C_2 -oxygenated compounds over Rh/SiO_2 and Rh/TiO_2 below atmospheric pressure using *in situ* FT-IR spectroscopy. In the case of Rh/SiO_2 , a resemblance was reported between the spectra obtained after decomposition of acetaldehyde and the spectra obtained during the $\text{CO} + \text{H}_2$ reaction. In the case of the sodium-promoted Rh/SiO_2 , two extra bands at 1577 and 1425 cm^{-1} appeared after decomposition of acetaldehyde, assigned to the asymmetric and symmetric modes of O-C-O stretching vibrations of adsorbed acetate ions stabilized by the presence of sodium cations. Adsorption of acetic acid resulted in bands at 1568 and 1417 cm^{-1} and at higher acetic acid pressures (> 10 torr) also at 1720 cm^{-1} . These bands were assigned to the CO stretching vibration of chemisorbed surface ester groups. In the case of the manganese-doped catalysts, bands observed at 1568 and 1414 cm^{-1} could be assigned to the symmetric and asymmetric modes of O-C-O stretching vibration of adsorbed acetate ions. Dynamic behaviour of the adsorbed species during replacement of $^{13}\text{CO} + \text{D}_2$ with $^{12}\text{CO} + \text{D}_2$ was studied. A rapid exchange of adsorbed ^{13}CO with ^{12}CO was observed. The band at 1745 cm^{-1} could be assigned to the CO stretching vibration of adsorbed acetyl species. This acetyl species was most stable towards evacuation or hydrogenation among all the adsorbed species including CO_{ads} suggesting that it is not adsorbed on Rh metal but on the support near Rh-particles. Combining these FT-IR studies with the already described isotope tracer studies (§ 1.4.3.3), Orita *et al.* suggested that acetate-like structures



with one oxygen atom being supplied by CO and the other by the support or promoter, are the intermediates forming acetaldehyde.

In the case of Rh/TiO_2 , the acetate-structures were also observed [91]. In

this case, the SMSI effect could be followed using FT-IR spectroscopy. After high temperature reduction, no CO_{ads} could be detected. After $\text{H}_2 + \text{CO}$ reaction, the CO_{ads} band increased, proving that during $\text{H}_2 + \text{CO}$ reaction, the SMSI state is (partly) broken probably due to H_2O formed during the synthesis gas reaction. The presence of chlorine enhanced the SMSI effect.

Van den Berg [69] studied Rh/SiO_2 and $\text{Rh-Mo-Mn}/\text{SiO}_2$ catalysts using *in situ* high-pressure FT-IR. On both catalysts chemisorbed CO appears to be the most dominant species under reaction conditions. Hydrocarbons are also present in significant amounts. His results indicate that these hydrocarbon species only cover a small fraction of the rhodium surface. The average length of these species increased during the reaction. A carbonyl vibration at 1770 cm^{-1} was assigned to an acetyl species. The isotope exchange confirmed that these species are active and can be reaction intermediates. Furthermore, a decrease in intensity of the silanol-bands during reaction was observed already before reaction products were observed in the gas phase. This may suggest that spillover adsorption of intermediates is responsible for this phenomenon.

1.4.3.5 General reaction scheme and reaction sites for C_2 -oxygenate formation

All measurements reviewed in the preceding paragraphs can be understood by the following general scheme for hydrogenation of CO over metal catalysts including the formation of oxygenates and hydrocarbons (see Figure 1.6) [92]:

- (1) non-dissociatively adsorbed CO is hydrogenated to methanol
- (2) dissociation of adsorbed CO to form CH_2/CH_3 (this step requires the largest ensemble of metal atoms)
- (3) growth of alkyl chains via CH_2 insertion
- (4) migratory insertion of CO into surface- CH_x bonds. Hydrogenation of the resulting species results in C_2 -oxygenates
- (5) hydrogenation or β -hydrogen elimination of surface alkyl groups resulting in saturated and unsaturated hydrocarbons, respectively.

The question we will consider now, is whether all these reaction steps can take place on one type of catalytic site, or whether a bifunctional operation is more likely.

Somorjai and coworkers [93-95] proposed a bifunctional reaction mechanism based on their measurements on rhodium foil, preoxidized rhodium foil

and LaRhO_3 catalysts. Rhodium metal is necessary for the production of CH_3 -groups, while an oxidized rhodium species is necessary to catalyse the CO insertion reaction, in a way analogous to the homogeneous catalytic reaction. Their Auger and XPS experiments revealed that the catalyst surface was composed of a mixture of oxidized and reduced rhodium species. Furthermore, their preoxidized rhodium foil and LaRhO_3 produced considerable amounts of oxygenates, while the Rh-foil only produced hydrocarbons. Van den Berg *et al.* [32] also proposed this dual-site mechanism, however they did not have evidence for the suggestion that the insertion reaction takes place on rhodium ions. However, Van der Lee *et al.* [95] observed an antipatic relation between the amount of C_2 -oxygenates produced and the amount of Rh ions as determined by extraction with acetyl acetone, while for the formation rate of methanol and the amount of extractable Rh ions a sympathetic correlation was found.

In accordance with this, Sachtler and Ichikawa [92] suggested that the hydroformylation of olefins (CO insertion) only requires very small rhodium metal ensembles. Basic metal additives like Fe and Zn ions on the rhodium surface effectively block the large Rh ensembles required for CO dissociation and H_2 dissociation. Their presence therefore results in a depression of methanation and of alkene hydrogenation. However, hydroformylation is even increased, which might be attributed to Zn ions inducing a Lewis acid promoted CO insertion, or to the Rh^{n+} , stabilized by ZnO, which are known centres of hydroformylation.

From the data reviewed in this chapter, it is obvious that the mechanism for the formation of C_2 -oxygenates and the nature of the sites required for the several steps in this mechanism, are not completely elucidated so far. Additional information is still desired.

1.5 SCOPE AND OUTLINE OF THIS THESIS

As already noticed in § 1.1, C_2 -oxygenates are the more desirable products in CO hydrogenation from an economic point of view. Rhodium catalysts are known to catalyse the formation of these products besides others, like methane and longer chain hydrocarbons. The improvement of the selectivity to C_2 -oxygenates is therefore one of the major challenges in the research efforts made in synthesis gas chemistry. The selectivity, activity and stability of the catalysts can be improved by a suitable choice of the support or a promoter.

This thesis describes a detailed characterization of supported rhodium

catalysts. V_2O_3 , ThO_2 , MoO_3 , ZrO_2 , La_2O_3 and alkali are used as promoters. Furthermore, the catalytic behaviour of these catalysts in CO hydrogenation is examined. Supported iridium catalysts are also characterized and tested in CO hydrogenation, because iridium, like rhodium, is placed on the line separating metals that adsorb CO dissociatively and metals that adsorb CO non-dissociatively under synthesis gas reaction conditions (see Figure 1.3).

The preparation methods, characterization techniques and experimental set-up for the high-pressure CO hydrogenation reaction are presented in chapter 2.

Chapter 3 deals with the preparation and characterization of alumina- and silica-supported iridium catalysts. Besides the classical incipient wetness technique, the urea technique was used to prepare highly dispersed iridium catalysts.

Hydrogen chemisorption was used to establish the degree of dispersion of the iridium catalysts. However, H/M ratios exceeding unity were measured. Because of the uncertainty in the H/M_{surface} stoichiometry, the hydrogen chemisorption results could not be used for a determination of the fraction of exposed metal atoms. Extended X-ray Absorption Fine Structure was used to calibrate the chemisorption measurements (chapter 4).

In chapter 5, alumina- and silica-supported rhodium and iridium catalysts are tested in the CO hydrogenation reaction at elevated pressure. Special attention is paid to the effect of chlorine remaining on the support after *in situ* reduction.

A review of the possible roles of promoter oxides in CO hydrogenation and the results of an explorative study of the promotion of silica-supported rhodium and iridium catalysts is presented in chapter 6.

In chapter 7 and 8, a detailed characterization of silica- and alumina-supported vanadium oxide-promoted rhodium catalysts and a study of the catalytic hydrogenation of CO over these catalysts at low (0.15 MPa) and relatively high (4.0 MPa) pressure are reported. The characterization and catalytic testing of silica-supported rhodium catalysts promoted by ThO_2 and MoO_3 are presented in chapter 9.

In order to further improve the catalysts of chapters 7-9, alkali was added. The effects of these additives are presented in chapter 10.

In chapter 11, the general discussion is presented.

The main conclusions arrived at in this thesis are summarized in chapter 12.

1.6 REFERENCES

1. A. Aquilo, J.S. Alder, D.N. Freeman and R.J.H. Voorhoeve, *Hydrocarbon Process*, 62 (1983) 57.
2. R.A. Sheldon, in "Chemicals from Synthesis Gas", D. Reidel, Publ. Comp., (1983).
3. F. Marschner and F.W. Moeller, *Appl. Industr. Catal.*, 2 (1983) 215.
4. J.F. Roth, J.H. Craddock, A. Hershmann and F.E. Paulik, *Chem. Techn.*, 1 (1971) 600.
5. H.D. Grove, *Hydrocarbon Process*, 51 (1972) 76.
6. F.E. Paulik, A. Hershmann, W.R. Knox and J.F. Roth, US Patent 3.769.329 (1973) to Monsanto.
7. S.L. Meisel, *Phil. Trans. Royal Soc. London*, A300 (1981) 157.
8. D.H. Bolton, *Chem. Eng. Techn.*, 41 (1969) 129.
9. J.M. Driessen, E.K. Poels, J.P. Hindermann and V. Ponc, *J. Catal.*, 82 (1983) 26.
10. L. Poutsma, L.F. Elek, P.A. Ibarbia, A.P. Risch and J.A. Rabo, *J. Catal.*, 52 (1978) 157.
11. A. Takeuchi and J.R. Katzer, *J. Phys. Chem.*, 85 (1981) 937.
12. M. Ichikawa, *Bull. Chem. Soc. Jap.*, 51 (1978) 2268.
13. M. Ichikawa, *Bull. Chem. Soc. Jap.*, 51 (1978) 2273.
14. M. Ichikawa, *J. Chem. Soc., Chem. Commun.*, (1978) 566.
15. P.R. Watson and G.A. Somorjai, *J. Catal.*, 72 (1981) 347.
16. P.R. Watson and G.A. Somorjai, *J. Catal.*, 74 (1982) 282.
17. M.M. Bhasin and G.L. O'Connor, Belgian Patent 824822, to Union Carbide Corp., (1975).
18. J.R. Katzer, A.W. Sleight, P. Gajardo, J. Michel, E.F. Gleason and S. McMillan, *Far. Disc. Chem. Soc.*, 72 (1981) 121.
19. S.J. Tauster and S.C. Fung, *J. Catal.*, 55 (1978) 29.
20. S.J. Tauster, S.C. Fung and R.L. Garten, *J. Am. Chem. Soc.*, 100 (1978) 170.
21. S.J. Tauster, S.C. Fung, R.T.K. Baker and J.A. Horsley, *Science*, 211 (1981) 1121.
22. J.A. Horsley, *J. Am. Chem. Soc.*, 101 (1979) 2870.
23. X.-Zh. Jing, T.F. Hayden and J.A. Dumesic, *J. Catal.*, 83 (1983) 168.
24. J. Santos, J. Phillips and J.A. Dumesic, *J. Catal.*, 81 (1983) 147.
25. P. Meriaudeau, J.F. Dutel, M. Dufaux and C. Naccache, *Stud. Surf. Sci. Catal.*, 11 (1982) 95.
26. D.E. Resasco and G.L. Haller, *J. Catal.*, 82 (1983) 279.
27. B.R. Powell and S.E. Whittington, *J. Catal.*, 81 (1983) 382.

28. A.J. Simoens, R.T.K. Baker, D.J. Dwyer, C.F.R. Lund and R.J. Madon, *J. Catal.*, 86 (1984) 359.
29. G.L. Haller, V.E. Henrich, M. McMillan, D.E. Resasco, H.R. Sadeghi and S. Sakellson, "Proc. of 8th Int. Congr. Catal., Berlin (1984)", vol. V, p. 135, Verlag Chemie, Weinheim, 1984.
30. Y.W. Chung, G. Xiong and C.C. Kao, *J. Catal.*, 87 (1984) 279.
31. M. Ichikawa, K. Shikakura and M. Kawai, in "Heterogeneous Catalysis Related to Energy Problems", Proc. Symp. in Dalion, China (1982) A.08-I.
32. F.G.A. van den Berg, J.H.E. Glezer and W.M.H. Sachtler, *J. Catal.*, 93 (1985) 340.
33. S.F. Alder and J.J. Keavney, *J. Phys. Chem.*, 64 (1960) 208.
34. V.S. Boronin, O.M. Poltorak and A.O. Turakulova, *Russ. J. Phys. Chem.*, 48 (1974) 156.
35. S.E. Wanke and N.A. Dougharty, *J. Catal.*, 24 (1972) 367.
36. G.B. McVicker, R.T.K. Baker, G.L. Garten and E.L. Kugler, *J. Catal.*, 65 (1980) 207.
37. S. Krishnamurthy, G.R. Landolt and H.J. Schoennagel, *J. Catal.*, 78 (1982) 319.
38. A.C. Yang and C.W. Garland, *J. Phys. Chem.*, 61 (1957) 1512.
39. J.W. Jenkins, B.D. McNickol and S.D. Robertson, *Chem. Techn.*, 7 (1977) 316.
40. N.W. Hurst, S.J. Gentry, A. Jones and B.D. McNickol, *Catal. Rev.-Sci. Eng.*, 24 (1982) 233.
41. T. Huizinga, J. van Grondelle and R. Prins, *Appl. Catal.*, 10 (1984) 199.
42. P.R. Wentrick, B.J. Wood and H.J. Wise, *J. Catal.*, 43 (1976) 363.
43. J.A. Rabo, A.P. Risch and M.L.J. Poutsma, *J. Catal.*, 53 (1978) 295.
44. P. Biloen and W.M.H. Sachtler, *Adv. Catal.*, 30 (1981) 165.
45. W.M.H. Sachtler, *Chem.-Ing. Techn.*, 54 (1982) 901.
46. J.A. Delmon and G.A.J. Martin, *J. Catal.*, 84 (1983) 45.
47. M. Araki and V. Ponec, *J. Catal.*, 44 (1976) 439.
48. V. Ponec and W.A. van Barneveld, *Ind. Eng. Chem., Prod. Res. Dev.*, 18 (1979) 268.
49. A.T. Bell, *Cat. Rev., Sci.-Ing.*, 23 (1981) 203.
50. R.C. Brady and R.J. Pettit, *J. Am. Chem. Soc.*, 102 (1980) 6181.
51. P. Biloen, J.N. Helle and W.M.H. Sachtler, *J. Catal.*, 58 (1979) 95.
52. P. Biloen, J.N. Helle, F.G.A. van den Berg and W.M.H. Sachtler, *J. Catal.*, 81 (1983) 450.
53. H. Yamazai, Y. Kobori, S. Naito, T. Onishi and K. Tamaru, *J. Chem. Soc., Faraday Trans. I*, 77 (1981) 2913; Y. Kobori, H. Yanazaki, S. Naito, T. Onishi and K. Tamaru, *ibid*, 78 (1982) 1473.

54. E.F.G. Herrington, *Chem. Ind.*, (1946) 347.
55. R.A. Friedel and R.B. Anderson, *J. Am. Chem. Soc.*, 72 (1950) 1212, 2307.
56. R.B. Anderson, R.A. Friedel and H.H. Storch, *J. Chem. Phys.*, 19 (1951) 313.
57. G.V. Schulz, *Z. Phys. Chem.*, 29 (1935) 299.
58. P.J. Flory, *J. Am. Chem. Soc.*, 58 (1936) 1877.
59. K. Klier, *Adv. Catal.*, 31 (1982) 243.
60. R.G. Herman, G.W. Simmons and K. Klier, in "New Horizons in Catalysis", *Proc. 7th Int. Congr. on Catal.*, Tokyo (1980), eds. T. Seiyama and K. Tanabe, Elsevier, Amsterdam (1981) A475.
61. R.G. Herman, K. Klier, G.W. Simmons, B.P. Finn, J.B. Bulko and T.P. Kobylinski, *J. Catal.*, 56 (1979) 407.
62. E.K. Poels, E.H. van Broekhoven, W.A.A. van Barneveld and V. Ponec, *React. Kinet. Catal. Lett.*, 18 (1981) 223.
63. E.K. Poels, *Far. Disc. Chem. Soc.*, 72 (1981) 194.
64. J.P. Hindermann, A. Kiennemann, A. Chakor-Alami and R. Kieffer, in "Proc. 8th Int. Congr. Catal., Berlin, 1984)", vol II, p. 163, Verlag Chemie, Weinheim, 1984.
65. E.K. Poels, Thesis, Leiden University, The Netherlands (1984).
66. C.S. Kellner and A.T. Bell, *J. Catal.*, 71 (1981) 296.
67. J. Saussy, J.C. Lavalley, T. Rais, A. Chakor-Alami, J.P. Hindermann and A. Kiennemann, *J. Molec. Catal.*, 26 (1984) 159.
68. N.A. Anikin, A.A. Bagatar'yants, G.M. Zhidomirov and V.B. Kazanskii, *Russ. J. Phys. Chem.*, 57 (1983) 393.
69. F.G.A. van den Berg, Thesis, Leiden University, The Netherlands, (1984).
70. H. Bahrmann and B. Cornils, in "New Synthesis with Carbon Monoxide" (J. Falk, Ed.) p. 226, Springer Verlag, Berlin, 1980.
71. M. Ichikawa, T. Fukushima and K. Shikakura, "Proc. Int. Congr. Catal., 8th (Berlin, 1984)", I-69, Verlag Chemie, Weinheim, 1984.
72. A. Takeuchi, J.R. Katzer and G.C.A. Schuit, *J. Catal.*, 82 (1983) 447.
73. A. Takeuchi, T. Matsuzaki, H. Arakawa and Y. Sugi, *Appl. Catal.*, 18 (1985) 325.
74. M. Pijolat and V. Perrichon, *Appl. Catal.*, 13 (1985) 321.
75. M. Ichikawa, K. Sekizawa and K. Shikakura, *J. Molec. Catal.*, 11 (1981) 167.
76. S.C. Chuang, J.G. Goodwin, Jr. and I. Wender, *J. Catal.*, 92 (1985) 416; S.C. Chuang, Y.H. Tian, J.G. Goodwin, Jr. and I. Wender, *J. Catal.*, 96 (1985) 396.
77. T.L.F. Favre, G. van der Lee and V. Ponec, *J. Chem. Soc., Chem. Commun.*, (1985) 230.
78. A. Takeuchi, J.R. Katzer and R.W. Creceley, *J. Catal.*, 82 (1983) 474.
79. A. Takeuchi and J.R. Katzer, *J. Phys. Chem.*, 86 (1982) 2438.

80. A. Deluzarche, J.P. Hindermann, R. Kieffer, R. Breault and A. Kiennemann, *J. Phys. Chem.*, 88 (1984) 4993.
81. H.H. Storch, N. Golumbic and R.B. Anderson, in "The Fischer-Tropsch and Related Synthesis", Wiley, New York (1951); R.B. Anderson in "Catalysis", Reinhold, New York (1956) vol 4.
82. G. Henrici-Olivé and S. Olivé, *Angew. Chem. Int. Ed. Engl.*, 15 (1976) 136.
83. H. Pichler and H. Schulz, *Chem. Ing. Techn.*, 18 (1970) 1162; H. Schulz, *Erdol, Kohle, Erdgas, Petrochem. Brennst. Chem.*, 30 (1977) 123.
84. G. Blyholder and P.H.J. Emmett, *J. Phys. Chem.*, 63 (1959) 962; *ibid* 64 (1960) 470.
85. A. Deluzarche, J.P. Hindermann and R.J. Kieffer, *Chem. Res. Synop.*, (1981) 72, *J. Chem. Res., Miniprint*, (1981) 934; J.P. Hindermann, A. Deluzarche, R. Kieffer and A. Kiennemann, *Can. J. Chem. Eng.*, 61 (1983) 21.
86. H. Orita, S. Naito and K. Tamaru, *J. Chem. Soc., Chem. Commun.*, (1984) 150.
87. H. Orita, S. Naito and K. Tamaru, *J. Catal.*, 90 (1984) 183.
88. M. Ichikawa and T. Fukushima, *J. Chem. Soc., Chem. Commun.*, (1985) 321.
89. T. Fukushima, H. Arakawa and M. Ichikawa, *J. Chem. Soc., Chem. Commun.*, (1985) 729.
90. T. Fukushima, H. Arakawa and M. Ichikawa, *J. Phys. Chem.*, 89 (1985) 4440.
91. H. Orita, S. Naito and K. Tamaru, *J. Phys. Chem.*, 89 (1985) 3066.
92. W.M.H. Sachtler and M. Ichikawa, *J. Phys. Chem.*, 90 (1986) 4752.
93. D.G. Castner, R.L. Blackador and G.A. Somorjai, *J. Catal.*, 66 (1980) 257.
94. P.R. Watson and G.A. Somorjai, *J. Catal.*, 72 (1981) 347.
95. P.R. Watson and G.A. Somorjai, *J. Catal.*, 74 (1982) 282.
96. G. van der Lee, B. Schuller, H. Post, T.L.F. Favre and V. Ponec, *J. Catal.*, 98 (1986) 522.

Chapter 2

EXPERIMENTAL METHODS

2.1 CATALYST PREPARATION

Most supported rhodium and iridium catalysts described in this thesis were prepared by the incipient wetness method. In this method, an accurately determined amount of metal salt is dissolved in just so much water that the volume of the solution will fill the pores of the support. The solution is added dropwise to the support, meanwhile shaking the support mechanically. After the impregnation the catalyst is dried at 395 K for 16 h. Some catalysts, especially the ones made from a nitrate precursor, were subsequently calcined at 723 K for 3 h.

For some catalysts the urea technique was used. In this technique, a solution of metal salt in water is added to a vigorously stirred and heated (365 K) aqueous suspension of the support and urea. The pH of the suspension increases slowly due to the decomposition of urea leading to the precipitation of metal hydroxides on the support.

Details about the supports and metal precursors used in this study are given in each of the following chapters.

2.2 CATALYST CHARACTERIZATION

It is of ultimate importance to obtain a good characterization of the catalysts used for the CO hydrogenation in order to understand the differences in catalytic behaviour. The following techniques were used to achieve this.

a. Temperature Programmed Reduction and Oxidation

Temperature programmed reduction (TPR) and oxidation (TPO) are very powerful techniques to study supported catalyst systems, as becomes obvious from an excellent review by Hurst *et al.* [1] and recent papers from our group [2-5]. During a TPR (TPO) experiment a gas mixture consisting of 4% H₂/Ar (4% O₂/He) flows over the catalyst while the temperature is increased at a linear programmed rate. The uptake of hydrogen (oxygen) is measured using a thermal conductivity detector. The resulting TPR (TPO)

profile is a "fingerprint" characterization of the reducibility (oxidizibility) of the catalyst. For a detailed description of the apparatus used and for aspects about reduction and oxidation of respectively metal oxides and metals, we refer to [5,6].

b. Chemisorption Techniques

One of the major characteristics of supported metal catalysts is the metal particle size. A certain metal particle size results in a certain degree of dispersion defined as the fraction of metal atoms exposed to the gasphase. Selective chemisorption of gaseous molecules, especially hydrogen and carbon monoxide, has been extensively used to estimate the degree of dispersion because this technique is relatively quick, cheap and easily feasible.

Hydrogen and carbon monoxide chemisorption measurements were performed in a conventional volumetric glass apparatus. The apparatus, the sequence of experimental actions and the theoretical background of the chemisorption measurements are extensively described in ref. [7,8].

c. Transmission Electron Microscopy

Some selected catalysts were studied by transmission electron microscopy in order to get more precise information about the mean metal particle size and the metal particle size distribution. These experiments were performed in cooperation with dr. H.W. Zandbergen of Gorlaeus Laboratories, State University of Leiden. The catalysts were examined with a Jeol 200 CX, operating at 200 kV (Centre for High Resolution Electron Microscopy, Antwerp).

d. Extended X-ray Absorption Fine Structure

EXAFS refers to the fine structure of the X-ray absorption coefficient that appears for photon energies in the range of approximately 20-1500 eV above the absorption edge. It is a final state effect involving scattering of the outgoing photo-electron by the neighbouring atoms. EXAFS is sensitive to short range order and can provide unique information about chemical and biological systems. Especially, this technique is very well suited for determining the coordination environment of very highly dispersed metal atoms in catalysts.

In this thesis EXAFS is used to determine the metal-metal coordination number, which is related to the metal particle size, for very highly dispersed metal atoms in catalysts. For these systems, hydrogen and carbon

monoxide chemisorption measurements do not provide reliable results and the metal particles are too small to be observed by TEM. EXAFS is the only technique available to provide information about the metal particle size.

We refer to Van Zon [9] en Van 't Blik [10] for a detailed description of the EXAFS measurement technique, the theory and the data analysis.

e. Temperature Programmed Desorption of Hydrogen

Temperature programmed desorption (TPD) of hydrogen was performed in the same apparatus as was used for the TPR and TPO experiments. These measurements were used to study the amounts of relatively strongly and relatively weakly adsorbed hydrogen. Argon was used as a carrier gas and the heating rate during a TPD experiment was 15 K min^{-1} .

f. Infrared Spectroscopy of Adsorbed CO

Chemisorption of carbon monoxide at 298 K was studied by infrared spectroscopy, in order to determine the binding sites for CO and to measure the CO adsorption capacity of the exposed metal atoms. For this purpose, a new *in situ* cell was designed, presented in Figure 2.1. Special attention was paid to the evacuability of the cell.

The infrared spectra were recorded using a Bruker IFS 113V Fourier transform infrared spectrometer equipped with a HgCdTe detector. Data were collected using an Aspect 2000 computer.

2.3 CO HYDROGENATION

CO hydrogenation was carried out in a continuous flow apparatus schematically depicted in Figure 2.2. The apparatus was designed to operate under pressures up to 10 MPa and temperatures up to 773 K. The entire apparatus is built of stainless steel (316) tubing. The different sections of the apparatus are described below.

a. H₂ and CO feed lines. CO and H₂ applied from 10 and 40 l pressure bottles (20 MPa maximum pressure) were dried over 4A molecular sieves. An extra feed line was present for addition of He or a mixture of ethylene and He. Each line was equipped with a Veriflo pressure regulator and a circle seal solenoid safety shut-off valve. Gass flows were regulated using thermal mass flow controllers from Brooks. During the CO hydrogenation experiments described in chapter 5, flows were regulated and measured using stainless steel fine metering valves and electronic bubble counters. The

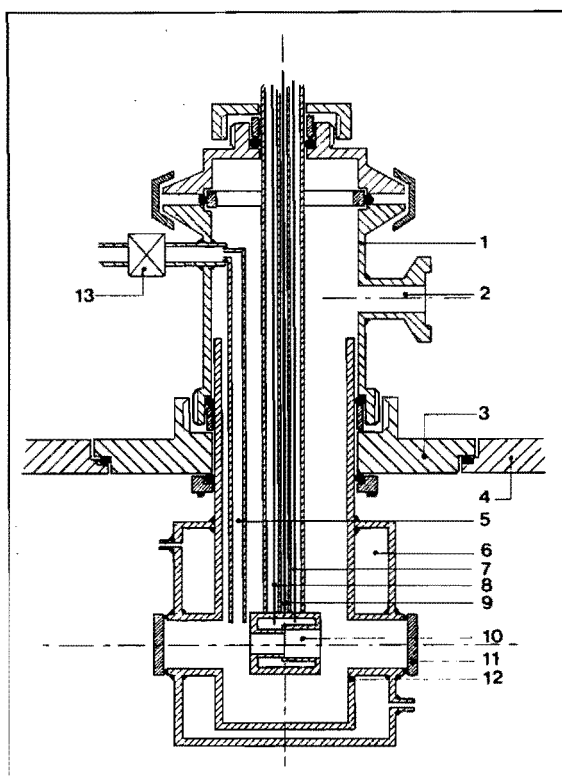


Figure 2.1: *In situ* infrared cell, upper part made of copper, lower part made of pyrex glass. 1. copper cell head, 2. connection ($\text{\O} = 1 \text{ cm}$) to high vacuum (oil diffusion pump) via a liquid nitrogen trap and to gas outlet, 3. support of the cell, 4. upper side of Bruker spectrometer, the pressure in the Bruker apparatus is 2 Torr, 5. gas inlet tube, 6. cooling mantle, 7. and 8. connecting wires for heating facility, 9. chromel-alumel thermocouple, separate tubing for heating wires and thermocouple, 10. sample holder for self-supporting wafer, the heating wires are not in contact with the gas atmosphere in the cell, 11. ZnSe window, 12. lower part of the cell, 13. shut-off valve.

pressure of the apparatus can be adjusted using the back pressure regulator at the end of the reactor system.

b. Reactor section. The apparatus contained two reactors that could be used simultaneously. The micro-flow reactors (Figure 2.3), made of stainless steel 321 (i.d. = 12 mm, o.d. = 29 mm) are surrounded by an electric

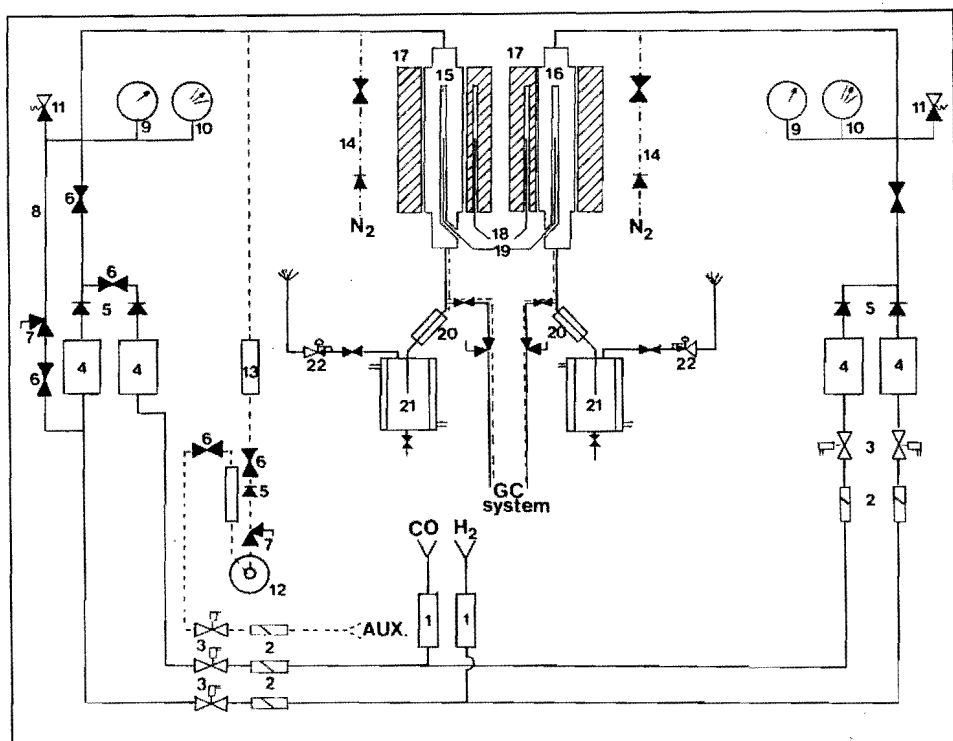


Figure 2.2: Flow scheme of microflow high pressure reactor system.

1. drying column, filled with molecular sieves 4A, 2. filter, 3. circle seal solenoid safety shut-off valve, 4. thermal mass flow controllers, Brooks, 5. check valve, 6. shut-off valve, 7. fine metering valve, 8. bypass H_2 feed line used for pressurizing the reactor, 9. precision manometer, 10. contact manometer, 11. spring loaded safety valve, 12. electronic bubble counter, 13. oil/gas separator, 14. low pressure N_2 purge line, 15. reactor I, 16. reactor II, 17. furnace, 18. regulating thermocouple, 19. measuring thermocouple, 20. water cooled mantle, 21. water cooled gas-liquid separator, 22. back pressure regulator, 23. heated tubes (423 K) to GC system (see Figure 2.4).

furnace, connected to a temperature programmer/controller. A chromel-alumel thermocouple, positioned in the pyrometer tube, was always placed in the middle of the catalyst bed. The reactor is lined with copper to prevent metal carbonyl formation.

c. Product section. Part of the product stream was fed to a gaschromatographic analysis system via a heated product line and a pressure reducer,

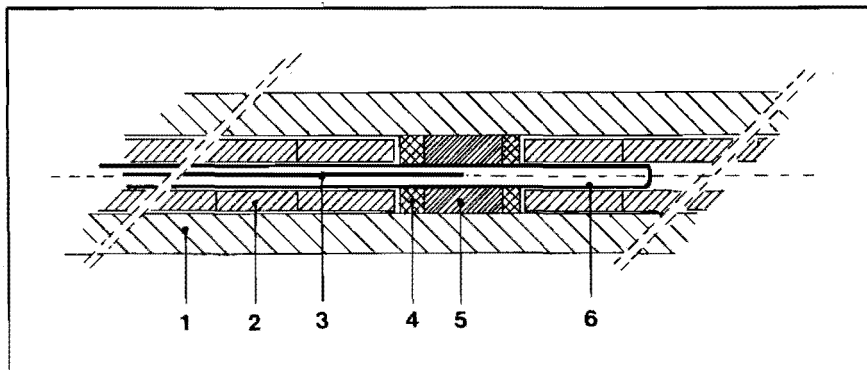


Figure 2.3: High pressure reactor, made of stainless steel 321.

1. reactor wall, 2. padding rings, 3. chromel-alumel thermocouple, 4. quartz wool, 5. catalyst bed, 6. pyrometer tube.

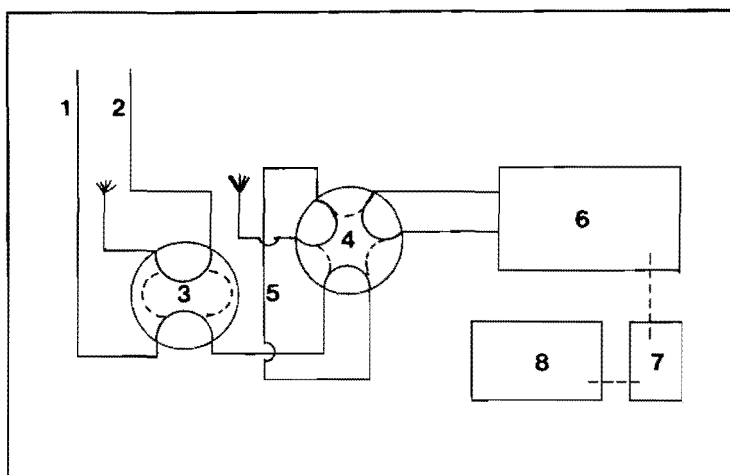


Figure 2.4: Sampling and gas chromatograph system, all tubes and valve are heated (423 K). 1. effluent of reactor I, 2. effluent of reactor II, 3. 4-way Valco valve to choose whether the effluent of reactor I or II has to be analyzed, 4. 6-way Valco sampling valve, 5. sample loop, 6. HP5890A gas chromatograph, 7. Nelson Analytical intelligent interface, 8. IBM-PC computer configuration with hard disc.

and could be analyzed on-line (see Figure 2.4). The remaining part of the product stream is vented via a condenser and the back pressure regulator. Two reactors are run simultaneously, using only one analysis system.

Therefore a Valco 4-port valve is used to switch between the two product streams. From the chosen product stream samples can be taken with a Valco 6-port valve (400 μl sampling volume).

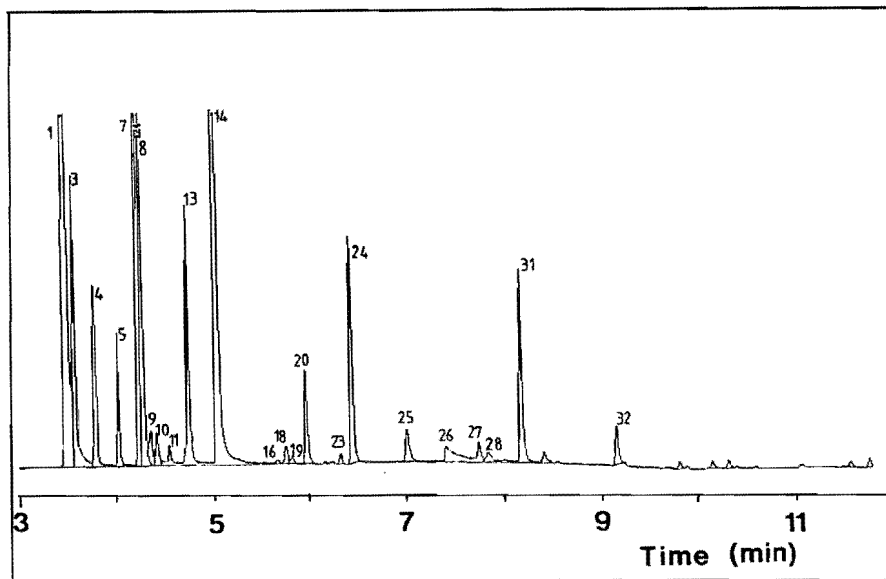


Figure 2.5: Example of chromatogram of reactor effluent, see Table 2.1 for identification of the peaks.

Since CO hydrogenation over group VIII metal catalysts may produce hydrocarbons (saturated, unsaturated and branched products), alcohols, aldehydes, ethers, acids, esters, water as well as carbon dioxide, it is obvious that a sophisticated analysis system is required. In cooperation with Hewlett Packard, we chose for a one column system: a crosslinked 5% phenyl methyl silicone capillary column (HP-5) with a film thickness of 1.0 μm , an internal diameter of 0.31 mm and a length of 50 m. This column was built in a capillary gaschromatograph (HP 5890A). A split ratio of 1:36 was used. Products were detected with a flame ionisation detector. The following temperature program enabled us to separate the products: initial temperature 303 K for 3.5 min, increasing the temperature at 20 K min^{-1} up to 423 K, holding this temperature for 0.5 min and subsequently increasing the temperature at 15 K min^{-1} up to 503 K. After reaching this temperature the oven was cooled again to 303 K. In this way, the amount of hydrocarbons up to C_8 , alcohols up to C_7 , aldehydes up to C_5 , ethers, esters and acetic acid could be measured in 16 min. Each 25 min a

sample could be analyzed. However, propylene and propane could not be separated using this method. If a starting temperature of 268 K was used, obtained by expanding CO₂, propylene and propane could also be analyzed separately. A representative chromatogram is shown in Figure 2.5 (starting temperature 303 K). Peaks were identified by injection of known compounds (see Table 2.1).

Table 2.1: Identification of products formed during CO hydrogenation, numbers correspond to numbers in Figure 2.5.

Nr.	compound	retention time (min)	Nr.	compound	retention time (min)
1	methane	3.51	19	pentane	5.89
2	ethene	3.57	20	diethylether	6.03
3	ethane	3.60	21	c-2-pentene	6.08
4	propene/propane	3.82	22	t-2-pentene	6.24
5	dimethylether	4.06	23	i-pentene	6.33
6	i-butane	4.17	24	methylacetate	6.52
7	methanol	4.27	25	propanol	7.06
8	acetaldehyde	4.32	26	acetic acid	7.54
9	n-butene	4.40	27	i-hexane	7.63
10	n-butane	4.47	28	n-1-hexene	7.81
11	i-butene	4.58	29	butyraldehyde	7.86
12	methylformate	4.76	30	n-hexane	7.99
13	methylethylether	4.78	31	ethylacetate	8.33
14	ethanol	5.09	32	butanol	9.29
15	i-pentane	5.52	33	i-heptane	9.91
16	1-pentene	5.73	34	n-heptane	10.08
17	i-propanol	5.80	35	n-1-heptene	10.17
18	propionaldehyde	5.83	36	ethylpropionate	10.23

d. Data collection and evaluation. Data were collected using a Nelson Analytical-IBM PC configuration and stored on a hard disc. Integrated peak areas were converted into volume percentages using experimentally determined response factors (methane, ethylene, methanol and ethanol) and response factors reported by Dietz [9]. From the peak areas the conversion α is calculated by

$$\alpha = \sum_N \frac{N[C_N]}{[CO]} \times 100\% \quad (2.1)$$

N = number of carbon atoms in product C_N

$[C_N]$ = molar concentration of a product with N carbon atoms

$[CO]$ = molar concentration of CO in feed.

From the conversion and flow data, the activity of the catalyst, expressed as mol CO converted into products (except CO_2) per mol of active metal per second, is calculated.

The selectivity for a certain product is calculated on the basis of carbon efficiency using:

$$S_P = P \frac{[C_P]}{\sum_N [C_N]} \times 100\% \quad (2.2)$$

C_P, C_N = molar concentration of a product with P or N carbon numbers, respectively,

P, N = number of carbon atoms in C_P and C_N , respectively.

2.4 REFERENCES

1. N.W. Hurst, S.J. Gentry and A. Jones, *Catal. Rev., Sci. Eng.*, 24 (1982) 233.
2. J.C. Vis, H.F.J. van 't Blik, T. Huizinga, J. van Grondelle and R. Prins, *J. Catal.*, 95 (1985) 333.
3. H.F.J. van 't Blik and R. Prins, *J. Catal.*, 97, (1986) 188.
4. J.H.A. Martens, H.F.J. van 't Blik and R. Prins, *J. Catal.*, 97 (1986) 200.
5. T. Huizinga, J. van Grondelle and R. Prins, *Appl. Catal.*, 10 (1984) 199.
6. H. Boer, W.J. Boersma and N. Wagstaff, *Rev. Sci. Instr.*, 52 (1982) 439. (1984).
7. B.J. Kip, J. van Grondelle, J.H.A. Martens and R. Prins, *Appl. Catal.*, 26 (1986) 353, chapter 3 of this thesis.
8. B.J. Kip, F.B.M. Duivenvoorden, D.C. Koningsberger and R. Prins, *J. Catal.*, to be published, chapter 4 of this thesis.
9. J.B.A.D. van Zon, Thesis, Eindhoven University of Technology (1984).
10. H.F.J. van 't Blik, Thesis, Eindhoven University of Technology (1984).
11. W.A. Dietz, *J. of Gas Chrom.* 2 (1967) 68.

Chapter 3

PREPARATION AND CHARACTERIZATION OF VERY HIGHLY DISPERSED IRIDIUM ON Al_2O_3 AND SiO_2

To obtain highly dispersed alumina- and silica-supported iridium catalysts, two preparation methods, the incipient wetness method and the urea technique, were investigated. Hydrogen and carbon monoxide chemisorption clearly showed that on $\gamma\text{-Al}_2\text{O}_3$ the incipient wetness method resulted in catalysts with a very high iridium dispersion ($\text{H}/\text{Ir} > 2.0$ for loadings < 2.5 wt% Ir and $\text{H}/\text{Ir} > 1.0$ up to 6.8 wt% Ir), in contrast with the catalysts made by this technique on SiO_2 ($\text{H}/\text{Ir} < 1.0$ for Ir loadings between 0.4 and 7.0 wt% Ir). Temperature programmed reduction, desorption and oxidation studies supported this conclusion. The behaviour of these systems in oxygen at elevated temperature also demonstrates a stronger interaction between iridium and alumina. The difference between the alumina- and silica-supported systems is caused by differences in adsorption processes during the impregnation. Using the urea technique, highly dispersed Ir/ SiO_2 and Ir/ Al_2O_3 catalysts were obtained ($\text{H}/\text{Ir} = 1.6$ for 1.5 wt% Ir/ SiO_2 and $\text{H}/\text{Ir} = 1.2$ for 5.5 wt% Ir/ SiO_2 , $\text{H}/\text{Ir} = 2.5$ for 1.5 wt% Ir/ Al_2O_3 and $\text{H}/\text{Ir} = 1.6$ for 5.7 wt% Ir/ Al_2O_3). Thus, the incipient wetness method proved successful for Al_2O_3 , whereas the urea technique resulted in highly dispersed iridium catalysts on both supports.

3.1 INTRODUCTION

As a result of many industrial applications, e.g. the purification of automobile exhaust gas, the reforming of petroleum naphthas and the hydroformylation of olefins, group VIII metals are studied extensively. Also in the hydrogenation of carbon monoxide to hydrocarbons and oxygenated products, group VIII metals are very important. Rhodium was found to be considerably selective for the production of oxygenated products [1-5]. Since in the periodic table iridium is placed below rhodium and to the left of platinum (which produces mainly methanol [6]), the catalytic behaviour of

iridium is of interest. Recently, we reported that the major products of the reaction of synthesis gas over alumina- and silica-supported iridium catalysts were methane, methanol and dimethylether [7].

Preparation and characterization of supported iridium catalysts starting from the $\text{Ir}_4(\text{CO})_{12}$ complex were reported by Anderson *et al.* [8-11], Tanaka *et al.* [12] and Ichikawa *et al.* [13]. The dispersion of these systems was comparable to that of systems prepared by ordinary impregnation of the support with a solution of IrCl_3 . McVicker *et al.* [14] reported the chemisorption properties of alumina-supported iridium catalysts prepared by incipient wetting $\gamma\text{-Al}_2\text{O}_3$ with an aqueous solution of chloro-iridic acid. They found that for 0.3 to 1.0 wt% $\text{Ir}/\text{Al}_2\text{O}_3$ catalysts H/Ir and CO/Ir ratios were close to two and that the particles could not be detected by high-resolution TEM, indicating that the particles were smaller than 6 Å. Their conclusion was that isolated iridium atoms can adsorb up to two hydrogen atoms, while iridium clusters ($d > 6 \text{ \AA}$) adsorb a single hydrogen atom per exposed metal atom. Krishnamurthy *et al.* [15], using temperature programmed desorption to characterize $\text{Ir}/\text{Al}_2\text{O}_3$ systems, also found that up to two atoms of hydrogen were chemisorbed per iridium atom. These results indicate that highly dispersed alumina-supported iridium catalysts can be prepared by the incipient wetness method. McVicker and Krishnamurthy both only used the relatively strongly bonded hydrogen (irreversibly adsorbed hydrogen) to calculate the H/Ir ratios. When the total amount of adsorbed hydrogen is taken into account, they both measured H/Ir values exceeding two (H/Ir = 2.5 for 0.5 wt% $\text{Ir}/\text{Al}_2\text{O}_3$).

Studies in our laboratory have shown that in the case of rhodium the incipient wetness method resulted in well dispersed alumina-supported systems [16] but less well dispersed silica-supported systems [17]. Geus *et al.* [18-20] showed that using the urea technique highly dispersed silica-supported nickel and copper catalysts could be prepared. In this method the pH of a suspension of SiO_2 and metal ions in water is increased slowly by means of the decomposition of urea. This leads to the formation of a homogeneously and well dispersed layer of Ni or Cu on the surface of the support. Until now, this method has not been used for the preparation of supported iridium catalysts.

Vis *et al.* [16,21] showed that chemisorption measurements and temperature programmed reduction (TPR) and oxidation (TPO) are very powerful techniques in characterization of supported noble metal catalysts. Using TPR and TPO, the state of an impregnated, reduced or oxidized catalyst could be studied successfully. Clearly, TPR/TPO as a characterization

technique has proven useful in a variety of fields in catalysis, e.g. Rh/Al₂O₃, Rh/TiO₂ and bimetallic catalysts like Co-Rh/TiO₂ [22] and Pt-Ir/Al₂O₃ [23-26]. In this paper, Al₂O₃- and SiO₂-supported iridium catalysts prepared via the incipient wetness method and the urea technique are discussed and it will be shown that these methods lead to very highly dispersed systems. Hydrogen and carbon monoxide chemisorption and temperature programmed reduction and oxidation are used to characterize the various catalysts.

3.2 EXPERIMENTAL

3.2.1 Preparation of the catalysts

Ir/Al₂O₃ and Ir/SiO₂ catalysts were prepared via the incipient wetness method and via the urea technique [18-20]. γ -Al₂O₃ was supplied by Ketjen (000-1.5E, surface area 200 m² g⁻¹, pore volume 0.6 ml g⁻¹, granulates with particle size 0.25-0.40 mm), SiO₂ by Grace (S.D. 2-324.382, surface area 290 m² g⁻¹, pore volume 1.2 ml g⁻¹, granulates with particle size 0.10-0.20 mm) and IrCl₃.xH₂O by Drijfhout (50.9 wt% Ir). The supports were used without thermal treatment. After incipient wetting the support with an aqueous solution of IrCl₃, the resulting catalysts were dried in air at 395 K for 16 h (heating rate 2 K min⁻¹). To prepare catalysts by the urea technique, a solution of IrCl₃.xH₂O in water was added to a vigorously stirred and heated (365 K) aqueous suspension of the support and urea (Merck, p.a., ten-fold excess of urea based on iridium) adjusted to pH=2.5 by addition of HCl. The reaction was allowed to proceed for 10 h, after which time the suspension was filtered, the residue washed with distilled water and dried at 395 K for 16 h (heating rate 2 K min⁻¹). Part of the dried catalyst was prerduced in flowing hydrogen at 773 K for 1 h (heating rate 5 K min⁻¹). Prior to removing the catalysts from the reduction reactor, they were passivated at room temperature by replacing the hydrogen-flow by nitrogen and subsequently slowly adding oxygen up to 20%. The dried, reduced and passivated catalysts were stored in a dessicator for further use. XPS studies have shown that in the case of 1.5 wt% Rh/Al₂O₃ a considerable amount of chlorine remained on the support after reduction (Cl/Rh_{surface} = 1.7), while in the case of 1.5 wt% Rh/SiO₂ almost no chlorine was present in the reduced samples (Cl/Rh_{surface} = 0.1) [7].

3.2.2 Characterization techniques

Chemisorption measurements. Volumetric hydrogen and carbon monoxide chemisorption measurements were performed in a conventional glass system at 298 K. The catalyst sample (typically 0.5 g) was placed in a quartz reactor attached to the chemisorption apparatus using greased quick fit glass joints. Hydrogen was purified by passing through a palladium diffusion cell, carbon monoxide (researchgrade) was used without further purification. Before measuring the H₂ and CO chemisorption the catalysts were reduced at 773 K (heating rate 8 K min⁻¹) for 1 h and evacuated at 773 K for 0.5 h resulting in an ultimate vacuum of 10⁻² Pa at the catalyst sample. After hydrogen admission at 473 K or carbon monoxide admission at 293 K desorption isotherms were measured at room temperature. The total amount of chemisorbed H atoms or CO molecules was obtained by extrapolating the linear high pressure part (20 kPa < P < 80 kPa) of the isotherm to zero pressure and by correcting for the extrapolated value of the bare support [27,28].

Hydrogen is admitted at 473 K because hydrogen adsorption at room temperature is a slow process. The H/Ir values obtained by admission at 473 K are somewhat higher than the H/Ir values obtained by admission at room temperature and waiting for 3 h, as was measured for 0.81 wt% Ir/Al₂O₃ (H/Ir(473 K)= 2.68, H/Ir(298 K)=2.49).

In literature, often a distinction is made between reversibly and irreversibly adsorbed hydrogen [14,15]. We think that this is not correct because the amount of reversibly adsorbed hydrogen is dependent on the apparatus and pump used. The question of reversibly and irreversibly adsorbed hydrogen is extensively discussed by Crucq *et al.* [27]. However, to get an idea of the amount of relatively weakly bonded hydrogen in our case, we have measured it for the 0.81 wt% Ir/Al₂O₃ catalyst. After 20 minutes of pumping, 23 % of the originally adsorbed hydrogen could be readsorbed (H/Ir_{irrev}= 2.07, H/Ir_{rev}=0.61).

Temperature programmed reduction, desorption and oxidation. TPR, TPD and TPO experiments were carried out in 4% H₂ in Ar, 100% Ar and 4% O₂ in He, respectively, with 200-400 mg catalyst in an apparatus as described by Boer *et al.* [29]. H₂, Ar and He were purified over molecular sieves (Union Carbide, 5A) for the removal of water and over a BTS column for the removal of traces of oxygen, O₂ was purified over molecular sieves. A Thermal Conductivity Detector (TCD) of the diffusion type, is used to detect the difference of hydrogen or oxygen concentration of the mixture

entering and leaving the reactor. The TCD signal monitored as a function of temperature, yields the TPR, TPD or TPO profile. The heating rate during all temperature programmed measurements was 10 K min^{-1} and the gas flow rate 5 ml min^{-1} . The temperature ramp started at 223 K and ended at 873 K. Since water is formed during reduction of the supported oxides, the reactor effluent is dried by molecular sieves before entering the thermal conductivity cell. We have already described the sequence of experiments used during temperature programmed reaction elsewhere [16,21,30]. In a standard experiment a TPR is done on a dried catalyst, followed by a TPD (of the now reduced catalyst covered with hydrogen), followed by a TPO (of the reduced catalyst without adsorbed hydrogen), followed by a TPR (of the now oxidized catalyst). The amount of gas consumed (TPR, TPO) or produced (TPD) is expressed per total amount of metal (H_2/Ir , O_2/Ir and H/Ir respectively).

Ultraviolet/Visible Spectroscopy. In order to get more insight in the adsorption processes during impregnation UV/VIS-spectroscopy was used. Spectra were recorded by means of a Hitachi 150-20 Spectrophotometer equipped with an integrating sphere reflection unit. The samples were ground and supported on a pellet by means of double sided adhesive tape. The scan speed was 200 nm min^{-1} .

3.3 RESULTS

3.3.1 Incipient wetness method catalysts

Hydrogen and carbon monoxide chemisorption. The hydrogen and carbon monoxide chemisorption results for the $\text{Ir}/\gamma\text{-Al}_2\text{O}_3$ and Ir/SiO_2 catalysts prepared by the incipient wetness method are represented graphically in Figure 3.1. For all $\text{Ir}/\text{Al}_2\text{O}_3$ catalysts, H/Ir is above 1.0, for the catalysts with metal loadings less than 2.5 wt%, H/Ir is even above 2.0. The H/Ir values for Ir/SiO_2 are below 1.0 for all metal loadings, indicating a lower dispersion for these systems. The CO chemisorption measurements support this conclusion, CO/Ir for alumina-supported iridium catalysts is higher than CO/Ir for silica-supported systems. CO/Ir values were corrected for adsorption on alumina ($20 \mu\text{mol CO g}^{-1}$), SiO_2 did not adsorb CO.

Temperature programmed desorption. In figure 3.2, the TPD profiles of some of the hydrogen covered catalysts are presented. These TPD profiles were measured subsequent to the first TPR measurements so hydrogen admission took place at 873 K. Note that for TPD the heating rate of 10 K

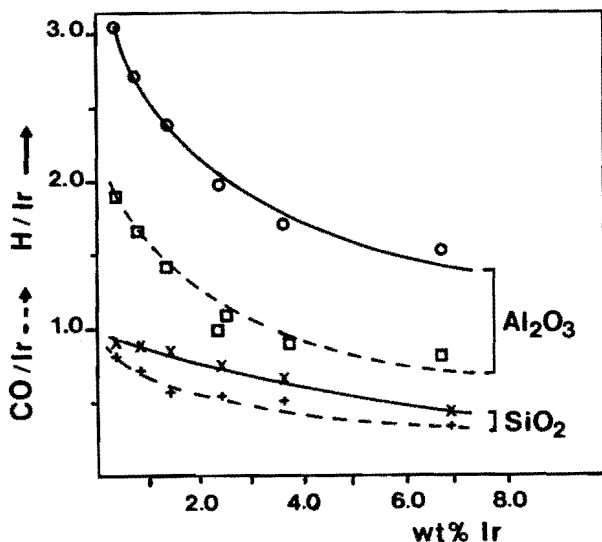


FIGURE 3.1: Hydrogen and carbon monoxide chemisorption of catalysts prepared by the incipient wetness method:

o : H/Ir for Ir/Al₂O₃ x : H/Ir for Ir/SiO₂
 □ : CO/Ir for Ir/Al₂O₃ + : CO/Ir for Ir/SiO₂

min⁻¹ is low so that readsorption of hydrogen will take place and no kinetic parameters for hydrogen desorption can be determined. Nevertheless, the results can be used to obtain information about dispersion and differences in strength of hydrogen adsorption. The TPD profile of 0.4 wt% Ir/SiO₂ is characterized by one broad peak around 473 K. Ir/SiO₂ catalysts with higher loadings show a second maximum in hydrogen desorption at lower temperatures (273-323 K) indicating weaker bonded hydrogen. The TPD profile of 0.4 wt% Ir/Al₂O₃ has a peak at 523 K, at somewhat higher temperature than the TPD peak of 0.4 wt% Ir/SiO₂ and a small peak around 823 K. For the higher loaded Ir/Al₂O₃ systems a third desorption area around 323 K is measured.

Although the hydrogen pressure range for the TPD measurements (0-5 kPa) differed from the hydrogen chemisorption measurements (20-80 kPa) and the temperature at which hydrogen was adsorbed is different, the H/Ir values obtained from the TPD experiments are in good agreement with the H/Ir values obtained from hydrogen chemisorption measurements for Ir/Al₂O₃ and Ir/SiO₂ systems (correlation coefficient R = 0.996, slope = 0.993, intercept = 0.023).

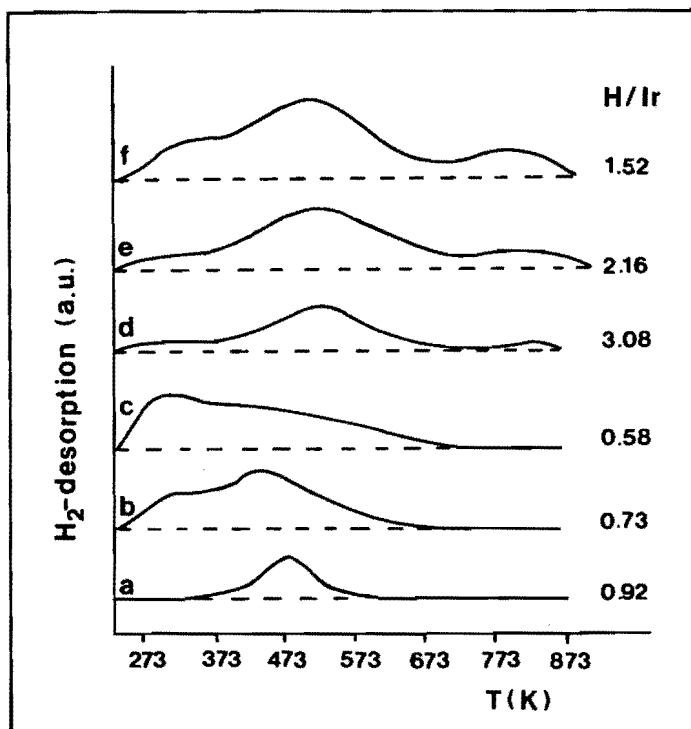


FIGURE 3.2: Temperature programmed desorption profiles of Ir/Al₂O₃ and Ir/SiO₂ catalysts prepared via the incipient wetness method: a. 0.4 wt% Ir/SiO₂, b. 2.3 wt% Ir/SiO₂, c. 7.0 wt% Ir/SiO₂, d. 0.4 wt% Ir/Al₂O₃, e. 2.6 wt% Ir/Al₂O₃, f. 6.8 wt% Ir/Al₂O₃.

Temperature programmed reduction and oxidation. The temperature programmed reduction profiles of the impregnated and dried Ir/SiO₂ catalysts are all similar. The TPR of 2.3 wt% Ir/SiO₂ is shown in Figure 3.3a. All Ir/SiO₂ catalysts start to reduce at 323 K, show a maximum in hydrogen consumption at 473-483 K and have a weak tail up to 673 K. The hydrogen consumption around 1.5 H₂/Ir is in agreement with the theoretical value for the reduction of Ir³⁺ to metallic Ir. The dried and impregnated Ir/Al₂O₃ systems (Figure 3.3b,c) start to reduce at 323 K, have a maximum in hydrogen consumption at 413 K and a shoulder at 433 K. Between 493 and 593 K desorption of hydrogen, adsorbed during the reduction, occurs. The net hydrogen consumption during the whole TPR run amounted to 1.4-1.7 H₂/Ir, indicating that the degree of reduction of iridium after a TPR run is 100% (\pm 5%). The TPR profile of 6.8 wt% Ir/Al₂O₃ (Figure 3.3d) shows a main peak around 420 K and a second peak around 480 K. Although the

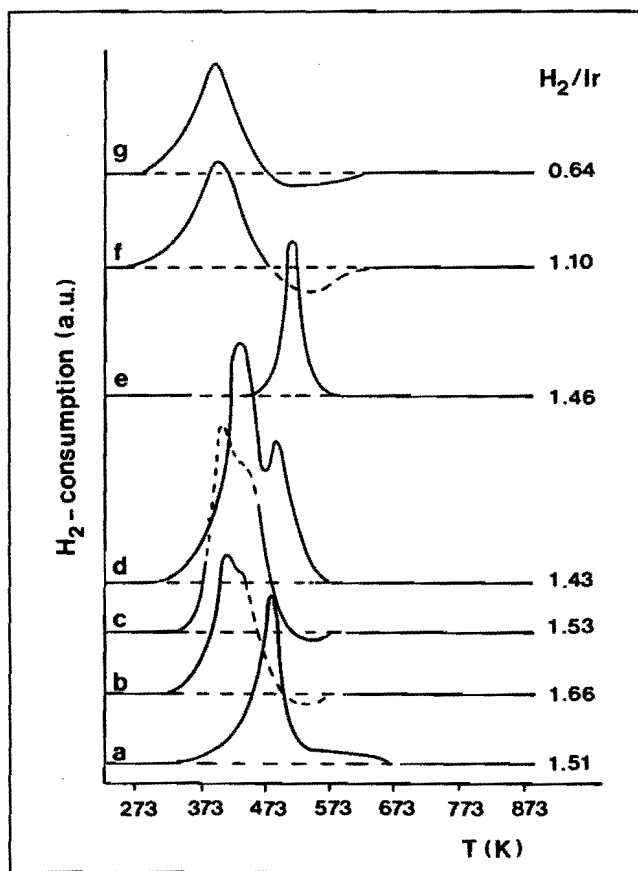


FIGURE 3.3: Temperature programmed reduction profiles of:

- impregnated and dried 2.3 wt% Ir/SiO₂ (a), 0.8 wt% Ir/Al₂O₃ (b), 2.6 wt% Ir/Al₂O₃ (c) and 6.8 wt% Ir/Al₂O₃ (d) catalysts,
- IrCl₃.xH₂O (e),
- reduced and passivated 3.8 wt% Ir/Al₂O₃ (f) and 3.7 wt% Ir/SiO₂ (g) catalysts.

experiments indicate that crystalline IrCl₃ is not present in Ir/Al₂O₃, nor in Ir/SiO₂ (crystalline IrCl₃ has a maximum hydrogen consumption at 503 K, Figure 3.3e), the reduction behaviour of Ir/SiO₂ resembles that of crystalline IrCl₃ most.

Figure 3.3f and g show the TPR profile of a passivated Ir/Al₂O₃ and Ir/SiO₂ catalyst. All passivated catalysts show a hydrogen consumption maximum around 373 K followed by a hydrogen desorption. The net

hydrogen consumption per iridium is dependent on the metal loading and the support. For Ir/Al₂O₃, H₂/Ir varied between 1.0 (high metal loading) and 1.3 (low loading), for Ir/SiO₂, H₂/Ir varied between 0.6 (high loading) and 1.1 (low loading). For highly dispersed Rh/Al₂O₃ Vis *et al.* [16] found that during passivation rhodium was almost completely oxidized. The present results show that for highly dispersed iridium systems this is not the case.

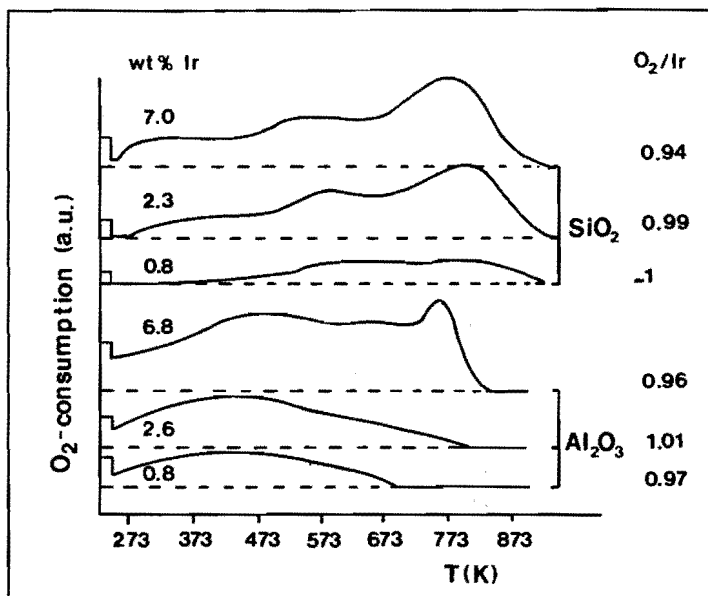


FIGURE 3.4: Temperature programmed oxidation profiles of reduced Ir/SiO₂ and Ir/Al₂O₃.

The TPO profiles of the Ir/Al₂O₃ and Ir/SiO₂ catalysts are shown in Figure 3.4. For all Ir/SiO₂ systems, oxygen consumption starts at 223 K. Furthermore, the oxygen consumption rises again at the beginning of the temperature ramp. Besides a broad oxygen consumption area around 325–373 K, two maxima around 573 and 773 K are visible. The third area around 773 K is becoming more important at higher metal loadings. For all catalysts the oxygen consumption per iridium is around 1.0, indicating the formation of IrO₂. The TPO's of the low loaded Ir/Al₂O₃ systems (< 3 wt%) showed some oxygen consumption at 223 K, a rise of O₂-consumption at the beginning of the temperature ramp and a maximum at 373–473 K. The TPO profiles of the reduced Ir/Al₂O₃ catalysts with higher loadings

also showed oxidation around 773 K. The total oxygen consumption for all catalysts amounted to 1.0, indicating the formation of IrO_2 .

The TPR profiles of the oxidized Ir/SiO_2 and $\text{Ir}/\text{Al}_2\text{O}_3$ systems were all the same, a very sharp reduction peak at about 493 K with a hydrogen consumption of $\text{H}_2/\text{Ir} = 1.9\text{--}2.1$ in agreement with the theoretical value of 2.0 for the reduction of IrO_2 . The reduction peak was rather sharp (width at half height is 30 K, while for the impregnated and dried systems this is 50–100 K) and no desorption was seen after the reduction peak (for $\text{Rh}/\text{Al}_2\text{O}_3$ and Rh/SiO_2 systems such desorption has been observed in the TPR of the oxidized systems [16]).

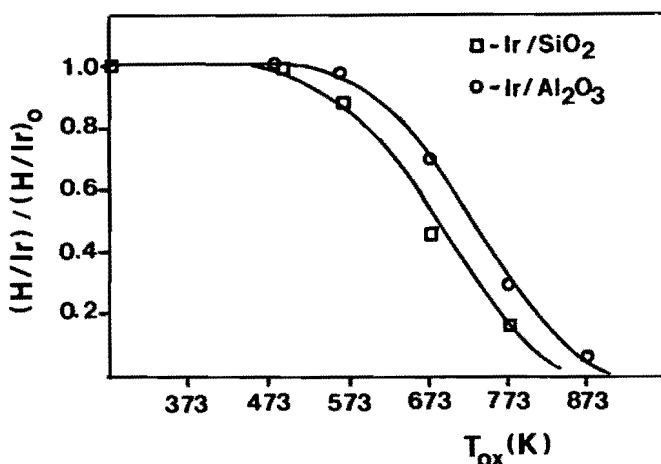


FIGURE 3.5: The influence of the oxidation temperature on the H/Ir for 2.3 wt% Ir/SiO_2 and 1.0 wt% $\text{Ir}/\text{Al}_2\text{O}_3$.

In literature several authors [23,35] reported that the dispersion of supported iridium systems is badly influenced by oxygen at elevated temperature. We have studied this effect for the $\text{Ir}/\text{Al}_2\text{O}_3$ and Ir/SiO_2 catalysts prepared by the incipient wetness method. In Figure 3.5, the relative dispersion for a 2.3 wt% Ir/SiO_2 ($\text{H}/\text{Ir} = 0.75$) and a 1.0 wt% $\text{Ir}/\text{Al}_2\text{O}_3$ ($\text{H}/\text{Ir} = 1.9$) catalyst is shown as a function of the oxidation temperature (oxidized in 5% O_2 in N_2 , starting temperature 298 K, heating rate 5 K min^{-1} , final temperature T_{ox} maintained for 1 h). The dispersion of the Ir/SiO_2 system starts to decrease after an oxidation for 1 h at 473 K and is very small ($\text{H}/\text{Ir} < 0.1$) after oxidation above 773 K. $\text{Ir}/\text{Al}_2\text{O}_3$ behaves similar although the decrease in dispersion is at a somewhat higher oxidation temperature (573 K), indicating a higher interaction between iridium oxide and the support in the latter case. TPR profiles of 1.0 wt% $\text{Ir}/\text{Al}_2\text{O}_3$ oxidized at

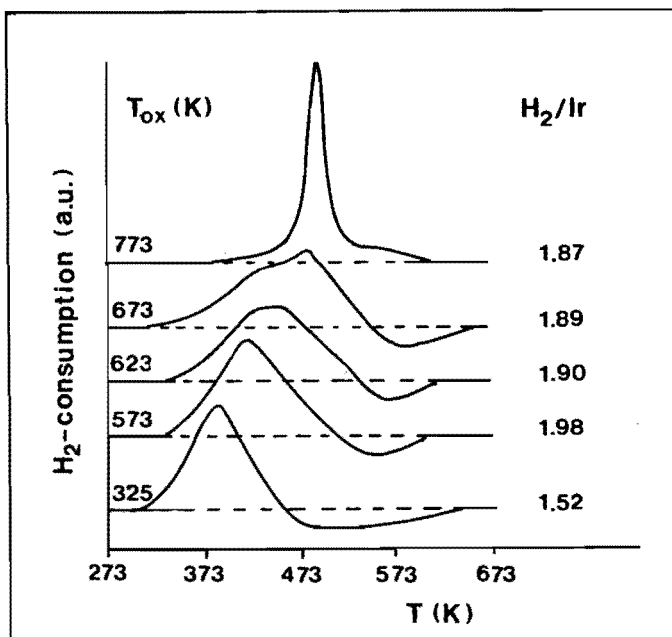


FIGURE 3.6: TPR profiles of 1.0 wt% Ir/Al₂O₃ oxidized at different temperatures after reduction.

different temperatures (the reduced and passivated system was oxidized in 4 % O₂ in He, $T_{start} = 298$ K, heating rate 5 K min⁻¹, 1 h at T_{ox}) are shown in Figure 3.6. After oxidation at higher temperature a reduction peak at 493 K becomes visible. Oxidation at 773 K results in one sharp peak at 493 K and the disappearance of hydrogen desorption.

UV/VIS-spectroscopy. In order to obtain more information about the adsorption processes during the incipient wetness method, UV/VIS spectroscopy was used. In Figure 3.7, the spectra for 3.8 wt% Ir/Al₂O₃, 3.7 wt% Ir/SiO₂ and physically mixed IrCl₃ and SiO₂ are presented. The adsorption spectrum of 3.7 wt% Ir/SiO₂ (Figure 7b) resembles that of physically mixed IrCl₃-SiO₂, an absorption peak at 300 nm and a shoulder at 390–400 nm. The spectrum of 3.8 wt% Ir/Al₂O₃ is quite different, it shows an absorption peak at 570 nm and one at 300 nm.

3.3.2 Catalysts prepared by the urea technique

Hydrogen chemisorption. The hydrogen chemisorption data for the Ir/Al₂O₃ and Ir/SiO₂ catalysts prepared by the urea technique are presented

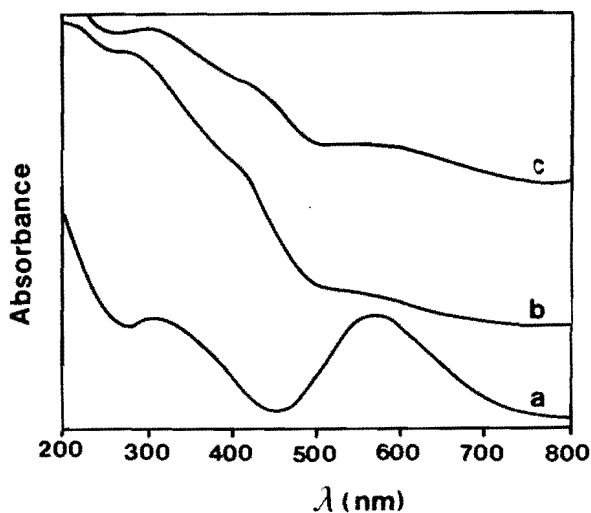


FIGURE 3.7: UV/VIS spectra of 3.8 wt% $\text{IrCl}_3/\text{Al}_2\text{O}_3$ (a), 3.7 wt% $\text{IrCl}_3/\text{SiO}_2$ (b) and $\text{IrCl}_3\text{-SiO}_2$, physically mixed (c).

in Table 3.1. The H/Ir values of the $\text{Ir}/\text{Al}_2\text{O}_3$ catalysts prepared by this method are comparable to those of $\text{Ir}/\text{Al}_2\text{O}_3$ systems prepared with the incipient wetness method, while the H/Ir values for the Ir/SiO_2 systems prepared by the urea method are by a factor 2-3 higher than those of the incipient wetness method, indicating that the urea technique produces highly dispersed iridium on both supports.

TABLE 3.1: Hydrogen chemisorption measurements of $\text{Ir}/\text{Al}_2\text{O}_3$ and Ir/SiO_2 catalysts prepared by the urea technique.

system	H/Ir	system	H/Ir
1.5 wt% $\text{Ir}/\text{Al}_2\text{O}_3$	2.45	1.5 wt% Ir/SiO_2	1.65
5.7 wt% $\text{Ir}/\text{Al}_2\text{O}_3$	1.62	5.3 wt% Ir/SiO_2	1.24

Temperature programmed reduction, desorption and oxidation. The TPR, TPD and TPO profiles of the catalysts prepared by the urea method are presented in Figure 3.8. The profiles of the alumina- and silica-supported systems are similar. The reduction of the dried samples starts at 373 K and proceeds up to 773 K. The H_2/Ir values are rather high (1.6-2.8), indicating that not only Ir^{3+} ($\text{H}_2/\text{Ir} = 1.5$) has been reduced. Elemental analysis, using

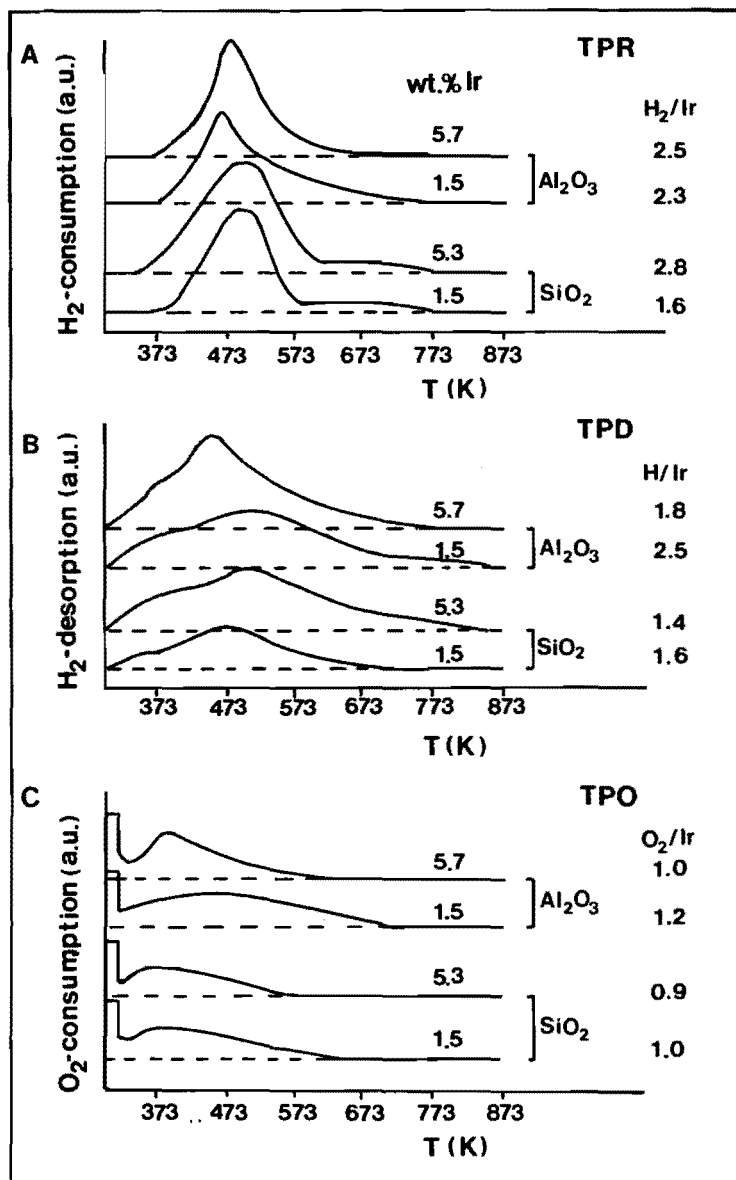


FIGURE 3.8: TPR, TPD and TPO profiles of Ir/Al₂O₃ and Ir/SiO₂ catalysts prepared by the urea technique:

TPR of dried catalysts (A), TPD of reduced and hydrogen covered catalysts (B), and TPO of reduced catalyst (C).

a Perkin Elmer Element Analyzer Model 240, shows that nitrogenous decomposition products of the urea are deposited on the catalyst (5.7 wt% Ir/Al₂O₃ : 0.14 wt% N, 5.3 wt% Ir/SiO₂ : 0.62 wt% N), no carbonaceous decomposition products were found. Hydrogenation of these nitrogenous deposits results in an increased hydrogen consumption. The hydrogen desorbed per iridium during the TPD is in agreement with the hydrogen chemisorption results (see Figure 3.8B). The TPD profiles of the Ir/SiO₂ and Ir/Al₂O₃ systems prepared by the urea technique resemble the TPD profiles of the Ir/Al₂O₃ systems prepared by the incipient wetness method, except for the desorption peak at high temperature which is only present in the TPD profiles of the Ir/Al₂O₃ systems. The TPO profiles of the reduced systems show a broad oxygen consumption area, already starting at 298 K. The high temperature oxygen consumption (around 773 K), measured for the Ir/SiO₂ systems and higher loaded Ir/Al₂O₃ systems prepared by the incipient wetness method, is absent.

3.4 DISCUSSION

Hydrogen chemisorption has been used through the years by many workers to characterize metal surfaces [1,14,15,23,31-36]. When attempts were made to calculate metal surface areas from hydrogen chemisorption data, a hydrogen to metal stoichiometry of one has been used. Recently several authors published H/M and also CO/M values exceeding unity. Wanke and Dougharty [31] reported the adsorption of more than one hydrogen atom per surface rhodium atom for Rh/Al₂O₃ catalysts, Vis *et al.* [16,21] reported H/Rh= 1.53 for 2.3 wt% Rh/Al₂O₃, Krishnamurthy *et al.* [15] showed that Ir/Al₂O₃ (0.2-1.0 wt%) chemisorbed up to two hydrogen atoms and carbon monoxide molecules per iridium atom using only the strongly bonded hydrogen. McVicker *et al.* [14] found the same upper limit of 2.0 adatoms per Ir. Taking into account the total amount of adsorbed hydrogen, McVicker and Krishnamurthy reported H/Ir values up to 2.5 for 0.5 wt% Ir/Al₂O₃. Crucq *et al.* [27] reported H/Pt = 1.32 for 5.7 wt% Pt/SiO₂. Recently Sato [36] described a Pt/TiO₂ system made by photoimpregnation of hexachloroplatinic acid with H/Pt = 2.5.

First of all, we want to exclude several trivial effects which could explain the high H/M values:

- unreduced Ir³⁺ was not present, as can be concluded from the TPR experiments. Within the experimental error (5 %), all Ir was reduced to Ir⁰.

- contamination of the catalyst with carbon did not occur. Elemental analysis (using Perkin Elmer Element Analyzer Model 240) showed that no carbon residues existed initially on the catalyst. Carbon residues could be produced by grease or oil vapours during evacuation. However, the TPD measurements are absolutely grease and oil vapour free, and resulted in similarly high H/Ir values.
- partial reoxidation during outgassing at high temperature, mentioned by Martin *et al.* for Fe [37] and Ni [38], can be excluded because oxygen consumption during oxidation at 773 K after reduction and evacuation at 773 K was measured to be 1.96 O/Ir for 1.5 wt% Ir/Al₂O₃ (H/Ir=2.4). IrO₂ is the most stable oxide of iridium, so this result shows that reoxidation can only account for an increase in hydrogen chemisorption of 0.08, proving that H/Ir values in excess of 1.0 are not caused by reoxidation of the metal during outgassing.

The high hydrogen chemisorption data are often explained by hydrogen spillover on the support. Although we cannot completely exclude this, we think that the H/Ir values (up to H/Ir = 3.0) presented here are real and that the chemisorbed hydrogen is all bound to the metal. Modeling calculations of the area around a small particle on a support confirm the idea that more than one hydrogen atom can be adsorbed per metal atom. A computer programme was made to determine the area available for chemisorption around a supported small metal particle. In the spirit of Wynblatt and Gjostein [39] the shape of the metal particle was calculated as a function of the relative magnitude of the metal-metal and metal-support interaction energy by minimizing the total energy. We assumed the support to consist of a flat (111) layer of oxygen anions, the size of which was taken equal to that of the metal atoms. The metal atoms were assumed to be fcc packed, and thus to fit epitaxially on the support surface. The shape of a metal particle with $n+1$ atoms was obtained from that of the particle with n atoms by putting the extra metal atom at the position of minimum energy. Such calculations were carried out over a whole range of α values, with α being the ratio of the metal atom-oxygen anion interaction $E(M-O^{2-})$ and the metal atom-metal atom interaction $E(M-M)$.

To obtain an estimate of the number of hydrogen atoms that can be placed around such a metal particle, we assumed that the hydrogen atoms will occupy the free fcc positions around the metal particle and that only one hydrogen atom per vacant fcc position is allowed. Although X-ray diffraction results for metal hydride complexes point to a hydrogen atom

radius which is much smaller than that of the Ir atoms [40], the same results also point out that H-H distances smaller than M-M distances are rarely observed. Our assumptions therefore seem very reasonable.

TABLE 3.2: Results of computer calculation on small metal particles.

Number of atoms in one particle	$\alpha = 0.5^a$					$\alpha = 2.0^a$				
	4	10	30	100	800	4	10	30	100	800
Empty positions ^b :										
1 metal neighbour	9	15	16	19	36	11	13	14	14	39
2 " "	9	8	21	35	81	6	10	21	41	85
3 " "	0	5	10	33	125	1	4	10	23	129
4 " "	0	2	4	15	113	0	1	6	21	92
5 " "	0	0	2	2	15	0	1	0	0	18
Dispersion	1.0	1.0	.80	.62	.36	1.0	1.0	.80	.60	.35
H/Ir ^c	4.5	3.0	1.8	1.0	.46	4.5	2.9	1.7	1.0	.45
H/Ir ^d	2.3	1.5	1.2	.85	.42	1.8	1.6	1.2	.85	.41
D (Å)	5.6	9.0	12	19	35	7.6	10	14	20	38

a) $\alpha = E(M-S)/ E(M-M)$.

b) empty f.c.c. positions around the metal particle that have at least one metal neighbour, which can be occupied by H atoms.

c) assuming that all f.c.c. positions around the particle with at least one metal neighbour, are filled by hydrogen.

d) assuming that only positions with more than one metal neighbour are filled by hydrogen.

Table 3.2 summarizes the results of the calculations for two situations, one in which the interaction between metal and oxygen is half that of the metal-metal interaction, $E(M-O^{2-}) = 0.5 E(M-M)$, which results in spherical particles, and one in which $E(M-O^{2-}) = 2 E(M-M)$, resulting in raft-like particles. Dispersions (defined as the fraction exposed metal atoms), diameters of the particles and H/M values are presented as a function of the number of atoms per particle. The H/M values were calculated on the basis of two assumptions. Very high H/M values (up to 4.5) were obtained if hydrogen was allowed to occupy all free fcc positions, even those where

hydrogen is bonded to only one metal atom. If only free positions, where the hydrogen atom is bonded to at least two metal atoms were considered, still a H/M value of 2.3 could be obtained.

On the basis of these calculations, one can conclude that geometrically very high H/M values can be obtained for fcc packed metals. For Ir, high H/M values are actually measured. For Rh and Pt, H/M values are not exceeding two. In a recent paper we studied metal particle sizes in Ir, Pt and Rh catalysts using hydrogen chemisorption and EXAFS [41]. The metal-metal coordination number N , which gives information about the metal particle size, versus H/M relationship could be described by a single straight line for each metal. Differences in adsorption stoichiometries between the metals were explained using electronical reasons. The order of H/M_{surface} stoichiometries for Pt, Rh and Ir was found to be analogous to the order of stability of the corresponding metal polyhydride complexes. This study also demonstrated that the high H/M stoichiometries cannot be a result of hydrogen spillover to the support.

The CO/Ir values also exceed unity. The measured values had to be corrected for adsorption on the support in the case of Al_2O_3 . Krishnamurthy *et al.* [15] also noted the adsorption of CO on Al_2O_3 , while McVicker [14] did not mention this effect.

As a consequence of the variability of the hydrogen-metal and carbon monoxide-metal stoichiometry, it is impossible to calculate particle sizes from chemisorption data for the highly dispersed systems. Nevertheless, the chemisorption data can be used to compare dispersions of different systems, taking into account the linear relationship between the metal-metal coordination number N and the measured H/Ir values [41].

The chemisorption measurements presented in this paper clearly show that using the incipient wetness method, well dispersed Ir/ SiO_2 catalysts and very highly dispersed Ir/ Al_2O_3 catalysts can be obtained. For both systems, a systematic decrease of the relative amount of adsorbed hydrogen (or carbon monoxide) with increasing iridium content is observed, reflecting a decrease in dispersion at higher metal loadings.

Temperature programmed desorption measurements support this conclusion. The amount of desorbed hydrogen per iridium atom agrees with the H/Ir values observed in the hydrogen chemisorption measurements. The TPD profiles (Figure 3.2) also show that in the case of high H/Ir values the hydrogen is adsorbed more strongly on the metal surface (desorbing at higher temperature). For the Ir/ Al_2O_3 systems, three species were detected during desorption, similar to the desorption spectra reported in literature

for supported Ir and Pt catalysts [42,43]. Candy *et al.* [39] detected two species desorbing at 223–323 K (β_1) and at 373–673 K (β_2) for supported Pt catalysts. The formation of β_2 is reported to be activated, with an activation energy of 5 ± 2 kcal mol⁻¹. From Figure 3.2, one can conclude that the higher loaded catalysts desorbed more hydrogen at low temperature, the β_1 type. For the alumina-supported systems a third desorption area around 823 K is observed. Candy *et al.* also reported this high temperature desorption peak (β_3), when hydrogen was admitted at high temperature (900 K) as also was done in our experiment (873 K). They interpreted this species as H atoms in bridged position between metal and support. However, Escard *et al.* [43] reported desorption of hydrogen around 800 K for a 36 % Ir/Al₂O₃ catalyst and for unsupported Ir. We therefore believe that the hydrogen desorbing at high temperatures is not linked to the support or support-iridium interface, but is really bonded to the metal.

Hydrogen on Ir/Al₂O₃ desorbs at a higher temperature than on Ir/SiO₂ and desorption of hydrogen adsorbed on samples with a high iridium loading occurs at a lower temperature, so hydrogen bond strength increases with decreasing particle size, as is expected if stronger bonding is associated with metal atoms of lower coordination number such as edge and corner sites [44]. In a recent study of the heat of adsorption on Pt catalysts, Vannice *et al.* [45] reported an opposite trend, a decrease in heat of adsorption with decreasing particle size. Thus, our hydrogen chemisorption and TPD experiments indicate very clearly that our Ir/Al₂O₃ catalysts are indeed highly dispersed.

The TPR profile of the dried IrCl₃/SiO₂ catalysts almost resembles the profile of pure IrCl₃.xH₂O, whereas the dried IrCl₃/Al₂O₃ catalysts reduce at much lower temperature. Hydrogen consumption during the TPR profile showed that within the uncertainty of the method complete reduction to metallic iridium occurred in both cases (H₂/Ir = 1.5).

The difference between the silica- and alumina-supported systems must be due to the adsorption properties of the supports. When an excess of IrCl₃ solution was added to alumina and silica in an adsorption experiment (2 h), a 3.8 wt% Ir/Al₂O₃ and a 0.01 wt% Ir/SiO₂ catalyst was obtained (when all metal salt would have been adsorbed, a 4.6 wt% Ir catalyst would have resulted in both cases). We also noticed that the pH of the IrCl₃ solution increased during the adsorption in the case of alumina. Thus, the pH of the starting IrCl₃ solution was 1.9, the pH of the solution after adsorption on alumina was 4.9, while the pH of the solution in the case of adsorption on silica remained 1.9. We think that alumina OH groups are protonated

during adsorption, forming adsorption sites for anionic iridium complexes in solution, probably $[\text{IrCl}_3(\text{H}_2\text{O})_2(\text{OH})]^-$. The UV/VIS-spectra supported this idea. The reflection spectrum of the impregnated $\text{IrCl}_3/\text{SiO}_2$ system resembled that of physically mixed IrCl_3 and SiO_2 , while the spectrum of the impregnated $\text{IrCl}_3/\text{Al}_2\text{O}_3$ system was completely different. The OH-groups of the silica can not be protonated in the pH-region used and therefore no adsorption sites are available for the negatively charged iridium complexes in the solution. Thus, during the incipient wetness method, the IrCl_3 adsorbs on alumina and a high dispersion is obtained. On the contrary, on SiO_2 no adsorption occurs (no sites are available) and during the drying process the IrCl_3 is deposited as crystallites on the surface of the support. Now we can understand the different TPR profiles of the impregnated and dried samples. The reduction profile of $\text{IrCl}_3/\text{SiO}_2$ resembles that of IrCl_3 because on silica crystallites of IrCl_3 are formed during the drying process. In case of alumina, with low metal loading, IrCl_3 is adsorbed as a complex on the surface and therefore its reduction behaviour is influenced by the support. Apparently single $[\text{IrCl}_3(\text{H}_2\text{O})_2\text{OH}]^-$ species are more easy to reduce than crystallites of $\text{IrCl}_3 \cdot x\text{H}_2\text{O}$. In the case of the 6.8 wt% $\text{Ir}/\text{Al}_2\text{O}_3$ catalyst, the iridium loading is above the loading that can maximally be obtained by adsorption (3.8 wt%), so only part of the IrCl_3 is adsorbed during the impregnation, the rest is deposited as larger particles during the drying of the catalyst, resulting in a bimodal particle size distribution. The first part reduces easily, like $\text{Ir}/\text{Al}_2\text{O}_3$ with a low metal loading, the latter part reduces at a higher temperature, like an Ir/SiO_2 catalyst. Summarizing the above mentioned results, the chemisorption and TPR measurements of the dried systems clearly show that the incipient wetness method provides very highly dispersed $\text{Ir}/\text{Al}_2\text{O}_3$ catalysts and reasonably dispersed Ir/SiO_2 catalysts.

The TPR profiles of the passivated catalysts (Figure 3.3f,g) show that during passivation no complete oxidation to IrO_2 has occurred ($0.6 < \text{H}_2/\text{Ir} < 1.3$). This is in contrast to the results published by Vis *et al.* [16,21] for the passivation of well dispersed $\text{Rh}/\text{Al}_2\text{O}_3$ systems. Two explanations for this effect can be given:

- during passivation the iridium particles are covered only by a layer of chemisorbed oxygen and real oxidation does not occur at all
- during passivation a protective oxide skin is formed, preventing further oxidation at room temperature.

The amount of hydrogen used per iridium during the reduction of the

passivated systems decreases with increasing metal loading and is higher for the Ir/Al₂O₃ systems than for the Ir/SiO₂ systems. Thus in the higher dispersed systems more oxygen molecules have adsorbed/reacted per iridium atom during passivation.

During TPO, oxygen consumption per iridium atom was close to 1.0, indicating the formation of the thermodynamically most stable IrO₂ phase. The TPO profiles of Ir/SiO₂ show three areas of oxygen consumption. The exact assignment of processes responsible for the oxygen consumption in these three areas is difficult since literature does not provide much information about the mechanisms of oxidation of supported metal catalysts. However, the theory of metal oxidation, dealing with bulk materials, does provide three phenomena as separated stages in oxidation processes, as we described before [16,21]. The first stage of oxidation is chemisorption, which is known to occur at clean surfaces [46] at low temperatures. Formation of an oxide film, the second stage, occurs at temperatures typically up to 573–673 K, following a logarithmic rate equation and leading to an oxide film [47–49]. Finally Wagner's oxidation theory [50] describes the third stage, the oxidation process of the bulk, rate controlled by volume diffusion of the reacting ions and/or electrons through the growing oxide scale, leading to parabolic rate equations. We suppose that analogous models can describe the oxidation processes in supported metal particles, dependent on their sizes. We think that the three processes mentioned, oxygen chemisorption, oxidation of the skin and thorough oxidation are related to the three observed oxygen consumption areas. The first two stages of oxygen consumption are visible for all catalysts. The third stage, the thorough oxidation, however, is absent for the low loaded Ir/Al₂O₃ samples, and increases for both Ir/Al₂O₃ and Ir/SiO₂ with metal loading. Since dispersions, as measured with H₂ and CO chemisorption, decrease with metal loading, there is clearly a relation between particle size and the high temperature oxygen consumption. For the very highly dispersed low loading Ir/Al₂O₃ catalysts thorough oxidation is absent, indicating that the particles are very small indeed. As the dispersion, related to the fraction of surface metal atoms, decreases, the particle size and the size of the metallic (bulk like) kernel will increase, accompanied with a higher oxygen consumption at high temperatures, as can be seen in Figure 3.4. The oxygen consumption during the first and second peak can also be used to determine the dispersion, since during these processes only the surface is oxidized. However, the third peak is badly separated from the first and second peak so no quantification can be made. Qualitatively, we observe a correlation between the H/Ir and CO/Ir values and the

amount of oxygen consumed during the first and second peak in the TPO. Note, that for 6.8 wt% Ir/Al₂O₃ (with H/Ir > 1), thorough oxidation is visible (high temperature oxidation peak), indicating that some of the metal particles have a (bulk like) kernel, as we also concluded from the TPR profile of the dried 6.8 wt% Ir/Al₂O₃ catalyst (Figure 3d). Thus, the TPO profiles support the conclusion of the chemisorption, TPD and TPR results that the Ir/Al₂O₃ catalysts are highly dispersed and the Ir/SiO₂ catalysts less well dispersed.

The TPR profiles of the oxidized samples show one very sharp reduction peak without any noticeable hydrogen desorption. This indicates the formation of large IrO₂ particles during the preceding TPO. Studies on the effect of the oxidation temperature on the dispersion of Ir/Al₂O₃ and Ir/SiO₂ confirm this. Oxidation at various temperatures followed by TPR clearly shows the formation of a distinct IrO₂ phase during oxidation, reducing in a very narrow temperature region (Figure 3.6). Several authors have described the loss of dispersion of supported iridium catalysts in oxygen atmosphere at elevated temperature. Wanke *et al.* [35] showed the loss of dispersion for Ir/Al₂O₃ systems, Foger *et al.* [23,51,52] for Pt-Ir/Al₂O₃, Pt-Ir/SiO₂ and Ir/TiO₂ systems. The latter authors concluded that if T_{ox} < 573 K, a surface oxide Ir₅O is formed, but that if T_{ox} > 573 K, IrO₂ grows out from metal particles as thin blades or sheets due to the fact that IrO₂ is volatile. The reduction of the iridium oxide is autocatalytic, once metal particles have been nucleated, atomic hydrogen is produced which nucleates further metal particles on the adjacent oxide. It is likely that the surfaces of the large IrO₂ particles are well defined. Thus, as all surfaces are very similar, reduction will start for all particles at about the same temperature. Since this first reduction is rate determining, this will result in a very sharp hydrogen consumption peak in TPR. We also see that the loss of dispersity due to the formation of large IrO₂ particles occurs at a lower temperature for Ir/SiO₂ (Figure 3.5), indicating an interaction between IrO₂ and alumina that prevents sintering of the iridium oxide at lower temperature.

From the results described above, we can conclude that IrCl₃, Ir and IrO₂ are very well dispersed on alumina, thus having an intimate contact with the support, while Ir, IrCl₃ and IrO₂ on SiO₂ are less well dispersed. Recent results of an EXAFS study of these catalysts [41,53] support these conclusions.

In order to get highly dispersed Ir/SiO₂ systems, the urea technique was used. H/Ir values exceeding unity and the absence of the high temperature oxidation area in the TPO's for the catalysts obtained by this method show

that the urea technique is very well suited to prepare highly dispersed Ir/SiO₂ and Ir/Al₂O₃ catalysts. Two explanations can be given for these results:

- during the decomposition of urea the pH is smoothly increasing, causing the formation of insoluble iridium hydroxide. The hydroxide will deposit on the support in the form of tiny crystallites.
- during the decomposition of urea iridium forms complexes with NH₃, the SiO₂ surface will slowly be deprotonated because of the increase of pH and adsorption of Ir complexes on the support will be possible.

Adsorption of the [Ir(NH₃)₅Cl]Cl₂ complex on silica at pH = 10 resulted in a catalyst with a loading of only 0.2 wt% Ir (when all the available complex would have been adsorbed, a 2.5 wt% Ir catalyst would have resulted). This disfavours the second explanation, so we think that the high dispersion in the case of the urea technique is a result of the formation of tiny crystallites of insoluble iridium hydroxide. The urea technique enables one to make very dispersive Ir/SiO₂ catalysts, much better than with the incipient wetness method.

3.5 CONCLUSIONS

With a limited number of techniques, chemisorption measurements and temperature programmed reduction, desorption and oxidation, we have obtained a good insight into the state a catalyst can be brought in by impregnation and reduction/oxidation. Hydrogen and carbon monoxide chemisorption and TPR/TPO clearly showed the difference between Ir/SiO₂ and Ir/Al₂O₃ prepared by the incipient wetness impregnation. On alumina H/Ir was above 2.0 up to an iridium loading of 2.5 wt% and still above 1.0 for 6.8 wt% Ir, whilst in the case of Ir/SiO₂ H/Ir was below 1.0 even for an iridium loading of 0.4 wt%. Temperature programmed desorption experiments gave the same results. Reduction behaviour of the dried systems, oxidation behaviour of the reduced systems and the loss of dispersity as a function of oxidation temperature support this conclusion. The difference in dispersion is caused by the absence of adsorption sites on the SiO₂ support during the incipient wetness impregnation. Thus, no mononuclear iridium species are adsorbed on this support and large salt crystallites are formed during the drying process. The urea method proved successful for both supports. During the decomposition of the urea (363 K), the pH of the solution increased slowly and small metal hydroxide particles were

deposited on the support resulting in H/Ir = 1.6 for 1.5 wt% Ir/SiO₂ and H/Ir = 1.2 for 5.5 wt% Ir/SiO₂. The results for the alumina-supported systems prepared via the urea method were comparable with those for the systems prepared via the incipient wetness method. Thus with these two methods we are able to prepare highly dispersed Ir/Al₂O₃ and Ir/SiO₂ systems.

3.6 REFERENCES

1. P.R. Watson and G.A. Somorjai, *J. Catal.*, **72** (1981) 3.
2. P.R. Watson and G.A. Somorjai, *J. Catal.*, **74** (1982) 282.
3. M. Ichikawa, *Bull. Chem. Soc. Jap.*, **51** (1978) 2268.
4. M. Ichikawa, *Bull. Chem. Soc. Jap.*, **51** (1978) 2273.
5. M. Ichikawa, *J. Chem. Soc., Chem. Comm.*, (1978) 566.
6. L. Poutsma, L.F. Elek, P.A. Ibarbia, A.P. Risch and J.A. Rabo, *J. Catal.*, **82** (1983) 20.
7. B.J. Kip, F.W.A. Dirne, J. van Grondelle and R. Prins, *Appl. Catal.*, **25** (1986) 43. Chapter 5 of this thesis.
8. J.R. Anderson, P.S. Elmes, R.F. Howe and D.E. Mainwaring, *J. Catal.*, **50** (1977) 508.
9. R.F. Howe, *J. Catal.*, **50** (1977) 196.
10. J.R. Anderson and R.F. Howe, *Nature* **268** (1977) 129.
11. K. Foger and J.K. Anderson, *J. Catal.*, **59** (1979) 325.
12. K. Tanaka, K.L. Watters and R.F. Howe, *J. Catal.*, **75** (1982) 23.
13. M. Ichikawa and K. Shikakura, *Proc. 7th Int. Congr. Catal.*, Tokyo (1980) 925.
14. G.B. McVicker, R.T.K. Baker, G.L. Garten and E.L. Kugler, *J. Catal.*, **65** (1980) 207.
15. S. Krishnamurthy, G.R. Landolt and H.J. Schoennagel, *J. Catal.*, **78** (1982) 319.
16. J.C. Vis, H.F.J. van 't Blik, T. Huizinga, J. van Grondelle and R. Prins, *J. Catal.*, **95** (1985) 333.
17. H.F.J. van 't Blik, D.C. Koningsberger and R. Prins, *J. Catal.*, **97** (1986) 210.
18. J.W. Geus, *Preparation of Catalysts III*, G. Poncelet, P. Grange and P.A. Jacobs, Eds., Elsevier, Amsterdam, (1983) 1.
19. L.A.M. Hermans and J.W. Geus, *Preparation of Catalysts II*, B. Delmon, P. Grange, P.A. Jacobs and G. Poncelet, Eds., Elsevier, Amsterdam (1983) 113.
20. J.A. Van Dillen, J.W. Geus, L.A.M. Hermans and J. v.d. Meyden, *Proc. 6th Int. Congr. Catalysts*, G.C. Bond, P.B. Wells, F.C. Tompkins, Eds., The Chemical Society, London (1976), 677.

21. J.C. Vis, H.F.J. van 't Blik, T. Huizinga, J. van Grondelle and R. Prins, *J. Molec. Catal.*, 25 (1984) 367.
22. J.H.A. Martens, H.F.J. van 't Blik and R. Prins, *J. Catal.*, 97 (1986) 200.
23. K. Foger and H. Jaeger, *J. Catal.*, 70 (1981) 53.
24. N. Wagstaff and R. Prins, *J. Catal.*, 59 (1979) 434.
25. N. Wagstaff and R. Prins, *J. Catal.*, 59 (1979) 446.
26. A.C. Faro Jr., M.E. Cooper, D. Garden and C. Kembball, *J. Chem. Res.*, paper E/183/82 (1983) 1114.
27. A. Crucoq, L. Degols, G. Lienard and A. Frennet, *Acta Chim. Acad. Sci. Hung.*, (1982) 111.
28. J.E. Benson and M. Boudart, *J. Catal.*, 4 (1965) 704.
29. H. Boer, W.J. Boersma and N. Wagstaff, *Rev. Sci. Instr.*, 52 (1982) 439.
30. T. Huizinga, J. van Grondelle and R. Prins, *Appl. Catal.*, 10 (1984) 199.
31. S.E. Wanke and N.A. Dougharty, *J. Catal.*, 24 (1972) 367.
32. M.A. Vannice, *J. Catal.*, 37 (1975) 449.
33. C.S. Brooks, *J. Colloid. Interface Sci.*, 34 (1970) 34.
34. T.P. Wibon, P.H. Kasai and P.C. Ellgen, *J. Catal.*, 69 (1981) 193.
35. R.M.J. Fiederow, B.S. Chabor and S.E. Wanke, *J. Catal.*, 51 (1978) 193.
36. S. Sato, *J. Catal.*, 70 (1985) 11.
37. R. Dutartre, P. Bussiere, J.A. Dalmon and G.A. Martin, *J. Catal.*, 59 (1979) 382.
38. J.A. Dalmon, C. Mirodatos, P. Turlier and G.A. Martin, in "Spillover of adsorbed species", G.M. Pajonk, S.J. Teichner and J.E. Germain, Eds., *Studies in surface science and catalysis*, Elsevier, Amsterdam 17 (1983) 169.
39. P. Wynblatt and N.A. Gjostein, *Progr. Solid State Chem.*, 9 (1975) 21.
40. G.G. Hlatky and R.H. Crabtree, *Coord. Chem. Rev.*, 65 (1985) 1.
41. B.J. Kip, F.B.M. Duivenvoorden, D.C. Koningsberger and R. Prins, *J. Am. Chem. Soc.*, 108 (1986) 5633. Chapter 4 of this thesis.
42. J.P. Candy, P. Fouilloux and A.J. Renouprez, *J. Chem. Soc. Faraday I*, 76 (1980) 616.
43. J. Escard, C. Leclere and J.P. Contour, *J. Catal.*, 29 (1973) 31.
44. R. van Hardenveld and F. Hartog, in "Advances in Catalysis", D.E. Eley *et al.*, Eds., vol. 22, Academic Press, New York (1972) 75.
45. M.A. Vannice, L.C. Hasselbring and B. Sen, *J. Catal.*, 95 (1985) 57.
46. G. Ehrlich, in "Conference on Clean Surfaces", *Ann. N. Y. Acad. Sci.*, 101 (1963) art. 3.
47. N. Cabrera, in "Semiconductor Surface Physics", R.H. Kingston, Ed., University of Pennsylvania Press, Philadelphia (1957).
48. N. Birks and H.G. Meier, *Introduction to high temperature oxidation of metals*, Edward Arnold Ltd., London (1983).

49. P. Kofstad, High temperature oxidation of metals, Wiley & Sons, New York (1966).
50. C. Wagner, Atom movements, Am. Soc. Metals, Cleveland (1951) 153.
51. K. Foger, J. Catal., 78 (1982) 406.
52. K. Foger and H. Jaeger, J. Catal., 67 (1981) 252.
53. F.B.M. Duivenvoorden, B.J. Kip, D.C. Koningsberger and R. Prins, to be published.

Chapter 4

DETERMINATION OF METAL PARTICLE SIZE OF HIGHLY DISPERSED Rh, Ir AND Pt CATALYSTS BY HYDROGEN CHEMISORPTION AND EXAFS

Hydrogen-to-metal (H/M) ratios exceeding unity for Pt and Rh and exceeding two for Ir were measured for highly dispersed Pt, Rh and Ir catalysts supported on Al_2O_3 and SiO_2 . Since the coordination of hydrogen to metal atoms is unknown for such highly dispersed catalysts, the metal surface area of these catalysts cannot be calculated from the hydrogen chemisorption values. Therefore EXAFS (Extended X-ray Absorption Fine Structure) measurements were performed to determine the metal particle size and thereby to calibrate hydrogen chemisorption results. The H/M ratio determined by hydrogen chemisorption is a linear function of the average metal coordination number determined by EXAFS. This linear relationship is independent of support but varies with the metal with the H/M ratio increasing in the order $\text{Pt} < \text{Rh} < \text{Ir}$. Several hypotheses for the high H/M values are discussed. Spillover and subsurface hydrogen are excluded as explanations and only multiple adsorption of hydrogen on metal surface atoms is shown to be capable of explaining all experimental observations. The $\text{H}/\text{M}_{\text{surface}}$ stoichiometry differs among Pt, Rh and Ir in the order $\text{H}/\text{Pt} < \text{H}/\text{Rh} < \text{H}/\text{Ir}$, analogous to the order of stability of corresponding metal polyhydride complexes and of theoretical expectation.

4.1 INTRODUCTION

Selective chemisorption of gaseous molecules, especially hydrogen, has been extensively used to estimate the degree of dispersion of group VIII metal catalysts [1-27]. Chemisorption methods are of special importance for highly dispersed metal catalysts, since it is often difficult to establish the degree of dispersion by other techniques such as X-ray diffraction or electron microscopy measurements [1]. Moreover, the chemisorption technique is relatively quick and cheap.

Hydrogen chemisorption data can be directly used to compare dispersions

of a metal in different catalysts in a relative way. However, when one wants to calculate metal surface areas in an absolute way the hydrogen-to-metal stoichiometry must be known. For the most widely used platinum metal usually a H/M stoichiometry of one has been used and this assumption has been justified by calibration with XRD and TEM [5-7]. Surface science studies furthermore proved that a maximum of one hydrogen atom per metal atom could be chemisorbed on the (111) faces of fcc metal single crystals [8]. Under the assumption that the surface of metal particles larger than say 2 nm consists largely of (111) faces, it is understandable that the empirical assumption of a H/M = 1 stoichiometry was rather successful in many studies. However, as early as 1960 data began to appear in the literature about stoichiometries exceeding one. The value of H/Pt = 1.5 - 1.65 has been measured for Pt/Al₂O₃ catalysts [9,10] and H/Pt = 1.3 - 1.6 has been quoted for Pt/SiO₂ catalysts [11,12], while a value of H/Pt = 2 has been observed by Rabo *et al.* for Pt deposited on a zeolite [13]. Recently, Sato [14] has described a Pt/TiO₂ system made by photo impregnation of hexachloroplatinic acid with H/Pt = 2.5, while Frennet and Wells [15] have reported H/Pt values around 1.2 for 6.3 wt% Pt/SiO₂. For Rh catalysts Wanke and Dougharty [16] have reported the adsorption of more than one hydrogen atom per surface rhodium atom for Rh/Al₂O₃ catalysts. For supported Ir catalysts even values near 3.0 have been measured. McVicker *et al.* [17] have found an upper limit of two adsorbed hydrogen atoms per Ir atom for Ir/Al₂O₃ systems, only using the strongly bonded hydrogen. When the total amount of adsorbed hydrogen is taken into account, they reported H/Ir values exceeding two. Krishnamurthy *et al.* [18] have shown that 0.48 wt% Ir/Al₂O₃ adsorbs up to 2.72 hydrogen atoms per iridium atom, part of which is weakly bound (H/Ir = 0.28).

In literature, several explanations have been given for H/M values exceeding unity. Often a distinction has been made between reversibly and irreversibly adsorbed hydrogen, and in many cases only the irreversibly adsorbed hydrogen has been assumed to be important for the determination of the metal surface area [17-22]. Several authors have ascribed the high H/M values to hydrogen spillover to the support [14,28-30], or to an increased hydrogen-to-metal stoichiometry for metal atoms situated at the corners and edges of the small metal particles [16-18]. Another explanation given for high H/M values has been the positioning of part of the hydrogen under the surface of the metal particle [31-33].

In our laboratory, Pt, Rh and Ir catalysts supported on Al₂O₃, SiO₂ and TiO₂ have been studied in the hydrogenation of carbon monoxide to

hydrocarbons and oxygenated products. We have also used hydrogen chemisorption to characterize the highly dispersed supported metal catalysts and have obtained H/M values exceeding unity for Rh and Pt catalysts [34-36] and H/M values even exceeding 2.0 for supported Ir systems [37]. Because of a lack of information on the hydrogen-to-metal stoichiometry for very small metal particles, we were unable to calculate the dispersion from the chemisorption results. Therefore, we have relied on another technique to obtain information about the particle size of the highly dispersed systems: Extended X-ray Absorption Fine Structure (EXAFS). With this technique, it is possible to determine the metal coordination number of a metal atom (N) in a particle and thus to get information about the particle size [36,38-43].

In this publication, the results of our hydrogen chemisorption and EXAFS measurements are compared for Pt, Rh and Ir catalysts supported on SiO_2 and Al_2O_3 . Several hypotheses for the observed high H/M values are discussed and it will be shown that multiple adsorption of hydrogen on metal surface atoms is the only one which can explain all experimental observations.

4.2 EXPERIMENTAL

4.2.1 Preparation of the catalysts

Pt, Ir and Rh catalysts were prepared from $RhCl_3$ and $IrCl_3$ via the incipient wetness technique [34,35,37], from $Pt(NH_3)_4(OH)_2$ and $Rh(NO_3)_3$ via the ion exchange technique [36,44], and from $IrCl_3$ via the urea method [37]. In the last method, the pH of a suspension of the support and metal ions in water is increased slowly by means of the decomposition of urea [45]. The following supports were used: $\gamma-Al_2O_3$ from Ketjen (000-1.5E, surface area $200\text{ m}^2\text{ g}^{-1}$, pore volume 0.60 ml g^{-1}), $\gamma-Al_2O_3$ obtained by heating boehmite (Martinswerk, GmbH, surface area $150\text{ m}^2\text{ g}^{-1}$, pore volume 0.65 ml g^{-1}), and SiO_2 (Grace, S.D. 2-324.382, surface area $290\text{ m}^2\text{ g}^{-1}$, pore volume 1.2 ml g^{-1}). The metal precursors ($IrCl_3 \cdot xH_2O$, $RhCl_3 \cdot xH_2O$ and $Pt(NH_3)_4(OH)_2$) were supplied by Drijfhout, Amsterdam. All catalysts were dried in air at 395 K for 16 h (heating rate 2 K min^{-1}).

4.2.2 Hydrogen chemisorption measurements

Volumetric hydrogen chemisorption measurements were performed in a conventional glass system at 298 K. Hydrogen was purified by passing

through a palladium diffusion cell. Before measuring the H_2 chemisorption isotherm the dried catalysts were reduced for 1 h (heating rate $5-8 \text{ K min}^{-1}$) and evacuated (10^{-2} Pa) for 0.5 h. The reduction temperatures, at which evacuation was also performed, are presented in Table 4.1. After hydrogen admission at 473 K, $P(H_2) = 93 \text{ kPa}$, desorption isotherms were measured at room temperature. The total amount of chemisorbed H atoms was obtained by extrapolating the linear high pressure part ($20 \text{ kPa} < P < 80 \text{ kPa}$) of the isotherm to zero pressure [2]). Correction for chemisorption on the bare support was not necessary, because the extrapolated values of the desorption isotherms for the bare supports, pretreated in the same way as the catalysts, were zero within the uncertainty of the measurements.

4.2.3 EXAFS measurements

Catalyst samples were measured at liquid nitrogen temperature as thin self-supporting wafers in H_2 , after *in situ* reduction. The Rh and Pt measurements were performed on beam line I-5 at the Stanford Synchrotron Radiation Laboratory (SSRL) at the Rh K-edge (23220 eV) and Pt L_{III} -edge (11564 eV), respectively. The data were analyzed with the use of reference compounds [38-40]). In the case of the Rh catalysts, Rh foil and Rh_2O_3 were used. For the Pt data, Pt foil and $Na_2Pt(OH)_6$ were used [36].

The Ir measurements were done on the Wiggler station 9.2 at the Synchrotron Radiation Source (SRS) in Daresbury, G.B. (2 GeV, 80-250 mA) at the Ir L_{III} -edge (11215 eV). As reference compounds Pt foil and $Na_2Pt(OH)_6$ were used. Both theoretically [46] and experimentally [47] the choice of Pt references for the analysis of Ir data can be justified.

The results of the analysis of the Rh data have been published before [38-40], as well as the results for the Pt catalyst with $H/M = 1.14$ [46].

The metal-metal coordination parameters of the Ir and other Pt catalysts were determined as follows [48]. A k^3 Fourier transform ($\Delta k = 2.7-15 \text{ \AA}^{-1}$) was applied to the EXAFS data. In the resulting spectrum in R-space, the peak representing the first M-M shell (but also including $M-O_{\text{support}}$ contributions) was back transformed ($\Delta R = 1.9-3.5 \text{ \AA}$) to k-space. In the resulting spectrum the $M-O_{\text{support}}$ contributions are only significant below $k = 8 \text{ \AA}^{-1}$, because a low Z element like oxygen does not scatter very much at high k-values. Therefore, the M-M coordination parameters were determined by fitting the data between $k = 7.9$ and 13.8 \AA^{-1} , in such a way that a good agreement was obtained in k- and in R-space.

4.3 RESULTS

4.3.1 Hydrogen chemisorption measurements

Since hydrogen chemisorption can be performed in many, slightly different ways, with often (slightly) different results, it is imperative to start with a description of our own method of measuring hydrogen chemisorption. After *in situ* reduction and evacuation we admit a certain amount of hydrogen at 473 K, as hydrogen adsorption at room temperature is a slow process. Subsequently, the sample is cooled to 298 K under hydrogen and the amount of adsorbed hydrogen is measured ($P_{\text{equilibrium}} \simeq 80$ kPa). Thereafter a so-called desorption isotherm is measured at room temperature by lowering the pressure step by step ($P \simeq 13$ kPa per step), while measuring the amount of desorbed hydrogen. The total amount of chemisorbed hydrogen is obtained by extrapolation of the linear high pressure part ($20 \text{ kPa} < P < 80 \text{ kPa}$) in the isotherm to zero pressure. The H/M values obtained in this way are slightly higher than those obtained by admission at room temperature and waiting for 3 h. As an example, we obtained H/Ir values of 2.68 and 2.49 for a 0.81 wt% Ir/Al₂O₃ catalyst, after admission of H₂ at 473 K and 298 K, respectively. The H/M values obtained for our catalysts are presented in Table 4.1.

Other, often lower, hydrogen pressures have been used in the literature. According to Crucq *et al.*, the hydrogen adsorption isotherms of supported Pt [49] and Rh [50] catalysts are Temkin-like (showing a linear relation between $\log(P)$ and H/M over a wide pressure range) due to a strongly decreasing heat of adsorption with coverage. Therefore they recommended the measurement of a single adsorption point at $P > 13$ kPa at room temperature, to obtain the amount of adsorbed hydrogen close to monolayer coverage. However, we always extrapolate our measurements to zero pressure. The experimental convenience of this is that the intercept is independent of the dead volume of the adsorption apparatus [16]. Consequently, it is possible to use an arbitrarily chosen dead volume or to ignore the dead volume entirely, since the zero-pressure condition implies no residual adsorbate in the gas phase, and there is thus no necessity for the experimental determination of dead volumes.

Several authors have reported that H/M increases with decreasing temperature. For instance Boronin *et al.* [12] reported that for Pt catalysts H/M increased to a value of 2 as the temperature of measuring chemisorption was lowered to 77 K. Most likely different metals will have different H/M

TABLE 4.1: Hydrogen chemisorption and EXAFS results for supported Rh, Ir and Pt catalysts.

catalyst ^{a,b}	reduction temp. (K)	H/M ^c	N ^d
4.2 %Pt/Al ₂ O ₃ , k, A	1100	0.23	10.0
4.2 % Pt/Al ₂ O ₃ , k, A	1058	0.43	10.2
4.2 % Pt/Al ₂ O ₃ , k, A	573	0.77	7.6
1.06 % Pt/Al ₂ O ₃ , k, A	673	1.14	5.2
2.00 % Rh/Al ₂ O ₃ , b, B	673	1.2	6.6
2.4 % Rh/Al ₂ O ₃ , b, A	473	1.2	6.3
1.04 % Rh/Al ₂ O ₃ , k, B	773	1.65	5.8
0.47 % Rh/Al ₂ O ₃ , k, B	773	1.7	5.1
0.57 % Rh/Al ₂ O ₃ , b, B	573	1.98	3.8
7.0 % Ir/SiO ₂ , g, B	773	0.43	11.1
1.5 % Ir/SiO ₂ , g, B	773	0.83	11.0
5.3 % Ir/SiO ₂ , g, C	773	1.24	8.6
1.5 % Ir/SiO ₂ , g, C	773	1.70	8.6
2.4 % Ir/Al ₂ O ₃ , k, B	773	1.96	7.7
1.5 % Ir/Al ₂ O ₃ , k, B	773	2.40	7.3
0.8 % Ir/Al ₂ O ₃ , k, B	773	2.68	6.0

(a) support: γ -Al₂O₃ Ketjen (k), γ -Al₂O₃ boehmite (b), SiO₂ Grace (g).

(b) Preparation method: ion exchange (A), incipient wetness (B), urea method (C).

(c) experimental error in H/M: $\pm 5\%$

(d) experimental error in N : $\pm 10\%$

temperature dependencies and there is no *a priori* reason why all metals should have the same H/M stoichiometry at a particular temperature. Furthermore, as also shown in this paper, the H/M stoichiometry is dependent on the metal particle size. For these reasons, and also to measure the H/M stoichiometries under identical conditions, we have opted to use a fixed measurement temperature for all three metals under study. For experimental reasons we have measured the desorption isotherms at 298 K. As a consequence, it should be kept in mind that the resulting calibration of the H/M values is only valid for chemisorption on Pt, Rh and Ir at 298 K.

We have not made any distinction between reversibly and irreversibly

adsorbed hydrogen, as is often done in the literature [17-22]. All chemisorption is reversible and one can only distinguish between weakly and strongly adsorbed hydrogen. The only difference between them is the heat of adsorption, which is a function of coverage. Goodwin *et al.* [21,22] have shown that hydrogen which is weakly adsorbed on supported Ru catalysts is associated with the metal, and not with the support. De Menorval and Fraissard [51] and Sanz and Rojo [52] have shown that the NMR chemical shifts of hydrogen atoms adsorbed on Pt/ Al_2O_3 and Rh/ TiO_2 catalysts, respectively, decrease with increasing hydrogen pressure, even at $P > 40$ kPa. This proves that even at such pressures additional hydrogen is still adsorbed on the metal when increasing the hydrogen pressure. Subtraction of the amount of 'reversibly' adsorbed hydrogen therefore does not result in a correction for the adsorption on the support, but instead to the elimination of hydrogen adsorbed weakly on the metal.

Moreover, we feel that the amount of weakly adsorbed hydrogen is difficult to determine objectively, as it depends on the apparatus, pump, and evacuation time used [49]. To obtain an idea of the amount of hydrogen which is relatively weakly bound to the metal under our conditions, measurements were done for the 0.81 wt% Ir/ Al_2O_3 catalyst. After 20 minutes of pumping, 23% of the original amount of adsorbed hydrogen could be readsorbed ($H/Ir_{\text{strong}} = 2.07$, $H/Ir_{\text{weak}} = 0.61$). It is obvious that even if only the strongly bonded hydrogen was considered, our H/M values would still exceed unity in many cases.

4.3.2 EXAFS measurements

In order to obtain the metal particle sizes of our catalysts, we used the EXAFS technique. Details about the data analysis used with some of the measurements have been reported earlier [36,38-40], or will be reported [47,48]. The quality of the fit obtained for the first metal-metal shell in the EXAFS data was always good. As an example the fits in R-space and in k-space are shown in Figure 4.1 for the 4.2 wt% Pt/ Al_2O_3 sample with a H/M value of 0.77. The fit has been obtained between $k = 7.9$ (below this limit Pt-O contributions are present) and 13.8 \AA^{-1} (signal-to-noise ratio is too low above this limit). In k-space a clear deviation is observed for $k < 7 \text{ \AA}^{-1}$ between the Pt-Pt spectrum calculated on the basis of the fit parameters, and the experimental spectrum. This deviation is caused by Pt-O contributions which cannot be neglected in this region [48].

The average numbers of metal atoms N obtained from the EXAFS

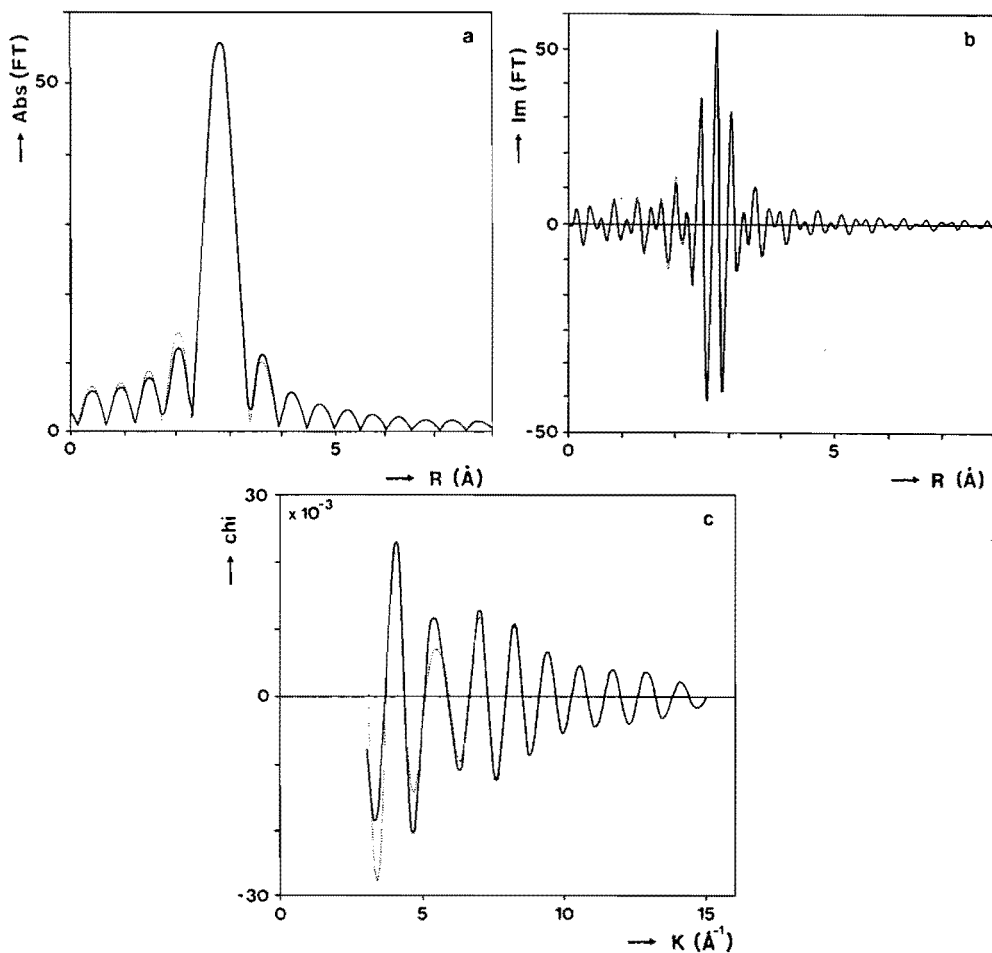


FIGURE 4.1: Fit obtained in the EXAFS analysis of 4.2 wt% Pt/ Al_2O_3 , $\text{H}/\text{Pt} = 0.77$; (—) experiment, (....) fit.

- (a) amplitude of the Fourier transform of the EXAFS obtained by a k^3 Fourier transform between $k = 7.9$ and 13.8 \AA^{-1}
- (b) imaginary part of the Fourier transform
- (c) fit in k -space. The Pt-Pt spectrum has been calculated on the basis of the fit for $7.9 < k < 13.8 \text{ \AA}^{-1}$, with $N = 7.6$, $R = 2.75 \text{ \AA}$, and $\Delta\sigma^2 = 0.0035 \text{ \AA}^2$.

analysis are presented in Table 4.1 and Figure 4.2. As can be seen in Table 4.1, two supports and a variety of preparation methods have been used. However, if any of these parameters has an effect on the hydrogen-to-metal

stoichiometry, it can only be a minor one since the metal-metal coordination number versus H/M relationship can be described by a single straight line for each metal. Rather unexpectedly there is a large difference between the three metals. This difference is very marked and experimentally significant above $H/M = 1$, but still exists at lower H/M values. For a given particle size (equal metal-metal coordination number) the H/M values increase in the sequence $H/Pt < H/Rh < H/Ir$.

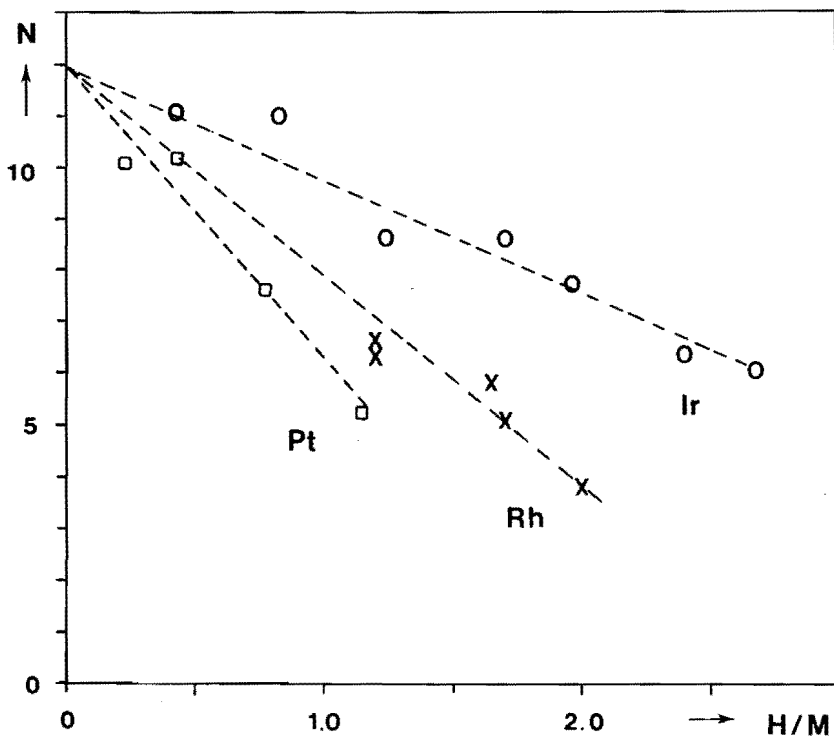


FIGURE 4.2: Metal-metal coordination number N from EXAFS versus H/M from chemisorption, for Pt (\square), Rh (x) and Ir (o).

4.3.3 Model calculations

To investigate if the high H/M values can be explained by adsorption at the surface metal atoms, model calculations were performed. A computer programme was made to determine the area available for chemisorption around a supported small metal particle. In the spirit of Wynblatt and Gjo-

stein [53] the shape of the metal particle was calculated as a function of the relative magnitude of the metal-metal and metal-support interaction energy by minimizing the total energy. We assumed the support to consist of a flat (111) layer of oxygen anions, the size of which was taken equal to that of the metal atoms. The metal atoms were assumed to be fcc packed, and thus to fit epitaxially on the support surface. The shape of a metal particle with $n+1$ atoms was obtained from that of the particle with n atoms by putting the extra metal atom at the position of minimum energy. Such calculations were carried out over a whole range of α -values, with α being the ratio of the metal atom-oxygen anion interaction $E(M-O^{2-})$ and the metal atom-metal atom interaction $E(M-M)$.

To obtain an estimate of the number of hydrogen atoms that can be placed around such a metal particle, we assumed that the hydrogen atoms will occupy the free fcc positions around the metal particle and that only one hydrogen atom per vacant fcc position is allowed. Although diffraction results for metal hydride complexes point to a hydrogen atom radius which is much smaller than that of the Pt, Rh, or Ir atoms [54], these same results also point out that H-H distances smaller than M-M distances are rarely observed. Similarly, in line with results obtained in surface science [8], our model predicts that the maximum number of hydrogen atoms which can adsorb on the (111) surface of an fcc metal single crystal is equal to the number of metal atoms in that surface. Our assumptions therefore seem reasonable. They lead to a lower bound for the number of hydrogen atoms that geometrically can be put around a supported metal cluster.

Table 4.2 summarizes the results of the calculations for two situations. One in which the interaction between metal and oxygen is half that of the metal-metal interaction, $E(M-O^{2-})/E(M-M) = \alpha = 0.5$, which results in spherical particles, and one in which $\alpha = 2$, resulting in raft-like particles. Dispersions (defined as the fraction exposed metal atoms), metal-metal coordination numbers, diameters of the particles (expressed in metal atom diameters) and H/M values are presented as a function of the number of atoms per particle. The H/M values were calculated on the basis of two assumptions. Very high H/M values (up to 4.5) were obtained if hydrogen was allowed to occupy all vacant fcc positions, even those where the hydrogen atom is bonded to only one metal atom. If only vacant positions were considered, where the hydrogen atom is bonded to at least two metal atoms, still a H/M value of 2.3 could be obtained. In Figure 4.3 we have plotted the two series of H/M values as a function of the total number of atoms in a metal particle, using $\alpha = 0.5$. In the same figure also the

TABLE 4.2: Results of the computer calculations on small metal particles.

α^a	0.5					2.0				
Number of atoms per particle	4	10	30	100	800	4	10	30	100	800
Empty positions ^b :										
1 metal neighbour	9	15	16	19	36	11	13	14	14	39
2 " "	9	8	21	35	81	6	10	21	41	85
3 " "	0	5	10	33	125	1	4	10	23	129
4 " "	0	2	4	15	113	0	1	6	21	92
5 " "	0	0	2	2	15	0	1	0	0	18
Dispersion	1.0	1.0	.80	.62	.36	1.0	1.0	.80	.60	.35
H/M ^c	4.5	3.0	1.8	1.0	.46	4.5	2.9	1.7	1.0	.45
H/M ^d	2.3	1.5	1.2	.85	.42	1.8	1.6	1.2	.85	.41
N ^e	3.0	4.8	6.8	8.5	10.2	2.5	4.2	6.5	8.3	10.2
D ^f	2.1	3.3	4.4	7.0	12.9	2.8	3.7	5.1	7.4	14.0

(a) $\alpha = E(M-O^{2-}) / E(M-M)$

(b) vacant fcc positions around the metal particle which have at least one metal neighbour, and which can be occupied by H atoms

(c) assuming that all vacant fcc positions around the particle are filled by hydrogen

(d) assuming that only vacant positions with more than one metal neighbour are filled by hydrogen

(e) metal-metal coordination number

(f) diameter of the particle expressed in metal atom diameters.

corresponding coordination number N, to be compared with the EXAFS results, and the dispersion are presented.

With the aid of these calculations, the metal-metal coordination numbers determined by EXAFS were used to calculate dispersions. These dispersions versus the measured H/M values are shown in Figure 4.4. It is clear from this figure that the H/M_{surface} stoichiometry cannot be taken as equal to one, and varies among the group VIII metals studied.

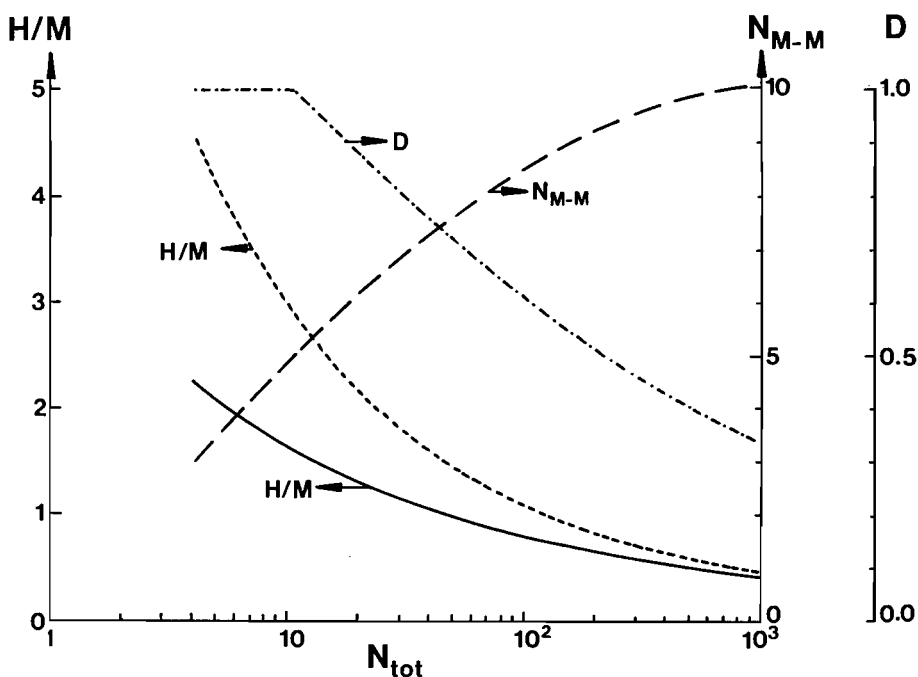


FIGURE 4.3: Results of model calculations for $\alpha = 0.5$. Calculated H/M, assuming that all free positions around the metal particle are filled with hydrogen (—), or that only the free positions with at least two metal neighbours are filled (---), versus total number of metal atoms in one particle N_{tot} , and calculated dispersion D (-·-·) and metal-metal coordination number N_{M-M} (---) versus N_{tot} .

4.4 DISCUSSION

First of all, we want to exclude several trivial effects which could explain the high H/M values:

- Unreduced M^{n+} was not present, as can be concluded from TPR experiments [34-37]. Within the experimental error (5%), all metal was reduced to M^0 .
- Contamination of the catalysts with carbon did not occur. Elemental analysis (using Perkin Elmer Element Analyzer Model 240) showed that no carbon residues existed initially on the catalysts. Carbon residues could be produced by grease or oil vapours during the evacuation. However, TPD experiments, which are absolutely free of grease and oil va-

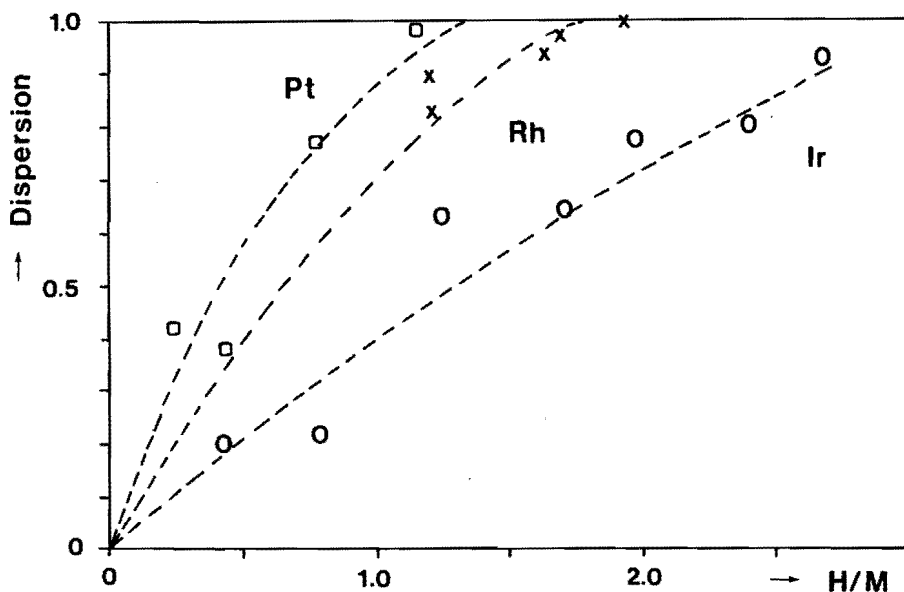


FIGURE 4.4: Dispersion ($M_{\text{surface}}/M_{\text{total}}$) obtained on the basis of model calculations ($\alpha = 0.5$) for Pt (\square), Rh (x) and Ir (o), versus H/M.

pour, resulted in similarly high H/M values [37].

- Partial reoxidation during outgassing at high temperature, mentioned by Martin *et al.* for Fe [55] and Ni [56], can be excluded, because oxygen consumption during oxidation at 773 K after reduction and evacuation at 773 K was measured to be O/Ir = 1.96 for 1.5 wt% Ir/Al₂O₃. IrO₂ is the most stable oxide of iridium, so these results prove that Ir was in the zero valent state after reduction and evacuation.

In the literature several explanations have been proposed for high H/M values. A common explanation is that in fact not all hydrogen is adsorbed by the small particles but that part of the hydrogen is adsorbed by the support through hydrogen spillover from the metal particles. Kramer and Andre [28] have reported the spillover of atomic hydrogen (formed by dissociation of H₂ on the platinum) on alumina and calculated a maximum surface capacity of their alumina for atomic hydrogen of $2 \cdot 10^{16}$ atoms m⁻². Cavanagh and Yates [29] have studied hydrogen spillover on alumina by exchange of D₂ with OH-groups and have shown that near 300 K, the rate of the exchange process is high in the presence of Rh particles on Al₂O₃. How-

ever, this experiment does not constitute proof for hydrogen spillover because the occurrence of exchange of hydrogen on the metal with hydrogen of the OH-groups on the support is a necessary but not sufficient condition for spillover to take place. Hydrogen spillover has also been reported on SiO_2 , especially by Teichner and coworkers [30].

We do not believe that spillover can explain our results. In the first place, it is not expected that the extent of spillover will differ greatly among the group VIII metals, and thus it cannot explain the observed differences between Pt, Rh and Ir. Besides, it is often said that spillover depends on the type of support used. In the case of Ir we have used two supports, SiO_2 and Al_2O_3 , and the H/Ir versus N values were found to lie on a straight line, independent of the support. Moreover, the reported number of sites on Al_2O_3 , available for hydrogen spillover ($2 \cdot 10^{16}$ H-atoms m^{-2} [28]), can only account for a fraction of the hydrogen chemisorbed by our catalysts. We can not imagine any trap for hydrogen on alumina or silica (what can be reduced ?) besides defects or impurities. The adsorbed amounts of hydrogen are far too high to be compatible with the concentration of impurities or defects.

Thus, we come to the conclusion that the main reason for the observed large H/M values must be an adsorption stoichiometry larger than one. There are two ways to achieve such a high adsorption stoichiometry:

A) adsorption beneath the metal surface, or

B) multiple adsorption on (parts of) the metal surface.

Both explanations have been proposed in the literature [31-33, 16-18]. In fact the difference is not that great, subsurface hydrogen can be considered as being bound to subsurface metal atoms, or alternatively as being bound to surface atoms. In the latter case the metal surface atom is multiply coordinated by hydrogen.

Subsurface hydrogen has already been observed for e.g. Pt(111), Ni(111) and Pd(111) by surface characterization techniques like XPS [32]. Also, Yates *et al.* [33] have invoked subsurface hydrogen to explain the delayed desorption of H_2 from a H_2/D_2 covered Ru (0001) surface, while Konvalinka and Scholten [31] have explained the TPD results of Pd/C with subsurface hydrogen. Because the hydrogen solubility in the bulk of Pt, Rh and Ir is rather low [57] the hydrogen can only be located just below the surface. Wells [58] has given an explanation for the different hydrogen absorption characteristics of the group VIII metals. He has related the degree of internal perfection of a metal particle to the amount of subsurface hydrogen (as

determined by butadiene titration and deuterium exchange) and stated that the degree of perfection is determined by the height of the reduction temperature, relative to the Hüttig temperature. The Hüttig temperature is taken as one third of the melting temperature, that is the temperature at which surface mobility becomes possible. For Pt this Hüttig temperature is 682 K, for Rh 746 K, and for Ir 894 K. Especially in the case of Ir, the Hüttig temperature is not reached during reduction, and thus the existence of internal defects is expected. These defects might accommodate subsurface hydrogen atoms.

While for large particles it is difficult to attribute the differences in H/M for Ir, Rh and Pt to multiple adsorption or subsurface adsorption exclusively, it is much easier to make a choice for the small metal particles. In the small metal particles almost all metal atoms occupy a surface position, and the number of subsurface atoms is not sufficient to accommodate a large number of extra hydrogen atoms. Besides, subsurface hydrogen can never explain a hydrogen-to-metal stoichiometry above one, because subsurface adsorption sites need subsurface metal atoms in order to exist.

Therefore, we conclude that multiple adsorption on exposed metal atoms must be the main reason for the high H/M values observed by ourselves and others. For very small particles almost all metal atoms will have an edge or corner position, independent of the type of metal and thus we are left with the conclusion, that certainly in the case of very small particles, high H/M values must be explained by high H/M_{surface} stoichiometries.

Multiple hydrogen adsorption has mostly been considered for edge and corner metal atoms, and a H/M stoichiometry of 2 has been assumed [16-18]. The results of our model calculations demonstrate that from a geometrical point of view high H/M values are acceptable, even those for the highly dispersed Ir catalysts with $H/M > 2.0$. Easing up our assumptions (no fcc structure for the smallest metal particles and more than one hydrogen atom filling an fcc vacancy at the surface of the metal particle), only results in still higher hydrogen-to-metal ratios. The calculations show that high H/M values can indeed be caused by multiple adsorption at the corners and edges of the metal particle. The extremely high H/M values found for the Ir catalysts lead to two possibilities on the basis of these calculations. Either a relatively large proportion of the metal surface atoms occupies a corner or edge position (irregular particle shape), or the H/M stoichiometry for corner and edge iridium atoms is relatively high. The first possibility is unlikely since in the EXAFS analysis no higher Debye-Waller factor has been found for the iridium systems [48], while a metal particle with many edges and

corners is expected to have a high degree of disorder and thus a high Debye-Waller factor.

Although the model calculations indicate that there is room enough around the metal particles to accommodate a large number of hydrogen atoms, they do in fact not constitute proof that all these hydrogen atoms are really bonded strong enough to stay adsorbed at room temperature at a pressure of tens of kPa. Recently Christmann *et al.* [59] performed studies of hydrogen adsorption on the Ni(110) and Rh(110) surfaces and found that at higher hydrogen pressure the Ni, respectively Rh atoms in the exposed rows all adsorb 1.5, respectively 2 hydrogen atoms. This proves that for Ni a stoichiometry of $H/Ni = 1.5$ and for Rh a stoichiometry of 2.0 is at least possible.

The calculations do not make clear either why there is such a difference in H/M values for Pt, Rh and Ir catalysts with the same dispersion, as shown in Figure 4.4. The explanation for these questions must come from electronic arguments. The most simple explanation, differences in heats of adsorption for hydrogen on Pt, Rh, or Ir, does not seem to be valid, because these heats do not differ markedly [60]. But the reported spread in the heats of adsorption is large and no real comparison for similar metal crystal surfaces at the same hydrogen coverage has been published yet. Theoretically one would indeed expect platinum to adsorb the least number of H atoms, because Pt has one (antibonding) electron more than Rh and Ir. The fact that Ir has a higher hydrogen adsorption capacity than Rh can be related to the larger size of 5d orbitals, which gives better overlap and stronger bonding.

But the difference in H/M values between Pt, Rh and Ir can also be explained by taking a closer look at the analogy between the hydrogen-covered small metal particles ($d < 15 \text{ \AA}$) and transition-metal polyhydride complexes. This can be justified by the fact that these very small particles are not truly metallic, because they consist of too few atoms. Thus, by using 1H NMR, Sanz and Rojo [52] have observed the similarity between the chemical shifts of chemisorbed hydrogen on Rh/TiO₂ at hydrogen pressures above 40 kPa, and of diamagnetic non-metallic hydride coordination compounds of the transition-metal elements.

In the case of Pt, hydride complexes with $H/Pt > 2$ are rarely mentioned in the literature [54]. Recently Minot *et al.* [61] performed extended Hückel calculations on the hydrogenation of small Pt_n ($n=2-13$) clusters and they reported stable complexes with rather high numbers of bound hydrogen atoms and dihydrogen molecules. Thus for Pt₄ and Pt₆ clusters the max-

imum amount of hydrogen which could be bonded corresponded to the $Pt_4H_{16}(H_2)_2$ and $Pt_6H_{12}(H_2)_4$ complexes, respectively (see Figure 4.5). These calculations indicated that in all cases the hydrogen atoms (hydride ions) were stronger bonded than the dihydrogen molecules and that the dissociation of the dihydrogen molecules in the complexes with maximum number of hydrogen and dihydrogen would lead to an increase, rather than a decrease in total energy.

While these theoretical results already suggest that dihydrogen molecules are much weaker bonded to a metal atom than hydrogen atoms, experimental results in the field of organometallics have presented convincing proof for this. Thus Kubas *et al.* [62] were the first to demonstrate that transition-metal complexes containing a coordinated dihydrogen molecule, bonded side-on in the η^2 mode, could be prepared. But the H_2 in their $M(CO)_3(PR_3)_2(H_2)$ complexes ($M = Mo, W$ and $R = \text{cyclohexyl, } i\text{-propyl}$) is extremely labile. Other authors have in the past years followed up on Kubas' work and have prepared other complexes in which one or two dihydrogen molecules are coordinated to a transition metal atom [63-68] (see Figure 4.6). In all cases the dihydrogen molecules are readily lost from these complexes and only a few complexes were isolable in crystalline form. For that reason we have assumed that also in our case, with small metal particles on a support at room temperature under a pressure of a few tens of kPa, the bonding of dihydrogen molecules to the metal particles is very weak and that the experimentally observed H/M values have to be explained in terms of hydrogen atoms (hydride ions) bonded to metal particles only.

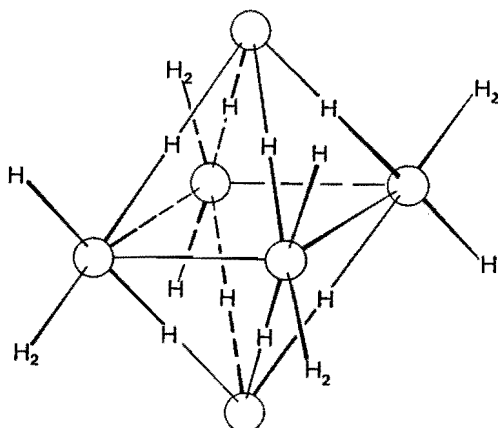


FIGURE 4.5: Representation of $Pt_6H_{12}(H_2)_4$ complex.

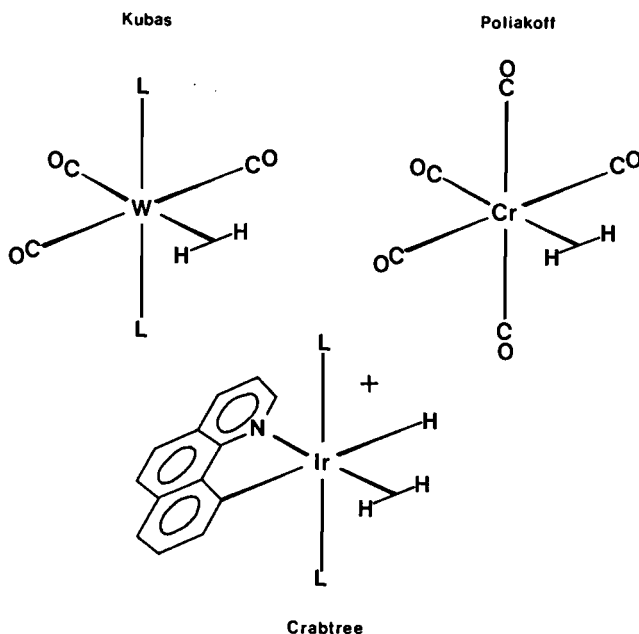


FIGURE 4.6: complexes with a dihydrogen molecule coordinated to a transition metal atom.

Besides direct quantum mechanical calculations such as the ones published by Minot *et al.* [61], also rules based on (semi-empirical) theory might shed a light on the number of hydrogen atoms which can be bonded to a particular metal cluster. Based on a topological approach and coupled with chemical intuition backed up by semi-empirical MO calculations, Wade [69], Mingos [70], Lauher [71] and Teo [72] developed rules to explain the existence of boron hydrides and metal carbonyl clusters. These rules have been very successful and can even explain the existence of high nuclearity clusters. Applying these rules to our metal particles, the binding of many hydrogen atoms to small metal clusters, with a resultant H/M stoichiometry above 1, is no surprise. Stoichiometries above 2 for Pt and above 3 for Rh and Ir are easily explained, if it is assumed that every H atom donates one electron. As examples we quote the existence of the $\text{Pt}_{38}(\text{CO})_{44}\text{H}_{12}^{2-}$ and $\text{Rh}_{13}(\text{CO})_{24}\text{H}^{4+}$ clusters, in which each CO molecule donates two electrons and each H atom one electron. According to the rules of Mingos, Lauher or Teo this means that complexes like $\text{Pt}_{38}\text{H}_{100}^{2-}$ and $\text{Rh}_{13}\text{H}_{49}^{2-}$ might be stable, resulting in stoichiometries of H/Pt = 2.6 and

H/Rh = 3.8, respectively.

Independent of the size of the metal cluster, all rules predict that all things being equal the H/M stoichiometry for a Pt atom should be smaller by one than for Rh and Ir particles, and that Rh and Ir should have equal stoichiometry. In essence the reason for that is the same as for mononuclear complexes, for which the 18 electron rule holds for octahedral and trigonal bipyramidal symmetry and the 16 electron rule for square planar symmetry. Since Rh and Ir atoms have one valence electron less than Pt atoms, they can coordinate one one-electron donating ligand more than Pt can. Therefore Pt is expected to have the lowest H/M value, and indeed it has. When Rh and Ir atoms or ions have the same valency, they have an equal number of valence electrons and therefore they are expected to coordinate an equal number of ligands. A difference between Rh and Ir is that Ir can reach a higher valency than Rh, Ir^{4+} ions are more stable than Rh^{4+} ions. As the M-H band can formally be described as M^+-H^- , we expect higher polyhydrides for Ir. Indeed many higher Ir polyhydrides are known, with H/Ir even as high as 6, while Rh polyhydrides are more rare, and are only known up to H/Rh = 5 [54]. This tendency is very clear in complexes of Ir and Rh that have the same ligands besides hydride ions. Thus Garlaschelli *et al.* [73] prepared $H_5Ir[P(i-Pr)_3]_2$ (i-Pr = isopropyl) from $HIrCl_2[P(i-Pr)_3]_2$, while the analogous procedure for Rh yielded only $H_2RhCl[P(i-Pr)_3]_2$. So the H/M stoichiometries in polyhydride complexes increase in the order Pt < Rh < Ir.

4.5 CONCLUSIONS

We conclude that the very high H/M values for the group VIII metals Pt, Rh and Ir are due to multiple adsorption of hydrogen on metal surface atoms. Differences in H/M values are due to different valencies of the three metals and are completely in line with the observed order of stability of corresponding metal polyhydride complexes. We do not want to fully exclude hydrogen spillover or subsurface hydrogen as explanation, but we think that they give only minor contributions to the high H/M values observed.

The results of this study clearly show that hydrogen chemisorption measurements cannot be used directly to determine particle sizes of highly dispersed metals, because of the uncertainty in the hydrogen-to-surface metal stoichiometry. Of course, for a particular metal the hydrogen chemisorption results can always be used to compare metal particle sizes in a qualita-

tive way. But by means of the EXAFS technique a calibration can be made, and by using this calibration H/M values can be quantitatively related to the percentage of exposed metal atoms as shown in Figure 4.4. At the moment, in this calibration we still have to rely on assumptions with regard to the metal particle shape. Thus in this work we relied on our model calculations to determine dispersion from metal coordination number. When in the future better EXAFS information becomes available, including second and third neighbor shells, then the calibration can really be made model independent.

4.6 REFERENCES

1. J.H. Sinfelt, *Ann. Rev. Mat. Sci.*, 2 (1972) 641.
2. J.E. Benson and M. Boudart, *J. Catal.*, 4 (1965) 704.
3. J.H. Sinfelt and D.J.C. Yates, *J. Catal.*, 8 (1967) 82.
4. J.H. Sinfelt, *J. Catal.*, 29 (1973) 308.
5. H.A. Benesi, R.M. Curtis and H.P. Studer, *J. Catal.*, 10 (1968) 328.
6. T.A. Dorling, M.J. Eastlake and R.L. Moss, *J. Catal.*, 14 (1969) 23; T.A. Dorling, B.W.J. Lynch and R.L. Moss, *J. Catal.*, 20 (1971) 190.
7. G.R. Wilson and W.K. Hall, *J. Catal.*, 24 (1972) 306.
8. K. Christmann, G. Ertl and T. Pignet, *Surface Sci.*, 54 (1976) 365.
9. S.F. Adler and J.J. Keavney, *J. Phys. Chem.*, 64 (1960) 208.
10. R.A. Herrmann, S.F. Adler, M.S. Goldstein and R.M. De Baun, *J. Phys. Chem.*, 65 (1961) 2189.
11. V.S. Boronin, V.S. Nikulina and O.M. Poltorak, *Russ. J. Phys. Chem.*, 37 (1963) 1174.
12. V.S. Boronin, O.M. Poltorak and A.O. Turakulova, *Russ. J. Phys. Chem.*, 48 (1974) 156.
13. J.A. Rabo, V. Schomaker and P.E. Pickert, *Proc. of the third Int. Congr. on Catal. (Amsterdam, 1964)*, p. II-1264.
14. S. Sato, *J. Catal.*, 92 (1985) 11.
15. A. Frennet and P.B. Wells, *Appl. Catal.*, 18 (1985) 243.
16. S.E. Wanke and N.A. Dougharty, *J. Catal.*, 24 (1972) 367.
17. G.B. McVicker, R.T.K. Baker, G.L. Garten and E.L. Kugler, *J. Catal.*, 65 (1980) 207.
18. S. Krishnamurthy, G.R. Landolt and H.J. Schoennagel, *J. Catal.*, 78 (1982) 319.
19. J.H. Sinfelt, Y.L. Lam, J.A. Cusumano and A.E. Barnett, *J. Catal.* 4 (1976) 227.

20. J.H. Sinfelt and G.H. Via, *J. Catal.*, 56 (1979) 1.
21. C. Yang and J.R. Goodwin, Jr., *J. Catal.*, 78 (1982) 182.
22. A. Sayari, H.T. Wang and J.G. Goodwin, Jr., *J. Catal.*, 93 (1985) 368.
23. M.A. Vannice, *J. Catal.*, 37 (1975) 449.
24. R.M.J. Fiederow, B.S. Chabor and S.E. Wanke, *J. Catal.*, 51 (1978) 193.
25. D.J.C. Yates, L.L. Murrell and E.B. Prestridge, *J. Catal.*, 57 (1979) 41.
26. P.R. Watson and G.A. Somorjai, *J. Catal.*, 72 (1981) 3.
27. T.P. Wibon, P.H. Kasai and P.C. Ellgen, *J. Catal.*, 69 (1981) 193.
28. R. Kramer and M. Andre, *J. Catal.*, 58 (1979) 287.
29. R.R. Cavanagh and J.T. Yates, Jr., *J. Catal.*, 68 (1981) 22.
30. D. Bianchi, M. Lacroix, G. Pajonk and S.J. Teichner, *J. Catal.*, 59 (1979) 467.
31. J.A. Konvalinka and J.J.F. Scholten, *J. Catal.*, 48 (1977) 374.
32. W. Eberhardt, F. Greuter and E.W. Plummer, *Phys. Rev. Lett.*, 46 (1981) 1085.
33. J.Y. Yates, Jr., C.H.F. Peden, J.E. Houston and D.W. Goodman, *Surface Sci.*, 160 (1985) 37.
34. J.C. Vis, H.F.J. van 't Blik, T. Huizinga, J. van Grondelle and R. Prins, *J. Catal.*, 95 (1985) 333.
35. J.C. Vis, H.F.J. van 't Blik, T. Huizinga, J. van Grondelle and R. Prins, *J. Molec. Catal.*, 25 (1984) 367.
36. D.C. Koningsberger and D.E. Sayers, *Solid State Ionics*, 16 (1985) 23.
37. B.J. Kip, J. van Grondelle, J.H.A. Martens and R. Prins, *Appl. Catal.* 26 (1986) 353. Chapter 3 of this thesis.
38. J.B.A.D. van Zon, D.C. Koningsberger, H.F.J. van 't Blik and D.E. Sayers, *J. Chem. Phys.*, 82 (1985) 5742.
39. D.C. Koningsberger, J.B.A.D. van Zon, H.F.J. van 't Blik, G.J. Visser, R. Prins, A.N. Mansour, D.E. Sayers, D.R. Short and J.R. Katzer, *J. Phys. Chem.*, 89 (1985) 4075.
40. D.C. Koningsberger, H.F.J. van 't Blik, J.B.A.D. van Zon and R. Prins, *Proc. of the 8th Int. Congr. on Catal. (Berlin, 1984)*, p. V-123.
41. F.W. Lytle, R.B. Greegor, E.C. Marques, D.R. Sandstrom, G.H. Via and J.H. Sinfelt, *J. Catal.*, 95 (1985) 546.
42. G.H. Via, J.H. Sinfelt and F.W. Lytle, *J. Chem. Phys.*, 71 (1979) 690.
43. G.H. Via, G. Meitzner, F.W. Lytle and J.H. Sinfelt, *J. Chem. Phys.*, 79 (1983) 1527.
44. T. Huizinga, J. van Grondelle and R. Prins, *Appl. Catal.*, 10 (1984) 199.
45. J.W. Geus, in "Preparation of Catalysts III" (G. Poncelet, P. Grange and P.A. Jacobs, Eds.), p. 1. Elsevier, Amsterdam, 1983.
46. B.K. Teo and P.A. Lee, *J. Am. Chem. Soc.*, 101 (1979) 2815.

47. F.B.M. Duivenvoorden, D.C. Koningsberger, Y.S. Uh and B.C. Gates, *J. Am. Chem. Soc.*, 108 (1986) 6254.
48. F.B.M. Duivenvoorden, B.J. Kip, D.C. Koningsberger and R. Prins, to be published.
49. A. Crucq, L. Degols, G. Lienard and A. Frennet, *Acta Chim. Acad. Sci. Hung.*, 111 (1982) 547.
50. A. Crucq, L. Degols, G. Lienard and A. Frennet, to be published.
51. L.C.X. De Menorval and J.P. Fraissard, *Chem. Phys. Lett.*, 77 (1981) 309.
52. J. Sanz and J.M. Rojo, *J. Phys. Chem.*, 89 (1985) 4974.
53. P. Wynblatt and N.A. Gjostein, *Progr. Solid State Chem.*, 9 (1975) 21.
54. G.G. Hlatky and R.H. Crabtree, *Coord. Chem. Rev.*, 65 (1985) 1.
55. R. Dutartre, P. Bussiere, J.A. Dalmon and G.A. Martin, *J. Catal.*, 59 (1979) 382.
56. J.A. Dalmon, C. Mirodatos, P. Turlier and G.A. Martin, in "Spillover of adsorbed species" (G.M. Pajonk, S.J. Teichner and J.E. Germain, Eds.) *Studies in surface science and catalysis*, vol. 17, p. 169. Elsevier, Amsterdam, 1983.
57. R.B. McLellan and W.A. Oates, *Acta Met.*, 21 (1973) 181.
58. P.B. Wells, *J. Catal.*, 52 (1978) 498.
59. R.J. Behm, K. Christmann, G. Ertl, V. Penka and R. Schwankner, in "The structure of surfaces" (M.A. van Hove and S.Y. Tong, Eds.), p. 257. Springer Verlag, Berlin, 1985; K. Christmann, to be published.
60. I. Toyoshima and G.A. Somorjai, *Catal. Rev.*, 19 (1979) 105.
61. C. Minot, B. Bigot and A. Hariti, *J. Am. Chem. Soc.*, 108 (1986) 196.
62. G.J. Kubas, R.R. Ryan, B.I. Swanson, P.J. Vergamini and H.J. Wasserman, *J. Am. Chem. Soc.*, 106 (1984) 451.
63. R.K. Upmacis, G.E. Gadd, M. Poliakoff, M.B. Simpson, J.J. Turner, R. Whyman and A.F. Simpson, *J. Chem. Soc. Chem. Commun.*, (1985) 27.
64. S.P. Church, F.W. Grevels, H. Hermann and K. Schaffner, *J. Chem. Soc. Chem. Commun.*, (1985) 30.
65. R.H. Crabtree and M. Lavin, *J. Chem. Soc. Chem. Commun.*, (1985) 794.
66. R.L. Sweany, *J. Am. Chem. Soc.*, 107 (1985) 2374.
67. R.H. Morris, J.F. Sawyer, M. Shiralian and J.D. Zubkowski, *J. Am. Chem. Soc.*, 107 (1985) 5581.
68. Compare also the abstracts of papers presented at the 191 st Meeting of the Am. Chem. Soc., New York, April 1986, Symposium on hydrogen-rich organometallic and inorganic complexes.
69. K. Wade, *Chem. Britain*, 11 (1975) 177; *Adv. Inorg. Chem. Radiochem.*, 18 (1976) 1.
70. D.M.P. Mingos, *J. Chem. Soc. Dalton Trans.*, (1974) 133; *ibid* (1976) 1173.
71. J.W. Lauher, *J. Am. Chem. Soc.*, 100 (1978) 5305; *ibid* 101 (1979) 2604.

72. B.K. Teo, *J. Chem. Soc. Chem. Commun.*, (1983) 1362; *Inorg. Chem.*, 23 (1984) 1251.
73. L. Garlaschelli, S.I. Khan, R. Bau, G. Longini and T.F. Koezle, *J. Am. Chem. Soc.*, 107 (1985) 7212.

Chapter 5

THE EFFECT OF CHLORINE IN THE HYDROGENATION OF CARBON MONOXIDE TO OXYGENATED PRODUCTS AT ELEVATED PRESSURE ON Rh AND Ir ON SiO₂ AND Al₂O₃

The catalytic behaviour of silica- and alumina-supported rhodium and iridium catalysts in synthesis gas reaction at elevated pressures was investigated. Temperature programmed reduction and hydrogen chemisorption measurements were used to characterize the catalysts. Rhodium was more active than iridium and had a better selectivity to higher hydrocarbons and C₂-oxygenates. For rhodium on silica high oxo-selectivities were obtained (40%), while on chlorine containing alumina this selectivity was rather low. When a chlorine-free metal precursor was used or when special pretreatments were applied to a RhCl₃/Al₂O₃ catalyst, oxo-selectivities of rhodium on alumina were also rather high (30%).

5.1 INTRODUCTION

The reaction of CO and H₂ over group VIII metals yields a wide range of products, such as alkanes, olefins and oxygenated hydrocarbons, the latter being the most interesting from an economic point of view. In recent investigations on supported rhodium catalysts a large percentage of oxygenated hydrocarbons has been reported (methanol, ethanol, acetaldehyde and acetic acid) [1-7]. The activity and selectivity depended markedly on the support and promoters. Ichikawa [2-4] used various oxides to support metal carbonyl clusters, and found better selectivities towards oxygenates on basic oxides than on acidic oxides at atmospheric pressures or below. Rh/ZnO and Rh/MgO mainly produced methanol, while on Rh/La₂O₃ the main product was ethanol and Rh/SiO₂ only produced hydrocarbons. Bhasin and O'Connor observed that Rh/SiO₂ can also produce C₂-oxygenates (ethanol, acetaldehyde and acetic acid) with selectivities up to 80 % [8] at higher pressures (7 MPa, high pressure assists in shifting equilibria to the oxygenated products side). Since rhodium can produce C₂-oxygenates and platinum was reported to produce large amounts of methanol [9], it might be of

interest to also investigate iridium in synthesis gas reaction at elevated pressures.

The mechanism for the formation of oxygenated products has not been elucidated so far. Recently Takeuchi and Katzer [10] and Tamaru *et al.* [11] demonstrated that the formation of methanol takes place by hydrogenation of nondissociatively adsorbed carbon monoxide. According to Watson and Somorjai [5-6] and Driessen *et al.* [12], the active sites for this reaction are metal ions. For C_2 -oxygenates, different mechanisms have been proposed. Takeuchi and Katzer [13] suggested a complicated mechanism involving CO insertion into adsorbed carbene species resulting in an adsorbed ketene or oxirene intermediate, thus indicating a common C_2 -intermediate for C_2 -hydrocarbons and C_2 -oxygenates. The Schulz-Flory distribution of hydrocarbons and oxygenates support this conclusion [14]. On the other hand Van den Berg *et al.* [1] and Tamaru *et al.* [7] proposed a mechanism in which carbon monoxide insertion in CH_x-Rh^{n+} intermediates takes place, leading to C_2 -oxygenates. In this mechanism C_1 -hydrocarbons and C_2 -oxygenates have a common intermediate.

In this work, the catalytic behaviour in synthesis gas reaction at elevated pressure (4 MPa) of Al_2O_3 - and SiO_2 -supported rhodium and iridium catalysts has been studied. Special attention has been paid to the effect of chlorine remaining on the support after reduction of catalysts prepared with metal chloride precursors. This chlorine might influence the acidity of the catalyst and the amount of metal ions present in the reduced catalyst and therefore the catalytic behaviour.

5.2 EXPERIMENTAL

5.2.1 Catalyst preparation

Catalysts were prepared by the incipient wetness technique using $RhCl_3 \cdot xH_2O$, $Rh(NO_3)_3 \cdot xH_2O$, $H_2IrCl_6 \cdot xH_2O$, $IrCl_3 \cdot xH_2O$ and $Ir(NO_3)_3$ in aqueous solution. SiO_2 from Grace (Type S.D. 2-324.382, surface area $290 \text{ m}^2 \text{ g}^{-1}$, pore volume 1.2 ml g^{-1}) and $\gamma-Al_2O_3$ from Ketjen (Type 000-1.5E, surface area $200 \text{ m}^2 \text{ g}^{-1}$, pore volume 0.6 ml g^{-1}) were used as support material. Impregnated catalysts were dried in air at 395 K for 16 h (heating rate 2 K min^{-1}). Some catalysts were calcined in air at 723 K for 2 h. *In situ* reduction of the catalysts was carried out in a high pressure reactor in pure hydrogen at 0.1 MPa, using a temperature ramp of 5 K min^{-1} between 298 K and 623 K, and holding that final temperature for 0.5 h.

5.2.2 Characterization techniques

Reducibility of the catalysts was studied by temperature-programmed reduction (TPR) using the apparatus described extensively in ref. [15-16]. Reduction was done in a flow of 4% H₂ in Ar at a heating rate of 5 K min⁻¹. Volumetric hydrogen chemisorption measurements were performed in a conventional glass system at 298 K. After reduction in flowing purified hydrogen for 1 h at 673 K (heating rate 8 K min⁻¹), evacuation at 673 K for 0.5 h, hydrogen admission at 473 K and cooling to room temperature, desorption isotherms were measured at room temperature. Following the method of Benson and Boudart [17] the total amount of chemisorbed H atoms was obtained by extrapolating the linear high pressure region (0.02 < P < 0.10 MPa) of the isotherm to zero pressure.

5.2.3 The CO-H₂ reaction

Hydrogenation of carbon monoxide was carried out in a continuous flow stainless-steel high pressure fixed-bed reactor. After *in situ* reduction of the catalysts (see catalyst preparation), the reactor was cooled down to the reaction temperature and pressurized with H₂ to the desired level. After stabilization an additional CO flow was started. All catalysts were measured under the same reaction conditions (GHSV = 4000 l l⁻¹ h⁻¹, H₂/CO = 3, P = 4 MPa). The reaction temperature was adjusted so that conversion of CO was around 2.0 %. The reactor effluent was analyzed using a column with Chromosorb 102 (3 m) and Porapak T (0.6 m) in series operated at 423 K. Peak area integration was carried out with a Nelson Analytical Interface-IBM PC configuration.

5.3 RESULTS AND DISCUSSION

5.3.1 Characterization

Hydrogen chemisorption measurements show that the silica-supported systems were well dispersed (H/Ir=0.7 for 2.5 wt% Ir and H/Rh=0.6 for 1.5 wt% Rh), and that the alumina-supported systems were even highly dispersed (H/Ir=1.7 for 2.5 wt% Ir and H/Rh=1.6 for 1.4 wt% Rh) as shown in Tables 5.1 and 5.2. Since most of the H/M ratios exceed unity, it is impossible to calculate particle sizes and dispersions from chemisorption data and use these for calculating turnover frequencies. Therefore, the H/M values were only used to compare dispersions in a not quantitative way.

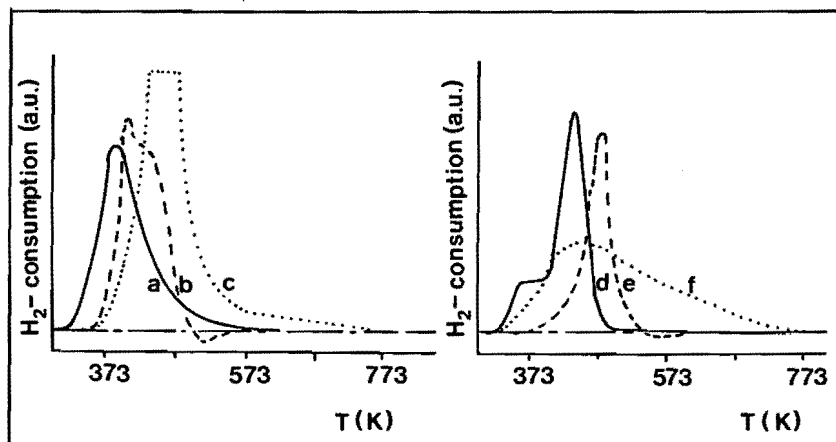


FIGURE 5.1: TPR profiles of impregnated catalysts dried at 393 K for 16 h. (a) $\text{RhCl}_3/\text{Al}_2\text{O}_3$, (b) $\text{IrCl}_3/\text{Al}_2\text{O}_3$, (c) $\text{Rh}(\text{NO}_3)_3/\text{Al}_2\text{O}_3$, (d) $\text{RhCl}_3/\text{SiO}_2$, (e) $\text{IrCl}_3/\text{SiO}_2$, (f) $\text{RhCl}_3/\text{Al}_2\text{O}_3$, calcined at 723 K, 2 h.

The TPR profiles of several catalysts are presented in Figure 5.1. The reduction of the silica-supported catalysts occurred at significant higher temperatures than the reduction of the alumina-supported catalysts (compare 5.1-a and -d, -b and -e). Figure 5.1-c shows that when a metal-nitrate precursor is used, the nitrate also reduces during the TPR-run, causing a huge hydrogen consumption. From these experiments it can be concluded that reduction at 623 K for 0.5 h in pure hydrogen will be sufficient to complete reduce the Rh and Ir catalysts, except may be for the calcined $\text{RhCl}_3/\text{Al}_2\text{O}_3$ sample, for which reduction during TPR was complete only at 773 K.

5.3.2 The CO- H_2 reaction

The catalytic properties of the various rhodium and iridium catalysts in the synthesis gas reaction at standard conditions after 11 h time on stream are shown in Tables 5.1 and 5.2. To keep the conversion below 5% (differential conditions) and above 0.5% (necessary for accurate product analysis), catalysts were tested at different temperatures between 506 and 633 K.

$\text{RhCl}_3/\text{Al}_2\text{O}_3$ catalysts (1.5 wt% Rh), dried at 383 K for 16 h before *in situ* reduction (Table 5.1-1) mainly produced methane, but also some methanol, dimethylether, ethanol, ethylmethylether, acetaldehyde and

TABLE 5.1: CO + H₂ reaction over various 1.5 wt% rhodium catalysts supported on Al₂O₃ and SiO₂.^a

no.	catalyst system ^b	H/Rh	Acti- vity ^c	Selectivity (%C) ^d				
				CH ₄	C ₂ ⁺ ^e	tot. ^f C ₁ -OH	tot. ^g C ₂ -OH	tot. ^h oxo
1	RhCl ₃ /Al ₂ O ₃ ⁱ , 1.8 mol% Cl	1.6	2.3	72.0	16.3	3.5	3.7	11.1
2	RhCl ₃ /SiO ₂ ^j , 0.1 mol% Cl	0.6	0.6	48.0	11.3	26.7	14.0	40.7
3	Rh(NO ₃) ₃ /Al ₂ O ₃	1.3	0.6	45.4	14.4	27.5	11.1	38.6
4	Rh(NO ₃) ₃ /Al ₂ O ₃ , calcined at 723 K	1.6	1.8	50.8	11.9	19.5	14.1	35.5
5	Rh(NO ₃) ₃ /Al ₂ O ₃ , calcined at 723 K, HCl treated, 1.4 mol% Cl	1.4	0.9	61.3	24.9	9.3	0.0	11.7
6	Rh(NO ₃) ₃ /SiO ₂ ^k	0.4	1.1	44.2	7.1	35.6	13.1	48.6
7	RhCl ₃ /Al ₂ O ₃ , 4% H ₂ O	1.6	2.6	63.9	4.1	14.7	14.8	29.5
8	RhCl ₃ /Al ₂ O ₃ , 1% H ₂ O ^l , 1.8 mol% Cl	1.6	1.5	72.8	15.3	4.9	4.9	11.9
9	RhCl ₃ /Al ₂ O ₃ , 1% H ₂ O, heating rate during reduc- tion 30 K min ⁻¹ , 1.5 mol% Cl	1.6	2.2	60.1	7.3	16.0	12.6	30.8
10	RhCl ₃ /Al ₂ O ₃ , 1% H ₂ O in- jection during reduction, 0.9 mol% Cl	1.3	4.0	57.0	5.8	9.5	17.0	29.6
11	RhCl ₃ /Al ₂ O ₃ , calcined	1.6	3.1	65.7	4.7	13.1	12.1	26.4
12	RhCl ₃ /Al ₂ O ₃ , calcined, reduction at 723 K	1.6	1.9	60.1	14.7	8.5	11.9	22.0

(a) T_{react} = 503 K, unless stated otherwise. (b) standard reduction conditions (see experi-
mental). (c) Activity in mmol CO (mol Rh)⁻¹ s⁻¹. (d) calculated by carbon efficiency. (e)
C₂⁺ = C₂ + C₃ + C₄ hydrocarbons. (f) tot. C₁-OH = C₁-OH + C₁-O-C₁ + 1/3
C₂-O-C₁. (g) tot. C₂-OH = C₂-OH + 2/3 C₂-O-C₁. (h) tot.oxo = tot.C₁-OH +
tot.C₂-OH + C₂=O. (i) dried *in situ* at 383 K, 16 h before reduction. (j) T_{react} = 623 K.
(k) T_{react} = 628 K. (l) T_{react} = 506 K.

TABLE 5.2: CO + H₂ reaction over various 1.5 wt% iridium catalysts supported on Al₂O₃ and SiO₂.^a

no.	catalyst system ^a	wt% Ir	H/Ir	Temp. (K)	Acti- vity ^b	Selectivity (%C) ^c		
						CH ₄	C ₂ ⁺	tot.oxo ^d
1	H ₂ IrCl ₆ /Al ₂ O ₃ ^e	2.5	1.7	593	2.5	73.2	15.6	11.2
2	H ₂ IrCl ₆ /Al ₂ O ₃ , 4% H ₂ O, heating rate reduction 30 K min ⁻¹	2.5	--	591	1.8	69.1	18.4	12.5
3	IrCl ₃ /Al ₂ O ₃ , 4% H ₂ O, heating rate reduction 30 K min ⁻¹	2.6	--	563	3.6	58.8	22.6	18.6
4	Ir(NO ₃) ₃ /Al ₂ O ₃	1.3	1.2	598	0.8	64.5	17.7	17.8
5	IrCl ₃ /SiO ₂	2.5	0.7	633	1.0	72.6	16.3	11.1
6	Ir(NO ₃) ₃ /SiO ₂	1.0	0.6	633	0.9	70.4	19.8	9.8

(a) Reduced in pure H₂, heating rate 5 K min⁻¹, 0.5 h at 623 K (b) Activity in mmol converted CO (mol Ir)⁻¹ s⁻¹. (c) Calculated by carbon efficiency. (d) tot.oxo = C₁-OH + C₁-O-C₁. (e) dried *in situ* at 383 K, 16 h before reduction.

higher hydrocarbons. The total oxo-selectivity was 11 %. The ethers are believed to be formed by dehydration of alcohols on acidic sites of the support. During the first hours of reaction a marked deactivation was observed, while after several hours all catalysts tested showed a small and constant relative deactivation (0-2 % h⁻¹). Total oxo-selectivity increased during the first hours and became constant after about 4 h.

The H₂IrCl₆/Al₂O₃ catalyst (2.5 wt% Ir, dried at 383 K before *in situ* reduction, cf. Table 5.2-1) differed significantly from the rhodium catalyst. To obtain an activity similar to that of the rhodium catalyst the reaction temperature had to be increased to 593 K. Using a value of 100 kJ mol⁻¹ for the total activation energy [1,7,18], it can be calculated that Rh/Al₂O₃ is 15 times more active than Ir/Al₂O₃. This difference in activity was also reported by Vannice [18], although he measured at atmospheric pressure. Ir/Al₂O₃ also showed a completely different selectivity. It only produced

methane, methanol, dimethylether and higher hydrocarbons, while C₂-oxygenates were absent. The total oxo-selectivity was 11 %. The chain-growth probability was found to be higher for the rhodium than for the iridium catalysts. The observed differences might be explained on the basis of the CO dissociation activity of transition metals [19]. Metals that easily dissociate CO catalyze hydrocarbon synthesis (i.e. Ru and Fe), metals that adsorb CO non-dissociatively at room temperature catalyze synthesis of methanol (i.e. Cu, Pd and Pt) [20]. Rh lies between Ru and Pd and catalyzes the formation of both alcohols and hydrocarbons from CO + H₂. Since it is capable of synthesizing both types of compounds, small effects can markedly alter its selectivity. There is no consensus in the literature about iridium. Poutsma *et al.* [20] reported non-dissociative adsorption of carbon monoxide on Ir, while van den Berg [21] reported dissociative adsorption. The results of the present study suggests that both Rh and Ir partly adsorb CO nondissociatively under reaction conditions and that Rh dissociates CO more easily than Ir. Vannice [18] suggested that the difference in activity between Rh and Ir is caused by a difference in heat of adsorption of CO (for Ir around 210 kJ mol⁻¹, for Rh around 185 kJ mol⁻¹).

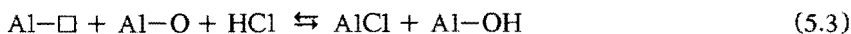
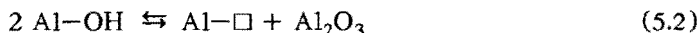
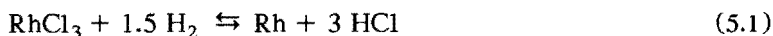
The silica-supported rhodium catalyst (RhCl₃/SiO₂, 1.5 wt% Rh, dried at 383 K for 16 h before *in situ* reduction, Table 5.1-2) was less active than the 1.5 wt% Rh/Al₂O₃ catalyst, since the reaction temperature had to be increased up to 623 K to obtain a corresponding conversion. In spite of this high temperature, its oxo-selectivity was much better, even though thermodynamically high temperature disfavours formation of oxygenates. Considerable amounts of methanol, dimethylether, ethanol and ethylmethylether were formed and total oxo-selectivity was 41 %.

The observed difference in oxo-selectivity between the alumina- and silica-supported rhodium catalyst might be due to the difference in chlorine content of the reduced catalysts. XPS showed that after reduction of the dried RhCl₃/Al₂O₃ and RhCl₃/SiO₂ (heating rate 5 K min⁻¹ 623 K) there was a large difference in chlorine content. The surface of the reduced Rh/Al₂O₃ contained 1.8 mol% Cl, whereas the surface of the reduced Rh/SiO₂ contained only 0.1 mol% Cl. To further investigate this chlorine effect, Al₂O₃ was impregnated with Rh(NO₃)₃ (Table 5.1-3). This catalyst showed a dispersion (H/Rh=1.3) comparable to that of RhCl₃, a relatively low activity and a high oxo-selectivity (39 %). Calcination of the dried Rh(NO₃)₃/Al₂O₃ catalyst before reduction (Table 5.1-4) resulted in an increased activity without much loss of oxo-selectivity (35 %), while the selectivity to C₂-oxygenates was increased. Thus, when a chlorine-free

precursor is used, the oxo-selectivity can amount to about 40 % on Rh/Al₂O₃, significantly higher than the 10 % obtained with the dried RhCl₃/Al₂O₃. Treating the calcined Rh(NO₃)₃/Al₂O₃ with gaseous HCl at 423 K in N₂ atmosphere before reduction (Table 5.1-5) caused a dramatically decrease in the oxo-selectivity. Only small amounts of methanol, dimethylether and acetaldehyde were formed, and ethanol and ethylmethylether were not formed at all and the total oxo-selectivity was only 12 %. Impregnation of SiO₂ with Rh(NO₃)₃ (Table 5.1-6) also resulted in a catalyst with a high oxo-selectivity (49 %). Further investigations showed that the pretreatment procedure before synthesis gas reaction has an important influence on the oxo-selectivity (Table 5.1-7,8,9,10,11,12). Normal reduction (heating rate 5 K min⁻¹, final temperature 623 K) of a rather wet RhCl₃/Al₂O₃ (stored for half a year and containing 4 wt% H₂O) resulted in a high oxo-selectivity (30%). RhCl₃/Al₂O₃ only stored for one week (1% H₂O) and reduced at 5 K min⁻¹ showed a low oxo-selectivity (12%), while reduction of this catalyst at 30 K min⁻¹ improved oxo-selectivity to 31%. Reduction of a dried RhCl₃/Al₂O₃ in the presence of water vapour (water injection in the reactor during reduction) also increased the oxo-selectivity (30%, Table 5.1-10). These results indicate that the water vapour pressure during reduction of RhCl₃/Al₂O₃ is an important factor. The observed differences can not be explained by differences in metal dispersions as can be seen in Table 5.1. RhCl₃/Al₂O₃, calcined at 723 K for 2 h followed by reduction at 623 K (Table 5.1-11) had a relatively high oxo-selectivity (26%), reduction of this catalyst at 723 K showed a somewhat lower oxo-selectivity caused by a decreased C₁-OH selectivity (Table 5.1-12).

For the alumina-supported iridium catalysts the differences in oxo-selectivity were smaller. Reduction of dried H₂IrCl₆/Al₂O₃ at 5 K min⁻¹, final temperature 623 K (Table 5.2-1) resulted in 11 % oxo-selectivity. Ir(NO₃)₃/Al₂O₃ (Table 5.2-4) showed an oxo-selectivity of 18%. Thus, also for iridium the chlorine-free precursor gives a higher oxo-selectivity. Reduction of the chlorine containing iridium catalysts in the presence of water vapour resulted in oxo-selectivities of 13 % and 19 % (Table 5.2-2,3). However, for silica-supported iridium catalysts the oxo-selectivities were low (10%).

The beneficial effect of water during reduction is due to the influence of water on the chlorine content of the catalyst. As the XPS results show, during reduction of RhCl₃ on Al₂O₃ a substantial part of the chlorine is retained by the catalyst. Most of this chlorine will be on the support, according to the reactions:



A high water vapour pressure during reduction of the metal chloride prevents retention of the chlorine by the alumina support. For SiO_2 the reaction corresponding to (2,3) is much less likely and therefore chlorine retention on SiO_2 is low and the oxo-selectivity is high.

Several explanations might be considered for the detrimental effect of chlorine on the oxo-selectivity. Since rhodium ions have been proposed to be the active sites for methanol formation [5-6,12], an explanation in terms of a change in (in)stability of such rhodium ions might be given. Chlorine has been said to stabilize transition metal ions under reducing conditions and therefore an explanation for the decreased methanol formation when chlorine is present on the catalyst might be that chlorine stabilizes higher inactive oxidation states of Rh. Another explanation along these lines might be that chlorine deactivates cation sites by binding too strongly and reducing the adsorption of the synthesis gas reactants.

A much more likely explanation, which can explain all observations in a natural way, is based on the assumption that oxo-products such as methanol and ethanol are formed in primary reactions of synthesis gas over rhodium and are subsequently transformed in secondary reactions into hydrocarbons. It is well known that ethanol is easily dehydrated to ethene over even weakly acidic catalysts. Methanol on the other hand is only dehydrated to dimethylether over acid catalysts, but in combination with a noble metal hydrocarbons are formed. Thus a $\text{Pt}/\text{Al}_2\text{O}_3$ catalyst transformed methanol into methane at 473 K with high conversion [22].

The negative influence of chlorine on the activity is not completely understood. Possibly chlorine enhanced the formation of coke, or alternatively it covers part of the active metal area.

In summary, $\text{Rh}/\text{Al}_2\text{O}_3$ was more active and had a higher chain-growth probability than $\text{Ir}/\text{Al}_2\text{O}_3$. Rhodium catalysts produced methanol, dimethylether, ethanol, ethylmethylether, acetaldehyde and hydrocarbons, while iridium catalysts produced only methanol, dimethylether and hydrocarbons. Chlorine, trapped by vacancies on the alumina surface, formed by dehydroxylation of OH-groups, disfavoured the formation of oxygenates in the hydrogenation of CO. On SiO_2 this effect was not observed. High water vapour pressure during the reduction of metal chloride on alumina

prevented the trapping the chlorine and high oxo-selectivities were measured in that case. Calcination of the $\text{RhCl}_3/\text{Al}_2\text{O}_3$ system caused removal of the chlorine resulting in high oxo-selectivities.

Although the influences of several supports [2-6,9] and promoters [3] have been described in the literature, the here observed effect has not been mentioned yet. Our study demonstrates that, in comparing the catalytic activity and selectivity of metal catalysts for CO hydrogenation the influence of the metal salt precursor and the pretreatment procedures should be taken into account.

5.4 REFERENCES

1. F.G.A. van den Berg, J.H.E. Glezer and W.M.H. Sachtler, *J. Catal.*, 93 (1985) 340.
2. M. Ichikawa, *Bull. Chem. Soc. Jap.*, 51 (1978) 2268.
3. M. Ichikawa, *Bull. Chem. Soc. Jap.*, 51 (1978) 2273.
4. M. Ichikawa, *J. Chem. Soc., Chem. Comm.*, (1978) 566.
5. P.R. Watson and G.A. Somorjai, *J. Catal.*, 72 (1981) 347.
6. P.R. Watson and G.A. Somorjai, *J. Catal.*, 74 (1982) 282.
7. H. Orita, S. Naito and K. Tamaru, *J. Catal.*, 90 (1984) 183.
8. M.M. Bhasin and G.L. O'Connor, Belgian Patent 824822, to Union Carbide Corp., 1975.
9. M. Ichikawa and K. Shikakura, *Proc. 7th Int. Congr. Catal.*, Tokyo (1980) 925.
10. A. Takeuchi and J.R. Katzer, *J. Phys. Chem.*, 85 (1981) 937.
11. Y. Kobori, H. Yamasaki, S. Naito, T. Onishi and K. Tamaru, *Chem. Lett.* (1983) 553.
12. J.M. Driessen, E.K. Poels, J.P. Hindermann and V. Ponec, *J. Catal.*, 82 (1983) 20.
13. A. Takeuchi and J.R. Katzer, *J. Phys. Chem.*, 86 (1982) 2438.
14. A. Takeuchi, J.R. Katzer and R.W. Creceley, *J. Catal.*, 82 (1983) 479.
15. H. Boer, W.J. Boersma and N. Wagstaff, *Rev. Sci. Instr.*, 53 (1982) 439.
16. T. Huizinga, J. van Grondelle and R. Prins, *Appl. Catal.*, 10 (1984) 199.
17. J.E. Benson and M. Boudart, *J. Catal.*, 4 (1965) 704.
18. M.A. Vannice, *J. Catal.*, 37 (1975) 462.
19. J.R. Katzer, A.W. Sleight, P. Gajardo, J.B. Michel, E.F. Gleason and S. McMillan, *Far. Disc. Chem. Soc.*, 72 (1981) 121.
20. L. Poutsma, L.F. Elek, P.A. Ibarbia, A.P. Risch and J.A. Rabo, *J. Catal.*, 52 (1978) 157.

21. F.G.A. van den Berg, Thesis, Leiden University (1983).
22. C.W.R. Engelen, J.P. Wolthuisen and J.H.C. van Hooff, *Stud. Surf. Sci. Catal.*, 20 (1985) 391.

Chapter 6

PROMOTERS IN SYNTHESIS GAS REACTIONS

The possible effects of promoters in synthesis gas reactions are briefly reviewed. Furthermore, an explorative study of the promotion of Rh and Ir catalysts is described. The promoter is provided as support or as an additive to a Rh/SiO₂ catalyst.

Rh catalysts are superior to Ir catalysts with respect to the activity and C₂-oxygenate selectivity. The promotion by additives to Rh/SiO₂ is more effective than the promotion by the support. From the studied promoter oxides delivered as additives to Rh/SiO₂, V₂O₃, ThO₂ and MoO₃ resulted in high activities; MoO₃, Fe₂O₃ and La₂O₃ resulted in high methanol selectivities and V₂O₃, ThO₂, CeO₂, Cr₂O₃, MnO and TiO₂ resulted in high C₂-oxygenate selectivities.

6.1 INTRODUCTION

Promoters are often added to supported metal catalysts to improve the behaviour of the systems. A promoter by itself does not catalyze the reaction under study but can change the activity, selectivity and stability of the catalysts.

In syngas reactions, promoters are often used to increase the production of oxygenated compounds. E.g. the addition of alkali increases the activity and average molecular weight of hydrocarbons of industrial iron catalysts [1,2], and it improves the methanol selectivity of Pd/SiO₂ [3] and Cu/ZnO [4] catalysts. Mori *et al.* showed that addition of alkali metals to Pd/Al₂O₃ [5] and Ru/Al₂O₃ [6] resulted in a decreased CO dissociation rate.

Addition of transition metal oxides also results in dramatic changes of the catalytic behaviour. Mori *et al.* [7] reported that addition of V₂O₅, Nb₂O₅, WO₃ and Re₂O₇ to a Ru/Al₂O₃ catalyst resulted in an increased CO dissociation rate. Ichikawa *et al.* [8] studied the production of ethanol for a series of silica-supported rhodium catalysts promoted with numerous metal oxides (see Figure 6.1). Vanadium oxide-promoted Rh/SiO₂ exhibited the highest ethanol formation rate, while thorium oxide-promoted Rh/SiO₂ exhibited the highest ethanol selectivity. Furthermore, Ichikawa *et al.* reported the enhancement of CO dissociation and stabilization of oxygen

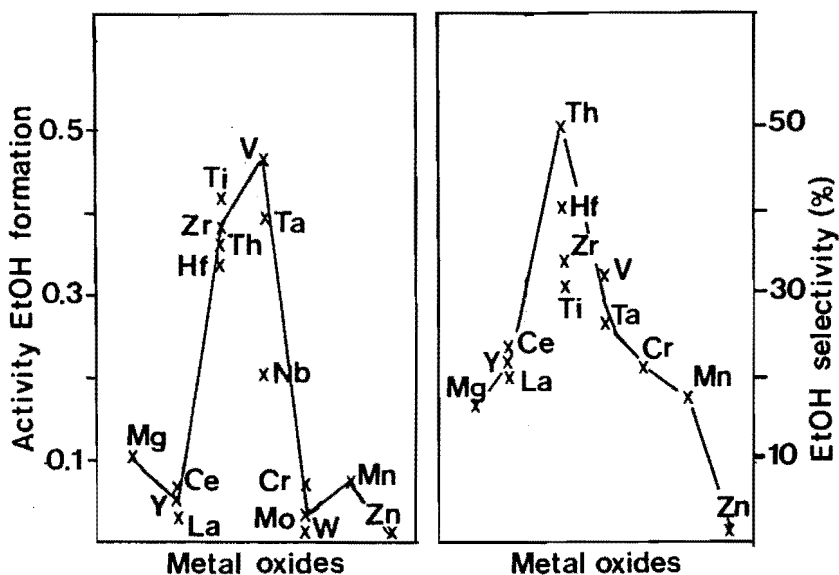


FIGURE 6.1: Yield and selectivity of ethanol for syngas reaction over Rh/SiO₂ promoted by various oxides, according to ref. [8].

intermediates for Fe-, Mn- and Ti-oxide promoted Rh/SiO₂ catalysts [9]. Van den Berg *et al.* [10] reported the promotion of Rh/SiO₂ by Mn- and Mo-oxide. These promoters resulted in an increased activity and C₂-oxygenate selectivity. Kiennemann *et al.* [11] reported CeO₂ to be very effective for the promotion of Rh/SiO₂, the activity and ethanol selectivity for the promoted system was considerably higher than for the unpromoted Rh/SiO₂ system.

Supports, used to disperse the active metals, are not always inert, but can also act as a promoter. Thus, Ichikawa showed that Rh dispersed on oxides like ZnO and MgO mainly produced methanol, while Rh dispersed on ZrO₂, TiO₂ and La₂O₃ also produced significant amounts of C₂-oxygenates [12]. Katzer *et al.* [13] also observed a considerable influence of the support on the catalytic behaviour. Van der Lee *et al.* [14] and Bastien *et al.* [15] made a detailed study of the role of the support in V₂O₃-supported Rh catalysts and concluded that during catalyst preparation part of the V₂O₃ support is transported onto the Rh metal particles. This V₂O₃ on top of the Rh metal was believed to be responsible for the observed promoting effect.

As can be seen from these examples, promoters may affect catalyst behaviour in different ways. In this chapter we will briefly review the effects of promoters reported in literature (§ 6.2) and will present the results of an explorative study of promotion of Rh and Ir catalysts by addition of several oxides and by the use of several oxides as support.

6.2 Possible effects of promoters in syngas reactions

In this paragraph, we will briefly describe the effects of promoters in syngas reactions. For an extended review on this subject we refer to Van der Lee [16].

a. Decrease of the active metal surface area. Addition of a promoter can decrease the ensemble size of the metal catalyst sites by physical blocking part of the active metal surface area. Especially the dissociation of CO requires a large ensemble. Thus, Ponc *et al.* [17], Luyten *et al.* [18] and Bond *et al.* [19] reported a sharp decrease of CO hydrogenation activity when group VIII metals were alloyed with an inactive metal like Cu. Decreases in activity of Rh and Ru catalysts by addition of alkali or transition metal oxides might also be caused by this ensemble size effect.

b. Stabilization of metal ions. As reported by Poels *et al.* [20,21] and Hindermann *et al.* [22], methanol is formed over metal ions. Van den Berg *et al.* [10] suggested that metal ions are also necessary for the CO insertion reaction (dual-site mechanism). The results of Van der Lee *et al.* [14] showed, however, that there is not a sympathetic correlation between the C₂-oxygenate formation and the amount of metal ions. But at least for the methanol formation, the amount of metal ions is important. This amount can be influenced by the addition of a promoter oxide. The promoter oxide might form mixed oxides with the oxide of the active metal and might therefore influence the reducibility of the active metal.

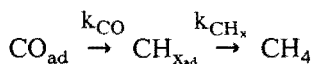
c. Neutralization of acid centers of the support. Acid sites of the support can influence the selectivity pattern by secondary reactions. E.g. alcohols can be dehydrated to ethers, esters and even to hydrocarbons [23]. Huang and Richardson [24] reported acid catalyzed formation of hydrocarbons by polymerization of CH_x groups, that could be suppressed by alkali addition, resulting in a decreased deactivation.

Additions of alkali metals or transition metal oxides can neutralize these acid sites and in this way change the properties of the catalyst [24-26].

d. Enhancement of the spreading of support material over the metal particle.

As already mentioned in § 1.2, certain types of support material cause a so-called SMSI effect, a suppression of the normal chemisorption capacity after high temperature reduction. This suppression is thought to be the result of spreading of the reduced support material over the metal particle and will result in a changed activity and selectivity pattern of the catalyst (see for instance references [14-16,25]). Spencer [27] observed an enhanced mobility and spreading of the "SMSI-support" when potassium compounds were added.

e. Activation of CO molecule. One of the essential steps in the formation of hydrocarbons and oxygenates is the dissociation of the adsorbed CO molecule. Mori *et al.* studied the influence of promoters on the dissociation of CO over Ru/Al₂O₃ catalysts using pulse surface reaction rate analysis, in which an emissionless infrared diffuse reflectance spectrometer cell is used as a pulse micro reactor and a flame ionisation detector is located downstream from the cell [5-7]. With this technique they could separately determine the rate constants for CO dissociation and subsequent hydrogenation, k_{CO} and k_{CH_x} respectively:



Their results are summarized in Figure 6.2. Clearly, the V-, Nb-, Mo-, W- and Re-oxide promoters increased the CO dissociation and suppressed the hydrogenation rate [7]. It must however, be noticed that these measurements are performed in a hydrogen rich atmosphere, in other words not under steady-state conditions. The increase in CO dissociation can explain the often observed increase in activity due to promotion by transition metal compounds [9,14-16,28].

Several models have been proposed for the activation of CO by the promoter oxide. Mori *et al.* [6,7] postulated a hydroxycarbene (M-CHOH) intermediate for C-O bond dissociation, based on an observed H₂-D₂ isotope effect for CO dissociation. A CO molecule is adsorbed on the metal, forming the M-CHOH intermediate. The promoter ion Pⁿ⁺ adjacent to the metal atom, to which the hydroxycarbene is attached, pulls the oxygen atom away from the M-CHOH fragment and forms a transition state that promotes the dissociation of CO to (CH_x)_{ad} and (OH)_{ad}. Simultaneously Pⁿ⁺ is oxidized to P⁽ⁿ⁺¹⁾⁺. The (OH)_{ad} species on P⁽ⁿ⁺¹⁾⁺ can be hydrogenated, forming H₂O and Pⁿ⁺. In this way the promoter oxide catalyzes the CO

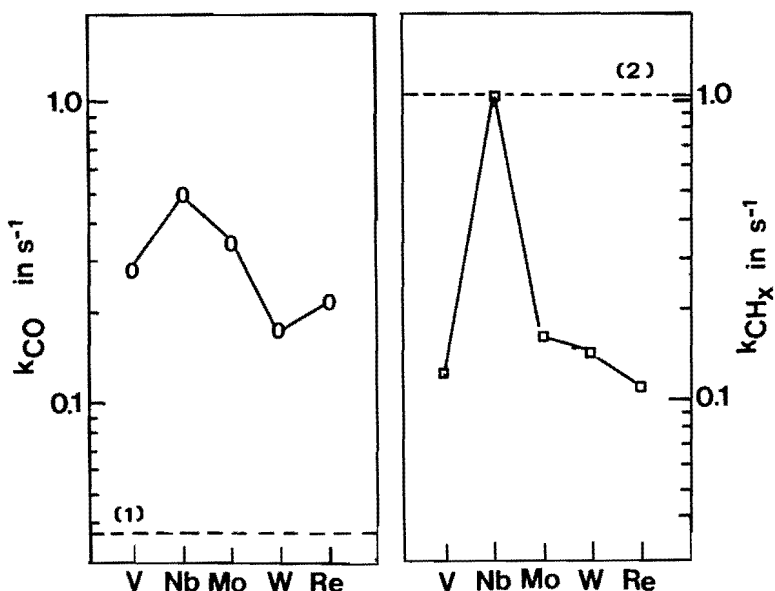


FIGURE 6.2: Rate constants of k_{CO} (o) and k_{CHx} (\square) at 445 K for the promoted Ru/Al₂O₃ catalysts. The dashed lines (1) and (2) represent k_{CO} and k_{CHx} at 445 K for the unpromoted Ru/Al₂O₃ catalyst, respectively, according to ref. [7].

dissociation by an oxidation/reduction cycle.

Burch *et al.* [29], Rieck and Bell [30] and Sachtler *et al.* [31,32] proposed a model based on the activation of CO by the interaction of a promoter ion with the oxygen atom of a chemisorbed carbonyl. This interaction was earlier extensively studied by Shriver *et al.* [33,34] for ligands in homogeneous transition metal catalysts. The ions of an electropositive metal (the promoter ion) on the surface of a metal particle might provide sites at which CO may be bonded with its carbon atom to a metal atom and with its oxygen atom to the promoter ion. This results in a weakened C-O bond, which shows up as a lowering of the CO stretching frequency in IR spectroscopy. Ichikawa *et al.* [9] and Sachtler *et al.* [28,31,32] indeed reported IR bands below 1750 cm^{-1} .

A third explanation is based on electronic arguments. The addition of the promoter will in this view increase or decrease the electron density on the active metal and in this indirect way change the properties of the active metal. Especially in the case of alkali addition, this effect is invoked by many authors [6,35-41]. The alkali additives showed electron-donor character, resulting in the weakening of the C-O bond due to the enhanced back-

donation of electrons from the metal to the antibonding 2π orbitals of adsorbed CO molecules [42]. This charge transfer can only occur when the alkali is present in the metallic form. However, under syngas reaction conditions, this will not be the case. Therefore Wilson *et al.* [43], studying alkali promotion of Rh-Mn/SiO₂ catalysts, suggested that the donation of electrons occurs by the negative counter ions of the added alkali.

Van Santen [44] proposed that when a positive charge is placed on the metal surface in the vicinity of CO, back-donation in the exposed and to a longer distance reaching antibonding π orbitals is enhanced by this electrostatic field, resulting in a weakened C-O bond.

f. Increase of CO insertion reaction. According to the now almost generally accepted mechanism (see Chapter 1), higher oxygenates are formed by CO insertion into a metal-alkyl chain. In organometallic reactions, an enhancement in the order of 10^3 for the CO insertion reaction in the presence of alkali metal ions, which are known to bind to carbonyl oxygen was reported [45], and aluminium trihalides bring about enhancement factors in the order of 10^8 [34]. Therefore, promoter ions in metal catalysts might increase the rate of CO insertion.

g. The promoter itself forms a catalytic center. The active centers for Cu/ZnO catalysts, used in methanol synthesis, were generally assumed to be the Zn sites of the ZnO support, whereas the role of Cu, present as C, is thought to be involved in hydrogen activation [46-48].

In a recent paper, we studied bimetallic Fe-Ir/SiO₂ catalysts [49]. Fukushima *et al.* [50], studying the same system, suggested that Ir is the active metal and Fe acts as a promoter. Our results however raise serious doubts about this conclusion.

Our results of the MoO₃-promoted Rh/SiO₂ catalysts [51] also indicate that the promoter oxide itself acts as a catalytic center, i.e. the Mo-ions are thought to be the active centers for methanol formation.

6.3 EXPERIMENTAL

6.3.1 Catalyst preparation

Catalysts were made by subsequent incipient wetness steps. After each impregnation step the catalysts were dried in air at 395 K for 16 h (heating rate 2 K min⁻¹) and subsequent calcination at 723 K for 3 h.

Various oxides were used as a support: Al₂O₃ (Ketjen 000-1.5E), SiO₂

(Grace Davison, type 113), TiO_2 (Tioxide, Eurotitania), ZnO (Merck), MgO (Merck), La_2O_3 (Merck), ZrO_2 (Merck), Nb_2O_5 (Merck), ThO_2 (Merck), WO_3 (Fluka AG) and MoO_3 (Merck). V_2O_3 was made by reduction of V_2O_5 (Merck) at 1100 K in pure hydrogen for 2 h (heating rate 10 K min^{-1}) and subsequent passivation.

Promoter oxides were added using: $\text{Mn}(\text{NO}_3)_2 \cdot 4\text{H}_2\text{O}$, $\text{Cr}(\text{NO}_3)_3 \cdot 9\text{H}_2\text{O}$, $[(\text{CH}_3)_2\text{CHO}]_4\text{Ti}$, $\text{Zr}(\text{NO}_3)_4$, $\text{La}(\text{NO}_3)_3 \cdot 6\text{H}_2\text{O}$, $(\text{NH}_4)_2\text{W}_4\text{O}_{13} \cdot 8\text{H}_2\text{O}$, $\text{Ce}(\text{NO}_3)_3 \cdot 6\text{H}_2\text{O}$, $\text{Fe}(\text{NO}_3)_3 \cdot 9\text{H}_2\text{O}$, $\text{RuCl}_3 \cdot x\text{H}_2\text{O}$, $\text{Co}(\text{NO}_3)_2 \cdot 6\text{H}_2\text{O}$, NH_4VO_3 , $(\text{NH}_4)_6\text{Mo}_7\text{O}_{24} \cdot 4\text{H}_2\text{O}$, $\text{Th}(\text{NO}_3)_4 \cdot x\text{H}_2\text{O}$.

Rhodium was added by impregnation with a solution of $\text{Rh}(\text{NO}_3)_3$ (Drijfhout, Amsterdam), iridium catalysts were made by impregnation with a solution of IrCl_3 (Drijfhout, Amsterdam). In case of the promoted Rh/SiO_2 and Ir/SiO_2 catalysts, first the promoter and then the active metal was impregnated.

6.3.2 CO hydrogenation reaction

The catalysts were tested at 4.0 MPa, $\text{H}_2/\text{CO} = 3.0$ and $\text{GHSV} = 4000 \text{ l l}^{-1} \text{ h}^{-1}$, using the apparatus described in Chapter 2.

6.4 RESULTS AND DISCUSSION

In Table 6.1 and 6.2, the results of CO hydrogenation over rhodium and iridium catalysts supported on various metal oxides are presented. The reactions were performed at different temperatures in order to measure at a comparable conversion level (around 2 %). To enable a comparison of the activities of the catalyst systems studied, activities were calculated at one temperature (538 K), using a total activation energy of 100 kJ mol^{-1} [10,25,52,53]. Clearly, large differences in activities were observed for the supported Rh catalysts (Table 6.1). Rh supported on TiO_2 and MoO_3 exhibits a high activity, while Rh supported on ZrO_2 , MgO and ZnO has a relatively low activity. The selectivity pattern is also highly dependent on the kind of support used. MgO - and ZnO -supported Rh catalysts have high methanol selectivities, as was already reported by Ichikawa [12]. WO_3 - MoO_3 - and Nb_2O_5 -supported Rh catalysts exhibit high hydrocarbon selectivities, while relatively high C_2 -oxygenate selectivities are obtained when SiO_2 , V_2O_3 and ThO_2 are used as support.

For almost all supports, the iridium catalysts exhibit a lower activity than the rhodium catalysts (compare Table 6.2 and 6.1). For the silica- and

TABLE 6.1: CO hydrogenation over 1.5 wt% Rh catalysts supported on several oxides. Experimental conditions: P = 4.0 MPa, GHSV = 4000 l l⁻¹ h⁻¹, H₂/CO = 3.0. All catalysts were reduced *in situ* at 723 K.

support	Temp (K)	corr. act. ^a	selectivity (%C) ^b					deact. % h ⁻¹
			CH ₄	C ₂ +	C ₁ OH ^c	C ₂ -oxy ^d	tot.oxo	
MgO	579	0.3	7.7	4.3	70.7	12.8	88.1	0.9
ZnO	583	0.2	1.4	0.5	98.1	0.0	98.1	0.4
La ₂ O ₃	523	1.4	26.9	5.5	58.5	7.5	67.6	n.a.
Al ₂ O ₃	501	8.3	46.3	6.6	22.4	21.6	47.1	0.4
SiO ₂	600	0.3	33.2	2.3	29.1	35.0	64.5	1.7
TiO ₂ ^e	473	34.5	31.7	17.5	20.8	27.5	50.9	n.a.
V ₂ O ₃	543	0.6	16.8	12.9	25.1	35.3	70.3	2.9
ThO ₂	535	1.4	35.6	7.3	11.6	41.0	57.2	3.8
MoO ₃	508	10.5	52.2	31.0	13.3	2.1	16.8	1.2
WO ₃	558	1.4	49.1	42.6	4.0	1.8	8.3	1.0
ZrO ₂	586	0.1	33.5	19.5	20.5	17.8	46.9	2.0
Nb ₂ O ₅	518	5.5	26.0	42.2	4.3	19.0	31.8	2.5

a. activity in mmol CO (mol Rh)⁻¹ s⁻¹ at 538 K, using E_{act} = 100 kJ mol⁻¹, b. selectivity calculated by carbon efficiency, c. total amount of C₁OH, including ethers and esters, d. total amount of C₂-oxygenates, including ethanol (and ethers, esters), acetaldehyde and acetic acid (including esters), e. 1.9 wt% Rh.

TABLE 6.2: CO hydrogenation of 2.5 wt% Ir catalysts supported on various oxides. For experimental conditions and notations see Table 6.1.

support	Temp (K)	corr. act.	selectivity (%C)				
			CH ₄	C ₂ +	C ₁ OH	C ₂ -oxy	tot.oxo
SiO ₂	623	0.05	72.6	16.3	11.1	0.0	11.1
Al ₂ O ₃	563	1.3	58.8	22.6	18.6	0.0	18.6
TiO ₂	536	2.3	40.6	31.0	21.2	5.6	28.4
V ₂ O ₃	523	5.3	35.7	18.8	27.3	12.8	44.0
La ₂ O ₃	593	0.1	40.1	4.8	44.5	4.8	49.3
ThO ₂	540	1.7	53.7	25.6	9.2	6.7	20.7
ZrO ₂	548	0.8	47.5	26.5	14.5	1.2	19.1

TABLE 6.3: CO hydrogenation over 1.5 wt% Rh/SiO₂ catalysts promoted by various transition metal oxides. Promoter/rhodium atomic ratio is one unless stated otherwise. For experimental conditions and notations see Table 6.1.

promoter	Temp (K)	corr. act.	selectivity (%C)					deact. % h ⁻¹
			CH ₄	C ₂ ⁺	C ₁ OH	C ₂ -oxy	tot.oxo	
-	600	0.3	33.2	2.3	29.1	35.0	64.5	1.7
V ₂ O ₃	503	8.5	20.3	8.8	25.1	39.6	70.9	2.6
MoO ₃	508	37.1	14.1	11.0	53.1	14.7	74.9	0.9
ThO ₂	528	8.7	32.3	5.8	7.7	51.8	61.9	2.4
ZrO ₂	548	1.7	24.5	7.9	30.1	32.5	67.6	n.m.
La ₂ O ₃	513	3.6	12.5	1.2	52.6	33.0	86.4	n.m.
CeO ₂ ^a	568	1.0	17.2	1.1	36.1	46.1	81.7	0.8
WO ₃	539	7.6	19.9	10.5	41.9	24.2	69.6	1.4
Cr ₂ O ₃	538	4.0	36.8	4.9	10.1	46.1	58.3	1.7
MnO	553	2.3	29.5	2.3	10.9	55.4	68.2	1.0
TiO ₂ ^a	538	2.3	27.5	5.5	18.7	44.0	67.0	2.8
Fe ₂ O ₃ ^b	560	2.1	10.9	1.4	58.2	28.6	87.7	0.9
Ir ^a	583	0.3	35.8	8.0	33.0	19.9	55.1	1.4
Ru ^a	538	1.8	14.4	42.1	10.5	18.3	43.5	3.0
Co ^a	568	0.6	21.5	4.0	39.1	33.2	74.5	1.1

a. 1.33 wt% Rh, P/Rh = 0.9, b. Fe/Rh = 0.3

TABLE 6.4: CO hydrogenation of 3.0 wt% Ir/SiO₂ catalysts promoted by some transition metal oxides. For experimental conditions and notations see Table 6.1.

promoter	P/Ir ratio	Temp (K)	corr. act.	selectivity (%C)				
				CH ₄	C ₂ ⁺	C ₁ OH	C ₂ -oxy	tot.oxo
-	0.0	623	0.05	72.6	16.3	11.1	0.0	11.1
ThO ₂	1.0	590	0.06	33.2	10.0	48.5	7.3	56.7
ThO ₂	4.0	593	0.13	69.1	22.9	7.0	1.0	8.0
La ₂ O ₃	1.0	588	0.03	55.6	16.7	27.1	2.7	30.6
La ₂ O ₃	4.0	593	0.05	37.4	12.2	43.1	5.9	50.4
Cr ₂ O ₃	1.0	588	0.43	49.0	16.6	26.1	6.4	34.4

alumina-supported Ir catalysts, the C_2 -oxygenate selectivity was 0. For the V_2O_3 -supported Ir catalyst, the C_2 -oxygenate selectivity was highest, but still only 12.8 %. The Ir catalyst supported by La_2O_3 exhibits a relatively high methanol selectivity. From Table 6.1 and 6.2 it is clear that the iridium catalysts are inferior to the rhodium catalysts with respect to activity and C_2 -oxygenate selectivity.

In Table 6.3, the results for the Rh/SiO₂ catalysts promoted by several transition metal oxides are presented. The V_2O_3 -, ThO₂- and MoO₃-promoted Rh/SiO₂ catalysts exhibit the highest activity. The increase in activity of the Rh/SiO₂ system due to addition of a promoter is smallest for the Ir- and Co-promoted catalysts. These promoters and Ru will be present in the metallic phase in contrast to the other promoters that will be present in the oxidic phase. The MoO₃-, Fe₂O₃- and La₂O₃-promoted Rh/SiO₂ catalysts have a high methanol selectivity (50-60 %). High C_2 -oxygenate selectivities are observed for V_2O_3 -, ThO₂-, CeO₂-, Cr₂O₃-, MnO- and TiO₂-promoted Rh/SiO₂. Except for MnO, Cr₂O₃ and CeO₂, these oxides were also reported by Ichikawa [8] to result in high C_2 -oxygenate selectivities. The Ru-promoted catalyst exhibits a high chain growth probability (large fraction of higher hydrocarbons), which is typical for Ru catalysts.

When the results of the promotion of Rh/SiO₂ by various oxides are compared with the catalysts in which rhodium is dispersed on the same oxides (Table 6.3 vs. Table 6.1), the following features are noticed. Almost all oxides studied are more effective in promoting rhodium when they are added to the Rh/SiO₂ catalyst. For the MoO₃- and WO₃-promoted catalysts, a large difference is observed in selectivity. The MoO₃- and WO₃-supported rhodium catalysts exhibit a very low oxygenate selectivity (< 20 %). The WO₃- and MoO₃-promoted Rh/SiO₂ catalysts exhibit a high oxo-selectivity (70-75), mainly consisting of methanol.

In Table 6.4, the results for the ThO₂-, La₂O₃- and Cr₂O₃-promoted Ir/SiO₂ catalysts are presented. Clearly the addition of these oxides did not result in a large increase of the activity. Even a promoter/iridium rate of 4.0 did not result in a high activity. C_2 -oxygenate selectivities were very low (< 8 %).

6.5 CONCLUSIONS

From the described measurements we can conclude that the rhodium catalysts, supported by various oxides or supported on SiO₂ and promoted by various oxides, are superior to the iridium catalysts in respect of the

activity and C₂-oxygenate selectivity.

For the Rh catalysts, the oxides are more effective promoters when they are used as additive in a Rh/SiO₂ catalyst, than when they are used as support. From the promoter oxides used, V₂O₃, ThO₂ and MoO₃ resulted in high activities, MoO₃, Fe₂O₃ and La₂O₃ resulted in high methanol selectivities, and V₂O₃, ThO₂, CeO₂, Cr₂O₃, MnO and TiO₂ resulted in high C₂-oxygenate selectivities.

In the following chapters we will study the promotion of Rh/SiO₂ by V₂O₃ (chapter 7 and 8, [25,54]), ThO₂ and MoO₃ (chapter 9, [51]) in more detail.

6.6 REFERENCES

1. M.E. Dry, in "Catalysis", vol. I (J.R. Anderson and M. Boudart, eds.), Springer Verlag (1981) p. 159.
2. R.B. Anderson, in "Catalysis", vol. IV (P.H. Emmett, ed.), Reinhold, New York (1956) p. 123.
3. Y. Kikuzono, S. Kagami, S. Naito, T. Onishi and K. Tamaru, *Far. Disc. Chem. Soc.*, 72 (1981) 135.
4. G.A. Vedage, P.B. Himelfarb, G.W. Simmons and K. Klier, *Solid State Chem. in Catal.* (ACS Symposium series 279) (R.K. Grasselli, J.C. Brazdil, eds.) (1985).
5. T. Mori, H. Masuda, H. Imai, A. Miyamoto, H. Niizuma, T. Hattori and Y. Murakami, *J. Molec. Catal.*, 25 (1984) 263.
6. T. Mori, A. Miyamoto, N. Takahashi, H. Niizuma, T. Hattori and Y. Murakami, *J. Catal.*, 102 (1986) 199.
7. T. Mori, A. Miyamoto, N. Takahashi, M. Fukagaya, T. Hattori and Y. Murakami, *J. Phys. Chem.*, 90 (1986) 5197.
8. M. Ichikawa, K. Shikakura and M. Kawai, in "Heterogeneous Catalysis Related to Energy Problems", *Proc. Symp. Dalian, China* (1982), A-08-I.
9. M. Ichikawa, T. Fukushima and K. Shikakura, in "Proc. 8th Int. Congr. Catal., Berlin, 1984" p.69, Weinheim, Berlin, 1984.
10. F.G.A. van den Berg, J.H.E. Glezer and W.M.H. Sachtler, *J. Catal.*, 93 (1985) 340.
11. A. Kiennemann, R. Breault, J.P. Hindermann and M. Laurin, *Far. Symp. Chem. Soc.*, 21 (1986) paper 14.
12. M. Ichikawa, *Bull. Chem. Soc. Jap.*, 51 (1978) 2268, 2273; M. Ichikawa, *J. Chem. Soc., Chem. Commun.*, (1978) 566.
13. J.R. Katzer, A.W. Sleight, P. Gajardo, J.B. Mitchel, E.F. Gleason and S. McMillan, *Far. Disc. Chem. Soc.*, 72 (1981) 121.
14. G. van der Lee, B. Schuller, H. Post, T.L.F. Favre and V. Ponec, *J. Catal.*, 98 (1986) 522; G. van der Lee, A.G.T.M. Bastein, J. van den Boogert, B. Schuller,

- H. Luo and V. Ponec, *Far. Symp. Chem. Soc.*, 21 (1986) paper 12.
15. A.G.T.M. Bastein, W.J. van den Boogert, G. van der Lee, H. Luo, B. Schuller and V. Ponec, *Appl. Catal.*, to be published.
 16. G. van der Lee, Thesis, Leiden University, The Netherlands (1986).
 17. M. Araki and V. Ponec, *J. Catal.*, 44 (1976) 439. W.A.A. van Barneveld and V. Ponec, *J. Catal.*, 51 (1976) 426.
 18. L.J.M. Luyten, M. van Eck, J. van Grondelle and J.H.C. van Hooff, *J. Phys. Chem.* 82 (1978) 2000.
 19. G.C. Bond and B.D. Turnham, *J. Catal.*, 45 (1976) 128.
 20. E.K. Poels, E.M. van Broekhoven, W.A.A. van Barneveld and V. Ponec, *React. Kinet. Catal. Lett.* 18 (1981) 223.
 21. J.M. Driessen, E.K. Poels, J.P. Hindermann and V. Ponec, *J. Catal.*, 82 (1983) 20.
 22. J.P. Hindermann, A. Kiennemann, A. Chakor-Alami and R. Kieffer, in "Proc. 8th Int. Congr. Catal., Berlin, 1984", vol. II, p. 163, Verlag Chemie, Weinheim, 1984.
 23. B.J. Kip, F.W.A. Dirne, J. van Grondelle and R. Prins, *Appl. Catal.*, 25 (1986) 32, chapter 5 of this thesis.
 24. C.P. Huang and J.T. Richardson, *J. Catal.*, 51 (1978) 1.
 25. B.J. Kip, P.A.T. Smeets, J. van Grondelle and R. Prins, submitted to *Appl. Catal.*, chapter 8 of this thesis.
 26. D.G. Blackmond, J.A. Williams, S. Kesraoui and D.S. Blazewick, *J. Catal.*, 10 (1986) 496.
 27. M.S. Spencer, *J. Phys. Chem.*, 88 (1984) 1046.
 28. W.M.H. Sachtler and M. Ichikawa, *J. Phys. Chem.*, 90 (1986) 4752.
 29. J.D. Bracey and R. Burch, *J. Catal.*, 86 (1984) 384; J.B.F. Anderson, J.D. Bracey and R. Burch, in "Proc. 8th Int. Congr. Catal., Berlin, 1984", vol. V, p. 251, Verlag Chemie, Weinheim, 1984.
 30. J.S. Rieck and A.T. Bell, *J. Catal.*, 96 (1985) 88 and 99 (1986) 262.
 31. W.M.H. Sachtler, D.F. Shriver, W.B. Hollenberg and A.F. Lang, *J. Catal.*, 92 (1985) 429.
 32. W.M.H. Sachtler, in "Proc. 8th Int. Congr. Catal., Berlin, 1984", vol. I, p. 151, Verlag Chemie, Weinheim, 1984.
 33. S.B. Butts, E.M. Holt, S.H. Strauss, N.W. Alcock, R.E. Stimson and D.F. Shriver, *J. Am. Chem. Soc.*, 101 (1979) 5864.
 34. T.G. Richmond, F. Basolo and D.F. Shriver, *Inorg. Chem.*, 24 (1982) 1272.
 35. M.M. McClory and R.D. Gonzalez, *J. Catal.*, 89 (1984) 392.
 36. D.L. King and J.B. Peri, *J. Catal.*, 79 (1983) 164.
 37. T. Okuhara, H. Tamaru and M. Misono, *J. Catal.*, 95 (1985) 41.
 38. E.L. Garfunkel, J.E. Crowell and G.A. Somorjai, *J. Phys. Chem.*, 86 (1982) 310; J.E. Crowell, E.L. Garfunkel and G.A. Somorjai, *Surf. Sci.*, 121 (1982)

- 303; J.E. Crowell and G.A. Somorjai, *Appl. Surf. Sci.*, 19 (1984) 73.
39. M. Kiskinova, *Surf. Sci.*, 11 (1981) 584.
 40. M.E. Dry, T. Shingles and L.J. Boskoff, *J. Catal.*, 25 (1972) 99.
 41. N.K. Ray and A.B. Anderson, *Surf. Sci.*, 125 (1983) 803.
 42. J. Blyholder, *J. Phys. Chem.*, 68 (1964) 2772.
 43. T.P. Wilson, P.C. Ellgen and W.J. Bartley, in "Advances in Catalytic Chemistry", Proc. Conf. in Salt Lake City (USA) (1982).
 44. R.A. van Santen, in "Proc. 8th Int. Congr. Catal., Berlin, 1984", vol. IV, p. 97, Verlag Chemie, Weinheim, 1984.
 45. J.P. Collman, R.G. Finke, J.N. Cawse and J.I. Brauman, *J. Am. Chem. Soc.*, 100 (1978) 4766.
 46. H.H. Kung, *Catal. Rev. Sci.*, 22 (1982) 235.
 47. R.G. Herman, K. Klier, G.W. Simmons, B.P. Finn, J.B. Bulko and T.P. Kobylinski, *J. Catal.*, 56 (1979) 407; R.G. Herman, G.W. Simmons and K. Klier, in "New Horizons in Catalysis", Proc. 7th Int. Congr. on Catal., Tokyo, 1980, Elsevier Amsterdam 1981, A475.
 48. K. Klier, in "Catalysis on the Energy Scene" eds. S. Kaliaguine and A. Mahay, Elsevier, Amsterdam, 1984.
 49. D.C. Koningsberger, C.P.J.H. Borgmans, A.M.J. van Elderen, B.J. Kip and J.W. Niemantsverdriet, *J. Chem. Soc., Chem. Commun.*, submitted for publication.
 50. T. Fukushima, Y. Ishii, Y. Onda and M. Ichikawa, *J. Chem. Soc., Chem. Commun.*, (1985) 1752.
 51. B.J. Kip, E.G.F. Hermans, J.H.M.C. van Wolput, N.M.A. Hermans, J. van Grondelle and R. Prins, *Appl. Catal.*, submitted for publication, chapter 9 of this thesis.
 52. H. Orita, S. Naito and K. Tamaru, *J. Catal.*, 90 (1984) 183.
 53. M.A. Vanice, *J. Catal.*, 37 (1975) 462.
 54. B.J. Kip, P.A.T. Smeets, J.H.M.C. van Wolput, H.W. Zandbergen, J. van Grondelle and R. Prins, *Appl. Catal.*, to be published, chapter 7 of this thesis.

Chapter 7

PREPARATION AND CHARACTERIZATION OF VANADIUM OXIDE-PROMOTED RHODIUM CATALYSTS

The location of the promoter element in rhodium on alumina and silica catalysts promoted by vanadium oxide has been studied by various techniques. Our results prove that an intimate contact between the active component, rhodium, and the promoter, vanadium oxide, is present in most catalysts studied.

For the silica-supported systems, temperature programmed reduction and diffuse reflectance infrared spectroscopy pointed to the formation of a mixed oxide (RhVO_4) during calcination. Reduction of this oxide phase resulted in a vanadium oxide layer on top of the metal particle, as could be concluded from carbon monoxide chemisorption experiments. CO chemisorption was suppressed in the $\text{Rh}/\text{V}_2\text{O}_3/\text{SiO}_2$ catalysts, while transmission electron microscopy showed that the rhodium particle size was not influenced by the addition of vanadium oxide. This indicates that the suppression of CO chemisorption is not due to a decrease of metal particle size, but due to covering of the metal particle. Infrared spectroscopy showed that the amount of linearly bonded and bridge-bonded CO was almost completely suppressed, while the amount of gem-dicarbonyl species remained unaffected. No suppression of hydrogen chemisorption was observed. From this and TPD experiments it could be concluded that hydrogen adsorption occurs both on the exposed Rh atoms, as well as on the vanadium oxide patches partly covering the surface Rh atoms, pointing to the formation of hydrogen bronzes.

Temperature programmed reduction experiments showed that RhVO_4 was not formed in $\text{Rh}/\text{V}_2\text{O}_3/\text{Al}_2\text{O}_3$ during calcination. For $\text{V}/\text{Rh} < 1.0$, Rh_2O_3 and V_2O_5 particles exist separately on the support, due to the strong interaction between V_2O_5 and Al_2O_3 . Only for catalysts with a V/Rh value around 7.0 (near-monolayer of vanadium oxide on alumina), oxidation at 898 K resulted in the formation of RhVO_4 . For these catalysts, Rh_2O_3 might be positioned on top of the vanadium oxide layer after calcination. Almost all adsorbed CO was present in the form of the gem-dicarbonyl species and only a minor suppression of CO adsorption was observed.

7.1 INTRODUCTION

Much attention has been paid to the effect of various promoters and supports on the activity and selectivity of group VIII metals in the hydrogenation of carbon monoxide [1-3]. It has been reported that V_2O_3 has a significant effect on this reaction. Kikuchi *et al.* [4] reported that V_2O_3 -supported Ru catalysts exhibited high turnover frequencies, high selectivities for heavier hydrocarbons and high olefin/paraffin ratios relative to Ru/ Al_2O_3 and other supported ruthenium catalysts. Mori *et al.* [5], using pulse surface reaction rate analysis, showed that addition of vanadium oxide greatly increased the rate of C-O bond dissociation of adsorbed CO in the methanation on Ru/ Al_2O_3 . Ichikawa *et al.* [6] and Van der Lee *et al.* [7] reported high selectivities to C_2 -oxygenates using V_2O_3 -supported Rh catalysts.

Like TiO_2 -, Nb_2O_5 - and Ta_2O_3 -supported noble metal catalysts, V_2O_3 -supported metal catalysts exhibit a significant suppression of hydrogen and carbon monoxide chemisorption after reduction at temperatures above 700 K [8-10]. Nowadays it is generally accepted that the high-temperature reduction causes the formation of a lower oxide that can diffuse onto the metal and spread over its surface (covering-model) [11-18]. These small patches of suboxide cause a suppression of the chemisorption capacity of the metal. Hicks *et al.* [19] studied the adsorption of H_2 and CO on La_2O_3 -supported Pd catalysts and observed a suppression of the CO chemisorption after reduction at 573 K (low temperature reduction), even though La_2O_3 has not been reported as an SMSI support. In contrast to the CO chemisorption, the hydrogen chemisorption was not suppressed. The suppression of CO adsorption was attributed to patches of partially reduced support material, LaO_x , already transferred to the surface of the Pd crystallites during catalyst preparation. The absence of a suppression of H_2 adsorption on Pd/ La_2O_3 indicated that H_2 adsorption occurred on the exposed Pd surface atoms as well as on the LaO_x patches covering the balance of the surface Pd atoms. Thus, in this case, the covering is not caused by the high reduction temperature, but by the fact that the overlayer of support oxide is already formed during catalyst impregnation.

In our laboratory we have studied the formation of C_2 -oxygenates from synthesis gas at elevated pressures. Rh/ V_2O_3 is of interest in this respect [6,7], but V_2O_3 has the disadvantage of a relatively low surface area ($< 10 \text{ m}^2 \text{ g}^{-1}$) and of a low mechanical and chemical stability. Therefore, we chose the route of promoting Rh/ SiO_2 and Rh/ Al_2O_3 systems with vanadium

oxide in order to combine the good structural properties of Al_2O_3 and SiO_2 (high surface area, high pore volume, high mechanical and chemical stability) with the good selectivity properties of V_2O_3 . In this publication we will describe the results of the characterization of the catalysts via a number of techniques, like temperature programmed reduction, hydrogen and carbon monoxide chemisorption, hydrogen desorption, transmission electron microscopy and infrared spectroscopy of adsorbed CO. In a subsequent paper [20] we will report the catalytic performance of the catalysts in the synthesis gas reaction.

7.2 EXPERIMENTAL

7.2.1 Catalyst preparation

As supports we used $\gamma\text{-Al}_2\text{O}_3$ (Ketjen, type 000-1.5E, surface area $200 \text{ m}^2 \text{ g}^{-1}$, pore volume 0.6 ml g^{-1}), SiO_2 (Grace, type 113, surface area $360 \text{ m}^2 \text{ g}^{-1}$, pore volume 1.1 ml g^{-1}) and V_2O_3 , obtained by reduction of V_2O_5 (Merck, p.a.) at 1100 K in pure hydrogen for 2 h (heating rate 10 K min^{-1}) and subsequent passivation. This resulted in V_2O_3 with a low surface area ($3 \text{ m}^2 \text{ g}^{-1}$, pore volume 0.32 ml g^{-1}). Vanadium oxide-promoted SiO_2 and Al_2O_3 were prepared by incipient wetting these supports with an aqueous solution of NH_4VO_3 (Merck, p.a.), drying at 395 K and calcining at 723 K (3 h). In this way, supports with a varying amount of vanadium oxide were obtained. We also tried to prepare a monolayer of vanadium oxide on Al_2O_3 , as described in the literature for vanadium oxide and molybdenum oxide monolayers on alumina [21-24], by batch adsorption of NH_4VO_3 . During the adsorption the pH was kept constant at 4 by adding HNO_3 . In this way we made a $\text{V}_2\text{O}_5/\text{Al}_2\text{O}_3$ support with 5.6 and 6.7 wt% V, the latter by two sequential adsorption steps. Drying and calcining were carried out as described above.

The catalysts were prepared by the incipient wetness method using an aqueous solution of $\text{Rh}(\text{NO}_3)_3$ (pH = 2.5, Drijfhout, Amsterdam), and were subsequently dried in air at 395 K for 16 h (heating rate 2 K min^{-1}). To remove nitrogenous residues from the precursor, the catalysts were calcined at 723 K for 3 h. Rhodium content was always around 1.5 wt%.

The following notations will be used: $\text{Rh}/\text{V}_2\text{O}_3/\text{SiO}_2$ for silica-supported rhodium catalysts promoted with vanadium oxide, $\text{Rh}/\text{V}_2\text{O}_3/\text{Al}_2\text{O}_3$ for alumina-supported rhodium catalysts promoted with vanadium oxide, and $\text{Rh}/\text{V}_2\text{O}_3$ for vanadium oxide-supported rhodium catalysts.

7.2.2 Characterization techniques

Volumetric hydrogen and carbon monoxide chemisorption measurements were performed in a conventional glass system at 298 K as described in [25]. Before measuring the H_2 and CO chemisorption the catalysts were reduced at 523 K or 723 K (heating rate 8 K min^{-1}) for 1 h and evacuated for 0.5 h, at the temperature indicated under RESULTS, to an ultimate vacuum of 10^{-2} Pa at the catalyst sample. The total amount of chemisorbed H atoms or CO molecules was obtained by extrapolating the linear part of the isotherm to zero pressure while correcting for the extrapolated chemisorption values of the bare support [26,27]. In a recent article we extensively discussed the method used (admission at 473 K, no distinction between reversibly and irreversibly adsorbed hydrogen, extrapolation to zero pressure) [28]. Al_2O_3 and V_2O_3/Al_2O_3 were found to adsorb CO, while SiO_2 , V_2O_3/SiO_2 and V_2O_3 did not adsorb CO. None of the supports adsorbed hydrogen.

The reduction behaviour of the supports and the reduction, oxidation and hydrogen desorption behaviour of the catalysts were studied by temperature programmed reduction (TPR), oxidation (TPO) and desorption (TPD), using the apparatus described extensively in ref. [29,30]. During TPR and TPO experiments, the heating rate was 5 K min^{-1} , while during TPD experiments the heating rate was 15 K min^{-1} . A final reduction temperature of 1073 K and 898 K was used for the supports and catalysts, respectively. In a standard experiment, a catalyst was characterized by a TPR of the calcined catalyst, followed by a TPO of the reduced catalyst, followed by a TPR of the oxidized system. TPD experiments were always preceded by a TPR. We have described the sequence of experiments used during the temperature programmed reactions elsewhere [25,30].

Carbon monoxide adsorption was also studied by infrared spectroscopy. A self-supporting catalyst wafer was placed in an evacuable glass reactor (ultimate pressure $5 \cdot 10^{-3}$ Pa). The catalyst was reduced *in situ* at 543 K in flowing H_2 (heating rate 5 K min^{-1}) for 0.5 h and evacuated at this temperature for 1 h unless stated otherwise. All gases were purified over molecular sieves and a BTS column. After cooling to room temperature, small doses of CO were introduced into the reactor, and the infrared spectrum was recorded after each dose. All spectra were recorded at 2 cm^{-1} resolution using a Bruker IFS 113V Fourier transform infrared spectrometer, equipped with a HgCdTe detector. A satisfactory signal-to-noise ratio was obtained by adding 128 interferograms. From these spectra information about the

relative amount of adsorbed carbon monoxide and the way in which CO is adsorbed on the metal particles was obtained.

Diffuse reflectance infrared spectroscopy was used to study V=O stretch bands. For that purpose, the Bruker IFS 113V Fourier transform spectrometer was equipped with a diffuse reflectance unit (Harrick). Spectra were recorded at 4 cm^{-1} resolution and 8192 interferograms were added to obtain a satisfactory signal-to-noise ratio. The samples were carefully ground and diluted in KBr (1:10). The same amount of sample was used for each measurement.

In order to get information about the metal particle size, Transmission Electron Microscopy (TEM) was used. Catalysts were pretreated by reduction at 523 K and subsequent passivation. The specimens were prepared by putting a few droplets of a suspension of the catalyst in methanol on a 'holey' carbon coated Formvar film. Similar images were obtained when the suspension of the catalyst was put in an ultrasonic bath or by dry mounting of the catalyst. The specimens were examined with a Jeol 200CX, operating at 200 kV. Very small particles ($< 1\text{ nm}$) could be observed best with an objective diafragma of about 7 nm^{-1} and a focus very close to zero. Especially when the support is crystalline, small metal particles are very difficult to see and to distinguish from artifacts, due to overlap of several support particles. In such cases only by comparison of images taken at different defocus values artifacts can be discriminated from metal particles.

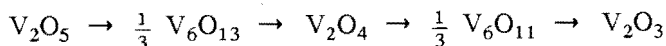
The vanadium content of the supports was determined by means of atomic adsorption spectrometry, while the rhodium content was determined colorimetrically.

7.3 RESULTS

7.3.1 Rh/V₂O₃

In order to compare the results of vanadium oxide-promoted Rh/SiO₂ and Rh/Al₂O₃ catalysts with Rh/V₂O₃, we started to study this system by temperature programmed reduction and hydrogen and carbon monoxide chemisorption.

In Figure 7.1a the reduction profile of V₂O₅ is presented. This profile is characterized by four different reduction peaks at 943, 973, 1013 and above 1073 K. These peaks are caused by the following reduction steps



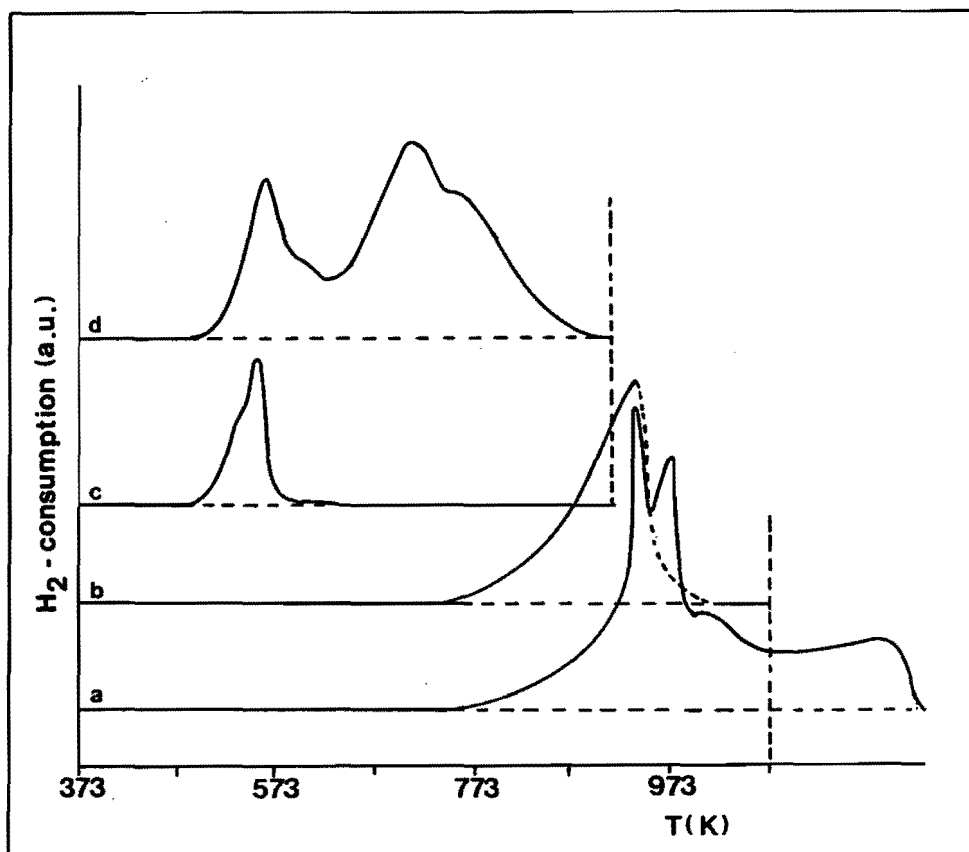


FIGURE 7.1: Temperature programmed reduction profiles of V_2O_5 (a), passivated V_2O_3 (b), Rh/ V_2O_3 after drying at 395 K (c), and Rh/ V_2O_5 after oxidation at 898 K (d). Note that the final reduction temperature for (a) and (b) was 1073 and for (c) and (d) was 898 K.

as shown by Bosch *et al.* [31] using X-ray diffraction. The final oxide formed in this reduction is V_2O_3 , as can be calculated from the amount of hydrogen consumed during the reaction.

The reduction profile of reduced and passivated vanadium oxide, used as support for the vanadium oxide-supported rhodium catalysts, shows one reduction peak around 923 K (cf. Figure 7.1b), caused by the reduction of the oxidized vanadium oxide surface layer, formed during the passivation and storage in air. Longer storage caused a deeper oxidized vanadium oxide layer (freshly prepared: 0.15 % V^{5+} , after one month storage: 2.2 % V^{5+}).

In Figure 7.1c the TPR profile of Rh/V₂O₃ is shown. This system is prepared by incipient wetting of the reduced and passivated vanadium oxide and by subsequent drying at 395 K. The hydrogen consumption starts at 473 K and has a maximum at 553 K. Reduction is complete at 593 K. Assuming that rhodium is reduced from the 3+ valency to zero valency and that vanadium is reduced from V⁵⁺ to V³⁺, one can calculate from the amount of hydrogen consumed that after drying about 10 % of the vanadium was in the 5+ valency state.

The TPR profile after TPO (oxidation up to 898 K) is presented in Figure 7.1d. The Rh/V₂O₅ system starts to reduce at 493 K and has a maximum at 573 K. Reduction peaks are also observed above 673 K and these must be due to the reduction of the fully oxidized vanadium oxide support, as judged from the amount of hydrogen consumed during the reduction.

Hydrogen chemisorption measurement of 1.5 wt% Rh/V₂O₃, reduced and evacuated at 523 K, resulted in a very high H/Rh value (3.8). Reduction at a higher temperature resulted in a strong decrease of the H/Rh value, 0.09 and 0.00 after reduction and evacuation at 723 and 823 K, respectively. The CO/Rh value after reduction and evacuation at 523 K was 0.36.

7.3.2 Rh/V₂O₃/SiO₂

Temperature programmed reduction. TPR profiles of V₂O₅/SiO₂ supports (Figure 7.2a,b) show that the major part of the vanadium oxide is reduced more easily when supported on SiO₂ than when unsupported, and that the characteristic peaks of the unsupported V₂O₅ are not present (compare with Figure 7.1a). The reduction starts around 673 K, has a maximum hydrogen consumption at 773–823 K, and is (almost) complete at the end of the temperature ramp (1073 K). The amount of hydrogen consumed during the TPR (H₂/V = 1.0) indicates that also in the case of V₂O₅/SiO₂ supports, V⁵⁺ is reduced to V³⁺. Almost no reduction was observed around 1073 K. This reduction behaviour indicates that no large crystalline V₂O₅ particles are formed, as is also supported by XRD. No crystalline V₂O₅ phase could be detected by this technique in the V₂O₅/SiO₂ samples.

Figures 7.2c-h show the TPR profiles of the Rh/V₂O₅/SiO₂ catalysts after calcination. A pronounced effect of the vanadium loading is observed. The Rh/SiO₂ system without vanadium (Figure 7.2c) starts to reduce at the beginning of the temperature ramp and has a maximum at 363 K. Reduction is complete at 463 K. A higher vanadium loading shifts the whole reduction profile. It causes an increase in the temperature at which the reduction is

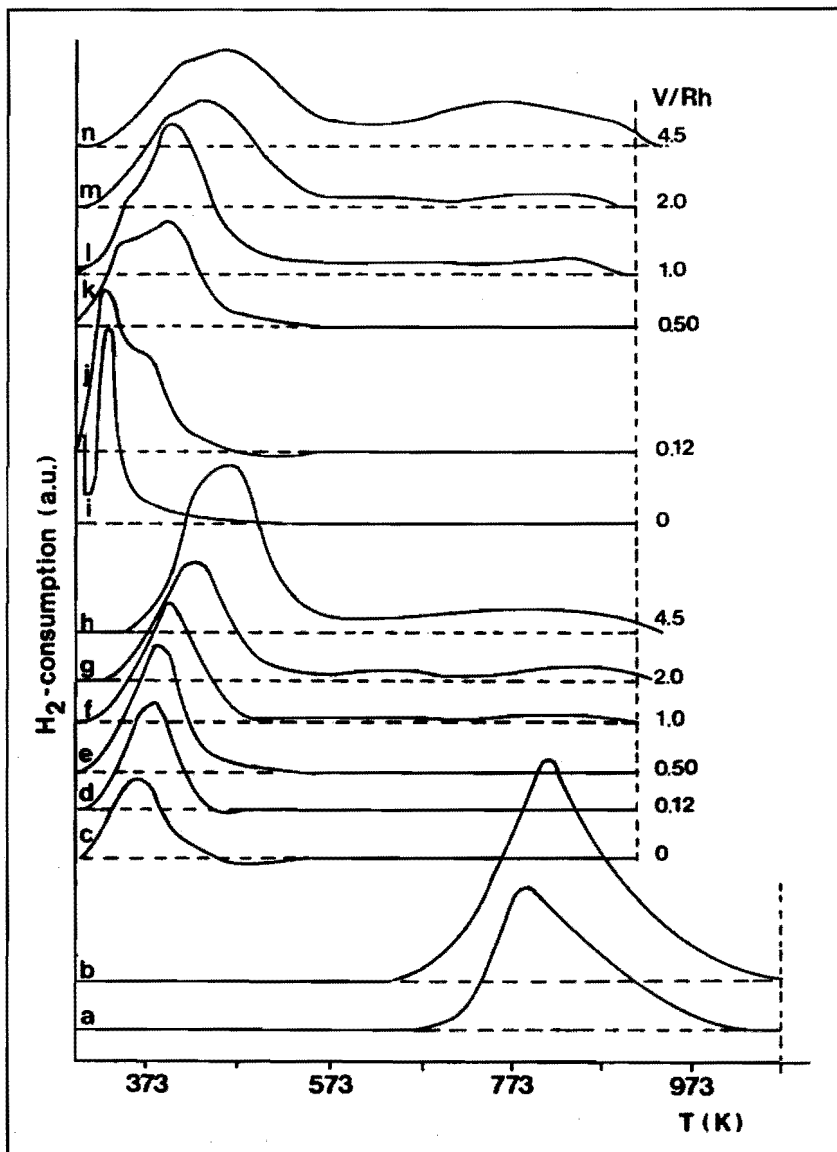


FIGURE 7.2: Temperature programmed reduction profiles of the silica-supported systems.

a. 0.8 wt% V_2O_5/SiO_2

b. 3.6 wt% V_2O_5/SiO_2

c-h. TPR after calcination of Rh/ V_2O_5/SiO_2 catalysts

i-n. TPR after oxidation at 898 K of Rh/ V_2O_5/SiO_2 catalysts.

Final reduction temperature 1073 K for a. and b. and 898 K for c-n.

starting, a shift to higher temperatures of the peak maximum and an increase in the temperature at which the reduction is complete. For vanadium loadings above $V/Rh = 1$, an additional hydrogen consumption is observed above 573 K. Also in this case total hydrogen consumption matches the calculated values assuming the following reduction reactions: $V^{5+} \rightarrow V^{3+}$ and $Rh^{3+} \rightarrow Rh^0$. Thus, for the silica-supported catalysts, rhodium oxide and part of the vanadium oxide are reduced around 373 K, and part of the vanadium oxide content is reduced at higher temperatures (673–898 K).

The TPR profiles of the $Rh/V_2O_5/SiO_2$ catalysts after TPO (oxidation up to 898 K) are presented in Figure 7.2i–n. Also in this case, a shift of the reduction process to higher temperatures is observed when the vanadium loading is increased. In contrast to the TPR profiles after calcination at 723 K (Figure 7.2c–h), now several reduction peaks are observed. Rh/SiO_2 starts to reduce at the beginning of the temperature ramp and has a maximum hydrogen consumption at 323 K. The system with $V/Rh = 0.12$ is characterized by an additional peak around 387 K at the cost of the peak at 323 K. Further increase of the vanadium loading causes a further decrease of the hydrogen consumption at the beginning of the temperature ramp up to 323 K and a further increase of the hydrogen consumption between 373 and 473 K. In the TPR profiles of catalysts with $V/Rh > 1.0$ a third hydrogen consumption peak is observed around 473 K. For these high vanadium loadings additional hydrogen consumption is measured above 673 K, with a peak around 773 K, like in V_2O_5/SiO_2 (cf. Figure 7.2b).

Temperature programmed desorption of hydrogen. Hydrogen TPD profiles for $Rh/V_2O_3/SiO_2$ catalysts with different V/Rh ratios are presented in Figure 7.3. After reduction at 523 K, hydrogen desorption is more difficult for catalysts with a high V/Rh ratio (see drawn line in Figure 7.3). From these TPD profiles we can conclude that after reduction and evacuation at 523 K all hydrogen will not be removed. Especially the catalysts with a high V/Rh ratio will still contain hydrogen. This has important implications for the H_2 and CO chemisorption measurements. Figure 7.3 shows that even evacuation at 723 K after reduction at 723 K will not remove all hydrogen (dashed line), because after a high reduction temperature part of the hydrogen is bonded strongly and only desorbs around 823 K. The high temperature desorption peak is most important for the highest vanadium loading ($V/Rh = 4.5$). The total amount of desorbed hydrogen was not influenced by the reduction temperature and the H/Rh ratio, calculated from these

TPD profiles, slightly increased with increasing vanadium content.

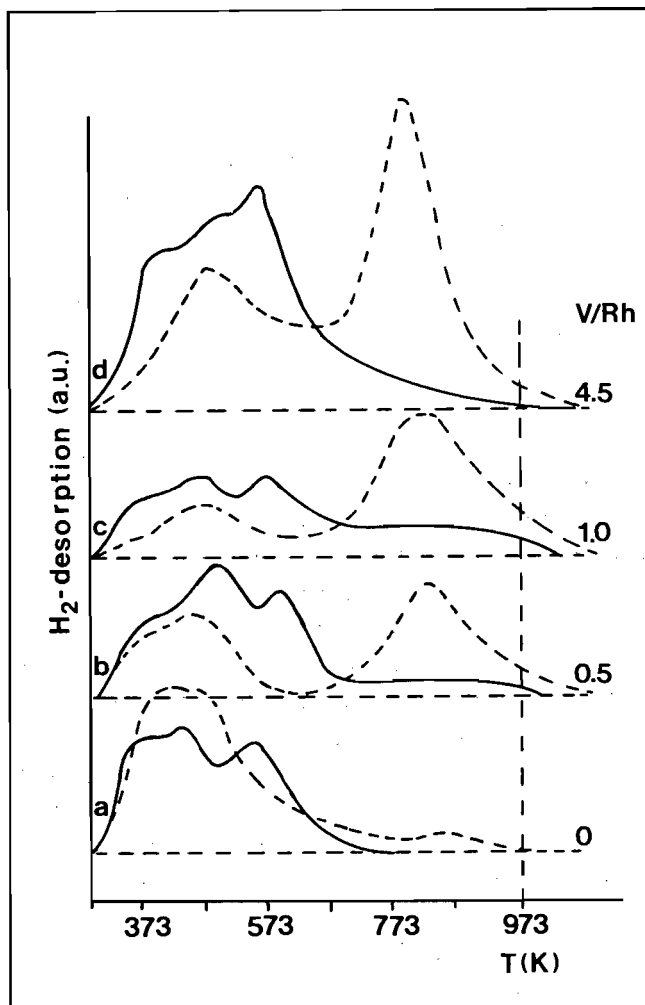


FIGURE 7.3: Temperature programmed desorption of hydrogen for Rh/ V_2O_3 /SiO₂ systems, reduced at 523 K (—) and reduced at 723 K (---).

H₂ and CO chemisorption measurements. Results of the hydrogen and carbon monoxide chemisorption measurements for the SiO₂-supported systems are presented in Figure 7.4. After reduction and evacuation at 523 K (low temperature reduction) the following features are observed (see Figure

7.4a1,b1). Up to $V/Rh = 1.0$, the hydrogen and carbon monoxide chemisorption capacity is strongly suppressed by addition of vanadium oxide. Further addition of vanadium oxide does not change the CO/Rh values and causes a gradual increase in the H/Rh values. After reduction and evacuation at a higher temperature (723 K), a similar behaviour is observed (see Figure 7.4a2,b2), the suppression of H/Rh and CO/Rh being even larger.

However, as shown by the TPD experiments, during the evacuation at the reduction temperature preceding the chemisorption measurements (at 523 K as well as 723 K), the hydrogen put on the catalyst during reduction is not removed completely and this effect is most important for the catalysts with a high V/Rh ratio. The observed decrease of the H/Rh and CO/Rh values with increasing V/Rh ratio (cf. Figure 7.4a,b) might be caused by this effect. We therefore performed chemisorption measurements after reduction at 523 K and evacuation at 723 K. The H/Rh and CO/Rh values obtained after this pretreatment are presented in Figures 7.4a3 and 7.4b3. H/Rh was more or less constant up to $V/Rh = 1.0$, and then increased with increasing vanadium content. However, the CO chemisorption still decreased with increasing V/Rh up to $V/Rh = 1.0$, although not to the same extent as in the case of evacuation at the reduction temperature.

Of course, it is important to check whether oxidation has taken place during the evacuation at a temperature above the final reduction temperature. During the high temperature evacuation, water formed by dehydration of the silica support might oxidize the rhodium and cause an increased hydrogen chemisorption, because in that case part of the hydrogen will be used to re-reduce the rhodium oxide. Therefore, after reduction at 523 K and evacuation at 723 K, oxygen was added to the catalyst at 723 K. The amount of oxygen consumed was 1.52 O/Rh for 1.5 wt% Rh/SiO_2 , proving that Rh was in the zero valent state after reduction at 523 K and evacuation at 723 K.

The hydrogen and carbon monoxide chemisorption measurements thus demonstrate that the vanadium oxide suppresses the carbon monoxide chemisorption, while it promotes the hydrogen chemisorption. Because suppression of CO/Rh can be caused by either an increase of the particle size or by an influence of the vanadium oxide on the chemisorption capacity of the rhodium metal (by a covering and/or electronic effect), we examined the rhodium particle size by TEM.

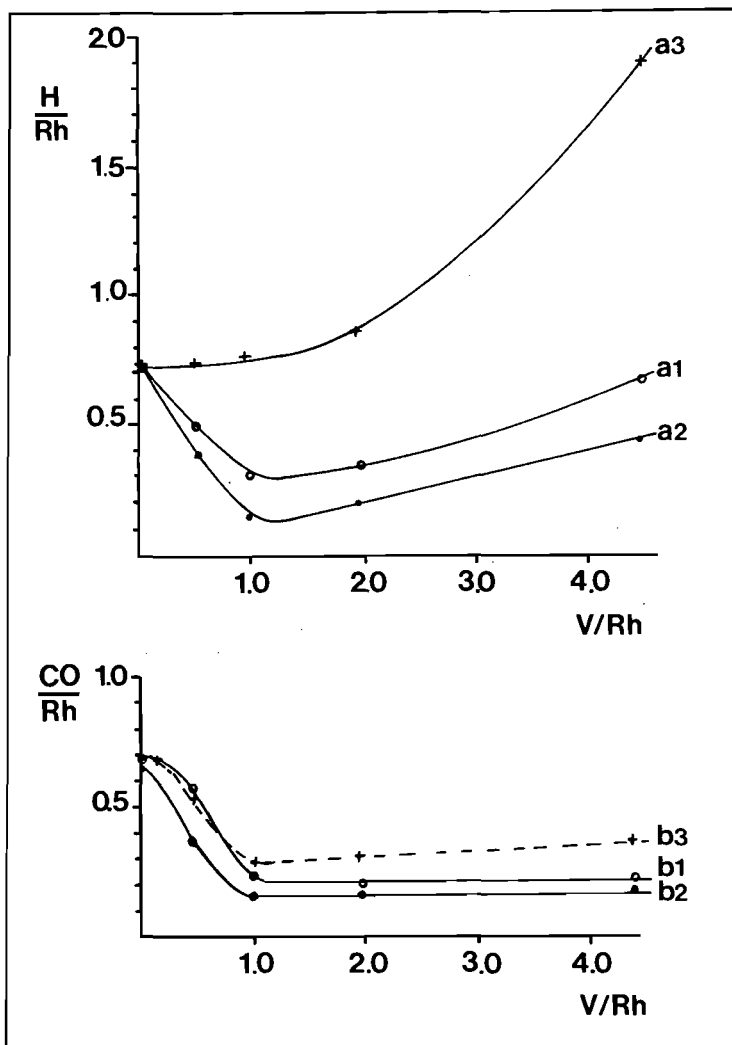


FIGURE 7.4: H_2 and CO chemisorption measurements of the 1.5 wt% Rh/ V_2O_3 / SiO_2 catalysts after several pretreatment procedures, as a function of the V/Rh ratio.

a1. H/Rh after reduction at 523 K and evacuation at 523 K

a2. H/Rh after reduction at 723 K and evacuation at 723 K

a3. H/Rh after reduction at 523 K and evacuation at 723 K

b1. CO/Rh after reduction at 523 K and evacuation at 523 K

b2. CO/Rh after reduction at 723 K and evacuation at 723 K

b3. CO/Rh after reduction at 523 K and evacuation at 723 K

Transmission electron microscopy. Figure 7.5 presents the metal particle size distribution for several Rh/V₂O₃/SiO₂ catalysts. A comparison of the Rh/V₂O₃/SiO₂ catalysts with different V/Rh ratios showed that all catalysts exhibited rhodium particles with an average particle size of 20 ± 2 Å. These data should be treated with some caution since electron microscopy, by its nature, sees only a limited part of the total catalyst surface. However, after analyzing several micrographs of each system, we feel confident that the systems studied do not differ significantly in their particle size distribution (cf. Figure 7.5). Spacings are observed in some of the particles and they point to the existence of Rh metal. The reduced and passivated catalysts, used for the TEM measurements, can easily be re-reduced (TPR peak around 353 K) by the electron beam in the microscope.

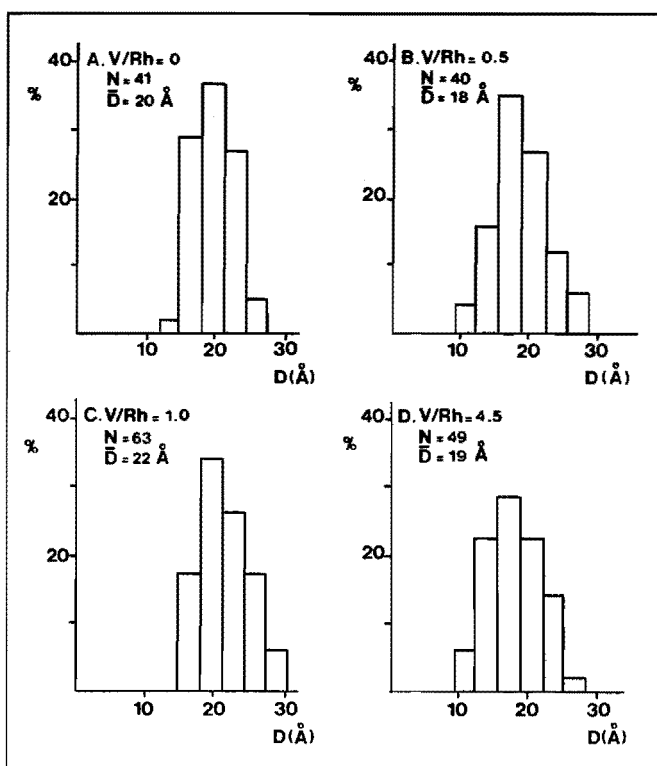


FIGURE 7.5: Rhodium particle size distributions for Rh/V₂O₃/SiO₂ catalysts with varying V/Rh ratio. N = number of particles used to determine particle size distribution. D = mean metal particle size.

Thus, the observed decrease in CO/Rh with increasing V/Rh ratio cannot

be caused by differences in metal particle size.

Infrared spectroscopy of adsorbed CO. Chemisorption of carbon monoxide at 298 K was also studied by infrared spectroscopy, in order to determine the binding sites for CO and to measure the CO adsorption capacity of the exposed rhodium. Spectra for CO adsorbed at 298 K on 1.5 wt% Rh/SiO₂, reduced *in situ* at 523 K and evacuated at 673 K (maximum temperature of the cell) are shown in Figure 7.6. Each spectrum was recorded after adding a dose of CO to the sample chamber containing the catalyst disc. Estimates of the amounts of CO in the cell, relative to the amount of rhodium are presented in the caption to Figure 7.6. The infrared spectrum of CO adsorbed on Rh/SiO₂ ($T_{ad} = 298$ K, CO/Rh = 250, Figure 7.6f) exhibited bands at 2092, 2068, 2022 and 1859 cm⁻¹. Following the original assignments of Yang and Garland [32], the band at 1859 cm⁻¹ is attributed to bridge-bonded CO (B), the band at 2068 cm⁻¹ to linearly bonded CO (L), and the bands at 2022 (T₁) and 2092 cm⁻¹ (T₂) to the symmetric and antisymmetric stretchings of the gem-dicarbonyl species (two CO molecules

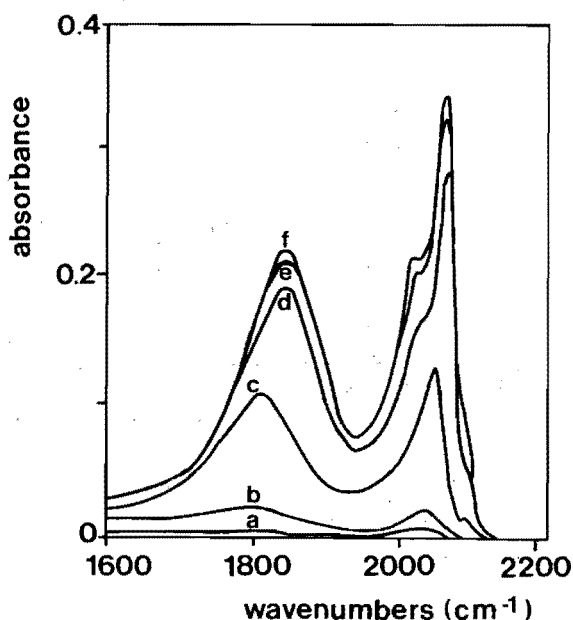


FIGURE 7.6: Infrared spectra of CO adsorbed on 1.5 wt% Rh/SiO₂ at 298 K, using an increasing dose of CO. (Reduction temperature 523 K, evacuation temperature 673 K). The approximate amounts of CO expressed as CO/Rh were: 0.05 (a), 0.2 (b), 0.8 (c), 2 (d), 20 (e) and 250 (f).

bonded to one rhodium cation). Recently, the existence and behaviour of these different structures for several supported Rh catalysts have been studied [32-40].

As is shown in Figure 7.6, the first aliquot of CO causes the B and L band to appear at 1800 and 2043 cm^{-1} , respectively. Addition of more CO leads to a large increase of the B and L band, and to the appearance of the shoulders at 2024 and 2090 cm^{-1} originating from the twin-species (T_1 and T_2). Only a modest increase in the band frequencies of the B and L bands is observed: $\Delta\sigma_B = 59 \text{ cm}^{-1}$ and $\Delta\sigma_L = 25 \text{ cm}^{-1}$. This increase has been ascribed to the fact that at higher CO coverage there is an increase in the dipole-dipole coupling between CO molecules and consequently an increase in the CO stretching frequency [41]. The shifts in band frequencies of the twin species T_1 and T_2 were negligible, as to be expected for CO molecules bonded to isolated Rh^+ cations.

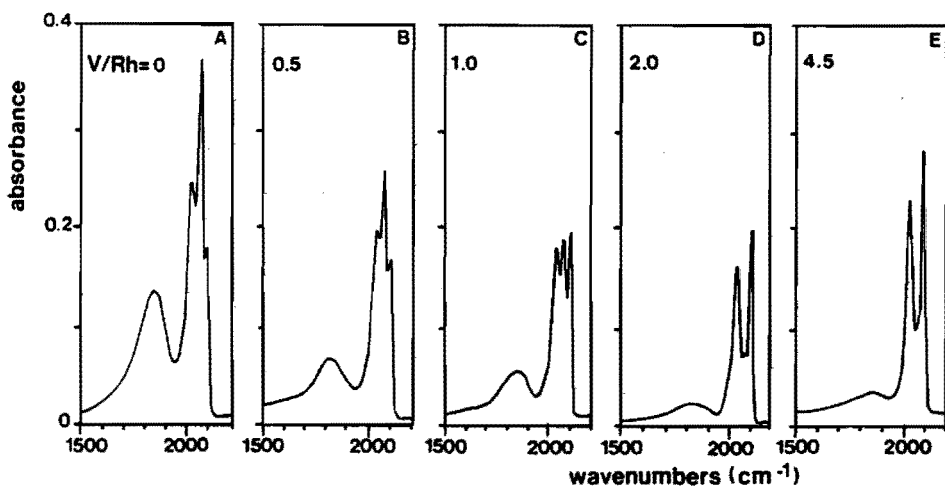


FIGURE 7.7: The infrared spectra of CO adsorbed on 1.5 wt% $\text{Rh}/\text{V}_2\text{O}_3/\text{SiO}_2$ catalysts with varying V/Rh ratios (adsorption at 298 K, $P_{\text{CO}} = 10$ Torr, reduction temperature 523 K, evacuation temperature 673 K).

The infrared spectrum of CO adsorbed on $\text{Rh}/\text{V}_2\text{O}_3/\text{SiO}_2$ was dramatically influenced by the presence of vanadium oxide, as shown in Figure 7.7. With increasing vanadium content, the amounts of bridge-bonded and linearly bonded CO, B and L respectively, strongly decreased and almost disappeared for $\text{V}/\text{Rh} = 4.5$. The bands, due to the dicarbonyl species, T_1

and T_2 , remain about constant.

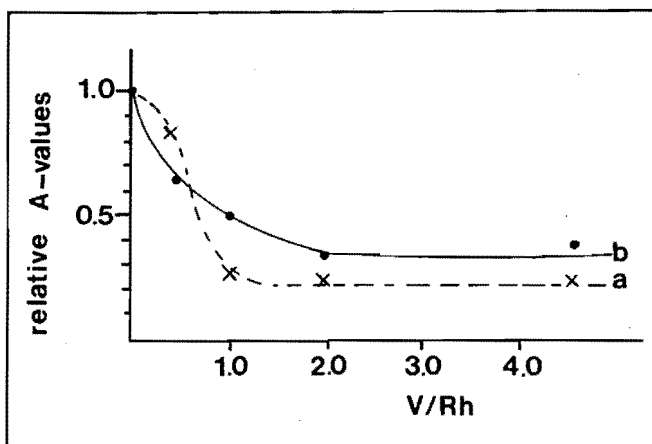


FIGURE 7.8: Relative integrated areas of the infrared absorbance spectra of the vanadium oxide-promoted 1.5 wt% Rh/SiO₂ catalysts relative to that of unpromoted 1.5 wt% Rh/SiO₂

a. after reduction at 523 K and evacuation at 523 K

b. after reduction at 523 K and evacuation at 673 K.

In order to compare the amounts of adsorbed CO for the systems with different V/Rh ratios, the adsorbance spectra were integrated:

$$A = \int_{1500}^{2200} {}^{10}\log I_0/I \, d\nu \quad (7.1)$$

where ${}^{10}\log (I_0/I)$ is the adsorbance and w_c is the amount of catalyst present in the cross-section of the beam. The A-values were normalized to the A-value of the Rh/SiO₂ catalyst (V/Rh = 0). The results are presented in Figure 7.8. A decrease of the A-value with increasing V/Rh ratio is observed. Of course, CO/Rh values cannot be calculated from these A-values because of differences in absorption coefficients for the different adsorption forms of carbon monoxide. Duncan *et al.* [42] reported the following infrared absorption coefficients for Rh/Al₂O₃: $\epsilon(L) = 26 \times 10^6$, $\epsilon(B) = 85 \times 10^6$, $\epsilon(T_{1,symm}) = 74 \times 10^6$ and $\epsilon(T_{2,asymm}) = 128 \times 10^6 \text{ cm mol}^{-1}$ for the linearly bonded and bridge-bonded CO, and symmetrical twin and asymmetrical twin structure, respectively. We could not determine the integrated areas of the adsorption bands separately and therefore can only use the A-values qualitatively. At high V/Rh values, the gem-dicarbonyl

structure is the most predominant form, and this structure has the highest ϵ -value. Therefore the real decrease in the CO/Rh ratio is higher than the observed decrease in the relative A-value (see Figure 7.8). The trend is similar to the trend observed for the CO chemisorption measurements (Figure 7.4). Thus, infrared spectroscopy shows that CO/Rh decreases along with increasing vanadium oxide content and that this decrease originates mainly from a decrease of the amount of linearly bonded and bridge-bonded CO. The amount of CO bonded in the twin structure remains almost constant.

Diffuse reflectance infrared spectroscopy. The diffuse reflectance infrared spectra of V_2O_5 , V_2O_5/SiO_2 (2.2 wt% V) and $Rh/V_2O_5/SiO_2$ (2.2 wt% V, 4.5 wt% Rh, calcined at 723 K) in the region of V-O stretching frequencies are presented in Figure 7.9. For V_2O_5/SiO_2 and V_2O_5 bands around 1010 and 920 cm^{-1} are observed. The band around 1010 cm^{-1} is ascribed to the V-O stretching vibration of V_2O_5 , the band at 920 cm^{-1} might be due to reduced vanadium oxide species like V_2O_4 [43,44]. Partial reduction of V_2O_5 at the surface of the sample was observed by a change in colour, and was a result of the fact that the infrared spectra were recorded in vacuum. For the $Rh/V_2O_5/SiO_2$ sample, the intensity of the band at 1010 cm^{-1} dramatically decreased and the band at 920 cm^{-1} completely disappeared, although the same amount of catalyst was present in the sample holder.

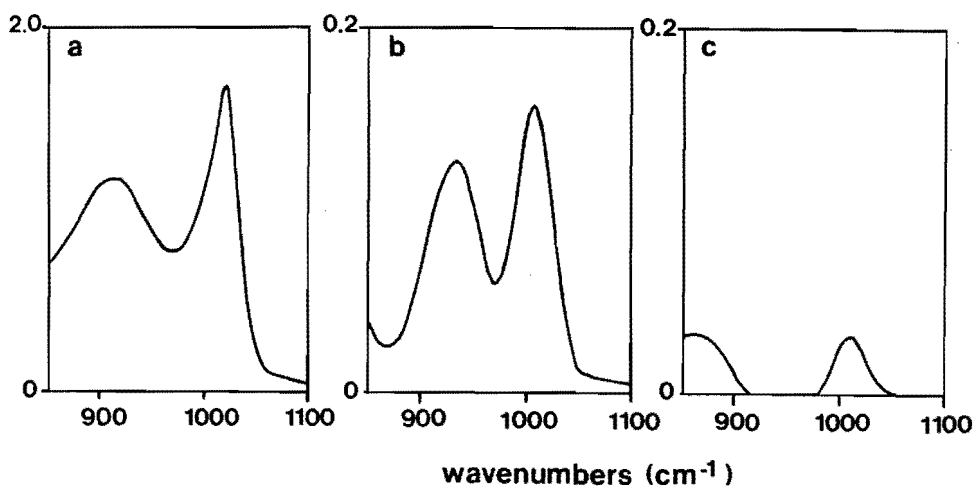


FIGURE 7.9: Diffuse reflectance infrared spectra (Kubelka-Munk units versus wavenumber) of V_2O_5 (a), V_2O_5/SiO_2 , 2.2 wt% V (b) and $Rh/V_2O_5/SiO_2$, 2.2 wt% V, 4.5 wt% Rh, calcined at 723 K (c).

7.3.3 Rh/ V_2O_5 / Al_2O_3

Temperature programmed reduction. We attempted to prepare a monolayer of vanadium oxide on the alumina support by adsorbing metavanadate at pH = 4 (using HNO_3). This resulted in a 5.6 wt% V loading. Calcination of this system followed by a second adsorption step resulted in a 6.7 wt% V loading. Assuming an area of 10.3 \AA^2 per $VO_{2.5}$ unit [45], one can calculate that 6.7 wt% V only occupies about 40% of the support surface. An explanation for a sub-maximum coverage is that during the preparation step the metavanadate is only adsorbed on one type of OH-group of the alumina. Evidence for this will be presented in a subsequent paper [20]. In Figure 7.10a the TPR profile of the 6.7 wt% V_2O_5/Al_2O_3 support after calcination is presented. The reduction of the vanadium oxide already starts around 573 K, and has a maximum around 773 K. Some extra hydrogen consumption is observed around 1023 K. With XRD no crystalline V_2O_5 phase could be detected in this support.

The reduction profiles of the Rh/ V_2O_5 / Al_2O_3 catalysts after calcination (Figure 7.10b-e) are all similar. Hydrogen consumption starts at the beginning of the temperature ramp (298 K) and has a maximum at 415-442 K. The amount of hydrogen consumed during the TPR run matches the theoretical value when assuming reduction of Rh^{3+} to Rh^0 and of V^{5+} to V^{3+} . For the systems with a high vanadium oxide loading, hydrogen consumption is also observed at temperatures above 673 K, the temperature region where reduction is observed for V_2O_5/Al_2O_3 (cf. Figure 7.10a). In contrast with the first TPRs (Figure 7.10b-e), in the TPR profiles obtained after oxidation up to 898 K during TPO (Figure 7.10f-h), an influence of the vanadium loading on the reduction temperature is observed for catalysts with a high V/Rh ratio. The systems with a higher vanadium loading exhibit a higher reduction temperature, as was also observed for the silica-supported systems after calcination.

H_2 and CO chemisorption, infrared spectroscopy of adsorbed CO. The results of the hydrogen and carbon monoxide chemisorption measurements of the Rh/ V_2O_5 / Al_2O_3 systems are presented in Figure 7.11. CO/Rh values decreased only slightly with increasing vanadium content, in contrast to those for the Rh/ V_2O_5 / SiO_2 catalysts. The H/Rh ratio is constant up to V/Rh = 1.0, but systems with high V/Rh ratios exhibit very high H/Rh ratios, as was also measured for the Rh/ V_2O_5 catalyst after a low temperature reduction. Rhodium particles were not observed by TEM in any

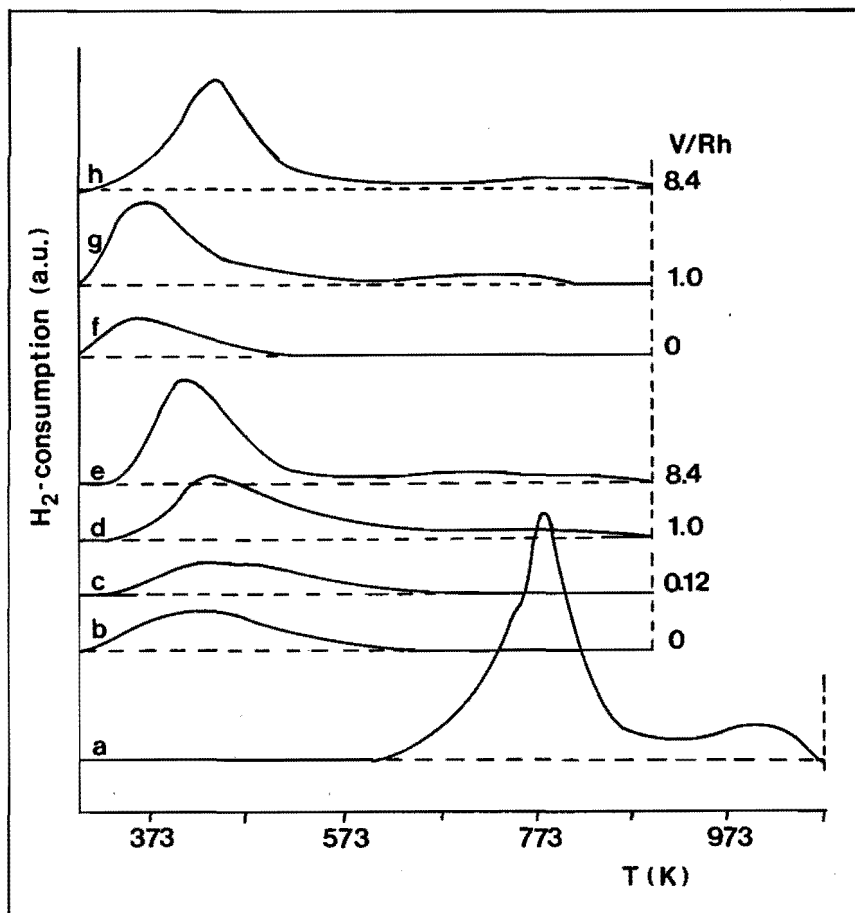


FIGURE 7.10: Temperature programmed reduction profiles of alumina-supported 1.5 wt% Rh catalysts.

a. 6.7 wt% V_2O_5/Al_2O_3

b-e. Rh/ V_2O_5/Al_2O_3 catalysts after calcination

f-h. Rh/ V_2O_5/Al_2O_3 catalysts after oxidation at 898 K.

Final reduction temperature 1073 K for a. and 898 K for b-h.

catalyst, pointing to a particle size less than 8 Å. The infrared spectra of Rh/ Al_2O_3 and Rh/ V_2O_5/Al_2O_3 with V/Rh = 7.0 are presented in Figure 7.12. Also in this case, the bridge-bonded and linearly bonded CO were suppressed by the presence of vanadium oxide, while the twin species were favoured. The Rh/ Al_2O_3 catalyst already had more twin-adsorbed CO than the Rh/ SiO_2 catalyst. A minor peak at 2181 cm^{-1} was observed for the vanadium oxide-promoted system and may be attributed to CO bonded to

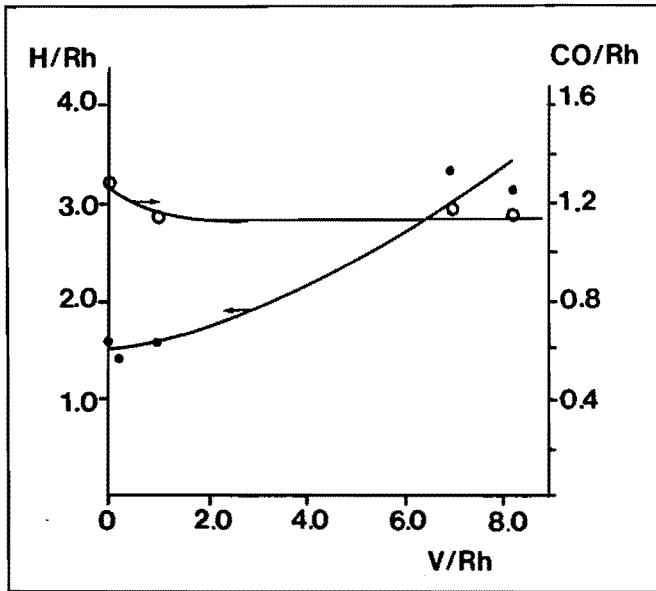


FIGURE 7.11: H_2 (●) and CO (○) chemisorption measurements of the 1.5 wt% Rh/ V_2O_3 / Al_2O_3 catalysts after reduction at 523 K and evacuation at 723 K, as a function of the V/Rh ratio.

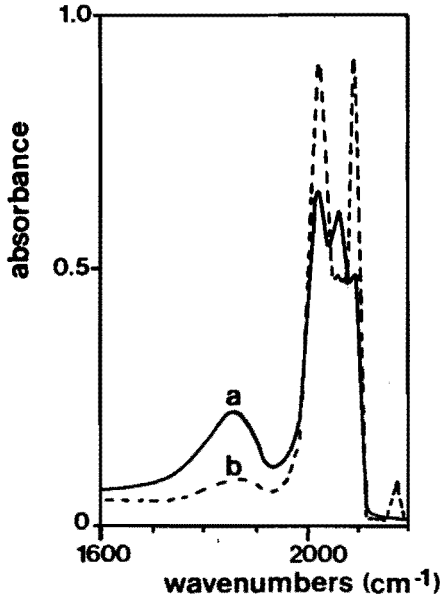


FIGURE 7.12: Infrared spectrum of adsorbed CO on 1.5 wt% Rh/ Al_2O_3 (a), and 1.5 wt% Rh/ V_2O_3 / Al_2O_3 (V/Rh = 7.0) (b), after reduction at 523 K and evacuation at 673 K ($P_{CO} = 10$ Torr, adsorption at 298 K).

Rh(III) [35].

7.4 DISCUSSION

7.4.1 Temperature programmed reduction

The TPR profiles of silica- and alumina-supported vanadium oxide exhibited only one prominent hydrogen consumption maximum. This contrasts with the reduction behaviour of bulk V_2O_5 , where several reduction steps can be distinguished [31]. Single peaks were also observed for titania-supported monolayers of V_2O_5 by Van Hengstum *et al.* [46] and Bond *et al.* [47], and for silica- and alumina-supported vanadium oxide by Kijenski *et al.* [48] and Roozeboom *et al.* [49]. The appearance of only one reduction peak suggests the presence of small amorphous vanadium oxide particles. In such particles no shear structures like V_6O_{13} and V_6O_{11} can be formed and therefore the reduction process proceeds in one step. However, taking into account the limited resolution of TPR measurements in the systems under study, the appearance of only one reduction peak does not decisively prove that the reduction occurs in a single step [48]. Nevertheless, it can be concluded that the supported vanadium oxide exhibits a completely different reduction behaviour than bulk V_2O_5 . Combining this with the results of XRD measurements, we can confidently conclude that large crystalline V_2O_5 particles are absent.

Temperature programmed reduction profiles of the calcined Rh/ V_2O_3 and Rh/ V_2O_5 /SiO₂ systems suggest that an intimate contact exists between the vanadium oxide promoter and the rhodium metal particles even at a low V/Rh ratio. The rhodium facilitates the reduction of the vanadium oxide, i.e. the reduction shifts to a lower temperature, and vanadium oxide hampers the reduction of rhodium oxide, i.e. its reduction temperature shifts to a higher value. The first effect could be explained by hydrogen spillover. However, the second cannot be explained by hydrogen spillover and proves that rhodium and vanadium oxide are in intimate contact in the Rh/ V_2O_5 /SiO₂ catalysts after calcination at 723 K. This effect is even more pronounced in the profiles of the second TPR (after oxidation at 898 K). In the profiles of the catalysts with low V/Rh values, one can even distinguish a peak due to the reduction of "free" rhodium oxide and a peak due to the reduction of rhodium oxide and vanadium oxide in close contact. The peak of the free rhodium oxide diminishes with increasing V/Rh ratio.

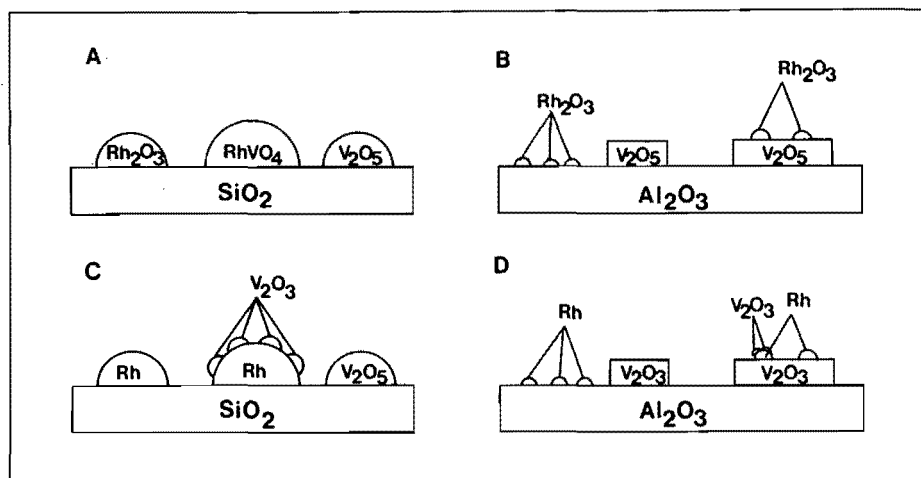


FIGURE 7.13: Schematic illustration of the model for the silica- and alumina-supported, vanadium oxide-promoted rhodium catalysts after calcination at 723 K (a and b), and after reduction at 523 K (c and d).

All this can be understood by assuming that a mixed oxide is formed. A mixed oxide of Rh_2O_3 and V_2O_5 , $RhVO_4$, is known to exist and can be formed by heating Rh_2O_3 and V_2O_5 under oxygen atmosphere at 923 K [50]. This temperature is higher than our calcination temperature (723 K), but surface reactions are known to proceed at lower temperatures than bulk reactions. This also clarifies the difference between the first TPR after calcination at 723 K and the second TPR after oxidation at 898 K. During the high temperature oxidation well defined phases of Rh_2O_3 and $RhVO_4$ are formed, reflected by distinct reduction peaks in the second TPR. For $V/Rh > 1.0$ a third hydrogen consumption peak around 453 K and a fourth consumption peak around 773 K can be observed. The third peak might be caused by the reduction of a mixed oxide with $V/Rh > 1.0$, like $Rh_2V_4O_{13}$, or by V_2O_5 layers positioned on top of the $RhVO_4$. The fourth reduction peak occurred around the temperature where V_2O_5/SiO_2 reduces (cf. Figure 7.2a,b) and must be caused by the reduction of V_2O_5 that is not in intimate contact with rhodium.

Although the assumption of the formation of a mixed oxide seems plausible, on the basis of the TPR profiles we cannot exclude that V_2O_5 is positioned on the nucleation sites of the reduction process of Rh_2O_3 , or that V_2O_5 totally covers the Rh_2O_3 . Furthermore we also cannot exclude that

part of the V_2O_5 is positioned between the Rh_2O_3 particle and the SiO_2 support. However, additional evidence for the formation of a mixed oxide is obtained from the diffuse reflectance infrared spectrometry measurements. In the IR spectrum of $Rh/V_2O_5/SiO_2$ (calcined at 723 K, $V/Rh = 0.9$) almost no V-O stretching bands were observed (Figure 7.9c), pointing to the absence of "free" V_2O_5 . This suggests that V_2O_5 and Rh_2O_3 formed a chemical compound. Bands of $RhVO_4$ have been reported below 900 cm^{-1} [50]. In this frequency region it was impossible to measure the infrared spectrum because of the strong absorption bands of SiO_2 and the insensitivity of the detector.

The present study clearly showed that after calcination at 723 K an intimate contact exists between the V_2O_5 promoter and the Rh_2O_3 particle, most probably in the form of a mixed oxide ($RhVO_4$). A schematic representation of this situation is presented in Figure 7.13a. For $V/Rh < 1$, after calcination and oxidation distinct Rh_2O_3 and $RhVO_4$ particles exist. For $V/Rh > 1$, V_2O_5 and mixed oxide particles like $RhVO_4$ are present on the support.

For the 1.5 wt% Rh/V_2O_5 catalyst, the first reduction peak is shifted to even higher temperatures than in the case of $Rh/V_2O_5/SiO_2$. This might be due to a covering of $RhVO_4$ by several layers of V_2O_5 .

The first TPRs of the alumina-supported vanadium oxide-promoted systems show that rhodium facilitates the reduction of vanadium oxide, but that the reduction of rhodium is not hampered by the presence of vanadium oxide. For the $Rh/V_2O_5/Al_2O_3$ catalysts with $V/Rh < 1$, even after oxidation at 898 K no hampering of the reduction of Rh_2O_3 was observed. We conclude that in this case the intimate contact between Rh_2O_3 and V_2O_5 in the form of a mixed oxide does not exist. Hydrogen spillover can explain the co-reduction of Rh_2O_3 and V_2O_5 . In agreement with this, the influence of V_2O_5 on the catalytic activity of Rh/Al_2O_3 for catalysts with $V/Rh < 1$ was negligible [20]. Thus, at least for $V/Rh < 1$, V_2O_5 and Rh_2O_3 particles exist separately on the Al_2O_3 support. During the impregnation of vanadium and rhodium, ammonium metavanadate and rhodium nitrate complexes rapidly adsorb on distinct sites on the alumina surface and, after calcination, these will result in Rh_2O_3 and V_2O_5 particles. The NH_4VO_3 and $Rh(NO_3)_3$ complexes do not adsorb on SiO_2 and therefore a mixed oxide can be formed on that support.

For $Rh/V_2O_5/Al_2O_3$ with $V/Rh = 7.0$ and 8.4, there clearly is an influence of the V_2O_5 on the reduction behaviour of Rh_2O_3 , the reduction of Rh_2O_3 is shifted to a higher temperature in the second TPR, pointing to the

formation of a mixed oxide. For these catalysts also an influence of the V_2O_5 on the catalytic behaviour is observed [20] and probably the Rh_2O_3 is (partly) positioned on top of the V_2O_5 layer. The mixed oxide ($RhVO_4$) can be formed only after oxidation at 898 K, because of the strong interaction between the V_2O_5 layer and the Al_2O_3 support. For the $Rh/V_2O_5/Al_2O_3$ catalysts with high V/Rh values, hydrogen consumption above 573 K is observed during the first and second TPR. This consumption must be due to the reduction of V_2O_5 positioned far away from the rhodium particles, so that hydrogen spillover cannot facilitate its reduction.

The resulting model which describes the state of the $Rh/V_2O_5/Al_2O_3$ catalysts is presented in Figure 7.13b. For $V/Rh < 1$, separate Rh_2O_3 and V_2O_5 particles exist on the support, with no interaction. For the catalysts with $V/Rh = 7.0$ and 8.4 , part of the Rh_2O_3 is positioned on V_2O_5 and only after oxidation at 898 K a mixed oxide is formed.

7.4.2 Hydrogen and carbon monoxide chemisorption

For the $Rh/V_2O_5/SiO_2$ catalysts, hydrogen and carbon monoxide chemisorption after reduction and evacuation at 523 K or 723 K showed a decrease of the H/Rh and CO/Rh values with increasing vanadium oxide content. However, from the temperature programmed desorption experiments we learned that the suppression of the hydrogen chemisorption is not real but is caused by incomplete desorption at the reduction and evacuation temperature. This effect aggravates with increasing vanadium content. After reduction at 723 K, part of the hydrogen is bonded even stronger (desorption peak at 823 K), and therefore also reduction and evacuation at 723 K is not sufficient to remove all hydrogen.

Considering the TPD results, reduction at 523 K and evacuation at 723 K seems to be the right pretreatment preceding hydrogen and carbon monoxide chemisorption. Using this pretreatment, CO/Rh still decreases with increasing vanadium content. This suppression of carbon monoxide chemisorption cannot be caused by a larger particle size since TEM measurements show that the rhodium particle size is not dependent on the vanadium content. The suppression of carbon monoxide chemisorption by promoters has also been reported by Van den Berg *et al.* [51] for Mo- and Mn-promoted Rh/SiO_2 , by Ichikawa *et al.* [52] for Fe- and Zr-promoted Rh/SiO_2 , and by Hicks *et al.* [19] for Pd/La_2O_3 . The suppression of CO chemisorption proves that the promoter oxide partially covers the metal particle. In fact, one can calculate that in order to decrease the CO chemisorption by a factor of 3,

(as was measured by carbon monoxide chemisorption and infrared spectroscopy) at a V/Rh ratio of 1.0, the vanadium oxide has to be spread over the rhodium surface as a near-monolayer. These results point to a model as depicted in Figure 7.13c.

The idea of the spreading of an oxidic overlayer over a noble metal received considerable support in recent work on the so-called strong metal-support interaction (SMSI). The support (e.g. TiO_2) is converted to a suboxide (e.g. Ti_4O_7) after high temperature reduction, and there is strong experimental evidence that this suboxide spreads over transition metals forming incomplete overlayers [11-18]. However, the observed covering effect for the Rh/ V_2O_3 / SiO_2 system does not originate from the high temperature reduction, but already exists after reduction at 523 K. The suppression in this case is caused by V_2O_3 layers, formed during the reduction of RhVO_4 , which was generated during calcination (Figure 7.13a,c).

For the alumina-supported catalysts, only a minor suppression of the CO chemisorption is observed, suggesting that covering by vanadium oxide did not occur. In this case, no mixed oxide is formed after calcination (see TPR results). For low V/Rh values, the vanadium oxide does not cover the rhodium metal particle but is positioned on separate locations on the Al_2O_3 surface. For V/Rh > 1, part of the rhodium particles might be positioned on vanadium oxide (Figure 7.13d).

7.4.3 Infrared spectroscopy of adsorbed CO

The infrared spectra of the Rh/ V_2O_3 / SiO_2 catalysts support and specify the conclusion from the CO chemisorption measurements (Figure 7.8). Bridge-bonded and linearly bonded carbon monoxide are almost completely suppressed, the twin structure of adsorbed CO is (almost) unaffected by the presence of vanadium oxide (Figure 7.7). Thus, the remarkable fact that the CO/Rh value is not completely suppressed above V/Rh = 1.0 is due to the absence of suppression of the gem-dicarbonyl species. As shown by EXAFS, in the gem-dicarbonyl species two CO molecules are bonded to a Rh^+ cation, formed by oxidation (using OH-groups of the support) of small Rh metal particles during CO adsorption [40]. Of course, this highly dispersed rhodium can not be seen by TEM. Apparently, particles covered by vanadium oxide still can provide Rh atoms which can be oxidized by OH-groups during adsorption of carbon monoxide, forming the $\text{Rh}(\text{CO})_2^+$ species. The same behaviour is seen for the Rh/ V_2O_3 / Al_2O_3 systems with V/Rh = 7.0. In that case, the linearly bonded and bridge-bonded CO are also

suppressed, suggesting that the rhodium particles are partially covered by vanadium oxide. The twin structure even increases when vanadium oxide is present. This may be caused by a better adsorption of the rhodium precursor on the vanadium oxide monolayer than on the bare alumina support, resulting in a smaller particle size in the vanadium oxide-promoted system. In the future, we will further study these systems by EXAFS.

7.4.4 Hydrogen ad- and desorption studies

In the case of $Rh/V_2O_3/SiO_2$, the hydrogen chemisorption is not suppressed, H/Rh is constant up to $V/Rh = 1$. However, the CO chemisorption results pointed to a partial coverage of the metal particles. This suggests that hydrogen will adsorb not only on the exposed rhodium atoms, but also on the surface of the V_2O_3 patches covering the metal particle. Such an adsorption has been reported before by Hicks *et al.* for Pd/La_2O_3 systems [19]. Evidence for the adsorption of hydrogen on V_2O_x patches is obtained from the desorption profiles after reduction at 723 K (Figure 7.3b,c,d, dashed profiles). We think that the first desorption area between 298 and 623 K is due to the desorption of hydrogen bonded to Rh, and that the second desorption area (673–973 K) is due to the desorption of hydrogen from the vanadium oxide, because the first peak decreases and the second peak increases with increasing vanadium oxide content.

The silica- and alumina-supported systems with $V/Rh > 1.0$, as well as the Rh/V_2O_3 systems, exhibit (very) high H/Rh ratios. These high ratios can not be explained by the assumption that all hydrogen is bonded to the metal. For instance, the 1.5 wt% Rh/V_2O_3 catalyst has a H/Rh value of 3.8, but TEM showed that the average particle size was 35 Å. Calculations based on half spherical metal particles indicate that the fraction of exposed metal atoms is 0.36 for an average particle size of 35 Å [25,28], in good agreement with the CO chemisorption measurement for this catalyst. However, a H/Rh value of 3.8 with all hydrogen bonded to the metal, would result in a H/Rh_{surface} stoichiometry of about 10, which is impossible. This must mean that the hydrogen is not only adsorbed on the metal but also on the support. However, vanadium oxide itself did not adsorb hydrogen. Thus, the presence of the metal is necessary to reach such high H/Rh values. From the chemisorption measurement of the silica-supported catalysts it can also be concluded that the extra hydrogen must be positioned on/in the vanadium oxide. Hydrogen chemisorption of these systems show that with equal rhodium particle size, the addition of an excess of vanadium oxide

(V/Rh > 1) results in a strong increase of the H/Rh value.

An explanation for the hydrogen atoms located in or on vanadium oxide might be the formation of bronzes. Recently, Tinet *et al.* [53,54] and Bond *et al.* [55] reported the formation of hydrogen bronzes like $H_{2x}V_2O_5$ ($x = 0-1.7$) at about 338 K from a V_2O_5 microcrystalline powder, coated with small Pt particles, in contact with gaseous molecular hydrogen, through hydrogen spillover. It is essential that hydrogen is provided in atomic form by dissociation on a noble metal. The hydrogen atoms then can insert in the host lattice, V_2O_5 . It has been shown that the proton is localized, creating V^{4+} and V^{3+} paramagnetic centers [54]. Thus, in our catalysts hydrogen adsorbs on exposed rhodium atoms, dissociates, and diffuses to vanadium oxide on the metal particle or support (by spillover), forming the hydrogen bronzes.

Recently, Lin *et al.* [56] proposed a similar spillover process from the rhodium metal to the vanadium oxide followed by hydrogen bronze formation. They observed a slow hydrogen adsorption rate and an increase in uptake with increasing pressure. Since we admitted hydrogen at 473 K at a relatively high pressure (around 80 kPa), the spillover and bronze formation will be more extended in our measurements. Lin's results also pointed to the importance of the impregnation and drying steps in the catalysts preparation.

7.5 CONCLUSIONS

Temperature programmed reduction studies showed that after calcination at 723 K, Rh facilitates the reduction of V_2O_5 , and V_2O_5 hampers the reduction of rhodium oxide in the case of $Rh/V_2O_5/SiO_2$ systems. Diffuse reflectance infrared spectrometry showed that a $Rh/V_2O_5/SiO_2$ catalyst with V/Rh = 0.9 did not contain "free" V_2O_5 . These results suggest the formation of the mixed oxide $RhVO_4$.

For $Rh/V_2O_5/Al_2O_3$ systems with V/Rh < 1, no evidence is found for an intimate contact between Rh_2O_3 and V_2O_5 . Separate Rh_2O_3 and V_2O_5 particles will exist on the Al_2O_3 support due to the strong interaction between the V_2O_5 and the Al_2O_3 support. For $Rh/V_2O_5/Al_2O_3$ catalysts with high V/Rh values (7.0 and 8.4) the formation of $RhVO_4$ was observed only after oxidation at 898 K. For these catalysts, Rh_2O_3 is believed to be partially positioned on top of a V_2O_5 layer. A higher oxidation temperature is required to form $RhVO_4$, because of the stronger interaction between V_2O_5 and Al_2O_3 .

CO chemisorption showed that CO/Rh was suppressed by the presence of vanadium oxide, proving a (partial) coverage of the rhodium metal by vanadium oxide in the Rh/ V_2O_5 /SiO₂ catalysts. TEM showed that the rhodium particle size was not influenced by the addition of vanadium oxide. Almost no suppression of CO chemisorption was observed for the Rh/ V_2O_5 /Al₂O₃ systems. Infrared spectroscopy showed that the linearly bonded and bridge-bonded CO were almost completely suppressed by vanadium oxide, especially present in the Rh/ V_2O_5 /SiO₂ systems, whereas the twin structure was unaffected.

Hydrogen chemisorption experiments showed that hydrogen is not only adsorbed by exposed rhodium atoms but also by vanadium oxide patches covering the rhodium. The systems with a high V/Rh ratio exhibit very high H/Rh values (up to H/Rh = 3.0), caused by the formation of hydrogen bronzes.

Our results prove that for the Rh/ V_2O_5 /SiO₂ catalysts an intimate contact between the active component, rhodium, and the promoter, vanadium oxide, is present. The weak interaction between V_2O_5 and SiO₂, and the strong interaction between Rh₂O₃ and V_2O_5 , result in the formation of a mixed oxide (RhVO₄) during catalyst preparation (calcination), which after reduction results in a vanadium oxide layer on top of the metal particle. On the other hand, for the Rh/ V_2O_5 /Al₂O₃ catalysts, a strong interaction between V_2O_5 and the Al₂O₃ support prevents mixed oxide formation, and Rh₂O₃ and V_2O_5 particles exist separately on the Al₂O₃ support. Only for Rh/ V_2O_5 /Al₂O₃ catalysts with a high V/Rh ratio (near mono-layer coverage of vanadium oxide), rhodium particles might be positioned on top of the V_2O_5 layer, after oxidation at 898 K leading the formation of RhVO₄.

7.6 REFERENCES

1. M. Ichikawa, Bull. Chem. Soc. Jap., 51 (1978) 2268.
2. M. Ichikawa, Bull. Chem. Soc. Jap., 51 (1978) 2273.
3. J.R. Katzer, A.W. Sleight, P. Gajardo, J.B. Mitchel, E.F. Gleason and S. McMillan, Far. Disc. Chem. Soc., 72 (1981) 121.
4. E. Kikuchi, H. Nomura, M. Matsumoto and Y. Morita, Appl. Catal., 7 (1983) 1.
5. T. Mori, A. Miyamoto, N. Takahashi, M. Fukagaya, H. Niizuma, T. Hattori and Y. Murakami, J. Chem. Soc., Chem. Commun., (1984) 678; T. Mori, A. Miyamoto, N. Takahashi, M. Fukagaya, T. Hattori and Y. Murakami, J. Phys. Chem., 90 (1986) 5197.
6. M. Ichikawa, K. Shikakura and M. Kawai, in "Heterogeneous Catalysis Related to Energy Problems", Proc. Symp. in Dalian, China, (1982) A.08-I.

7. G. van der Lee, B. Schuller, H. Post, T.L.F. Favre and V. Ponc, *J. Catal.*, 98 (1986) 522.
8. S.J. Tauster and S.C. Fung, *J. Catal.*, 55 (1978) 29.
9. S.J. Tauster, S.C. Fung and R.L. Garten, *J. Am. Chem. Soc.*, 100 (1978) 170.
10. S.J. Tauster, S.C. Fung, R.T.K. Baker and J.A. Horsley, *Science*, 211 (1981) 1121.
11. X.-Zh.Jing, T.F. Hayden and J.A. Dumesic, *J. Catal.*, 83 (1983) 168.
12. J. Santos, J. Phillips and J.A. Dumesic, *J. Catal.*, 81 (1983) 147.
13. P. Meriaudeau, J.F. Dutel, M. Dufaux and C. Naccache, *Stud. Surf. Sci. Catal.*, 11 (1982) 95.
14. D.E. Resasco and G.L. Haller, *J. Catal.*, 82 (1983) 279.
15. B.R. Powell and S.E. Whittington, *J. Catal.*, 81 (1983) 382.
16. A.J. Simoens, R.T.K. Baker, D.J. Dwyer, C.F.R. Lund and R.J. Madon, *J. Catal.*, 86 (1984) 359.
17. G.L. Haller, V.E. Henrich, M. McMillan, D.E. Resasco, H.R. Sadeghi and S. Sakellson, "Proc. of the 8th Int. Congr. Catal.", Berlin (1984), vol. V, 135, Verlag Chemie, Weinheim 1984.
18. Y.W. Chung, G. Xiong and C.C. Kao, *J. Catal.*, 87 (1984) 279.
19. R.F. Hicks, Q. Yen and A.T. Bell, *J. Catal.*, 89 (1984) 498.
20. B.J. Kip, P.A.T. Smeets, J. van Grondelle and R. Prins, to be published, chapter 8 of this thesis.
21. F. Roozeboom, J. Medema and P. Gellings, *Z. Phys. Chem. Neue Folge*, 111 (1979) 215.
22. A. Iannibello, S. Marenga and F. Trifiro, "Preparation of Catalysts II", Elsevier, Amsterdam (1979) 65.
23. A. Iannibello and P. Mitchell, "Preparation of Catalysts II", Elsevier, Amsterdam (1979) 25.
24. F. Roozeboom, T. Fransen, P. Mars and P. Gellings, *Z. Anorg. Allg. Chem.*, 449 (1979) 25.
25. B.J. Kip, J. van Grondelle, J.H.A. Martens and R. Prins, *Appl. Catal.*, 26 (1986) 353, chapter 3 of this thesis.
26. A. Crucq, L. Degols, G. Lienard and A. Frennet, *Acta Chim. Acad. Sci. Hung.*, (1982) 111.
27. J.E. Benson and M. Boudart, *J. Catal.*, 4 (1965) 704.
28. B.J. Kip, F.B.M. Duijvenvoorden, D.C. Koningsberger and R. Prins, *J. Catal.*, to be published, chapter 4 of this thesis.
29. H. Boer, W.J. Boersma and N. Wagstaff, *Rev. Sci. Instr.*, 52 (1982) 439.
30. T. Huizinga, J. van Grondelle and R. Prins, *Appl. Catal.*, 10 (1984) 199.
31. H. Bosch, B.J. Kip, J.G. van Ommen and P.J. Gellings, *J. Chem. Soc., Faraday Trans. I*, 80 (1984) 2479.

32. A.C. Yang and C.W. Garland, *J. Phys. Chem.*, 61 (1957) 1510.
33. D.J.C. Yates, T.M. Duncan, S.D. Worley and R.W. Vaughan, *J. Chem. Phys.*, 70 (1979) 1219.
34. C.A. Rice, S.D. Worley, C.W. Curtis, J.A. Guin and A.R. Tarrer, *J. Chem. Phys.*, 74 (1981) 6487.
35. S.D. Worley, C.A. Rice, G.A. Mattson, C.W. Curtis, J.A. Guin and A.R. Tarrer, *J. Chem. Phys.*, 76 (1982) 20; *J. Phys. Chem.*, 86 (1982) 2714.
36. F. Solymosi and M. Pasztor, *J. Phys. Chem.*, 89 (1985) 4789.
37. R.R. Cavenagh and J.T. Yates, Jr., *J. Catal.*, 68 (1981) 22.
38. J.T. Yates, Jr. and K. Kolanski, *J. Chem. Phys.*, 79 (1983) 1026.
39. H.P. Wang and J.T. Yates, Jr., *J. Catal.*, 89 (1984) 79.
40. H.F.J. van 't Blik, J.B.A.D. van Zon, T. Huizinga, J.C. Vis, D.C. Koningsberger and R. Prins, *J. Am. Chem. Soc.*, 107 (1985) 3139.
41. P. Hollins, *Ads. Science and Techn.*, 2 (1985) 177.
42. T.M. Duncan, J.T. Yates, Jr. and R.W. Vaughan, *J. Phys. Chem.*, 73 (1980) 975.
43. M. Inomata, A. Miyamoto and Y. Murakami, *J. Phys. Chem.*, 85 (1981) 2372.
44. J.L.G. Fierro, L.A. Ganbaro, T.A. Cooper and G. Kremenec, *Appl. Catal.*, 6 (1983) 363.
45. W. Hanke, R. Bienert and H.G. Jerschke, *Z. Anorg. Allg. Chem.*, 414 (1975) 109.
46. A.J. van Hengstum, J.G. van Ommen, H. Bosch and P.J. Gellings, in "Proc. 8th Int. Congr. Catal.", Berlin (1984) IV-297, Verlag Chemie, Weinheim 1984.
47. G.C. Bond, J.P. Zurita, S. Flamerz, P.J. Gellings, H. Bosch, J.G. van Ommen and B.J. Kip, *Appl. Catal.*, 22 (1986) 361.
48. J. Kijenski, A. Baiker, M. Glinski, P. Dollenmeier and A. Wokaun, *J. Catal.*, 101 (1986) 1.
49. F. Roozeboom, M.C. Mittelmeyer-Hazelegger, J.A. Moulijn, J. Medema, V.H.J. de Beer and P.J. Gellings, *J. Phys. Chem.*, 84 (1980) 2783.
50. I.S. Shaplygin, I.I. Prosychev and V.B. Lazarev, *Russ. J. Inorg. Chem.*, 23 (1978) 773.
51. F.G.A. van den Berg, J.H.E. Glezer and W.M.H. Sachtler, *J. Catal.*, 93 (1985) 340.
52. M. Ichikawa, T. Fukushima and K. Shikakura, in "Proc. 8th Int. Congr. Catal.", Berlin (1984) II-69, Verlag Chemie, Weinheim 1984.
53. D. Tinet and J.J. Fripiat, *Rev. Chim. Miner.*, 19 (1982) 612.
54. D. Tinet, M.H. Legay, L. Gatineau and J.J. Fripiat, *J. Phys. Chem.*, 90 (1986) 948.
55. G.C. Bond, P.A. Shermon and C.J. Wright, *Mater. Res. Bull.*, 19 (1984) 701.
56. Y.J. Lin, R.J. Fenoglio, D.E. Resasco and G.L. Haller, in "Preparation of Catalysts IV", Louvain-la-Neuve (Belgium) (1986) A10.

Chapter 8

HYDROGENATION OF CARBON MONOXIDE OVER VANADIUM OXIDE-PROMOTED RHODIUM CATALYSTS

The effect of vanadium oxide as support and promoter on supported rhodium catalysts on the CO hydrogenation has been investigated at 0.15 and 4.0 MPa. Rh/V₂O₃ reduced at 723 K has a good selectivity toward oxygenated products, especially C₂-oxygenates, but has a low activity and stability. Vanadium oxide added as a promoter to catalysts consisting of rhodium supported on silica and alumina showed a remarkable effect on the activity of these systems. For the silica-supported systems the activity increased by a factor of 40, the deactivation of these catalysts was low (2 % h⁻¹) and the oxo-selectivity was very high (70 %). Although the vanadium oxide blocks part of the active metal surface, as became evident from a suppressed chemisorption capacity, it also enhances the rate of CO dissociation in those locations where reaction is still possible. The enhancement prevails over the blocking in the case of silica- and alumina-supported vanadium oxide-promoted catalysts, while blocking dominates for the vanadium oxide-supported catalyst after high temperature reduction. Experiments in which ethylene was added to a working catalyst, provided indications that the main promoter action of the vanadium oxide is to increase the CO dissociation, thereby increasing the activity of the catalyst.

For the alumina-supported catalysts, most of the vanadium oxide is scavenged by the support and only at a high V/Rh ratio, the activity of the Rh/Al₂O₃ catalyst is increased. The addition of vanadium oxide to the alumina-supported catalysts caused a suppression of the formation of ethers. The vanadium oxide probably covers the acidic ether-forming sites of the alumina support. During the first hours of reaction no acetic acid was observed for the alumina-supported catalysts due to a chromatographic effect. Initially, the acetic acid that was produced was adsorbed by basic sites of the support and only after prolonged reaction was acetic acid observed at the reactor outlet.

8.1 INTRODUCTION

The hydrogenation of carbon monoxide over rhodium catalysts produces a variety of products. The product distribution can be influenced by using different supports or promoters [1-11]. Since C_2 -oxygenates are desirable products from an economic point of view [12], much attention has been paid to improve catalyst activity and selectivity to C_2 -oxygenates. Vanadium oxide used as a support [9] or as a promoter [5,13,14] is reported to be of interest in this respect.

In the preceding paper we reported the synthesis and characterization of such V_2O_3 -promoted Rh/SiO₂ and Rh/Al₂O₃ systems [15]. For the Rh/V₂O₃ catalyst, a complete suppression of hydrogen chemisorption was observed after high temperature reduction, as previously reported by Tauster and Fung [16] for Ir/V₂O₃. They called this effect Strong Metal Support Interaction (SMSI). The now generally accepted explanation for the SMSI effect is that during high-temperature reduction a lower oxide is formed (for TiO₂ this suboxide is for instance Ti₄O₇) and that this oxide spreads over the metal particle, leading to a suppression of hydrogen and carbon monoxide chemisorption [16-22]. For the vanadium oxide-promoted Rh/SiO₂ catalysts, temperature programmed reduction experiments showed that rhodium facilitates the reduction of vanadium oxide and that vanadium oxide hampers the reduction of rhodium oxide, indicating that an intimate contact exists between rhodium and vanadium oxide. These and diffuse reflectance infrared spectroscopy experiments suggest the formation of RhVO₄ [15]. Carbon monoxide chemisorption was suppressed by the presence of vanadium oxide, but metal particle size was not influenced by the presence of vanadium oxide, as determined by TEM. This points to covering of the rhodium particles by patches of vanadium oxide. In this case, covering is not caused by reduction at high temperatures as normally in SMSI systems, but is due to the formation of RhVO₄ during the calcination step. Infrared spectroscopy of adsorbed carbon monoxide showed that only the linearly bonded and bridge-bonded CO were suppressed and that the amount of the gem-dicarbonyl species slightly increased with increasing V/Rh ratio [15]. Since absorption bands were not found at low wave numbers (around 1500 cm⁻¹), we did not find evidence for a weakening of the C-O bond by the promoter, as suggested by Sachtler *et al.* [23-25] and Ichikawa *et al.* [11]. The measurements, described above suggest a model for the Rh/V₂O₃/SiO₂ systems as shown in Figure 8.1a and 8.1c.

For the vanadium oxide-promoted Rh/Al₂O₃ systems, only for catalysts

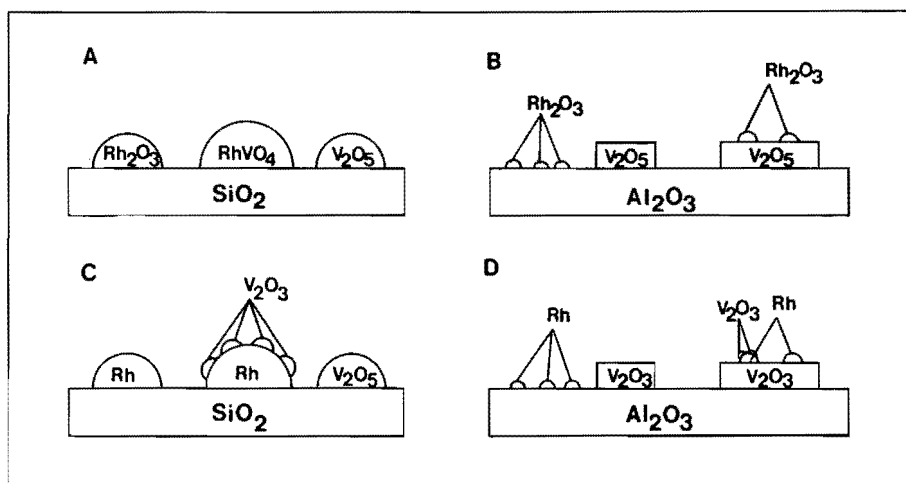


FIGURE 8.1: Schematic illustration of the model for the silica- and alumina-supported, vanadium oxide-promoted rhodium catalysts after calcination at 723 K (a and b) and after reduction at 523 K (c and d).

with a high V/Rh ratio (around 7) indications for an intimate contact between the vanadium oxide and the rhodium were found. For these catalysts only after oxidation at 898 K a mutual affection of the reduction of rhodium and vanadium oxide was observed in TPR, suggesting the formation of RhVO_4 . For these catalysts, rhodium might be positioned on V_2O_5 layers and after reduction some vanadium oxide might be located on top of the rhodium particles. For $\text{V/Rh} < 1$, no indication for an intimate contact was present. Rh_2O_3 and V_2O_5 are believed to be present as separate particles on the alumina support due to the strong interaction between vanadium oxide and the alumina support. The model for the $\text{Rh}/\text{V}_2\text{O}_5/\text{Al}_2\text{O}_3$ catalysts is summarized in Figure 8.1b and d.

In this study we report the results of the H_2/CO reaction over $\text{Rh}/\text{V}_2\text{O}_3$ and vanadium oxide-promoted Rh/SiO_2 and $\text{Rh}/\text{Al}_2\text{O}_3$. Attention will be paid to the role of the promoter element. Ethylene addition is carried out on a working catalyst with and without promoter in order to compare the *in situ* rate of hydrogenation and CO insertion.

8.2 EXPERIMENTAL

8.2.1 Catalyst preparation and characterization

Since the catalysts used in this study were the same as those used in the characterization studies reported earlier [15], we refer to that study for information on catalyst preparation. The following notations will be used in the present article: Rh/ V_2O_3 /SiO₂ for silica-supported vanadium oxide-promoted rhodium catalysts, Rh/ V_2O_3 /Al₂O₃ for alumina-supported vanadium oxide-promoted rhodium catalysts, and Rh/ V_2O_3 for vanadium oxide-supported rhodium catalysts.

The results of the characterization of the catalysts by temperature programmed reduction, hydrogen and carbon monoxide chemisorption, transmission electron microscopy, hydrogen desorption and IR studies of adsorbed carbon monoxide have been reported before [15]. The results are summarized in Table 8.1.

Transmission electron microscopy was used to study the metal particle size before and after the syngas reaction. The catalysts were examined with a Jeol 200 CX, operating at 200 kV.

8.2.2 CO hydrogenation

A continuous flow stainless-steel high pressure reactor, lined with copper to prevent metal carbonyl formation, was used to study the hydrogenation of carbon monoxide. The catalysts were reduced *in situ* in this reactor in pure hydrogen at 0.1 MPa, using a temperature ramp of 5 K min⁻¹ between 298 and 723 K (unless stated otherwise), and holding the final temperature for 1 h. The reactor was subsequently cooled to reaction temperature and pressurized with H₂ to the desired level. After stabilization an additional CO flow was started. Flows were regulated accurately by means of thermal mass flow controllers. All catalysts were measured under the same reaction conditions (GHSV = 4000 l l⁻¹ h⁻¹, H₂/CO = 3, P = 0.15 or 4.0 MPa, catalyst bed 1 ml). The reaction temperature was adjusted so that conversion of CO was around 2%. The product stream was fed to a GC system via a heated sampling line and analyzed on-line. A capillary column (crosslinked 5% phenyl methyl silicone, film thickness 1.0 μm, internal diameter 0.31 mm, length 50 m, split ratio 1:36) enabled us to determine accurately the amount of saturated and unsaturated hydrocarbons up to C₈, alcohols up to C₇, aldehydes up to C₅, ethers, esters and acetic acid in 16 min. Peak area integration was carried out with a Nelson Analytical

TABLE 8.1: Results and characterization of vanadium oxide-supported or -promoted 1.5 wt% Rh catalysts.

Systems	V/Rh ^a	H/Rh ^b	CO/Rh ^b	D(Å) ^c
Rh/V ₂ O ₃ ^d	---	3.8	0.36	52
Rh/SiO ₂	0	0.72	0.71	20
Rh/V ₂ O ₃ /SiO ₂	0.13	0.71	0.70	22
Rh/V ₂ O ₃ /SiO ₂	0.50	0.73	0.56	18
Rh/V ₂ O ₃ /SiO ₂	1.0	0.76	0.27	22
Rh/V ₂ O ₃ /SiO ₂	2.0	0.86	0.32	n.m. ^e
Rh/V ₂ O ₃ /SiO ₂	4.5	1.89	0.36	19
Rh/Al ₂ O ₃	0	1.6	1.3	n.o. ^e
Rh/V ₂ O ₃ /Al ₂ O ₃	0.13	1.4	n.m.	n.m.
Rh/V ₂ O ₃ /Al ₂ O ₃	1.0	1.6	1.1	n.o.
Rh/V ₂ O ₃ /Al ₂ O ₃	7.0	3.3	1.2	n.o.
Rh/V ₂ O ₃ /Al ₂ O ₃	8.4	3.1	1.1	n.m.

a) atomic ratio, b) determined after reduction at 523 K and evacuation at 723 K by back extrapolation of the desorption isotherm to room temperature, c) mean diameter of rhodium particles, determined by TEM, d) Rh/V₂O₃ system in non-SMSI state, after reduction at 523 K. H/Rh was 0.09 and 0.00 after reduction at 723 and 823 K, respectively, e) n.m. is not measured, n.o. is not observable (diameter less than 8 Å).

Interface-IBM PC configuration. The integrated product signals were converted into volume percentages using experimental determined calibration factors (methane, ethane, methanol and ethanol) and calibration factors from literature. Conversion and selectivity were calculated on carbon basis.

8.3 RESULTS

8.3.1 Rh/V₂O₃

Table 8.2 summarizes the results of the hydrogenation over vanadium oxide-supported rhodium catalysts at 4.0 MPa. As vanadium oxide is a SMSI support, we reduced the Rh/V₂O₃ system *in situ* at 523, 723 and 823 K. The influence of the reduction temperature is clearly observed. The higher reduction temperature caused a strong decrease in activity. Therefore the catalysts reduced at a high temperature had to be tested at a higher

reaction temperature, in order to obtain a conversion high enough to enable accurate measurements. To compare activities for all catalysts studied in this paper, the activities were corrected for differences in temperature, and calculated at 503 K, using $E_{act} = 100 \text{ kJ mol}^{-1}$. This activation energy was measured for the catalyst $Rh/V_2O_5/SiO_2$ with $V/Rh = 4.5$.

TABLE 8.2: Results of H_2 -CO reaction for 1.5 wt% Rh/V_2O_5 systems after 15 h time on stream, $H_2/CO = 3$, GHSV = $4000 \text{ l l}^{-1} \text{ h}^{-1}$.

Reduction temp. (K)	523	723	823	723
P (MPa)	4.0	4.0	4.0	0.15
React. temp. (K)	513	543	543	513
Activity ^a	3.4	0.8	0.8	0.6
corr. act. ^b	2.1	0.1	0.1	0.4
sel. (%) ^c				
CH ₄	75.8	16.8	11.3	28.2
C ₂ ^d	10.6	12.9	8.4	33.6
C ₁ OH ^e	6.8	25.1	23.2	0.3
C ₂ OH ^f	5.4	26.1	28.6	6.9
C ₂ =O ^g	0.4	6.4	10.3	27.9
C ₂ OOH ^h	0.5	2.8	4.0	1.8
C ₃ O _x ⁱ	0.6	4.6	14.6	1.3
oxo. sel. ^j	13.6	70.3	80.3	38.2
Deact. (% h ⁻¹)	4.0	2.9	11.1	8.4
C ₂ =/C ₂	0.1	0.2	0.4	5.9
C ₃ =/C ₃	0.2	0.7	2.1	>10
C ₄ =/C ₄	0.4	1.2	1.9	10.0

a) activity in mmol converted CO (mol Rh)⁻¹ s⁻¹, b) calculated activity at 503 K using $E_{act} = 100 \text{ kJ mol}^{-1}$, c) selectivities expressed as %C efficiency, d) hydrocarbons containing two or more C atoms, e) total amount of methanol, ethers and esters included, f) total amount of ethanol, ethers and esters included, g) acetaldehyde, h) acetic acid, esters included, i) oxygenated products containing three or more C atoms, j) total oxo-selectivity.

Not only was the activity influenced by the reduction temperature, but also the selectivity changed markedly. Oxo-selectivity increased dramatically with increasing reduction temperature, from 13.6 to 70.3 and 80.3 %

when using $T_{\text{red}} = 523, 723$ and 823 K, respectively, and so did the proportion of unsaturated hydrocarbons.

We also performed an experiment at low pressure (0.15 MPa) after a high temperature reduction. In that case activity was low too. The methanol selectivity was below 1.0 %. The total amount of other oxygenates was comparable to that obtained in the high pressure experiment. The relative amount of unsaturated hydrocarbons was high and considerable amounts of longer hydrocarbons were measured.

In all cases the deactivation was high (3-11 % h^{-1}). The selectivity changed markedly as a function of time on stream, especially after reduction at high temperature. Methanol and ethanol selectivities increased and hydrocarbon selectivity decreased with reaction time. The total oxo-selectivity increased from 29% after 0.5 h to 81% after 16 h time on stream for the Rh/V₂O₃ catalyst reduced at 823 K.

Thus, Rh/V₂O₃ catalyst reduced at high temperature (> 723 K) exhibits a relatively high oxo-selectivity, but a low activity and strong deactivation. During high temperature reduction the rhodium particles become covered by V₂O₃, as suggested by Van der Lee *et al.* [9]. The V₂O₃ patches covering the Rh particles will be partly removed by water (formed as a product during the syngas reaction), but the remaining vanadium oxide still has an effect on activity and selectivity. This was also shown by Lin *et al.* [26]. They reported that a few pulses of CO + H₂ reversed the SMSI-state for Rh/TiO₂ reduced at high temperatures, whereas this was not the case for Rh/V₂O₃ after high temperature reduction.

However, the activity and stability of these catalysts is low and V₂O₃ has bad structural properties (low surface area, low pore volume, relatively high solubility in water). Rh/Al₂O₃ exhibits a high activity and stability [3,27,28], and SiO₂ and Al₂O₃ are stable supports with good structural properties (high surface area, high pore volume). We therefore tried to combine the selectivity properties of Rh/V₂O₃ reduced at a high temperature and the activity and stability properties of alumina- and silica-supported systems by promoting Rh/Al₂O₃ and Rh/SiO₂ with varying amount of vanadium oxide. Especially, we attempted to prepare a monolayer of vanadium oxide on alumina, so that the resulting catalyst would have the good structural properties of alumina, and the described promoter activity of vanadium oxide.

8.3.2 Rh/V₂O₃/SiO₂

As shown above, the influence of the reduction temperature on the catalytic performance of Rh/V₂O₃ was significant. However, for the Rh/V₂O₃/SiO₂ systems, the reduction temperature had a minor influence. The Rh/V₂O₃/SiO₂ system with V/Rh = 2, was reduced at 523 and 723 K (cf. Table 8.3). In comparison with the catalyst reduced at high temperature, the catalyst reduced at low temperature showed a slightly higher selectivity to methane and acetaldehyde and a lower selectivity to methanol and ethanol. Total oxo-selectivity after reduction at 523 K was 57 %, whereas this selectivity was 70 % after reduction at 723 K. We used the reduction at 723 K as a standard for all catalysts.

TABLE 8.3: Results of H₂-CO reaction after 15 h time on stream for vanadium oxide-promoted 1.5 wt% Rh/SiO₂ systems reduced *in situ* at 723 K. For definitions see Table 2. Experimental conditions: GHSV = 4000 l⁻¹ h⁻¹, H₂/CO = 3.0.

V/Rh ^a	0	0.12	0.5	1.0	2.0	2.0 ^b	4.5	0	0.5	2.0
P (MPa)	4.0	4.0	4.0	4.0	4.0	4.0	4.0	0.15	0.15	0.15
T (K)	600	546	523	503	504	503	501	591	523	504
activity	2.8	1.7	1.6	1.8	2.9	2.5	3.0	1.8	2.4	1.8
corr. act.	0.06	0.3	0.6	1.8	2.7	2.5	3.3	0.05	1.0	1.7
sel. (%)										
CH ₄	33.2	20.3	21.8	20.3	20.4	31.6	19.5	85.4	36.2	26.5
C ₂ ⁺	2.3	2.2	5.2	8.8	9.9	11.1	12.4	13.5	28.1	37.8
C ₁ OH	29.1	27.8	20.4	25.1	27.5	15.3	27.2	0.5	0.8	2.5
C ₂ OH	20.5	20.2	24.2	25.9	26.9	20.9	25.9	0.2	23.2	26.4
C ₂ =O	4.3	7.6	7.6	3.7	1.2	6.3	1.1	0.4	10.2	6.4
C ₂ OOH	10.2	20.6	17.1	10.0	8.7	9.4	7.0	0.0	0.8	0.7
C ₃ O ⁺	0.6	1.4	3.7	6.2	5.4	5.4	6.9	0.0	0.7	2.1
oxo. sel.	64.5	77.5	73.0	70.9	69.7	57.3	68.1	1.1	35.7	35.7
Deact. ^c	1.7	3.5	3.8	2.6	1.9	2.0	1.8	n.m.	3.8	3.0
C ₂ =/C ₂	0.0	0.2	0.2	0.5	0.4	n.m.	0.6	0.0	0.9	1.1
C ₃ =/C ₃	0.0	1.1	1.8	2.1	2.1	n.m.	2.7	0.0	> 10	> 10
C ₄ =/C ₄	0.0	0.2	1.2	1.6	1.3	n.m.	1.7	0.0	3.8	3.8

a) V/Rh, atomic ratio, b) reduced at 523 K, c) in % h⁻¹.

Table 8.3 summarizes the effect of vanadium oxide promotion on Rh/SiO₂ at 4.0 and 0.15 MPa. In the high pressure case, a sharp increase in activity with increasing V/Rh ratio was observed. Using an activation energy of 100 kJ mol⁻¹, as was measured for Rh/V₂O₃/SiO₂ with V/Rh = 4.5, it is calculated that the vanadium oxide-promoted Rh/SiO₂ catalysts with V/Rh = 4.5 is 40 times more active than the unpromoted Rh/SiO₂ catalyst, and almost 20 times more active than Rh/V₂O₃ reduced at 723 K (see Figure 8.2). The extent of deactivation of these catalysts decreased with increasing V/Rh ratio and was considerably lower than that of Rh/V₂O₃. Clearly the promoted catalysts were considerably more active than the unpromoted catalyst.

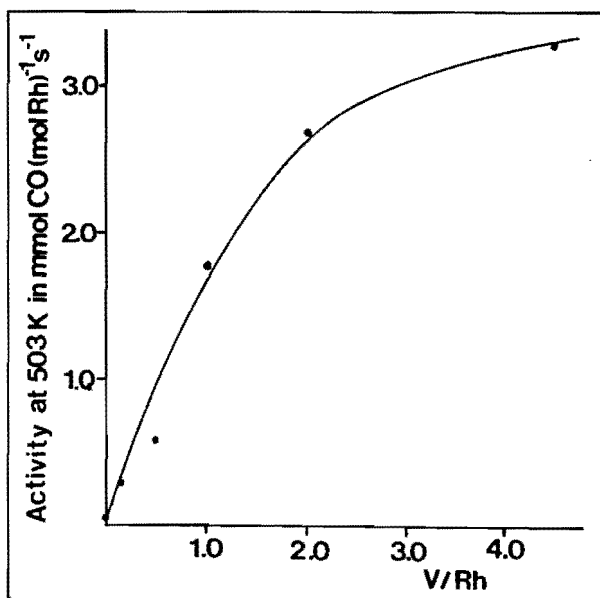


FIGURE 8.2: Corrected activity at 503 K vs V/Rh ratio for Rh/V₂O₃/SiO₂ catalysts.

The total oxo-selectivity slightly decreased with increasing V/Rh ratio, mainly due to a decreased methanol and acetic acid selectivity, but still was around 70%, comparable to those obtained for the Rh/V₂O₃ systems reduced at high temperature. The increase of the relative amount of unsaturated hydrocarbons with increasing V/Rh ratio up to V/Rh = 1 must be due to differences in reaction temperature.

To exclude the influences of temperature on selectivity, we tested Rh/SiO₂ and Rh/V₂O₃/SiO₂ (V/Rh = 1.0) at the same temperature (548 K). In order to measure at the same conversion level (about 3 %), we adjusted the GHSV for these systems by changing the amount of catalyst and the total gas flow. The results are presented in Table 8.4. Activities and selectivities for the different product groups are compared. Clearly the formation rate of all products is increased by the presence of vanadium oxide, but the rates for hydrocarbons and C₂O⁺ formation are increased most, while the formation rate of methanol is only increased by a factor of six.

TABLE 8.4: Rh/SiO₂ and Rh/V₂O₃/SiO₂ (V/Rh = 1.0) catalyst tested at the same reaction temperature (548 K), GHSV for Rh/SiO₂ = 660 l l⁻¹ h⁻¹, GHSV for Rh/V₂O₃/SiO₂ = 8000 l l⁻¹ h⁻¹, P = 4.0 MPa, H₂/CO = 3.0.

	Selectivity(%C)		Activity (mmol converted CO (mol Rh) ⁻¹ s ⁻¹)		factor of increase of formation
	Rh/SiO ₂	Rh/V ₂ O ₃ /SiO ₂	Rh/SiO ₂	Rh/V ₂ O ₃ /SiO ₂	
CH ₄	11.6	30.7	0.051	3.75	74
C ₂ ⁺	1.4	10.9	0.006	1.33	222
C ₁ OH	57.2	12.4	0.252	1.51	6
C ₂ OH	13.7	25.2	0.060	3.07	51
C ₂ =O	0.0	6.9	0.000	0.84	∞
C ₂ OOH	14.7	10.5	0.065	1.28	20
C ₃ O ⁺	1.4	3.4	0.006	0.41	68
C ₂ -oxo	28.4	42.6	0.125	5.20	42
tot. oxo	87.0	58.4	0.383	7.12	19
tot. act.			0.440	12.2	28

In the low pressure case (P = 0.15 MPa, see Table 8.3), almost no methanol was formed. However, relatively high oxo-selectivities were measured (up to 36 %) because of a high selectivity to ethanol and acetaldehyde. During the low pressure experiments, the deactivation and the proportion of unsaturated hydrocarbons were high. The presence of vanadium oxide had a remarkable influence on the total oxo-selectivity. The unpromoted Rh/SiO₂ catalysts had a total oxo-selectivity of 1 %, whereas the promoted Rh/SiO₂ catalysts had a total oxo-selectivity of 36 %.

A separate experiment was conducted to investigate the CO hydrogenation

activity of the vanadium oxide itself. A V_2O_3/SiO_2 catalyst containing 1.6 wt % V was tested at 591 K, but no products could be detected.

Rhodium particle size can have a significant influence on the activity of Rh/SiO_2 catalysts in the synthesis gas reaction [27,29]. Therefore the improvement of the activity by addition of vanadium oxide might be caused by a decrease in particle size. But as shown in Table 8.1, rhodium particle size did not differ significantly for the silica-supported systems with or without vanadium oxide. The average particle size was $20 \pm 2 \text{ \AA}$. Particle size can be increased by sintering due to adsorption of CO [30] or syngas reaction [31]. The metal particle size distribution of $Rh/V_2O_3/SiO_2$, $V/Rh = 1.0$ had not changed at all during reaction. The unpromoted catalyst showed some larger particles ($25\text{--}35 \text{ \AA}$), but the majority of the particles remained unchanged. The presence of some larger particles will originate from a more pronounced sintering process at the higher reaction temperature needed for the Rh/SiO_2 catalyst. Thus, the observed higher activity for the promoted catalyst cannot be caused by the presence of larger particles in this catalyst.

The catalytic performance of Rh/SiO_2 and $Rh/V_2O_3/SiO_2$ ($V/Rh = 2.0$) at 4.0 MPa as a function of time on stream is presented in Figure 8.3a and 8.3b, respectively. Clearly, for Rh/SiO_2 the moderate decrease in overall activity (1.7 \% h^{-1}) is mainly correlated with the decrease in activity to methane (3.6 \% h^{-1}). The formation rate of methanol was almost constant, while the other products showed an intermediate deactivation. For the $Rh/V_2O_3/SiO_2$ ($V/Rh = 2.0$) catalyst, a similar behaviour of activity versus time on stream is observed. After several hours on stream an almost constant formation rate of methanol and a slight deactivation for the other products is observed. This deviating deactivation behaviour of methanol can be explained by the assumption that methanol is formed on sites different from those for the other products, such as metal ions [32–34].

In Figure 8.4a and b, the influence of the H_2/CO ratio and the reaction temperature on the activity for Rh/SiO_2 and $Rh/V_2O_3/SiO_2$, $V/Rh = 4.5$ is presented. From the temperature dependence of the activity, activation energies can be calculated. For the promoted system a total activation energy of 100 kJ mol^{-1} was measured. The activation energies for methane, methanol and ethanol were 135, 65 and 105 kJ mol^{-1} , respectively. For the unpromoted system, the total activation energy and the activation energy for methane were 89 and 160 kJ mol^{-1} , respectively. As can be seen in Figure 8.4b, the formation rate of methanol and ethanol cannot be described by an Arrhenius equation. This might be due to successive reactions, to thermodynamic limitations (in the case of methanol), or to changes in the catalyst

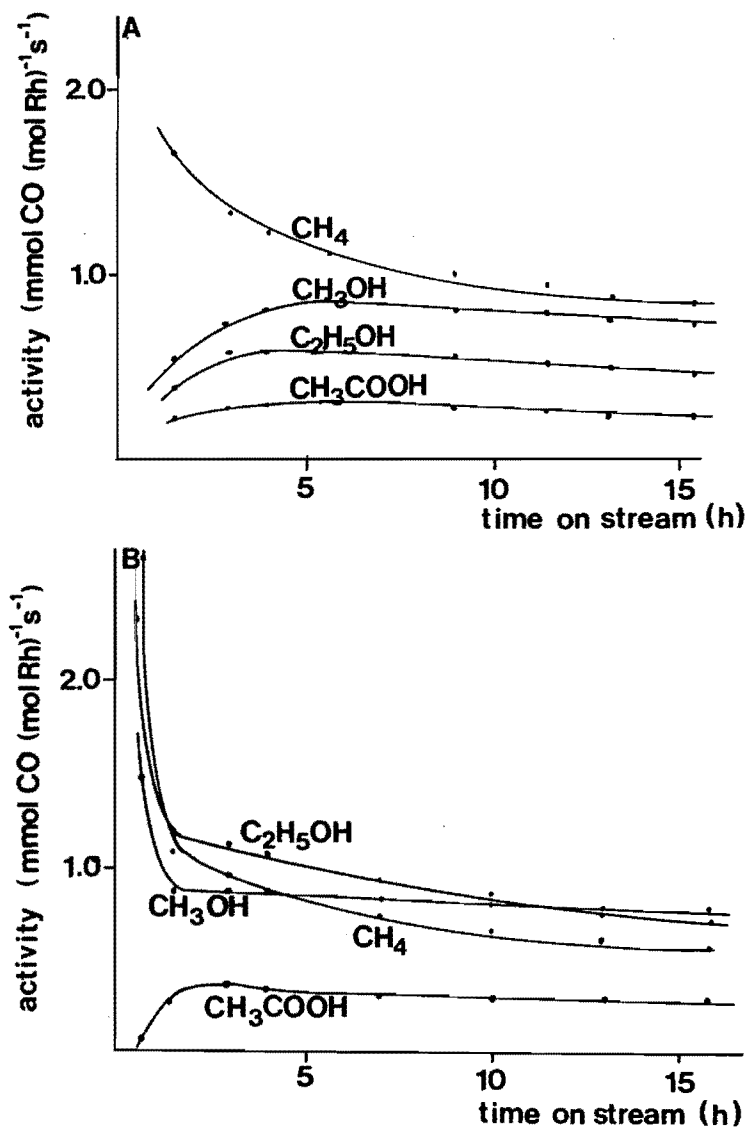
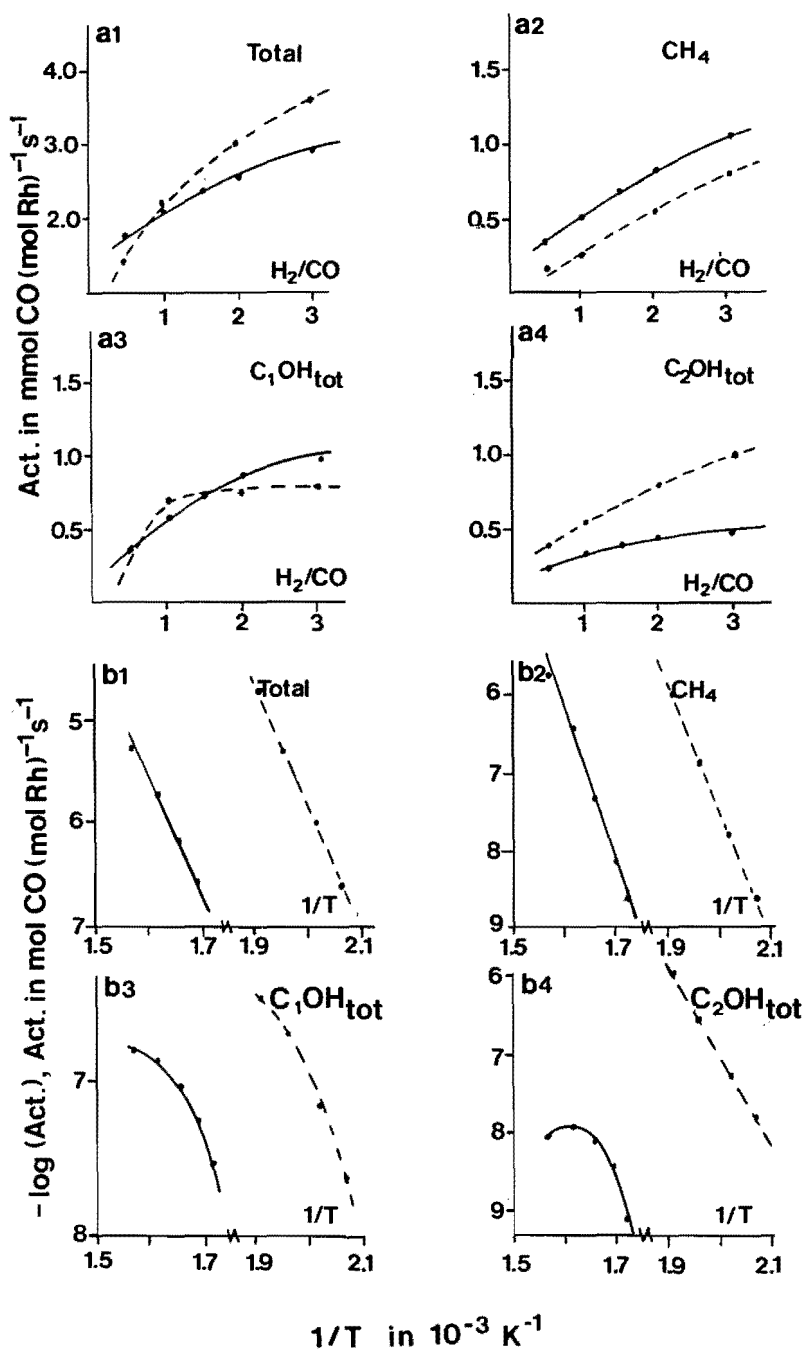


FIGURE 8.3: Formation rates of several products as a function of time on stream ($P = 4.0$ MPa, $GHSV = 4000$ l l^{-1} h $^{-1}$, $H_2/CO = 3.0$), expressed in mmol converted CO (mol Rh) $^{-1}$ s $^{-1}$.

a. 1.5 wt% Rh/SiO₂, $T_{react} = 600$ K

b. 1.5 wt% Rh/V₂O₃/SiO₂, $V/Rh = 2.0$, $T_{react} = 504$ K.

(e.g. less rhodium ions at high temperatures). In all cases the total activity and the formation rates to CH₄, C₁OH and C₂OH increased with increasing H₂/CO ratio. Only for the promoted system, the formation rate of



←
FIGURE 8.4: Influence of H_2/CO and reaction temperature on formation rates of the most important products after 15 h on stream,

a. influence of H_2/CO ratio on overall reaction rate (a1), methane formation rate (a2), methanol formation rate (a3) and ethanol formation rate (a4)

b. influence of reaction temperature on overall reaction rate (b1), methane formation rate (b2), methanol formation rate (b3) and ethanol formation rate (b4).

Activities are expressed in mmol converted CO $(\text{mol Rh})^{-1} \text{ s}^{-1}$. Drawn lines represent data of Rh/SiO dotted lines of Rh/ V_2O_3 /SiO₂, V/Rh = 4.5. Reaction conditions: GHSV = 4000 l l⁻¹ h⁻¹, P = 4.0 MPa, reaction temperature for a-series: 593 K for Rh/SiO₂ and 503 K for Rh/ V_3 /SiO₂, H_2/CO for b-series = 3.0.

methanol became almost constant above $H_2/CO = 1.0$. Note that the measurements of the promoted and unpromoted catalysts took place at different temperatures. In Table 8.5, the selectivity data for the promoted system as a function of temperature and H_2/CO ratio are given. Clearly, an increase in temperature and a decrease in H_2/CO ratio induced a higher C_2 -

TABLE 8.5: Influence of temperature and H_2/CO ratio on syngas reaction at 4.0 MPa over Rh/ V_2O_3 /SiO₂ (V/Rh = 4.5), GHSV = 4000 l l⁻¹ h⁻¹.

T (K)	Temperature influence				H_2/CO influence			
	483	495	510	524	503	503	503	503
H_2/CO	3.0	3.0	3.0	3.0	0.5	1.0	2.0	3.0
Act.	1.3	2.4	4.9	8.9	1.4	2.2	3.0	3.6
Sel. (%C)								
CH ₄	14.0	17.4	21.7	27.9	10.1	11.6	19.4	22.3
C ₂ ⁺	9.7	9.7	10.6	12.3	12.1	9.3	12.4	11.6
C ₁ OH	36.6	31.5	25.2	17.4	25.1	33.7	25.3	22.9
C ₂ OH	26.1	27.7	28.4	28.9	27.9	25.2	27.2	28.5
C ₂ =O	0.4	0.2	0.7	1.5	3.0	2.8	1.0	0.9
C ₂ OOH	7.2	7.4	7.6	7.3	13.8	10.3	8.9	7.9
C ₃ O ⁺	6.1	6.1	5.8	4.7	8.1	7.1	6.6	5.9
C ₂ -oxo	33.7	35.3	36.7	37.7	44.7	38.3	37.1	37.3
tot. oxo	76.4	72.9	67.7	59.8	77.9	79.1	69.0	66.1

oxygenate selectivity and a lower methanol selectivity. The methane selectivity increased with increasing temperature and H_2/CO ratio. A low H_2/CO ratio resulted in a high acetic acid selectivity.

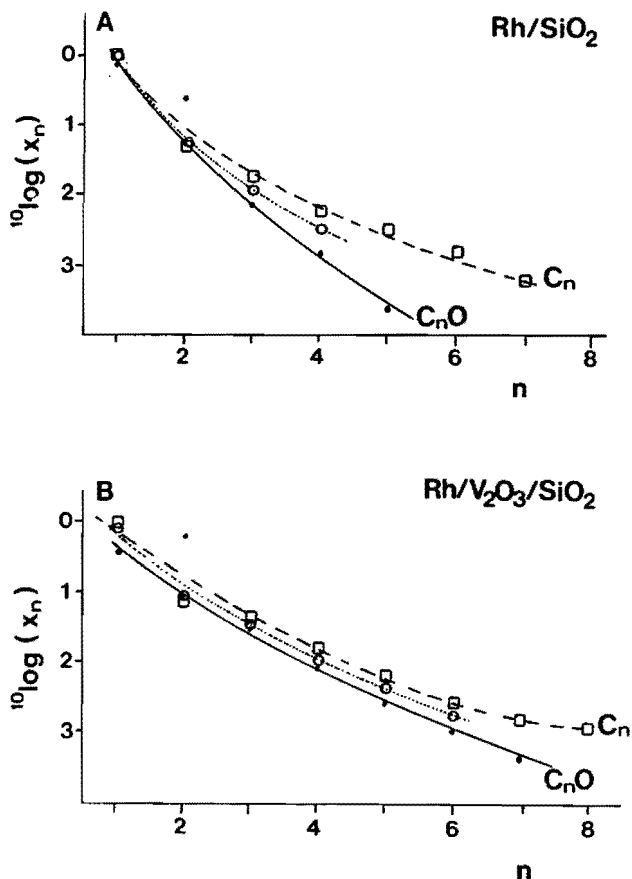


FIGURE 8.5: Flory Schulz distribution for hydrocarbons (\square), oxygenates (\bullet) and the sum of hydrocarbons and oxygenates, counted as $C_n + C_{n+1}O$ (\circ) after 15 h on stream. a. Rh/SiO_2 b. $Rh/V_2O_3/SiO_2$, $V/Rh = 4.5$.

From a detailed analysis of the products, Flory-Schulz distributions were obtained for the unpromoted and promoted catalysts, presented in Figure 8.5a and b, respectively. No straight lines were found in the Flory-Schulz plots and therefore chain-growth probabilities for low and high carbon numbers (n) were calculated. For the promoted catalyst ($V/Rh = 4.5$), the chain-growth probability for hydrocarbons $\alpha(C_n)$ ranged from 0.4 ($n = 3$ -

8) to 0.6 ($n = 5-8$). The chain-growth probability for oxygenates $\alpha(C_nO)$ ranged from 0.3 ($n = 1-5$) to 0.4 ($n = 4-7$). Thus we observed a significantly higher α -value for the hydrocarbons than for the oxygenates. Since the most accepted mechanism for the formation of oxygenates is the insertion of CO in a growing alkylgroup, hydrocarbons with n and oxygenates with $n+1$ C-atoms were taken together to calculate the total chain-growth probability. The total chain-growth probability $\alpha(C_n+C_{n+1}O)$ was 0.4 ($n = 3-6$). The following chain-growth probabilities were measured for the unpromoted Rh/SiO₂ catalyst: $\alpha(C_n)$ ranged from 0.3 ($n = 3-4$) to 0.5 ($n = 4-7$), $\alpha(C_nO)$ was 0.2 ($n = 3-5$) and $\alpha(C_n+C_{n+1}O)$ was 0.3 ($n = 2-4$). Furthermore, in both cases an overshoot of C₂-oxygenated products and a deficit of C₂-hydrocarbons was observed, compared with the expected amounts based on the Flory-Schulz plots. In the experiments at low pressure, a higher chain-growth probability was observed for Rh/V₂O₃/SiO₂, V/Rh = 4.5: $\alpha(C_n) = 0.6$ ($n=3-5$), $\alpha(C_nO) = 0.4$ ($n=3-6$) and $\alpha(C_n+C_{n+1}O) = 0.5$ ($n=3-5$).

8.3.3 Rh/V₂O₃/Al₂O₃

The results for the vanadium oxide-promoted alumina-supported rhodium catalysts are presented in Table 8.6. In the low as well as the high pressure cases, 0.15 and 4.0 MPa respectively, an increase in activity was observed with increasing V/Rh ratio. However, the increase in activity was not as pronounced as in the case of vanadium oxide promotion of the Rh/SiO₂ catalyst. Low amounts of vanadium oxide (V/Rh < 1) had a negligible influence on the activity, in contrast to the silica-supported catalysts. For the catalysts with V/Rh = 7.0 and 8.4, the catalysts with a near mono-layer of vanadium oxide on the alumina surface, the vanadium oxide caused an increase of the activity by a factor of three and increased selectivities to C₂-oxygenates and longer hydrocarbons, whereas the selectivities to methane and methanol were suppressed. The total oxo-selectivity was slightly increased by the presence of vanadium oxide (up to 52 %), but was considerably lower than for the Rh/V₂O₃/SiO₂ (70 %) and Rh/V₂O₃ (70-80%) catalysts. The deactivation was low and increased slightly with increasing V/Rh ratio.

A noteworthy effect of the vanadium oxide content on the formation of dimethyl ether was observed (see Table 8.6). Dimethyl ether is thought to be formed on acidic sites of the Al₂O₃ by dehydration of methanol [28]. The low dimethyl ether concentrations for V/Rh = 7.0 and 8.4 suggest that

TABLE 8.6: Results of H₂-CO reaction after 15 h time on stream for vanadium oxide-promoted 1.5 wt% Rh/Al₂O₃ systems reduced *in situ* at 723 K. For definitions see Table 8.2. Experimental conditions: GHSV = 4000 l l⁻¹ h⁻¹, H₂/CO = 3.0.

V/Rh ^a	0.0	0.12	1.0	7.0	8.4	0.12	1.0	7.0
P (MPa)	4.0	4.0	4.0	4.0	4.0	0.15	0.15	0.15
React. temp. (K)	501	493	493	493	493	503	493	493
activity	1.6	1.0	1.3	3.8	3.6	0.8	0.8	2.8
corr. act.	1.8	1.7	2.1	6.2	5.9	0.8	1.3	4.5
sel. (%)								
CH ₄	46.3	39.5	39.7	37.5	36.2	54.1	48.8	39.1
C ₂ ⁺	6.6	8.8	8.2	11.8	11.6	21.1	27.0	35.6
C ₁ OH	22.4	29.3	23.9	15.6	16.0	15.4	10.2	3.6
C ₂ OH	19.1	17.0	19.9	21.2	21.4	7.6	10.8	18.1
C ₂ =O	1.6	1.4	1.7	1.6	1.6	0.0	0.6	1.0
C ₂ OOH	0.9	0.9	3.6	7.3	7.5	0.2	0.3	1.0
C ₃ O ⁺	3.1	3.1	3.0	5.0	5.7	1.6	2.3	1.5
oxo. sel.	47.1	51.7	52.1	50.7	52.2	24.8	24.2	25.2
Deact. (% h ⁻¹)	0.4	0.5	0.7	1.9	1.7	3.0	3.3	2.3
ether formation ^b	.51	.39	.23	.02	.01	.32	.15	0.0

a) V/Rh, atomic ratio, b) 2*COC/(C₁OH+2*COC).

there are almost no free acidic sites available in these systems, otherwise the ether formation would not be suppressed that much. We conclude that the vanadium oxide has covered the alumina sites responsible for the dehydration of methanol.

The rate of formation of acetic acid changed markedly as a function of time on stream (see Figure 8.6). For the alumina and low-vanadium oxide loaded alumina-supported catalysts, the acetic acid concentration started to increase after about 12 h time on stream, whereas in the case of high vanadium oxide loaded aluminas, the increase in acetic acid formation took place after about 5 h time on stream. The silica-supported systems (with or without vanadium oxide) started to produce acetic acid during the first hour of reaction. We think that the fact that acetic acid is only observed after prolonged reaction on the alumina-supported catalysts, is due to a

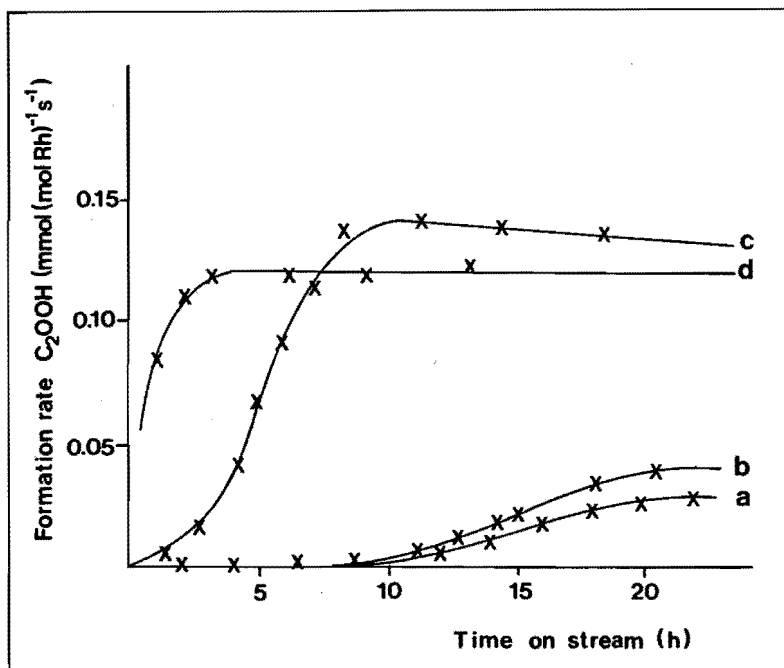


FIGURE 8.6: Formation rate of acetic acid (in $\text{mmol C}_2\text{OOH}/(\text{mol Rh})^{-1} \text{s}^{-1}$) as a function of time on stream. For reaction conditions see Table 8.2 and 8.3.

- a. $\text{Rh}/\text{Al}_2\text{O}_3$
b. $\text{Rh}/\text{V}_2\text{O}_3/\text{Al}_2\text{O}_3$, $\text{V}/\text{Rh} = 1$
c. $\text{Rh}/\text{V}_2\text{O}_3/\text{Al}_2\text{O}_3$, $\text{V}/\text{Rh} = 7.0$ d. $\text{Rh}/\text{V}_2\text{O}_3/\text{SiO}_2$, $\text{V}/\text{Rh} = 2$

chromatographic effect. Already during the first hours acetic acid or its reaction-intermediate is formed, but is bonded by basic sites on the support. When these sites are filled, acetic acid can leave the catalyst surface and be detected as one of the products in the gas stream. The following experiment proved this chromatographic effect. Downstream of the $\text{Rh}/\text{Al}_2\text{O}_3$ catalyst bed an additional bed of 1 ml of Al_2O_3 was placed. The amount of acetic acid that could be adsorbed during the first hours of reaction thus was doubled, and indeed acetic acid appeared in the product stream only after 23 h time on stream. Since acetic acid is observed almost immediately after the start of the reaction for the silica-supported systems, these adsorption sites will not be available on SiO_2 . In the case of the alumina-supported catalysts with high V/Rh ratios, the quicker breakthrough of acetic acid (cf. Figure 8.6c) is caused by the higher formation rate of acetic acid. The amount of acetic acid which stays adsorbed on the catalyst can be estimated from Figure 8.6 assuming that the formation rate of acetic acid in the beginning is

the same as after prolonged reaction. The amounts of adsorbed acetic acid are 0.20, 0.28 and 0.34 mmol C_2OOH $(g Al_2O_3)^{-1}$ for Rh/Al_2O_3 , $Rh/V_2O_3/Al_2O_3$ ($V/Rh=1$) and $Rh/V_2O_3/Al_2O_3$ ($V/Rh=7.0$), respectively.

8.3.4 Ethylene addition

In order to study the reaction mechanism and the role of the vanadium oxide promoter, we examined the influence of ethylene addition to a working catalyst as has been done before for other catalyst systems [35-37]. Since addition of a gas is not easy in high pressure experiments, and since oxo-selectivity is relatively high in the low pressure experiment with the vanadium oxide-promoted catalysts, we used the $Rh/V_2O_3/SiO_2$ ($V/Rh = 1.0$) catalyst in the low pressure syngas reaction (0.15 kPa) for this experiment. We added 0.3 vol% C_2H_4 to the catalyst after prolonged reaction (23 h) at 503 K and stopped addition 3 h later. Subsequently, after another 2.5 h we again added ethylene, now in a concentration of 0.95 vol%, and after another 2.5 h we stopped this addition. While most of the added ethylene remained in the C_2 -hydrocarbon fraction, part of it was hydrogenated to ethane. The hydrogenation activity was $1.0 \text{ mmol } H_2 \text{ (mol Rh)}^{-1} \text{ s}^{-1}$ (0.30 vol% C_2H_4). The normal Fischer Tropsch activity of this catalyst was $2.85 \text{ mmol CO (mol Rh)}^{-1} \text{ s}^{-1}$. The amount of propanol and propanal increased dramatically and was dependent on the amount of added ethylene (see Table 8.7). None of the other products was influenced by this addition.

TABLE 8.7: Effect of ethylene addition to $H_2 + CO$ reaction over $Rh/V_2O_3/SiO_2$ ($V/Rh = 1$) catalyst. Reaction conditions: $P = 0.15 \text{ MPa}$, $GHSV = 4000 \text{ l l}^{-1} \text{ h}^{-1}$, $H_2/CO = 3.0$, $T_{\text{react}} = 503 \text{ K}$. All data are expressed in 10^{-2} vol\% . (so not as selectivities, but as volume percentages of the gas stream).

Addition of	CH_4	C_2H_4	C_2H_6	C_3H_{6-8}	C_3OH	$C_3=O$
-----	8.06	1.15	0.71	1.56	0.15	0.06
0.30 vol% C_2H_4	7.34	15.8	16.4	1.45	1.21	0.43
-----	7.03	1.10	0.49	1.33	0.16	0.05
0.95 vol% C_2H_4	6.51	76.2	13.7	1.34	3.16	1.02
-----	6.09	0.95	0.37	1.10	0.17	0.04

Ethylene addition was also studied for the unpromoted Rh/SiO_2 catalyst (see Table 8.8). During reaction at 593 K, no extra propanol and propanal were found after addition of ethylene. All added ethylene was

TABLE 8.8: Effect of ethylene addition to $H_2 + CO$ reaction over Rh/SiO₂ catalyst. Reaction conditions: $P = 0.15$ MPa, GHSV = 4000 l l⁻¹ h⁻¹, $H_2/CO = 3.0$. All data are expressed in 10⁻² vol%.

T (K)	Addition of	CH ₄	C ₂ H ₄	C ₂ H ₆	C ₃ H ₆₋₈	C ₃ OH	C ₃ =O
593	---	19.6	0.0	0.53	0.39	0.0	0.0
593	0.24 vol% C ₂ H ₄	18.8	0.0	24.4	0.42	0.0	0.0
593	0.83 vol% C ₂ H ₄	19.2	0.0	83.1	0.55	0.0	0.0
503	---	0.16	.014	.008	0.01	0.0	0.0
503	0.27 vol% C ₂ H ₄	0.16	13.6	11.6	0.01	0.83	1.16

hydrogenated, even after addition of 0.83 vol% C₂H₄. We also studied addition of ethylene at 503 K, the temperature used for the experiments with the promoted catalyst (Rh/V₂O₃/SiO₂ (V/Rh = 1.0)). At this temperature the normal syngas reaction rate was very low. However, addition of ethylene now caused the formation of a remarkable amount of propanol and propanal and the hydrogenation activity was rather high. Half of the amount of added ethylene was hydrogenated.

8.4 DISCUSSION

8.4.1 Rh/V₂O₃/SiO₂

Influence of promoter on activity. In a previous study [15], we already discussed the location of the vanadium oxide promoter in Rh/V₂O₃/SiO₂ catalysts. Results of temperature programmed reduction and diffuse reflectance spectroscopy measurements suggest the formation of a mixed oxide (RhVO₄) during calcination of the catalyst. Reduction of this oxide phase resulted in a decoration of the rhodium metal particles by patches of vanadium oxide during the reduction, causing a suppression of the CO chemisorption. Thus, intimate contact between the promoter and the active metal exists. In the syngas reaction further evidence is found for this. Even small amounts of vanadium oxide added to Rh/SiO₂ cause a large increase in activity pointing to an intimate contact. Thus, although it is not known if the covering, which exists after reduction, is continued during syngas reaction conditions (since water formed during the reaction may undo the covering), there must be intimate contact between metal and promoter after prolonged reaction.

Clearly, the addition of vanadium oxide to Rh/SiO₂ dramatically enhances the activity of the catalyst system. First we want to exclude a trivial effect that could cause this increase in activity. Rhodium particle size can dramatically affect the activity [27,29]. However, after analyzing several micrographs of promoted and unpromoted catalysts before and after synthesis gas reaction, we feel confident that the systems studied did not differ significantly in their rhodium particle size. Thus, the increase in activity due to promotion cannot be caused by an increase in particle size and must originate from the interaction between vanadium oxide and rhodium, influencing the rate determining step of the reaction and/or creating more reactive sites.

Figure 8.7 represents a mechanism for the formation of oxygenates and hydrocarbons as proposed by several groups [10,11,23]. The main initiating steps in this mechanism are believed to be the dissociation of CO and the hydrogenation of the resulting carbon atoms to CH_x species ($x = 1-3$). Once formed, these CH_x species can undergo a number of competing reactions, such as hydrogenation to methane, addition to an alkyl-group to cause chain-growth, and CO insertion to form intermediates for oxygenated hydrocarbons.

For a number of catalyst systems, it has been possible to conclude that CO dissociation is not the rate determining step under reaction conditions. For nickel catalysts it was found that the slowest step in the methanation reaction was the hydrogenation of CH_x species [38] and that the concentration of adsorbed hydrogen atoms on the surface is the limiting factor [39]. On iron catalysts, CO dissociation is rapid compared with the rate of the overall reaction as reported by Van Dijk *et al.* [40]. Using transient isotope techniques, Biloen *et al.* [41] obtained evidence showing that CO dissociation is rapid over nickel, cobalt and ruthenium. This observation led Van den Berg *et al.* [10] to assume that the hydrogenation of surface carbon is the rate determining step in the hydrogenation of CO over rhodium catalysts. The role of their promoter, MnO and MoO₂, is then to increase the rate of hydrogenation. Ellgen *et al.* [42] studied the kinetics of the CO/H₂ reaction and reported a decrease in the H₂ pressure dependence by adding a Mn promoter, indicating that the concentration of hydrogen adsorbed on the catalyst has indeed become less limiting.

Two reasons were mentioned by Van den Berg *et al.* for the increase in the hydrogenation rate by promoting [10]. Firstly, the promoter oxides can act as a hydrogen reservoir via spillover of adsorbed hydrogen and/or formation of hydroxyl groups. Secondly, the function of the promoter might be

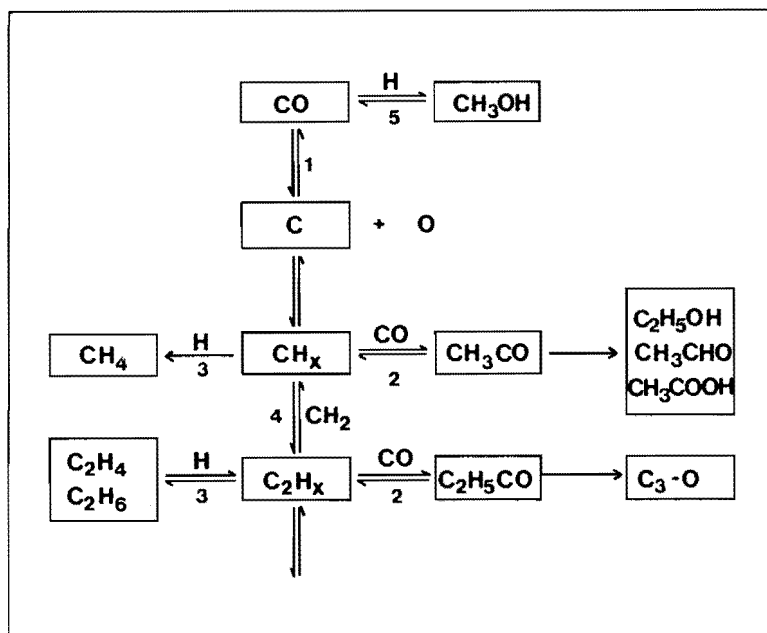


FIGURE 8.7: Schematic models of the elementary steps for the synthesis of hydrocarbons and oxygenates during carbon monoxide hydrogenation:

- (1) CO dissociation followed by the formation of an alkyl group,
- (2) CO insertion in alkyl group forming acyl species that is the precursor for C₂+ oxygenates,
- (3) H-addition and β -H elimination of surface alkyl groups forming hydrocarbons,
- (4) growth of carbon chain,
- (5) CO insertion in metal-H, resulting in methanol.

to decrease the heat of adsorption of CO via the formation and stabilization of rhodium ions. Since the surface of the catalyst is practically completely covered with CO under reaction conditions, a small change in the heat of chemisorption of CO, leading to a small decrease in θ_{CO} (e.g. from 0.999 to 0.990), could result in a 10-fold increase in θ_H and therefore a 10-fold increase in activity. Thus, Van den Berg *et al.* proposed that the role of MoO₂ and MnO is to change the relative surface concentration of CO and H₂, thereby accelerating the rate-determining step.

However, our ethylene-addition experiments are in contradiction with this conclusion in the case of vanadium oxide promotion. Conclusions from addition of reactive compounds must be considered with care. As noted by

Chuang *et al.* [35], the added and adsorbed ethylene is not equivalent to the precursor for ethylene formed during the CO hydrogenation reaction. This is obvious since the chance for the added ethylene to enter chain growth rather than to be hydrogenated to ethane is significantly different from that for the C_2H_x surface intermediates formed during CO hydrogenation. This effect was also seen for the promoted and unpromoted catalysts used in this study. The amount of ethylene incorporated in high hydrocarbons was negligible compared with the chain growth probability of C_2H_x intermediates formed during CO hydrogenation. However, the added ethylene can serve as a probe to determine hydrogenation and CO insertion activities under reaction conditions.

From Table 8.7 and 8.8 the following picture emerges. If $Rh/V_2O_3/SiO_2$ and Rh/SiO_2 are tested at the same temperature (503 K), the reaction rate for $Rh/V_2O_3/SiO_2$ is very much higher than that of Rh/SiO_2 . However, under these reaction conditions, the amount of ethylene converted to ethane is about the same for these two systems and therefore their hydrogenation rates are comparable. Thus, the fact that Rh/SiO_2 has a low activity at 503 K can not be due to a low hydrogenation activity. The same conclusion can be drawn from the experiments in which the H_2/CO ratio is varied (Figure 8.4a). The increase in activity with increasing H_2/CO ratio is comparable for the two systems. Therefore, the hydrogenation rate is not rate determining for the Rh/SiO_2 catalyst. A further indication that the presence of hydrogen is not rate limiting is the fact that during reaction over Rh/SiO_2 at 591 K, the amount of unsaturated hydrocarbons is very low pointing to a high hydrogenation activity.

The other possibility is that the CO dissociation is the rate determining step. Mori *et al.* [14] have used a combination of pulse surface reaction rate analysis and emissionless diffuse reflectance infrared spectrometry to measure the rate constants for C-O bond dissociation (k_{CO}) and methane formation (k_{HC}) separately. The influence of several promoters, e.g. V, Mo, W and Re, on a Ru/Al_2O_3 catalyst was studied. They reported that vanadium oxide enhanced the CO dissociation (k_{CO} increased), while the influence of the vanadium oxide on the hydrogenation was small (k_{HC} decreased by addition of vanadium oxide). Furthermore, k_{HC} was much higher than k_{CO} and an IR absorption band at 2926 cm^{-1} was observed for the V-promoted catalysts only. Mori *et al.* assigned this band to the C-H stretching vibration of the CH_x species. These results suggest that the main role of the vanadium oxide promoter is to enhance the rate of dissociation of CO. We will pursue this suggestion by further studying the vanadium oxide

promotion of Rh catalysts by means of ^{13}C -NMR.

The promoter effect of vanadium oxide on the activation of the CO band can be caused by an interaction of the oxygen atom of the chemisorbed CO with a positively charged promoter centre (V^{3+}), as was proposed by Sachtler *et al.* [24] for promoted systems in general. Burch *et al.* [43] and Bell *et al.* [44] proposed a similar activation of CO by an ion of the support for Pd catalysts. Sachtler *et al.* studied a Mn-promoted Rh catalyst with IR spectroscopy (CO adsorbed at 298 K) and observed a CO band at low frequency, around 1530 cm^{-1} [23-25]. Ichikawa *et al.* [11] reported the existence of a similar band for Mn-promoted rhodium catalysts. The band at 1530 cm^{-1} is ascribed to C- and O-bonded carbon monoxide and a model was proposed in which ions of an electropositive metal (promoter) on the surface of the rhodium metal particle provide sites at which CO may be "C"-bonded to a metal surface and "O"-bonded to a promoter ion [23-25,11]. Recently, Sachtler and Ichikawa [25] reported that the band position of the bridge-bonded CO for the vanadium oxide-promoted Rh/SiO₂ was shifted to lower wavenumbers compared with the unpromoted Rh/SiO₂ catalyst (Rh-V/SiO₂ had a broad strong band at 1760 cm^{-1} , and a shoulder at 1650 cm^{-1} , while Rh/SiO₂ had a strong band at $1880\text{--}1900\text{ cm}^{-1}$). They ascribed this shift also to a tilted mode of CO adsorbed on Rh and the promoter, resulting in a weakened C-O bond. As a result, C-O bond dissociation is facilitated. For our catalysts, the shift of the bridge-bonded CO due to the promotion of vanadium oxide was less (shift of 50 cm^{-1} to lower wavenumbers) [15] and can also be caused by the lower CO coverage, as vanadium oxide decreases the amount of CO adsorbed in the bridged form. Therefore, it is questionable whether shifts in this order of magnitude point to the formation of C- and O-bonded CO. However, it is still possible that these species are formed under reaction conditions.

Mori *et al.* [14] proposed a mechanism in which a CO molecule adsorbs on the metal and is transformed into a M-CHOH intermediate. An adjacent V^{3+} -ion pulls the oxygen atom away from this hydroxycarbene intermediate, and forms a transition state that promotes the dissociation of CO into $(\text{CH}_x)_{\text{ad}}$ and $(\text{OH})_{\text{ad}}$. Simultaneously V^{3+} is oxidized to V^{4+} . The vanadium oxide promoter catalyzes the CO dissociation by an oxidation/reduction cycle.

From our measurements we can not exclude one of described models for the promoter action.

Influence of promoter and reaction conditions on selectivity. At first sight, the influence of the promoter on the selectivity is high. While the Rh/SiO₂ catalyst has a high selectivity to methanol and methane, the Rh/V₂O₃/SiO₂ catalysts have a relatively high selectivity to C₂-oxygenates and higher hydrocarbons. However, this can be caused by the differences in reaction temperature. As can be seen in the ethylene addition experiment, ethylene is completely hydrogenated at the reaction temperature necessary for Rh/SiO₂ to obtain sufficient conversion (593 K) and no insertion of CO in ethylene took place to form propionaldehyde or propanol. However, ethylene addition at 503 K showed that, although the activity for CO hydrogenation is very low at that temperature for Rh/SiO₂, CO insertion takes place with approximately the same reaction rate as on the Rh/V₂O₃/SiO₂ catalyst. This proves that the presence of vanadium oxide is not necessary for the CO insertion reaction in ethylene. To exclude temperature influences, we tested Rh/SiO₂ and Rh/V₂O₃/SiO₂ (V/Rh = 1.0) at the same temperature (see Table 8.4). The difference is even more pronounced. Rh/SiO₂ produced mainly methanol (57 %), and C₂-oxygenates (28 %) at 548 K. At the same temperature the promoted system had a relatively low methanol selectivity (9 %), and produced much methane (29 %), C₂-oxygenates (42 %) and heavier products. From the formation rates of the different products at 548 K, we can conclude that the methanol formation rate is only increased by a factor of six, while the formation rate to the other product groups is increased by a factor of fourty to two hundred. The higher formation rates of the products, except for methanol, can be understood by the assumption that vanadium oxide enhances the dissociation of CO and increases the chain-growth probability.

Vanadium oxide not only enhanced the dissociative path leading to hydrocarbons and higher oxygenated products, but also the associative pathway leading to methanol, as methanol has been proven to be formed non-dissociatively [45]. As methanol is thought to be formed over metal ions [32-34], this suggests that the presence of vanadium oxide increased the amount of rhodium ions. Unfortunately, we do not have information about the amount of rhodium ions in our catalysts. However, temperature programmed reduction studies showed that in vanadium oxide-promoted catalysts, the reduction of rhodium oxide is shifted to higher temperatures [15]. Thus, it is plausible to assume that in the vanadium oxide-promoted catalysts the amount of rhodium ions is higher than in the unpromoted Rh/SiO₂ catalyst. The amount of metal ions does not influence the formation rate of C₂-oxygenates, as demonstrated by Van der Lee *et al.* [9].

Not only did the amount of vanadium oxide influence the selectivity pattern during syngas reaction, but also the reaction conditions (temperature, pressure and H_2/CO ratio) had an important effect. For the vanadium oxide-promoted catalyst, an increase in temperature caused a decrease in methanol selectivity, while the methane selectivity increased and the C_2 -oxygenate selectivity increased slightly (see Table 8.5 and Figure 8.4b). Temperatures above 573 K disfavour the formation of oxygenates, as can be seen in Figure 8.4b for the unpromoted Rh/SiO₂ catalyst (compare the increase in activity to C₁OH (8.4b3) and C₂OH (8.4b4) with the increase in activity to methane (8.4b1)). Probably, CH_x species, once formed, are readily hydrogenated to methane, and do not have the chance to grow to longer carbon chains or undergo a CO insertion reaction. This was also concluded from the ethylene addition experiments at 593 K.

A higher H_2/CO ratio caused an increase in the formation rates of all products (see Figure 8.4a and Table 8.5). The C_2 -oxygenate and methanol selectivity are higher at low H_2/CO ratios. The methanol formation rate of the promoted catalyst was almost constant above $H_2/CO = 1.0$.

For the promoted catalyst, the pressure mainly affected the formation rate of methanol. A remarkably high selectivity to C_2 -oxygenates is observed at 0.15 MPa. For the unpromoted Rh/SiO₂, the major product at 0.15 MPa is methane. A high pressure (4.0 MPa) results in a better total oxo-selectivity due to an increased methanol and C_2 -oxygenate selectivity. Thus, at a high reaction temperature, the increase in pressure is positive for C_1 - and C_2 -oxygenates, while for low temperatures, a higher pressure mainly affects the methanol selectivity. Therefore, if one is interested in a high total oxo-selectivity, the best reaction conditions for the promoted catalyst are a low reaction temperature, a low H_2/CO ratio and a high pressure. If one is only interested in a high C_2 -oxygenate selectivity, a low H_2/CO ratio and a higher reaction temperature are required, while a high pressure is not necessary.

Besides influencing the selectivity pattern of catalysts via differences in reaction kinetics, successive reaction and/or thermodynamic limitations, the reaction conditions (pressure, H_2/CO , temperature and GHSV) can also affect the catalyst system itself. For instance the extent of covering by V_2O_3 and/or the amount of rhodium ions will be influenced by the reaction conditions. The surface concentration of oxygen, formed by dissociation of CO, and the amount of water are affected by the reaction parameters and will play an important role. Low conversions, as a result of a low temperature, and a high GHSV will result in relatively low water vapour pressures. This

will in turn result in a relatively low amount of rhodium ions. A high pressure will result in a high water vapour pressure, which can result in a relatively high amount of metal ions. The water vapour pressure also can influence the extent of coverage by vanadium oxide, as the SMSI state is known to be reversed by water or oxygen.

From the detailed study of the products and the Flory-Schulz distributions we can conclude that the chain-growth probability for hydrocarbons is higher than for the oxygenated products. This is in contrast to the measurements reported by Van den Berg and Sachtler [24,46]. Studying a Rh-Mn-Mo/SiO₂ catalyst at 10 MPa, they showed that the Flory-Schulz distributions of hydrocarbons and oxygenates exhibit the same chain-growth probability and from this fact they concluded that the chain-growth mechanisms for hydrocarbons and oxygenates are identical. However, this is not a necessary condition. Assuming an identical chain-growth mechanism for hydrocarbons and oxygenates, we must conclude from our measurements that the CO insertion rate is dependent on the chain-length of the carbon fragment into which it inserts. In agreement with several groups [24,46,47] we observed an undershoot of C₂-hydrocarbons and an overshoot of C₂-oxygenated products in the Flory-Schulz plots.

8.4.2 Rh/V₂O₃/Al₂O₃

Although not to the same extent, the vanadium oxide promoter also caused an increase in the activity for Rh/Al₂O₃ catalysts. Small amounts of vanadium oxide (up to V/Rh = 1.0) did not influence the activity. This confirms the conclusion from the characterization studies that rhodium and vanadium oxide particles exist separately on the alumina support. The Rh/V₂O₃/Al₂O₃ catalysts with a high V/Rh ratio (7.0 and 8.4) had an activity three times larger than the unpromoted Rh/Al₂O₃ catalyst. Clearly, large amounts of vanadium oxide are required to promote the Rh/Al₂O₃ catalyst. This is due to the strong interaction between vanadium oxide and alumina, the first amount of vanadium oxide is scavenged by the alumina support. This also explains why the vanadium oxide promoter in the study of Mori *et al.* [14] only had a limited positive effect on their Ru/Al₂O₃ catalyst. The rate of formation of C₂-oxygenates and hydrocarbons containing two or more carbon atoms is increased to a higher extent than the formation rate of methanol and methane, causing a shift in the selectivity pattern to heavier products.

The alumina-supported catalysts produced more methanol than the

silica-supported ones. As could be concluded from chemisorption and TEM measurements, the rhodium particle size of the alumina-supported catalysts is much smaller than the particle size of the silica-supported catalysts. This might result in a higher amount of rhodium ions, thus causing a higher methanol formation rate.

Two interesting, special features were observed for the Rh/ V_2O_5 / Al_2O_3 catalysts. Firstly, part of the alcohols formed are converted into ethers over acidic sites of the alumina in the case of Rh/ Al_2O_3 [28]. In the present study we found that the amount of ether formed from alcohols decreased with increasing vanadium content. For the high vanadium oxide loaded catalysts, the amount of dimethylether was negligible. This suggests that the sites responsible for the ether formation are covered completely by vanadium oxide. It also offers an explanation for the fact that in the preparation of the catalysts we did not succeed in the formation of a 100% monolayer coverage. The maximum V/Rh ratio of 8.4 (6.7 wt% V) which we obtained corresponds to a coverage of 40 % of the surface area of the Al_2O_3 used in this study, assuming that all vanadium oxide is present as a monomolecular layer on the support. The catalytic results suggest that during preparation of the monolayer of vanadium oxide on alumina the ammonium metavanadate ions adsorb only on the sites which are responsible for ether formation during Fischer Tropsch reaction. Apparently, at V/Rh = 8.4, these sites are all filled with vanadium oxide, therefore no more ether formation takes place and there are no further sites available for adsorption of vanadium, leading to a maximum coverage of 40 %.

The second feature is related to other, non acidic sites on the alumina support. Studying the catalytic activity as a function of time on stream, a chromatographic effect was observed for acetic acid. For Rh/ Al_2O_3 , only after prolonged reaction (12 h) was acetic acid detected, whereas for Rh/ V_2O_5 / Al_2O_3 , V/Rh = 7.0, acetic acid was already found after 5 h time on stream. However, the amount of strongly adsorbed acetic acid increased slightly with increasing V/Rh ratio (in a shorter time more acetic acid is formed in the promoted case due to a higher formation rate). The chromatographic effect is due to adsorption of acetic acid or of a precursor of acetic acid on basic sites on the support, as was proven by the experiment in which an additional amount of alumina was placed downstream of the catalyst bed. Once the adsorption sites are filled, acetic acid appeared as products in the gas stream at the reactor outlet. These type of sites increased with increasing V/Rh ratio, suggesting that the addition of vanadium oxide converts sites responsible for ether formation (acid sites) into sites

responsible for adsorption of acetic acid (basic sites).

Using the surface model for γ - Al_2O_3 proposed by Knözinger and Ratnasamy [48], one can understand the coexistence of acidic and basic sites on an alumina surface. Under syngas reaction conditions (water is formed and the temperature is relatively low), the alumina surface will be hydroxylated to a high extent. Knözinger and Ratnasamy expect a maximum of five different OH configurations, their actual occurrence and relative concentration depending on the relative contributions of the different crystal faces. The OH-groups in the various configurations bear slightly different net charges, and as a consequence have slightly different properties. One would expect an OH-group which is coordinated to three cations in octahedral interstices (Type III according to Knözinger and Ratnasamy, with a net positive charge of + 0.5) to be the most acidic, since abstraction of a proton would lead to an oxygen atom bearing a net negative charge of only -0.5, which is close to the value of zero necessary for electroneutrality. By the same arguments, OH-groups with a more negative net charge, like an OH-group coordinated to a single tetrahedral Al^{3+} cation (Type IA, net charge -0.25) or an OH-group coordinated to a single cation in an octahedral interstice (Type IB, net charge -0.5) have a higher basicity. Thus, the model proposed by Knözinger and Ratnasamy allows us to suggest that, while sites with a more basic character and sites with a more acidic character coexists on the alumina surface, the acidic ones are responsible for the ether formation and the basic ones responsible for the adsorption of acetic acid.

8.4.3 Rh/ V_2O_3

The activity and the selectivity of the CO hydrogenation over 1.5 wt% Rh/ V_2O_3 catalysts depend critically on the reduction temperature. After reduction at 823 K, the oxo-selectivity was very high (80%), but the activity was low. We also saw a complete suppression of hydrogen chemisorption after high temperature reduction [15]. These results point to a covering of the metal particles as in the SMSI systems [16-22]. Van der Lee *et al.* [9] also observed similar effects of the reduction temperature. Using a 4.5 wt% Rh/ V_2O_3 catalyst, they reported that a high reduction temperature was always beneficial for the selectivity to oxygenates, and that a more extended covering of the metal particles induced by a reduction at higher temperature sometimes caused a decrease and sometimes caused an increase in activity. Probably, the vanadium oxide promoter induces two counteracting effects [9]. Firstly, the vanadium oxide blocks a part of the active metal

surface and selectively suppresses reactions which need a large ensemble of metal atoms. This blocking also results in suppressed hydrogen and carbon monoxide chemisorption. Secondly, the vanadium oxide patches enhance the rate of CO dissociation at the metal-vanadium oxide interface, that is at the perimeter of the V_2O_3 patches on the Rh particles (see also Rh/ V_2O_3 /SiO₂ catalysts). In a recent study Levin *et al.* [49] reported the influence of TiO_x and AlO_x submonolayers deposited on a polycrystalline Rh foil. AlO_x deposition suppressed the rate of CO hydrogenation in direct proportion to the AlO_x coverage, but the product distribution and kinetics were unaffected, indicating that the only effect of AlO_x is to block Rh sites. With increasing TiO_x coverage, the methanation rate passed through a maximum at a TiO_x coverage of 0.15 monolayer. Kinetics and catalyst selectivity were also changed by the TiO_x layer. They attributed the unusual behaviour of TiO_x-promoted Rh to the occurrence of highly active catalytic sites near the perimeter of the TiO_x islands making up the overlayer. Thus, also in the case of TiO_x-promotion, the effect of blocking of sites and the creation of highly active sites compete. Which effect prevails is strongly dependent on the extent and structure of the overlayer and explains why covering in the case of Rh/ V_2O_3 /SiO₂ resulted in an increased activity (the second effect is stronger), and covering in the case of our 1.5 wt% Rh/ V_2O_3 catalyst caused a decrease in activity (the blocking effect is stronger). Similar explanations can be given for the difference in the influence of vanadium oxide promotion of Ru/Al₂O₃. As already mentioned, Mori *et al.* [14] reported an increase in activity, whereas Enomoto *et al.* [50] showed that the activity in carbon monoxide hydrogenation decreased after vanadium oxide promotion.

In contrast to the SMSI-state of Rh/TiO₂, obtained after high temperature reduction, the SMSI-state of Rh/ V_2O_3 is maintained during the syngas reaction and is not reversed by water formed during the reaction, as has also been reported by Lin *et al.* [26].

Our results, as well as the results of Van der Lee *et al.* [9] and Levin *et al.* [49] suggest that the vanadium oxide patches which cover the metal particle not only have a positive effect on the CO dissociation, but also have a positive effect on the formation of oxygenated intermediates. Furthermore, the extent of covering seems to affect the hydrogenation activity. The 1.5 wt% Rh/ V_2O_3 catalyst reduced at 523 K has a high hydrogenation activity, low amounts of unsaturated hydrocarbons are formed and the ethanol/acetaldehyde ratio is high (ethanol is thought to be formed by hydrogenation of acetaldehyde). This catalyst has a high methane selectivity, probably caused by the high hydrogenation rate. Once C₁-

intermediates are formed, they are readily hydrogenated to methane before CO can insert (which results in C₂-oxygenates), or before the C₁-intermediate can grow to longer carbon chains. Reduction at a high temperature (723 or 823 K) resulted in a lower activity (due to site blocking), a lower methane and higher oxygenate selectivity. This will be due to a lower hydrogenation rate, as is also reflected in a higher acetaldehyde/ethanol ratio and a higher amount of unsaturated hydrocarbons. This also explains the high deactivation of this catalysts. Due to the low hydrogenation activity long unsaturated hydrocarbons can accumulate on the surface leading to coke formation. For the Rh/V₂O₃/SiO₂ catalysts, the lower amount of unsaturated hydrocarbons and acetaldehyde and the lower deactivation point to a relatively high hydrogenation rate. This is consistent with the model described before in which the covering by vanadium oxide was less in these systems, compared with the Rh/V₂O₃ catalyst reduced at a high temperature.

8.5 CONCLUSIONS

Addition of vanadium oxide to Rh/SiO₂ caused an important increase in the activity. The results suggest that the rhodium particles are partially covered by vanadium oxide and that the role of the vanadium oxide promoter is to enhance the CO dissociation. The results of Rh/V₂O₃ show that this rate enhancing can be dominated by the blocking of reaction sites by patches of vanadium oxide present on the metal particles. There will be an optimum positive influence of the vanadium oxide promoter on the activity and this optimum will depend on the impregnation, drying, calcination and reduction steps. The oxo-selectivities were high for the Rh/V₂O₃/SiO₂ and Rh/V₂O₃ catalysts. The insertion reaction of CO into ethylene was not influenced by the presence of vanadium oxide patches in the Rh/V₂O₃/SiO₂ catalysts.

For the alumina-supported vanadium oxide-promoted catalysts, high V₂O₃ loadings are required to improve the activity. In these catalysts, the vanadium oxide covered the acidic sites on the alumina support and this resulted in a complete suppression of the ether formation. Furthermore, a chromatographic effect for acetic acid was observed for these catalysts. During the first hours of reaction the formed acetic acid is adsorbed in the support. Only after prolonged reaction acetic acid is found in the gas stream.

So, Rh/V₂O₃/SiO₂ is the better catalyst system. Because of a weak interaction between V₂O₃ and the SiO₂ support, Rh₂O₃ and V₂O₃ are in

intimate contact. After reduction V_2O_3 partially covers the Rh particles, resulting in a relatively high activity and oxo-selectivity (70 %). For the Rh/ V_2O_3 catalyst, reduced at a high temperature, the covering of the Rh particles by V_2O_3 is substantial. In this case, blocking of active sites dominates the promoting effect of V_2O_3 on the CO dissociation, resulting in a relatively low activity. Oxo-selectivity is high for this system (70-80 %). Because of the strong interaction between V_2O_3 and Al_2O_3 most of the V_2O_3 is scavenged by the Al_2O_3 support, and a high V_2O_3 loading is required to affect the activity of Rh/ Al_2O_3 . For this system, the oxo-selectivity is relatively low (50 %).

8.6 REFERENCES

1. P.R. Watson and G.A. Somorjai, *J. Catal.*, 72 (1981) 347.
2. M. Ichikawa, *Bull. Chem. Soc. Japan*, 51 (1978) 2268.
3. J.R. Katzer, A.W. Sleight, P. Gajardo, J.B. Mitchel, E.F. Gleason and S. McMillan, *Faraday Disc. Chem. Soc.*, 72 (1981) 121.
4. E.K. Poels, P.J. Magnus, J. van Velzen and V. Ponec, "Proc. Int. Congr. on Catal., 8th (Berlin, 1984)", vol II, p.59. Verlag Chemie, Weinheim, 1984.
5. M. Ichikawa, K. Shikakura and M. Kawai, in "Heterogeneous Catalysis Related to Energy Problems", Proc. Symp. in Dalian, China, 1982 A.08-I.
6. M. Ichikawa, *Bull. Chem. Soc. Japan*, 51 (1978) 2273.
7. M.M. Bhasin and G.L. O'Connor, Belgian Patent 824822, to Union Carbide Corp., 1975.
8. T.P. Wilson, P.H. Kasai and P.C. Ellgen, *J. Catal.*, 69 (1981) 193.
9. G. van der Lee, B. Schuller, H. Post, T.L.F. Favre and V. Ponec, *J. Catal.*, 98 (1986) 522; G. van der Lee, A.G.T.M. Bastein, J. van den Boogert, B. Schuller, H. Luo and V. Ponec, *Far. Symp. Chem. Soc.*, 21 (1986) paper 12.
10. F.G.A. van den Berg, J.H.E. Glezer and W.M.H. Sachtler, *J. Catal.*, 93 (1985) 340.
11. M. Ichikawa, T. Fukushima and K. Shikakura, "Proc. Int. Congr. on Catal., 8th (Berlin, 1984)", vol 1, p. 69, Verlag Chemie, Weinheim, 1984.
12. A. Aquilo, J.S. Alder, D.N. Freeman and R.J.H. Voorhoeve, *Hydrocarbon Process*, 62 (1983) 57.
13. E. Kikuchi, H. Nomura, M. Matsumoto and Y. Morita, *Appl. Catal.*, 7 (1983) 1.
14. T. Mori, A. Miyamoto, N. Takahashi, M. Fukagaya, H. Niizuma, T. Hattori and Y. Murakami, *J. Chem. Soc., Chem. Commun.*, (1984) 678; N. Takahashi, T. Mori, A. Miyamoto, T. Hattori and Y. Murakami, *Appl. Catal.*, 22 (1986) 137; T. Mori, A. Miyamoto, N. Takahashi, M. Fukagaya, T. Hattori and Y. Murakami, *J. Phys. Chem.*, 90 (1986) 5197.

15. B.J. Kip, P.A.T. Smeets, J.H.M.C. van Wolput, H. Zandbergen, J. van Grondelle and R. Prins, submitted to *Appl. Catal.*, chapter 7 of this thesis.
16. S.J. Tauster and S.C. Fung, *J. Catal.*, 55 (1978) 29.
17. P. Meriaudeau, J.F. Dutel, M. Dufaux and C. Naccache, *Stud. Surf. Sci. Catal.*, 11 (1982) 95.
18. D.E. Resasco and G.L. Haller, *J. Catal.*, 82 (1983) 279.
19. B.R. Powell and S.E. Whittington, *J. Catal.*, 81 (1983) 382.
20. A.J. Simoens, R.T.K. Baker, D.J. Dwyer, C.F.R. Lund and R.J. Madon, *J. Catal.*, 86 (1984) 359.
21. G.L. Haller, V.E. Henrich, M. McMillan, D.E. Resasco, H.R. Sadeghi and S. Sakellson, "Proc. Int. Congr. on Catal., 8th (Berlin, 1984)", vol. V, p. 135, Verlag Chemie, Weinheim, 1984.
22. Y.W. Chung, G. Xiong and C.C. Kao, *J. Catal.*, 87 (1984) 279.
23. W.M.H. Sachtler, "Proc. Int. Congr. on Catal., 8th (Berlin, 1984)", vol. I, p. 151, Verlag Chemie, Weinheim, 1984.
24. W.M.H. Sachtler, D.F. Shriver, W.B. Hollenberg and S.I. Lang, *J. Catal.*, 92 (1985) 429.
25. W.M.H. Sachtler and M. Ichikawa, *J. Phys. Chem.*, 90 (1986) 4752.
26. Y.J. Lin, D.E. Resasco and G.L. Haller, *Far. Symp. Chem. Soc.*, 21 (1986) paper 11.
27. H.F.J. van 't Blik, J.C. Vis, T. Huizinga and R. Prins, *Appl. Catal.*, 19 (1986) 405.
28. B.J. Kip, F.W.A. Dirne, J. van Grondelle and R. Prins, *Appl. Catal.* 25 (1986) 32, chapter 5 of this thesis.
29. H. Arakawa, T. Takeuchi, T. Matsuzaki and Y. Sugi, *Chem. Lett.*, (1984) 1607; H. Arakawa, T. Fukushima, M. Ichikawa, K. Takeuchi, T. Matsuzaki and Y. Sugi, *Chem. Lett.*, (1985) 23.
30. H.F.J. van 't Blik, J.B.A.D. van Zon, T. Huizinga, D.C. Koningsberger and R. Prins, *J. Am. Chem. Soc.*, 107 (1985) 3139.
31. H.F.J. van 't Blik, J.B.A.D. van Zon, D.C. Koningsberger and R. Prins, *J. Molec. Catal.*, 25 (1984) 379.
32. E.K. Poels, E.M. van Broekhoven, W.A.A. van Barneveld and V. Ponec, *React. Kinet. Catal. Lett.*, 18 (1981) 223.
33. J.M. Driessen, E.K. Poels, J.P. Hindermann and V. Ponec, *J. Catal.*, 82 (1983) 20.
34. J.P. Hindermann, A. Kiennemann, A. Chakor-Alami and R. Kieffer, "Proc. Int. Congr. Catal., 8th (Berlin, 1984)", vol. II, p. 163, Verlag Chemie, Weinheim, 1984.
35. S.C. Chuang, J.G. Goodwin, Jr. and I. Wender, *J. Catal.*, 92 (1985) 416; S.C. Chuang, Y.H. Tian, J.G. Goodwin, Jr. and I. Wender, *J. Catal.*, 96 (1985) 396.

36. M. Ichikawa, K. Sekizawa, K. Shikakura and M. Kawai, *J. Molec. Catal.*, 11 (1981) 167.
37. M. Pijolat and V. Perrichon, *Appl. Catal.*, 13 (1985) 321.
38. J. Happel, I. Suzuki, P. Kokayeff and V. Fthenakis, *J. Catal.*, 65 (1980) 59.
39. R.S. Pilizzoti and J.A. Schwarz, *J. Catal.*, 77 (1982) 1.
40. W.L. van Dijk and H.S. van der Baan, *J. Catal.*, 78 (1982) 24.
41. P. Biloen, J.N. Helle, F.G.A. van den Berg and W.M.H. Sachtler, *J. Catal.*, 81 (1983) 450.
42. P.C. Ellgen, W.J. Bartly, M.M. Bhasin and T.P. Wilson, *Adv. Chem. Ser.*, 178 (1979) 147.
43. J.D. Bracey and R. Burch, *J. Catal.*, 86 (1984) 384; J.B.F. Anderson, J.D. Bracey and R. Burch, "Proc. Int. Congr. Catal., 8th (Berlin, 1984)", vol. V, p. 251, Verlag Chemie, Weinheim, 1984.
44. J.S. Rieck and A.T. Bell, *J. Catal.*, 99 (1986) 262.
45. A. Takeuchi and J.R. Katzer, *J. Phys. Chem.*, 85 (1981) 937.
46. F.G.A. Van den Berg and J.H.E. Glezer, *Proc. Kon. Ned. Akademie Wetensch.*, B86 (1983) 227.
47. A. Takeuchi, J.R. Katzer and G.C.A. Schuit, *J. Catal.*, 82 (1983) 477.
48. H. Knözinger and P. Ratnasamy, *Catal. Rev.- Sci. Eng.*, 17 (1978) 31.
49. M.E. Levin, M. Salmeron, A.T. Bell and G.A. Somorjai, *Faraday Symp. Chem. Soc.*, 21 (1986) paper 10.
50. T. Enomoto, T. Okuhara and M. Misono, *Bull. Chem. Soc. Japan*, 58 (1985) 1490.

Chapter 9

HYDROGENATION OF CARBON MONOXIDE OVER Rh/SiO₂ CATALYSTS PROMOTED WITH MOLYBDENUM OXIDE AND THORIUM OXIDE

The promotion of silica-supported rhodium catalysts in the hydrogenation of carbon monoxide by molybdenum and thorium oxide has been examined. Temperature programmed reduction studies indicated the formation of rhodium molybdates, while no evidence was found for the formation of such mixed oxides in the ThO₂-promoted catalysts. Hydrogen and carbon monoxide chemisorption were suppressed by the presence of molybdenum oxide, pointing to a coverage of the rhodium particles by this promoter oxide. The catalysts with Mo/Rh ratios exceeding one even exhibited an almost complete suppression of the rhodium chemisorption capacity. In the ThO₂-promoted catalysts the chemisorption of hydrogen and carbon monoxide were not suppressed. Infrared spectroscopy of adsorbed CO showed that MoO₃ completely suppressed bridge-bonded and linearly bonded CO, as well as the gem-dicarbonyl species. ThO₂ addition resulted in a minor decrease of the linearly bonded CO, while the bridge-bonded CO was suppressed to a greater extent. The IR spectra of the ThO₂-promoted catalysts also exhibited a broad absorption band between 1300 and 1750 cm⁻¹, which is thought to be due to CO bonded with the carbon atom to the metal and with the oxygen atom to the promoter ion.

Carbon monoxide hydrogenation was greatly enhanced by the presence of both molybdenum oxide and thorium oxide. Thorium oxide-promoted catalysts had a high selectivity to C₂-oxygenates, while the molybdenum oxide-promoted catalysts exhibited a high methanol selectivity. Ethylene addition to a working catalyst showed that the CO insertion reaction, which is thought to be responsible for the formation of oxygenates, was not enhanced by MoO₃, nor by ThO₂. The ethylene addition experiments indicated that the role of the promoter is to enhance CO dissociation. The results can be understood by assuming that side-bonded CO, with its weakened C-O bond, is responsible for the higher CO dissociation activity.

9.1 INTRODUCTION

In a previous study [1,2] we observed a sharp increase in the activity of CO hydrogenation when vanadium oxide was added to silica- and alumina-supported rhodium catalysts. The major role of the vanadium oxide promoter was to enhance the CO dissociation, and thus to increase the activity. The increase in activity was also observed by Mori *et al.* [3,4] for vanadium oxide-promoted Ru/Al₂O₃ catalysts. A high oxo-selectivity was measured for the V₂O₃-promoted Rh/SiO₂ catalyst [2]. The CO insertion reaction, which is thought to be an important step in the formation of oxygenated hydrocarbons, was not influenced by the presence of vanadium oxide, as could be concluded from ethylene addition experiments.

Temperature programmed reduction and diffuse-reflectance infrared measurements of calcined vanadium oxide-promoted silica-supported rhodium catalysts indicated that during the calcination a mixed oxide of rhodium oxide and vanadium oxide (RhVO₄) was formed. But the size of the rhodium particles formed after reduction was not influenced by the presence of the promoter oxide. Suppression of carbon monoxide chemisorption after reduction at 523 K proved that the rhodium particles were (partly) covered by vanadium oxide patches. The absence of hydrogen chemisorption suppression was explained by the adsorption of hydrogen by vanadium oxide via the formation of vanadium hydrogen bronzes.

From these observations we concluded that on the one hand the vanadium oxide blocks part of the active metal surface, resulting in a suppressed chemisorption capacity, while on the other hand, the vanadium oxide patches enhance the rate of CO dissociation along their perimeter. This enhancement effect is most important for silica-supported vanadium oxide-promoted rhodium catalysts. For vanadium oxide-supported rhodium catalysts, however the covering and blocking effect dominates after high temperature reduction.

Mori *et al.* [4] proposed a catalytic redox cycle to explain the role of the vanadium oxide promoter, in their V₂O₃-promoted Ru/Al₂O₃ catalyst. The V³⁺ ion adjacent to the Ru atom, to which a hydroxycarbene fragment (M-CHOH) is attached, pulls the oxygen atom away from this M-CHOH fragment. Thus a transition state is formed, which eases the dissociation of the C-O bond into (CH_x)_{ad} and (OH)_{ad}. Simultaneously V³⁺ is oxidized to V⁴⁺. The (OH)_{ad} species on the V⁴⁺ ion is hydrogenated to H₂O, reforming V³⁺. In this way, the oxidation-reduction cycle of the promoter oxide may explain the dissociation of the C-O bond during the hydrogenation of CO.

In the present paper we will extensively study two other promoters, molybdenum oxide and thorium oxide. Ellgen *et al.* [5,6] and Van den Berg *et al.* [7] examined the promotive effect of molybdenum oxide and observed a positive effect on the activity and oxo-selectivity. Jackson *et al.* [8] reported that the activity of a Rh/MoO₃ catalyst was 20 times higher than the activity of Rh/SiO₂. Ichikawa *et al.* [9] reported an enhanced formation rate of C₂-oxygenates by the addition of thorium oxide. Other rare earth oxides have also been reported to influence the hydrogenation of CO over Rh. Underwood and Bell reported large differences between Rh supported on SiO₂ and Rh supported on La₂O₃, Nd₂O₃ and Sm₂O₃ [10]. Kiennemann *et al.* [11] reported CeO₂ to be very effective for the promotion of ethanol formation. The molybdenum oxide promotion has a similarity with vanadium oxide promotion. The MoO₃ can be reduced under our reduction conditions and rhodium oxide can form rhodium molybdates with MoO₃ [12]. On the contrary, thorium oxide can not be reduced under normal conditions and no thorium rhodates have been reported [13]. However, for the promoter influence on the CO dissociation as described by Mori *et al.* [4] one needs a reduction-oxidation cycle. For these reasons we studied the promotion of Rh/SiO₂ by molybdenum oxide and thorium oxide using a number of characterization techniques like temperature programmed reduction, hydrogen and carbon monoxide chemisorption, transmission electron microscopy, infrared spectroscopy of adsorbed CO, and carbon monoxide hydrogenation at elevated pressure.

9.2 EXPERIMENTAL

9.2.1 Catalyst preparation

As supports we used SiO₂ (Grace, type 113, surface area 360 m² g⁻¹, pore volume 1.1 ml g⁻¹), ThO₂ (Merck, surface area 3.9 m² g⁻¹, pore volume 0.11 ml g⁻¹) and MoO₃ (Merck, surface area 4.0 m² g⁻¹, pore volume 0.13 ml g⁻¹). Molybdenum oxide- and thorium oxide-promoted SiO₂ were prepared by incipient wetting the SiO₂ support with an aqueous solution of (NH₄)₆Mo₇O₂₄·4H₂O (Merck, p.a.) and Th(NO₃)₄·xH₂O (Merck, p.a.) respectively, drying at 395 K and calcining at 723 K (3 h). In this way, supports with a varying amount of molybdenum and thorium oxide were obtained. The catalysts were prepared by the incipient wetness method using an aqueous solution of Rh(NO₃)₃ (pH = 2.5, Drijfhout, Amsterdam), and were subsequently dried in air at 395 K for 16 h (heating rate 2 K min⁻¹). To remove nitrogenous residues from the precursor, the catalysts

were calcined at 723 K for 3 h. Rhodium content was always around 1.5 wt%.

9.2.2 Characterization techniques

Volumetric hydrogen and carbon monoxide chemisorption measurements were performed as described elsewhere [1,14]. Catalysts were reduced at 723 K (heating rate 8 K min⁻¹) for 1 h and evacuated for 0.5 h at 723 K before the chemisorption experiment.

The reduction behaviour of the supports and the reduction, oxidation and hydrogen desorption behaviour of the catalysts were studied by temperature programmed reduction (TPR) and oxidation (TPO), using the apparatus described extensively in ref. [15,16]. During TPR and TPO experiments the heating rate was 5 K min⁻¹.

Carbon monoxide adsorption was also studied by infrared spectroscopy. The glass reactor and spectrometer were described in ref. [1]. The catalysts were reduced *in situ* at 543 K in flowing H₂ (heating rate 5 K min⁻¹) for 0.5 h and evacuated at 543 K for 1 h. The IR spectrum was obtained by adding 512 interferograms. From these spectra information about the relative amount of adsorbed carbon monoxide and the way in which CO is adsorbed on the metal particles was obtained.

In order to get information about the metal particle size Transmission Electron Microscopy (TEM) was used. Catalysts were pretreated by reduction at 523 K and subsequent passivation. The specimens were examined with a Jeol 200CX, operating at 200 kV.

9.2.3 CO hydrogenation

The high pressure reactor and analysis system were described in detail elsewhere [2]. The catalysts were reduced *in situ* in pure hydrogen at 0.1 MPa, using a temperature ramp of 5 K min⁻¹ between 298 and 723 K and holding the final temperature for 1 h. All catalysts were measured under the same reaction conditions (GHSV = 4000 l l⁻¹ h⁻¹, H₂/CO = 3, P = 0.15 or 4.0 MPa). The reaction temperature was adjusted so that conversion of CO was around 2%.

9.3 RESULTS

9.3.1 Temperature programmed reduction

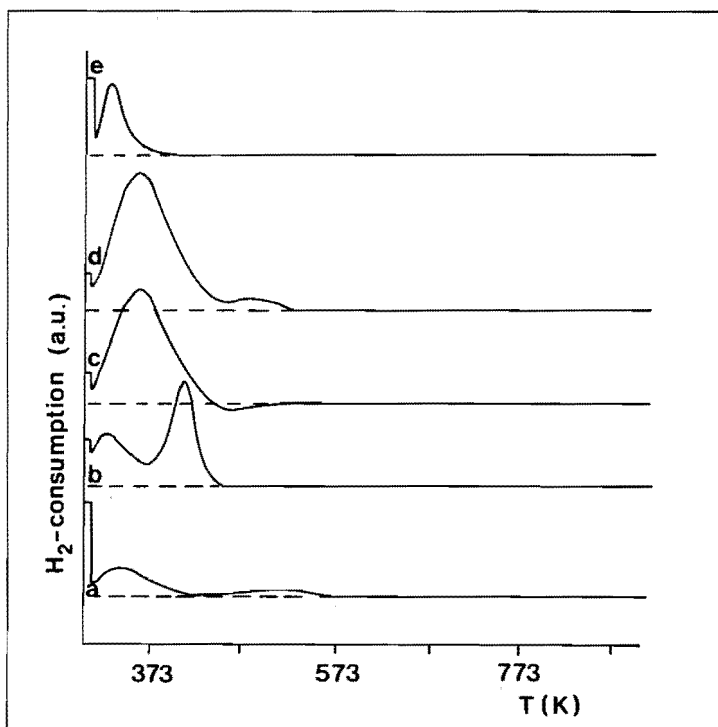


FIGURE 9.1: Temperature programmed reduction profiles of ThO_2 -promoted catalysts.

- 1.5 wt% Rh/ ThO_2 , after calcination at 723 K,
- 1.5 wt% Rh/ ThO_2 , after oxidation at 898 K,
- 1.5 wt% Rh/ SiO_2 , after calcination at 723 K,
- 1.5 wt% Rh/ $\text{ThO}_2/\text{SiO}_2$ (Th/Rh = 1.0), after calcination at 723 K
- 1.5 wt% Rh/ $\text{ThO}_2/\text{SiO}_2$ (Th/Rh = 1.0), after oxidation at 898 K.

ThO₂ promotion. TPR profiles of the thorium oxide-promoted rhodium catalysts are presented in Figure 9.1. For ThO_2 and $\text{ThO}_2/\text{SiO}_2$ no measurable amount of hydrogen consumption was found up to 898 K. For the 1.5 wt% Rh/ ThO_2 catalysts calcined at 723 K, the major part of the hydrogen consumption (about 70 %) was found before the start of the temperature ramp (cf. Figure 9.1a). Hydrogen consumption maxima were found at 346 and

502 K. The TPR profile of this catalyst after oxidation at 898 K (the TPR after a TPO experiment) exhibited a minor hydrogen consumption before the start of the temperature ramp (about 13 %) and two consumption maxima at 325 and 410 K (Figure 9.1b). Similar TPR profiles were observed by Vis *et al.* [17] for Rh/TiO₂ catalysts after oxidation at 873 K. They found two reduction maxima at 330–340 and 385–400 K, respectively, and ascribed the two peaks to two different kinds of Rh/Rh₂O₃ particles. The first kind was easy to reduce and consisted of flat, raftlike particles, the second was harder to reduce and consisted of spherical particles. In our case, this second Rh₂O₃ phase was only observed for 1.5 wt% Rh/ThO₂ and not for 1.5 wt% Rh/SiO₂, indicating that for Rh/ThO₂, the particle size was larger. Hydrogen chemisorption measurements also pointed to a larger particle size for the Rh/ThO₂ catalyst (*vide infra*).

The amount of hydrogen consumed during the TPR run matched the calculated values, assuming that reduction of Rh³⁺ to Rh⁰ took place. Within the experimental error (5%) it can be concluded that no Th⁴⁺ is reduced.

Only a minor influence of ThO₂ on the reduction behaviour of Rh/SiO₂ was seen. For the calcined samples (Figures 9.1c–d) the major peak was found between 353 and 378 K. Some hydrogen consumption was observed around 473 K, and its amount increased with increasing thorium oxide content. This extra peak is ascribed to CO₂ adsorbed to ThO₂ during catalyst preparation [18]. In the TPR profile after oxidation at 898 K (Figure 9.1e) no influence of the thorium oxide on the reduction behaviour was found at all. The amount of hydrogen consumed during the TPR runs of the calcined and oxidized Rh/ThO₂/SiO₂ catalysts pointed to the reduction of Rh³⁺ to Rh⁰. Within the experimental error no ThO₂ was reduced.

The TPR results do not present evidence for an intimate contact between the thorium oxide promoter and the rhodium metal. ThO₂ itself cannot be reduced, not even with the use of the rhodium metal.

MoO₃ promotion. In Figure 9.2a the TPR profile of MoO₃ is presented. The reduction started at 853 K and had a maximum at 993 K. At 1073 K, the maximum reduction temperature obtainable in our apparatus, the average oxidation state was close to Mo⁴⁺. Arnoldy *et al.* [19] showed that the reduction of MoO₃ is highly dependent on the H₂O content of the reducing mixture. They reported reduction of MoO₃ to Mo between 600 and 1100 K. In our case the MoO₃ reduction is more difficult because of the low hydrogen concentration (5% H₂/Ar versus 67% H₂/Ar) and a high sample size/flow rate ratio (4 mg MoO₃/(ml min⁻¹) versus 0.5 mg MoO₃/(ml

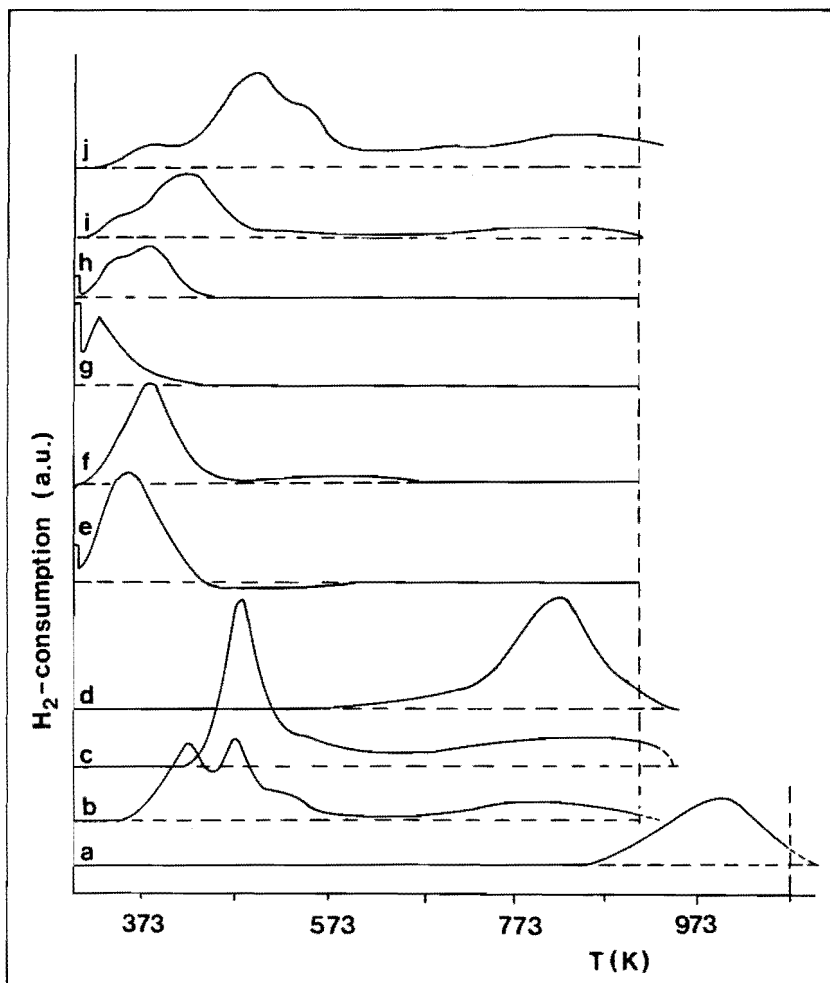


FIGURE 9.2: Temperature programmed reduction profiles of MoO_3 -promoted catalysts.

- a. MoO_3
- b. 1.5 wt% Rh/ MoO_3 , after calcination at 723 K
- c. 1.5 wt% Rh/ MoO_3 , after oxidation at 898 K
- d. $\text{MoO}_3/\text{SiO}_2$ (1.4 wt% Mo), after calcination at 723 K
- e-f. 1.5 wt% Rh/ $\text{MoO}_3/\text{SiO}_2$ after calcination at 723 K, e: Mo/Rh = 0, f: Mo/Rh = 1.0
- g-i. 1.5 wt% Rh/ $\text{MoO}_3/\text{SiO}_2$ after oxidation at 898 K, Mo/Rh = 0, 0.12, 1.0 and 4.0 for g, h, i and j, respectively.

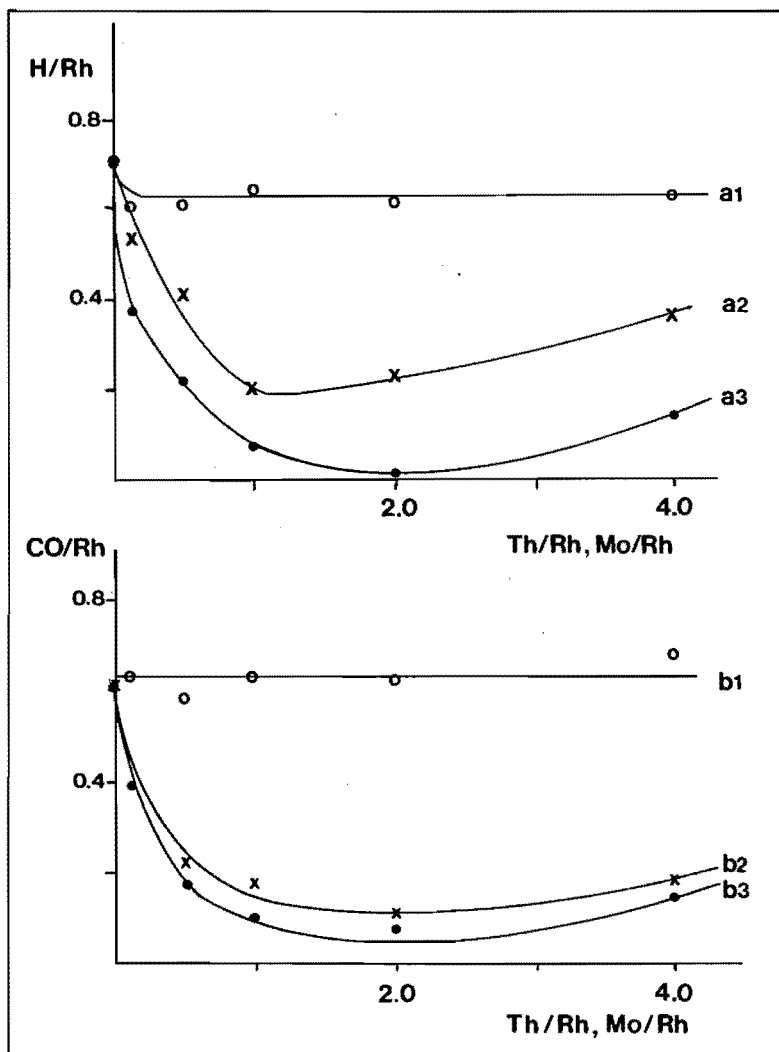


FIGURE 9.3: H₂ and CO chemisorption measurements of the 1.5 wt% Rh/ThO₂/SiO₂ and Rh/MoO₃/SiO₂ catalysts as a function of the Th/Rh and Mo/Rh ratio. Evacuation was performed at the reduction temperature.

- a1. H/Rh after reduction at 723 K for ThO₂-promoted catalysts,
- a2. H/Rh after reduction at 523 K for MoO₃-promoted catalysts,
- a3. H/Rh after reduction at 723 K for MoO₃-promoted catalysts,
- b1. CO/Rh after reduction at 723 K for ThO₂-promoted catalysts,
- b2. CO/Rh after reduction at 523 K for MoO₃-promoted catalysts,
- b3. CO/Rh after reduction at 723 K for MoO₃-promoted catalysts.

min⁻¹) used by Arnoldy *et al.*). This results in a relatively high H₂O/H₂ ratio during our reduction process.

Clearly, rhodium facilitated the reduction of molybdenum oxide in the 1.5 wt% Rh/MoO₃ catalyst, calcined at 723 K (Figure 9.2b). The major hydrogen consumption for this catalyst took place below 573 K. Two peaks were observed at 428 and 478 K. A broad hydrogen consumption maximum was found between 573 and 873 K, caused by the reduction of MoO₃ not in direct contact with rhodium. In the TPR profile after oxidation at 898 K, only the peak at 478 K and the broad hydrogen consumption area between 573 and 873 K were present (Figure 9.2c). The amount of hydrogen consumed during the TPR (after calcination at 723 K and oxidation at 898 K) pointed to the reduction of Rh³⁺ to Rh⁰ and of Mo⁶⁺ to Mo²⁺. Apparently, the low hydrogen concentration and high sample weight/flow rate ratio resulted in a relatively high water vapour pressure causing thermodynamical limitations for a complete reduction of the MoO₃ to Mo.

The reduction of MoO₃/SiO₂ started slowly around 573 K and had a maximum around 773 K (Figure 9.2d). The amount of hydrogen consumed pointed to the reduction reaction Mo⁶⁺ to Mo²⁺. Arnoldy *et al.* [20] reported for 11.7 wt% MoO₃/SiO₂ a hydrogen consumption maximum around 750 K and a second maximum around 920 K. The position of the second maximum was highly dependent on the H₂O vapour pressure and shifted to 1050 K if a H₂O/H₂/Ar mixture was used. They reported that the total hydrogen consumption (first and second peak together) pointed to the complete reduction of MoO₃ to Mo. As already pointed out before, our experimental conditions result in a relatively high H₂O/H₂ ratio, which can explain the differences between the observed TPR profiles in this study and the TPR profiles observed by Arnoldy *et al.* [19,20].

The TPR profiles of calcined Rh/MoO₃/SiO₂ catalysts (Figures 9.2e-f) show that rhodium enhanced the reduction of MoO₃. Almost all hydrogen consumption took place below 573 K and the amount of hydrogen consumed in this temperature region pointed to the reduction of Rh₂O₃ (Rh³⁺ to Rh⁰) and MoO₃ (Mo⁶⁺ to Mo²⁺). Only for catalysts with high Mo/Rh ratios hydrogen consumption was seen above 573 K. On the other hand, MoO₃ slightly hampered the reduction of Rh₂O₃. A shift to higher reduction temperatures was observed for the main TPR peak when the Mo/Rh ratio was increased and also the start of the reduction occurred at a higher temperature. These effects were more pronounced for the oxidized catalysts (Figures 9.2g-i), different peaks could even be observed. Higher Mo/Rh ratios caused a decrease of the amount of hydrogen consumed before the temperature

ramp, and of the peak around 323 K, and an increase of the hydrogen consumption peak between 373 and 473 K. From the TPR profiles it can be concluded that Rh facilitated the reduction of MoO₃ and that MoO₃ hampered the reduction of Rh₂O₃.

Thus, the TPR profiles of calcined and oxidized Rh/MoO₃/SiO₂ clearly provide evidence for a mutual affection of the active metal (Rh) and the promoter (MoO₃).

9.3.2 Hydrogen and carbon monoxide chemisorption

In Figure 9.3 the hydrogen and carbon monoxide chemisorption measurements for the ThO₂- and MoO₃-promoted catalysts are presented. For the Rh/MoO₃/SiO₂ catalysts, reduced and evacuated at 573 K, a suppression of the H/Rh and CO/Rh ratios by the presence of MoO₃ was observed (Figures 9.3a2 and 9.3b2, respectively). Reduction and evacuation at 723 K resulted in an even higher suppression of the chemisorption capacity (Figures 9.3a3 and 9.3b3, respectively). At high Mo/Rh ratios (Mo/Rh=4.0) a slight increase of the H/Rh and CO/Rh ratios was observed.

The 1.5 wt% Rh/ThO₂/SiO₂ catalysts did not exhibit any suppression of the chemisorption capacity, their H/Rh and CO/Rh values did not vary with increasing Th/Rh ratio (Figures 9.3a1 and 9.3b1).

The chemisorption capacity of the 1.5 wt% Rh/ThO₂ catalyst was low. H/Rh was equal to 0.19 and CO/Rh was equal to 0.18. This was also concluded from the TPR profile after TPO, where the presence of a reduction peak at 410 K pointed to the presence of large spherical particles [17].

For the 1.5 wt% Rh/MoO₃ catalyst, very high H/Rh and CO/Rh values were observed, pointing to an anomalous effect. After reduction and evacuation at 723 K, the H/Rh and the CO/Rh ratios were 2.2 and 5.2, respectively.

9.3.3 Transmission electron microscopy

The decrease of the chemisorption capacity for the Rh/MoO₃/SiO₂ catalysts can be caused by an increased metal particle size, or by a more direct influence of the promoter on the chemisorption capacity of the rhodium metal particles due to a covering and/or electronic effect. To exclude the first explanation TEM measurements were performed. The addition of the MoO₃ promoter did not significantly change the rhodium particle size: D(Rh/SiO₂) = 20 Å and D(Rh/MoO₃/SiO₂) = 21 Å (Mo/Rh = 1.0). MoO₃ particles were not seen by TEM, because molybdenum oxide is not a well defined oxide

under TEM conditions. For the Rh/ThO₂/SiO₂ catalyst (Th/Rh = 1.0) particles with a diameter of around 30 Å were observed. However, the characteristic spacings of Rh metal (2.1 and 2.6 Å), present in the particles of Rh/SiO₂ and Rh/Mo/SiO₂, were not observed in any of the particles of the Rh/ThO₂/SiO₂ catalysts. On the contrary, spacings of about 3.1 Å were seen which originate from ThO₂ particles.

Thus, the suppression of the chemisorption capacity for the MoO₃-promoted rhodium catalysts is not due to a decreased metal particle size.

9.3.4 Infrared spectroscopy of adsorbed CO

Chemisorption of CO at 298 K was also studied by infrared spectroscopy, in order to determine the binding sites for CO and to measure the CO adsorption capacity of the exposed rhodium. In a recent study, we already showed that vanadium oxide had a remarkable influence on the infrared spectrum of adsorbed CO. The addition of vanadium oxide only suppressed the linearly bonded and bridge-bonded CO, while the amount of CO present in the gem-dicarbonyl form remained about constant [1].

In Figure 9.4 the IR spectra of CO adsorbed on Rh/SiO₂ catalysts, promoted with a varying amount of molybdenum oxide and thorium oxide, are presented. The infrared spectrum of CO adsorbed on Rh/SiO₂ was dramatically influenced by the presence of molybdenum oxide. With increasing molybdenum oxide content, the amount of linearly bonded and bridge-bonded CO, as well as the number of gem-dicarbonyl species strongly decreased and almost disappeared for Mo/Rh = 4.0. For the catalysts with Mo/Rh > 1.0, an additional peak around 1890 cm⁻¹ is observed. The intensity of this peak decreased less than the intensity of the other peaks. In order to compare the amounts of adsorbed CO for the systems with different Mo/Rh ratios, the absorbance spectra were integrated as described before [1], resulting in an integrated absorption value (A-value) for every Mo/Rh ratio. These A-values were normalized to the A-value of the Rh/SiO₂ catalyst (Mo/Rh = 0). The relative A-values for the MoO₃-promoted catalysts are presented in Figure 9.5, together with the relative CO/Rh values (compared with Rh/SiO₂) obtained by CO chemisorption. Of course, the A-values can not be used to calculate the CO/Rh values because of differences in absorption coefficients for the different adsorption forms of carbon monoxide, as reported by Duncan et al. [21]. However, from the trends observed in Figure 9.5, one can conclude that the CO adsorption sites on rhodium measured by IR are suppressed completely, whereas CO chemisorption showed that for

absorbance

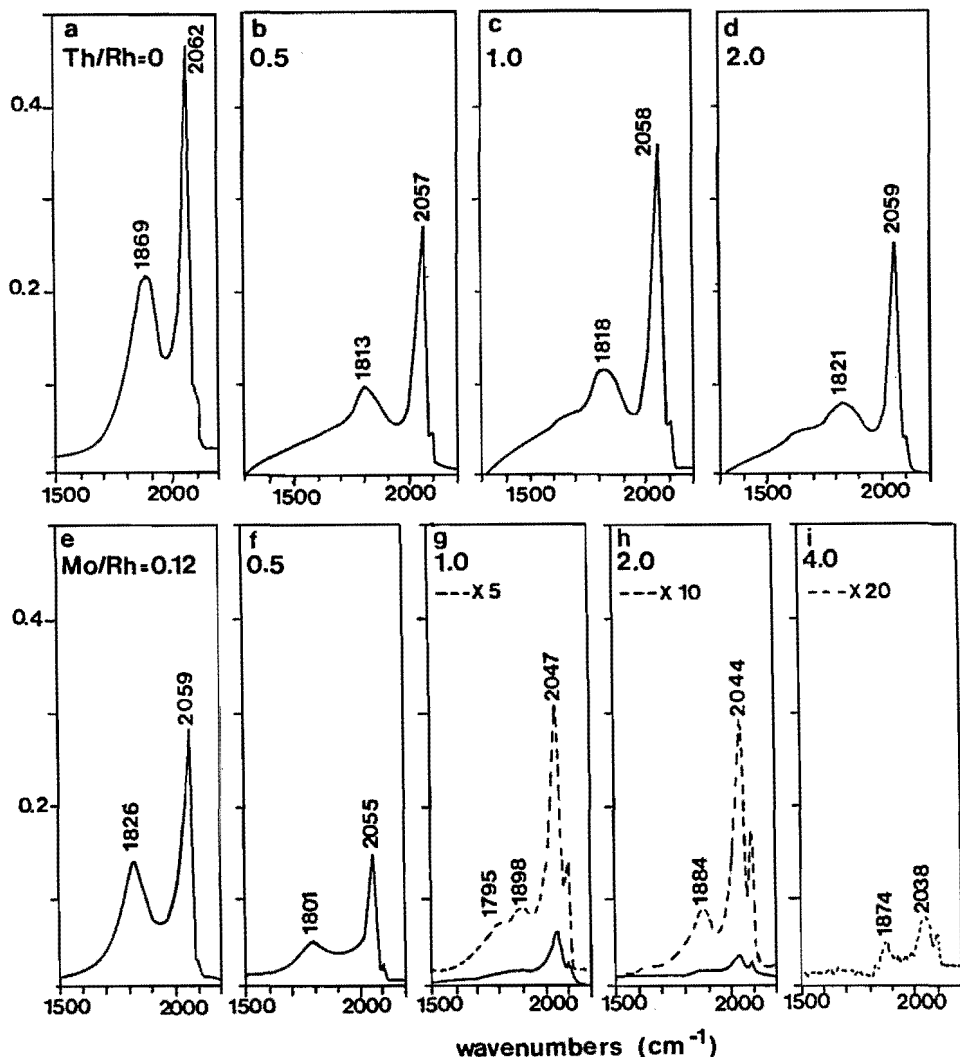


FIGURE 9.4: Infrared spectra of CO adsorbed at 298 K ($P_{\text{CO}} = 10$ Torr, reduction and evacuation temperature 523 K) for 1.5 wt% Rh/SiO₂ catalysts.

a. Rh/SiO₂ b-d. Rh/ThO₂/SiO₂ g-i. Rh/MoO₃/SiO₂.

Mo/Rh ratios > 1.0 , there still is a small chemisorption of carbon monoxide. We think that this CO is adsorbed on the molybdenum oxide promoter. However, this kind of adsorbed CO should also have been seen by IR spectroscopy. This difference between the IR results and the chemisorption results will be a result of differences in CO pressure. During chemisorption measurements, the CO pressure was in the 100–600 Torr range, whereas

during IR measurements, 10 Torr of CO was introduced into the cell and subsequently, the cell was evacuated to 10^{-3} Torr, in order to remove gas phase CO. This evacuation was harder for catalysts with a high Mo/Rh ratio, suggesting that additional CO was weakly adsorbed on the molybdenum oxide promoter.

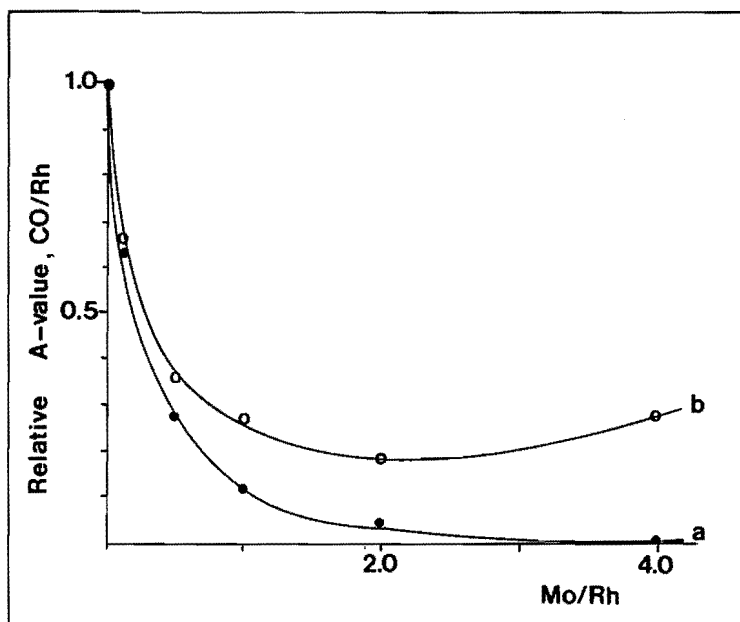


FIGURE 9.5: Relative integrated areas of infrared absorbance spectra of the MoO_3 -promoted Rh/SiO_2 catalysts relative to the unpromoted Rh/SiO_2 catalyst using the integrated infrared spectra of Figure 9.4 (a) and relative CO/Rh ratios from CO chemisorption measurements (b).

The position of the gem-dicarbonyl species was unaffected by the presence of MoO. The position of the linearly bonded CO shifted to lower wavenumbers with increasing MoO_3 content ($\Delta\sigma_L = 20 \text{ cm}^{-1}$). The shift of the bridge-bonded CO to lower wavenumbers with increasing MoO_3 content was around 70 cm^{-1} . No bands at lower wavenumbers ($< 1800 \text{ cm}^{-1}$) were observed. The shifts of the linearly bonded and bridge-bonded CO were comparable with the shifts found when changing the amount of CO adsorbed on Rh/SiO_2 ($\Delta\sigma_L = 25 \text{ cm}^{-1}$ and $\Delta\sigma_B = 59 \text{ cm}^{-1}$) [1].

The influence of ThO_2 on the IR spectrum of adsorbed CO is shown in Figures 9.4b-d. The amount of linearly adsorbed CO for the catalyst with $\text{Th}/\text{Rh} = 0.5$ was slightly lower than that for the unpromoted catalyst.

Further addition of ThO₂ did not result in a further decrease of the amount of linearly adsorbed CO and also the position of this band was not influenced by ThO₂ promotion. The amount of bridge-bonded CO was considerably lower for the ThO₂-promoted catalysts than for the unpromoted catalyst and decreased with increasing Th/Rh ratio. The position of the bridge-bonded CO band for the ThO₂-promoted catalysts was shifted to lower wavenumbers by the presence of ThO₂ compared with the unpromoted catalyst ($\Delta\sigma_B = 51 \text{ cm}^{-1}$). For the ThO₂-promoted catalysts, also a band around 1650-1700 cm^{-1} was observed and between 1300 and 1650 cm^{-1} still absorption was seen. The integrated areas of the ThO₂-promoted catalysts amounted to about 75 % of the integrated area of the Rh/SiO₂ catalyst and did not decrease with increasing Th/Rh ratio. This is in contrast with the chemisorption measurements which showed that the CO/Rh value was not influenced by the addition of ThO₂. However, the CO causing the broad low-frequency absorption bands will have a relatively low extinction coefficient (see Discussion) and therefore will result in an underestimation of the amount of adsorbed CO.

9.3.5 Hydrogenation of CO

ThO₂ and MoO₃ promotion. In Table 9.1 and 9.2 the results of the CO + H₂ reaction over ThO₂-promoted and MoO₃-promoted catalysts are presented, respectively. The results are given after 15 h time on stream, when a constant small decrease of the activity is reached. The selectivity patterns were constant at that time. The catalysts were compared at a similar conversion level in order to obtain differential reaction conditions (conversion < 5%) and to obtain accurate measurement of the different products by GC (conversion > 1%). Therefore the reaction temperature was adjusted. The other reaction conditions, H₂/CO, P and GHSV were held constant. In order to compare activities at the same temperature (523 K), the measured activities were corrected for temperature differences using an activation energy of 100 kJ mol^{-1} , as was measured for Rh/ThO₂/SiO₂ at Th/Rh = 1.0. Of course, the different systems have different activation energies, and therefore the calculated activities are only an estimate of the activity at that temperature.

The 1.5 wt% Rh/ThO₂ catalyst had a moderate activity and a reasonably high C₂-oxygenate selectivity (41 %). Compared with 1.5 wt% Rh/SiO₂, the activity of the ThO₂-supported catalyst was 5 times larger. The ThO₂-promoted silica-supported catalysts had high selectivities to C₂-oxygenates

TABLE 9.1: Results of H₂-CO reaction after 15 h time on stream for ThO₂-promoted 1.5wt% catalyst reduced *in situ* at 723 K. Experimental conditions: GHSV = 4000 l l⁻¹ h⁻¹, H₂/CO = 3.0.

	Rh/ThO ₂	Rh/ThO ₂ /SiO ₂							
Th/Rh ^a	---	0	0.12	0.5	1.0	2.0	4.0	0	1.0
P (MPa)	4.0	4.0	4.0	4.0	4.0	4.0	4.0	0.15	0.15
T (K)	535	600	535	528	528	508	507	591	528
activity ^b	1.2	2.8	2.3	3.9	5.7	2.0	2.4	1.8	6.1
corr. act. ^c	0.7	.14	1.4	3.1	4.6	4.0	5.0	0.1	4.9
sel. (%C) ^d									
CH ₄	35.6	33.2	25.5	30.8	32.3	24.5	26.4	85.4	53.8
C ₂ + ^e	7.3	2.3	2.1	4.5	5.8	5.4	5.8	13.5	23.9
C ₁ OH ^f	11.6	29.1	14.3	11.0	7.7	16.2	16.9	0.5	0.7
C ₂ OH ^g	16.7	20.5	31.3	30.6	30.7	30.0	30.4	0.2	16.9
C ₂ =O ^h	12.8	4.3	7.1	5.4	6.5	4.0	2.8	0.4	4.1
C ₂ OOH ⁱ	11.5	10.2	18.4	15.6	14.6	17.0	14.8	0.0	0.5
C ₃ O+ ^j	4.6	0.6	1.3	2.1	2.4	3.0	3.0	0.0	0.2
C ₂ oxy ^k	41.0	35.0	56.8	51.6	51.8	51.0	48.0	0.6	21.5
oxo. sel. ^l	57.2	64.5	72.4	64.7	61.9	70.1	67.9	1.1	22.3
Deact. ^m	3.8	0.9	1.7	2.1	2.4	1.7	1.4	n.m.	n.m.

a) Th/Rh, atomic ratio, b) activity in mmol converted CO (mol Rh)⁻¹ s⁻¹, c) calculated activity at 523 K using E_{act} = 100 kJ mol⁻¹, d) selectivities expressed as %C efficiency, e) hydrocarbons containing two or more C atoms, f) total amount of methanol, ethers and esters included, g) total amount of ethanol, ethers and esters included, h) acetaldehyde, i) acetic acid, esters included, j) oxygenated products containing three or more C atoms, k) C₂-oxygenate selectivity, l) total oxo-selectivity, m) deactivation in % h⁻¹.

(48-57 %), more than half of it being ethanol. ThO₂ also had a remarkable effect on the activity of the Rh/SiO₂ catalysts. The activity sharply increased with increasing Th/Rh ratio up to Th/Rh = 0.5. Further addition of ThO₂ only resulted in a slight increase of the activity. The activity of the Rh/SiO₂ catalyst was increased 36 times for the catalyst with Th/Rh = 4.0, which is similar to the increase in activity observed for V₂O₃ promotion [2]. The methanol selectivity is rather low (7-17 %). The deactivation for the

TABLE 9.2: Results of H₂-CO reaction after 15 h time on stream for MoO₃-promoted 1.5wt% catalyst reduced *in situ* at 723 K. Experimental conditions: GHSV = 4000 l l⁻¹ h⁻¹, H₂/CO = 3.0. For notations see Table 9.1.

	Rh/MoO ₃	Rh/MoO ₃ /SiO ₂							
Mo/Rh ^a	----	0	0.12	0.5	1.0	2.0	4.0	0	1.0
P(MPa)	4.0	4.0	4.0	4.0	4.0	4.0	4.0	.15	.15
T (K)	508	600	544	508	508	508	500	591	503
activity	2.8	2.8	2.9	7.9	9.9	7.7	4.7	1.8	1.7
corr. act.	5.6	.14	1.1	15.7	19.7	15.3	13.6	.13	2.5
sel. (%C)									
CH ₄	52.2	33.2	17.2	12.4	14.1	16.5	19.4	85.4	30.5
C ₂ ⁺	31.0	2.3	4.5	8.1	11.0	12.3	18.4	13.5	25.4
C ₁ OH	13.3	29.1	38.0	51.7	53.1	52.3	43.6	0.5	27.3
C ₂ OH	1.6	20.5	25.8	18.0	13.8	12.4	12.3	0.2	12.7
C ₂ =O	0.0	4.3	0.0	0.0	0.0	0.0	0.0	0.4	0.0
C ₂ OOH	0.5	10.2	10.5	1.5	0.9	0.3	0.4	0.0	0.2
C ₃ O ⁺	1.4	0.6	4.0	8.4	7.1	6.2	6.0	0.0	3.9
C ₂ oxy	2.1	35.0	36.3	19.5	14.7	12.7	12.7	0.6	12.9
oxo. sel.	16.8	64.5	78.3	79.6	74.9	71.2	62.3	1.1	44.1
Deact.	1.2	0.9	1.1	1.1	0.9	<0.5	<0.5	n.m.	1.0

a) Mo/Rh atomic ratio

ThO₂-promoted catalysts was lower than for the Rh/ThO₂ catalyst (2% h⁻¹ versus 4% h⁻¹).

CO hydrogenation at 0.15 MPa for 1.5 wt% Rh/SiO₂ and 1.5 wt% Rh/ThO₂/SiO₂ (Th/Rh = 1.0) shows that the promotive effect of thorium oxide was also present at low pressure, the activity of the promoted catalyst was 38 times larger than that of the unpromoted catalyst. In the low pressure experiments the methane selectivity was high and the methanol selectivity was low. However, also the C₂-oxygenate selectivity was considerably lower than in the high pressure case (21.5 versus 51.8 %). This is different from V₂O₃ promotion, where high C₂-oxygenate selectivities were also measured in the low pressure experiment.

The 1.5 wt% Rh/MoO₃ catalyst had a low C₂-oxygenate (2%) and methanol (13%) selectivity (see Table 9.2). The catalyst showed a substan-

tial activity and a moderate deactivation. These results were comparable with the results of Jackson *et al.* [8].

From the TPR experiments we concluded that after reduction at 898 K, Mo was in the 2+ state. However, we do not have information about the valency of the Mo under reaction conditions. Nevertheless we will use the following notation for the SiO₂-supported molybdenum oxide-promoted systems: Rh/MoO/SiO₂.

Promotion of 1.5 wt% Rh/SiO₂ by molybdenum oxide considerably increased the activity, even more than promotion by thorium and vanadium oxide. A maximum increase in activity was observed for a Mo/Rh ratio of 1.0. Compared with the unpromoted 1.5 wt% Rh/SiO₂, the activity of the Rh/MoO/SiO₂ (Mo/Rh = 1.0) catalyst was increased by a factor of 141. For Mo/Rh ratios > 1.0 the activity decreased with increasing Mo/Rh ratio. The molybdenum oxide-promoted catalysts had a high methanol selectivity (around 50%) and a relatively low C₂-oxygenate selectivity (12-20 %). Total oxo-selectivity was high (60-80 %), and deactivation was low (around 1% h⁻¹).

The effect of molybdenum oxide promotion was less effective in the low pressure experiment (0.15 MPa). The activity of the promoted catalyst (Mo/Rh = 1.0) was 19 times larger than the activity of the unpromoted catalyst. Total oxo-selectivity was lower than in the high pressure case (44 versus 75 %), mainly due to a decreased methanol selectivity.

For the molybdenum oxide-promoted catalysts a lower deactivation was observed than for the ThO₂-promoted catalysts (1.0 and 2.0 % h⁻¹, respectively). The decrease of the methanol formation rate was lower (< 0.5 % h⁻¹) than the decrease of the formation rate of the other products (2-3 % h⁻¹) for both catalysts. The low overall deactivation of the molybdenum oxide-promoted catalysts is therefore a result of the high selectivity to methanol. The different deactivation behaviour for methanol compared with the other products, suggests that methanol is formed on other sites than the other products. This suggestion has been made before by Poels *et al.* [22,23] and Hindermann *et al.* [24]. They proposed that methanol is formed over metal ions, while the other products are formed over well-reduced metal particles.

From Table 9.1 and 9.2 it can be concluded that the addition of molybdenum oxide and thorium oxide to a 1.5 wt% Rh/SiO₂ catalyst resulted in an increased activity. Thorium oxide resulted in a high C₂-oxygenate selectivity, while molybdenum oxide led to a high methanol selectivity. However, different reaction temperatures were used to test the several catalyst sys-

TABLE 9.3: H₂-CO reaction over Rh/SiO₂ and Rh/Promoter/SiO₂ (Promoter = ThO₂, MoO and V₂O₃, Promoter/Rh = 1.0) catalysts at 548 K, H₂/CO = 3.0 and P = 4.0 MPa. GHSV for Rh/SiO₂ 660, for Rh/ThO₂/SiO₂ 8000, for Rh/MoO/SiO₂ 64000 and for Rh/V₂O₃/SiO₂ 16000 l l⁻¹ h⁻¹. For definitions see Table 1.

	Selectivity (%C)				Activity ^a				Factor of increase ^b		
	Unp.	Mo	Th	V	Unp.	Mo	Th	V	Mo	Th	V
CH ₄	11.6	15.4	42.8	29.1	0.051	11.5	5.91	5.22	225	116	102
C ₂ ⁺	1.4	8.6	3.3	14.0	0.006	6.4	0.46	2.52	1067	77	426
C ₁ OH	57.2	57.7	4.1	9.5	0.252	43.2	0.57	1.71	171	3	7
C ₂ OH	13.7	13.3	25.0	23.9	0.060	10.0	3.45	4.30	167	58	72
C ₂ =O	0.0	0.0	11.1	9.7	0.000	0.0	1.53	1.75	0	∞	∞
C ₂ OOH	14.7	0.7	11.4	8.8	0.065	0.5	1.57	1.58	8	24	24
C ₃ O ⁺	1.4	4.3	2.0	5.0	0.006	3.2	0.28	0.90	537	47	150
C ₂ oxy	28.4	14.0	47.5	42.4	0.125	10.5	6.56	7.63	84	52	61
tot oxo	87.0	76.0	53.6	56.9	0.383	56.9	7.40	10.24	149	19	27
Tot act					0.440	74.9	13.8	17.98	170	31	41
CO dis ^c					0.126	26.4	10.0	12.46	210	79	99

a) Formation rate of several product groups expressed as mmol CO converted (mol Rh)⁻¹ s⁻¹.

b) Effect of promoter on formation rates of several product groups related to the unpromoted catalyst.

c) CO dissociation rate is total activity minus formation rate of methanol minus half of formation rate of C₂-oxygenates.

tems and this may have influenced the selectivity patterns. Therefore, we tested the unpromoted 1.5 wt% Rh/SiO₂ and promoted 1.5 wt% Rh/promoter/SiO₂ catalysts, (promoter = ThO₂, MoO₃ and V₂O₃, promoter/Rh = 1.0) at the same temperature, i.e. 548 K. The GHSV was adjusted in such a way that the conversion level was around 2%. The results of these measurements are presented in Table 9.3. The selectivity pattern is greatly influenced by the promoter used. The molybdenum oxide-promoted catalysts had a high methanol selectivity, while thorium oxide and vanadium oxide resulted in a high C₂-oxygenate selectivity. (The results of the V₂O₃-promoted catalysts differ slightly from the results reported in [2] due to a different Rh(NO₃)₃ batch). Furthermore, one can see that longer chain

products like C_2+ and C_3O^+ are favoured by the presence of vanadium oxide.

These observations might lead us to the conclusion that molybdenum oxide promotes the formation of methanol, and thorium oxide and vanadium oxide promote the formation of C_2 -oxygenates. However, it is better to compare formation rates for the different product groups. In Table 9.3 these formation rates of several product groups and the influence of the promoter oxides on these formation rates, expressed as a factor of increase of the formation rates to the several products groups relative to the unpromoted catalyst, are presented. From these factors of increase (F) a clear picture of the role of the promoter emerges. The formation rate of methanol is mostly enhanced by the molybdenum oxide promoter ($F_{Mo}:F_{Th}:F_V = 171:3:7$). The formation rate of methane is increased by ThO_2 and V_2O_3 by a factor of about 100 and for MoO promotion by a factor of 225. The formation rate of C_2 -oxygenates is increased by roughly the same factor for all three promoters ($F_{Mo}:F_{Th}:F_V = 84:52:61$). The lower selectivity to C_2 -oxygenates for the molybdenum oxide-promoted catalysts therefore does not originate from a low formation rate of C_2 -oxygenates, but from a high methanol formation rate. Because methanol is most probably formed by a completely different mechanism as the rest of the products (hydrogenation of associatively adsorbed CO versus hydrogenation of dissociatively adsorbed CO [25]), the factor of increase of the formation rate of all products except methanol was also calculated. The effect of V_2O_3 and ThO_2 on this combined product group was approximately the same, $F_{Th} = 70$ and $F_V = 87$. MoO promotion resulted in a higher increase factor ($F_{Mo} = 169$). The increase factor for the longer chain products (C_2+ and C_3O^+) decreased in the order $F_{Mo} > F_{Th} > F_V$.

Ethylene addition. As shown by Chuang *et al.* [26], Jordan and Bell [27], Ichikawa *et al.* [28], Van den Berg *et al.* [29] and Pijolat and Perrichon [30] ethylene addition to a working catalyst is a very powerful method to study the mechanism of CO hydrogenation. Possible reactions of ethylene are the formation of methane, hydrogenation to ethane, chain-growth reaction forming propane and propylene and the CO insertion reaction forming propanol and propionaldehyde. The latter reaction is thought to be responsible for the formation of C_2+ -oxygenates [26-30]. In this study we examined the influence of the promoter on these specific reaction steps in order to investigate the role of the promoter in the CO hydrogenation.

Since addition of a gas is not easy in a high pressure experiment and the

TABLE 9.4: The effect of ethylene addition to H₂ + CO reaction over Rh/SiO₂ and promoted Rh/Promoter/SiO₂ (Promoter = MoO, ThO₂, or V₂O₃, Promoter/Rh = 1.0) catalysts. Reaction conditions: P = 0.15 MPa, H₂/CO = 3.0 and GHSV = 4000 l l⁻¹ h⁻¹. All data are expressed in 10⁻² vol% compound.

Promoter	T (K)	added C ₂ H ₄ (10 ⁻² vol%)	CH ₄	C ₂ H ₄	C ₂ H ₆	C ₃ H ₆₋₈	C ₃ OH	C ₃ =O
---	503	---	0.16	0.01	0.01	0.01	0.00	0.00
---	503	27	0.16	13.6	11.6	0.01	0.83	1.16
---	593	---	19.6	0.0	0.53	0.39	0.00	0.00
---	593	24	18.8	0.0	24.4	0.42	0.00	0.00
---	593	83	19.2	0.0	83.1	0.55	0.00	0.00
MoO	503	---	7.84	0.36	1.52	0.64	0.16	0.06
MoO	503	33	6.84	1.42	29.8	2.35	1.91	0.14
MoO	503	78	6.16	4.14	67.2	3.93	5.22	0.31
MoO	528	---	26.8	0.66	6.23	2.15	0.12	0.14
MoO	528	35	25.4	0.00	39.9	4.27	0.19	0.14
ThO ₂	503	---	9.72	0.29	0.30	0.64	0.02	0.00
ThO ₂	503	25	8.64	8.6	16.3	0.66	1.03	0.23
ThO ₂	503	66	7.56	20.2	42.8	0.76	2.60	0.53
ThO ₂	503	---	8.55	0.29	0.32	0.54	0.15	0.02
ThO ₂	528	---	48.7	0.52	2.39	2.90	0.17	0.05
ThO ₂	528	29	45.4	1.35	29.5	2.96	0.82	0.16
V ₂ O ₃	503	---	8.06	1.15	0.71	1.56	0.15	0.06
V ₂ O ₃	503	30	7.34	15.8	16.4	1.45	1.21	0.43
V ₂ O ₃	503	---	7.03	1.10	0.49	1.33	0.16	0.05
V ₂ O ₃	503	95	6.51	76.2	13.7	1.34	3.16	1.02
V ₂ O ₃	503	---	6.09	0.95	0.37	1.10	0.17	0.04

promoter effect was also present in the reaction at low pressure, we studied ethylene addition at 0.15 MPa. Ethylene was added after prolonged reaction (15 h time on stream). The results for Rh/SiO₂ and Rh/promoter/SiO₂, promoter/Rh = 1.0 (promoter = MoO, ThO₂ and V₂O₃) are presented in Table 9.4.

In order to compare the results of ethylene addition for the different catalysts at identical conditions, we calculated the vol% of the several pro-

ducts formed after addition of 0.30 vol% ethylene at 503 K, assuming first order kinetics in ethylene. The amount of ethylene hydrogenated to ethane increased in the order unpromoted < V_2O_3 < ThO_2 < MoO (0.13 : 0.16 : 0.20 : 0.27). The amount of CO inserted into added ethylene forming C_3 -oxygenates increased in the order V_2O_3 , ThO_2 , MoO < unpromoted (0.014 : 0.015 : 0.017 : 0.022). The chain-growth for the unpromoted and V_2O_3 -promoted catalysts was negligible, while ThO_2 exhibited a small incorporation of ethylene and MoO considerably enhanced the incorporation of ethylene.

These results prove that CO insertion is not increased by the presence of the promoter oxide. A higher temperature disfavoured the CO insertion reaction. Furthermore, the hydrogenation reaction of ethylene is not the rate limiting step in the CO hydrogenation, because part of the added ethylene is hydrogenated without a significant decrease of the CO hydrogenation reaction rate. The hydrogenation rate is higher for the MoO - and ThO_2 -promoted catalysts than for the V_2O_3 -promoted and unpromoted catalysts. Incorporation of ethylene into a growing chain, resulting in an increased amount of C_3 -hydrocarbons, is present for Rh/SiO_2 tested at 593 K, for MoO -promoted catalysts tested at 503 K and only in a modest way for ThO_2 . The ethylene incorporation reaction was absent for the V_2O_3 -promoted catalyst and for Rh/SiO_2 tested at 503 K.

9.4 DISCUSSION

9.4.1 Temperature programmed reduction

Temperature programmed reduction studies of the $Rh/MoO_3/SiO_2$ catalysts after calcination at 723 K showed that there is an intimate contact between the MoO_3 promoter and Rh_2O_3 . The reductions of Rh_2O_3 and MoO_3 can not be distinguished in the TPR profile. The reduction of MoO_3 is facilitated by the presence of Rh metal, the reduction of MoO_3 shifts to a lower temperature, and the reduction of Rh_2O_3 is hampered by the presence of MoO_3 , the reduction peak of Rh_2O_3 shifts to a higher temperature. This effect is more pronounced in the TPR profiles of the samples oxidized at 898 K. The easier reduction of the MoO_3 points to an intimate contact between Rh_2O_3 and MoO_3 , but can also be explained by assuming hydrogen spillover. Once Rh_2O_3 is reduced to Rh metal, hydrogen molecules can dissociate on the Rh metal and the H atoms formed can spillover and reduce the MoO_3 , resulting in a lower reduction temperature of MoO_3 . However, the

hampered reduction of Rh₂O₃ proves that there must be an intimate contact between Rh₂O₃ and MoO₃ in the Rh/MoO₃/SiO₂ catalysts after calcination at 723 K and oxidation at 898 K.

The hampered reduction of Rh₂O₃ can be understood by assuming that a mixed oxide of Rh₂O₃ and MoO₃ is formed, or that the Rh₂O₃ particles are completely covered with a layer of MoO₃, preventing the H₂ molecules from reaching the Rh₂O₃ at a low temperature. A mixed oxide of Rh₂O₃ and MoO₃, Rh₂MoO₆, is known to exist and can be formed by heating RhCl₃ and MoO₃ in a molar ratio of 2:1 in air for 60 h at 773 K and for 48 h at 923 K [12,13]. This temperature is higher than the calcination temperature used for the Rh/MoO₃/SiO₂ catalysts, but surface reactions are known to proceed at lower temperatures than bulk reactions. This also clarifies the difference between the TPR profiles after calcination at 723 K and after oxidation at 898 K. The latter profiles show distinct reduction peaks which may be due to better defined distinct phases, "free" Rh₂O₃ and Rh₂MoO₆.

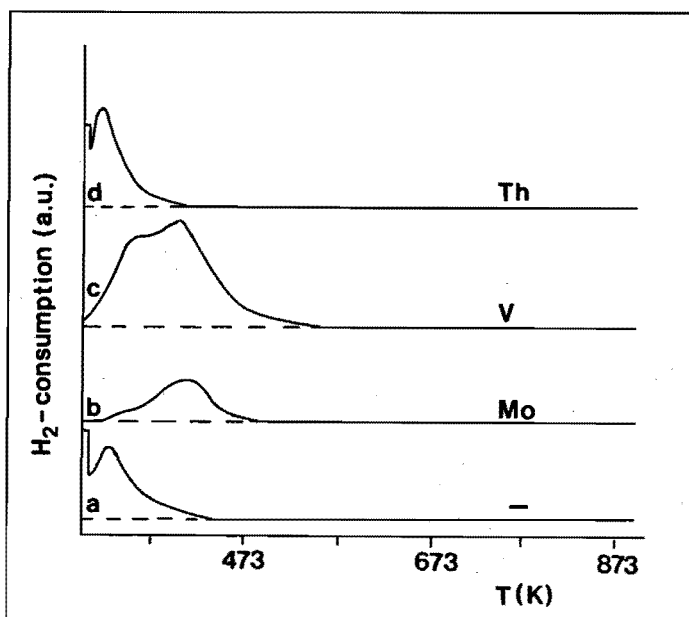


FIGURE 9.6: Temperature programmed reduction profiles after oxidation at 898 K.

a. 1.5 wt% Rh/SiO₂

b. 1.5 wt% Rh/MoO₃/SiO₂, Mo/Rh=0.5

c. 1.5 wt% Rh/V₂O₅/SiO₂, V/Rh=0.5

d. 1.5 wt% Rh/ThO₂/SiO₂, Th/Rh=0.5

Similar influences of the promoter oxide on the reduction behaviour of Rh₂O₃ were observed for V₂O₅-promoted Rh/SiO₂ catalysts [1]. In Figure

9.6 the influences of V_2O_5 and MoO_3 on the TPR profile of Rh/SiO_2 after oxidation at 898 K are compared. For promoter/ $Rh = 0.5$ the amount of "free" Rh_2O_3 , reducing below 373 K, almost completely vanished in the MoO_3 -promoted catalysts (Figure 9.6b), while this amount was only decreased by a factor of 2 for the V_2O_5 promoted catalyst (Figure 9.6c). This supports the assumption of the formation of mixed oxides, because for MoO_3 a mixed oxide with $Rh:Mo = 2$ is most stable (Rh_2MoO_6), while for V_2O_5 a mixed oxide with $Rh:V = 1$ is most stable ($RhVO_4$). The same amount of promoter thus decreases the amount of "free" Rh_2O_3 twice as much for MoO_3 promotion, than for V_2O_5 promotion. However, this phenomenon does not completely exclude the possibility of covering of the Rh_2O_3 by MoO_3 and V_2O_5 . MoO_3 may spread better over Rh_2O_3 and may form a more complete layer of oxide and thus may shield Rh_2O_3 better at a lower promoter/ Rh ratio. However, for V_2O_5 -promoted systems, diffuse-reflectance infrared spectroscopy showed that the $V=O$ stretching band which was present in the V_2O_5/SiO_2 system, was not present in the $Rh/V_2O_5/SiO_2$ ($V/Rh = 0.9$) catalyst after calcination, indicating that no "free" V_2O_5 was present. This proves that Rh_2O_3 and V_2O_5 are not present in a "free" form and therefore must have formed a compound. By analogy, we assume that this is also the case for the $Rh/MoO_3/SiO_2$ catalysts.

For Mo/Rh ratios > 1.0 , hydrogen consumption is also observed at temperatures between 573 and 873 K, i.e. the temperature region where reduction was found for MoO_3/SiO_2 . Thus for this system, part of the MoO_3 is not in intimate contact with Rh_2O_3 .

From the TPR profiles of the ThO_2 -promoted catalysts, we can not conclude whether or not there is an intimate contact between the promoter oxide and Rh_2O_3 . ThO_2 did not reduce at all and the reduction profile of Rh_2O_3 after calcination was only slightly influenced by the presence of ThO_2 , due to CO_2 adsorbed on ThO_2 . The TPR profiles of the oxidized samples were not at all influenced by the presence of ThO_2 . In the literature, no information is available about the formation of a mixed oxide of ThO_2 and Rh_2O_3 [13].

9.4.2 H_2 and CO chemisorption

Hydrogen and carbon monoxide chemisorption measurements showed a decrease of H/Rh and CO/Rh for the molybdenum oxide-promoted catalysts with increasing Mo/Rh ratio. For the thorium oxide-promoted catalysts, such a suppression of H_2 and CO chemisorption was not observed.

The decrease of the H/Rh and CO/Rh ratios with increasing promoter/Rh ratio was also seen for vanadium oxide-promoted catalysts and may originate from an increased rhodium metal particle size or from an influence of the promoter oxide on the chemisorption capacity of the rhodium metal (electronic or covering effect). A TEM study showed that the rhodium metal particle size was not influenced by the promoter oxide (MoO and V₂O₃). A similar suppression of chemisorption was observed for noble metals supported on transition metal oxides like TiO₂ and V₂O₃ after reduction at higher temperatures ($T_{\text{red}} > 723$ K) [31–33]. The almost generally accepted explanation for this so-called Strong Metal Support Interaction (SMSI) effect is the covering of the metal particle by suboxides of the support (like Ti₄O₇) formed during the high-temperature reduction [34–41]. However, for the MoO- and V₂O₃-promoted catalysts, the suppression of CO and H₂ chemisorption was already present after reduction at a much lower temperature (523 K). The suppression was more pronounced after reduction at 723 K. We think that also in our case the rhodium metal particles are covered with molybdenum and vanadium oxide, even after a low temperature reduction. Hicks *et al.* [42] reported similar results for La₂O₃-supported Pd catalysts. They observed a suppression of the CO chemisorption after reduction at 573 K (low temperature reduction) and attributed this suppression to patches of partially reduced support material, LaO_x, already transferred to the surface of the Pd crystallites during catalyst preparation.

For Mo/Rh ratios > 1.0 , a slight increase of the H/Rh and CO/Rh ratios with increasing Mo/Rh ratio was observed, pointing to adsorption of H₂ and CO on the molybdenum oxide. In recent studies, Tatsumi *et al.* [43] and Concha *et al.* [44] reported CO hydrogenation over silica-supported molybdenum oxide catalysts at 573 K and 1.6 MPa and at 623 K and 0.14 MPa, respectively. Of course, for this reaction to occur, molybdenum oxide must be able to adsorb both H₂ and CO. Hall *et al.* [45,46] reported that reduced alumina-supported molybdenum oxides chemisorbed CO and H₂. The very high H/Rh and CO/Rh ratios found for 1.5 wt% Rh/MoO₃ also point to the adsorption of both H₂ and CO on MoO_x.

So, for the MoO₃-promoted catalysts, hydrogen and carbon monoxide chemisorption and TEM pointed to a coverage of the rhodium particles by patches of molybdenum oxide, even after low temperature reduction. For the thorium oxide-promoted catalysts, the H₂ and CO chemisorption measurements did not indicate any coverage of the metal particles.

9.4.3 Infrared spectroscopy

The IR spectra of CO adsorbed on Rh/MoO/SiO₂ catalysts prove that MoO completely suppressed the CO chemisorption capacity of rhodium. For Mo/Rh > 1.0, almost no CO adsorbed on Rh in the bridge-bonded, linearly bonded or gem-dicarbonyl form. The CO bonded to the MoO_x is not seen in the IR studies, due to the evacuation after CO admission.

An increasing Mo/Rh ratio resulted in shifts to lower wavenumbers of the bands of the linearly bonded and bridge-bonded CO. We do not think that this is caused by an electronic effect of the promoter on the rhodium metal, but ascribe this effect to the lower CO coverage, resulting in a decrease of the dipole-dipole coupling between CO molecules and consequently a decrease in the CO stretching frequency [47]. This conclusion is supported by the observation that the shifts of the linearly bonded and bridge-bonded CO with increasing CO pressure and thus increasing CO coverage, observed for the unpromoted Rh/SiO₂ catalysts, were similar.

For the ThO₂-promoted catalysts, the amount of linearly adsorbed CO was slightly lower for the promoted catalysts and the corresponding absorption band shifts to slightly lower wavenumber. The amount of bridge-bonded CO decreased with increasing Th/Rh ratio and shifted to lower wavenumbers, which can be a result of a decreased dipole-dipole coupling caused by the decreased CO coverage. Also a broad absorption band between 1300 and 1800 cm⁻¹ and a band maximum around 1680 cm⁻¹ were observed. The origin of this band is ascribed to C and O bonded CO (see the discussion about the CO hydrogenation reaction).

From the IR study we conclude that MoO₃ dramatically suppressed all forms of CO adsorbed on Rh, while ThO₂ mainly influenced the bridge-bonded CO and caused the appearance of a broad absorption band between 1300 and 1800 cm⁻¹.

9.4.4 CO hydrogenation reaction

From the results presented in Table 9.3 we conclude that the total activity of the Rh/SiO₂ catalyst was greatly enhanced by the presence of the promoter oxides used in this and the preceding study: MoO, ThO₂ and V₂O₃. The increase of the total activity was largest for the molybdenum oxide-promoted catalysts. The large increase in activity by the presence of the promoter oxides points to an intimate contact between the promoter oxide and the rhodium metal. For MoO and V₂O₃, H₂ and CO chemisorption measurements and IR spectroscopy pointed to a covering of the rhodium

metal particle by patches of MoO and V₂O₃. During CO hydrogenation, this covering can be removed by water, one of the products of the CO hydrogenation reaction, as has been reported for TiO₂-supported Rh and Pt catalysts [48]. The highest activity was measured for the Mo/Rh = 1.0 catalyst and further addition of MoO caused a decrease in activity. We think that this is due to two counteracting effects. Firstly, the MoO patches block part of the active metal surface and selectively suppress reactions which need a large ensemble. This blocking also results in a suppressed hydrogen and carbon monoxide chemisorption. Secondly, the molybdenum oxide patches enhance the CO hydrogenation reaction at the metal-molybdenum oxide interface, that is at the perimeter of the molybdenum oxide patches on the Rh particle. The latter effect prevails for Mo/Rh < 1 and the first dominates for Mo/Rh > 1. This explanation was also proposed for the V₂O₃ promotion effect [2].

Hydrogen and carbon monoxide chemisorption measurements indicate that within the experimental error of the measurements (5 %), for the Rh/ThO₂/SiO₂ catalysts no covering of the rhodium metal particles by ThO₂ occurred. However, it is still possible that a limited number of ThO₂ molecules is positioned on top of the Rh particles. This would explain the small influence of ThO₂ on the IR spectra of adsorbed CO. Other possible locations for the thorium oxide are the perimeter of the rhodium particle, or the area between the rhodium particle and the SiO₂ support. It is also possible that the major part of the thorium oxide is not in contact with the rhodium metal particle at all. However, TEM studies showed that almost no distinct Rh particles (characteristic spacing of 2.1 and 2.6 Å) were present in the Rh/ThO₂/SiO₂ catalyst, suggesting that the major part of the rhodium particles was in intimate contact with the ThO₂ particles.

In order to further study the position of the ThO₂ promoter, a 0.5 wt% Rh/ThO₂/SiO₂ (Th/Rh = 3.0) catalyst was made. The H/Rh chemisorption value was 0.87 and the CO/Rh value was 0.97. This catalyst contained the same amount of ThO₂ as the 1.5 wt% Rh/ThO₂/SiO₂ catalyst with Th/Rh = 1.5. One can calculate that in this catalyst roughly twice as many Rh atoms should be positioned at the perimeter of the rhodium particles as in the 1.5 wt% Rh/ThO₂/SiO₂ catalysts (H/Rh = 0.64) [14,49]. If ThO₂ is positioned at the perimeter of the rhodium metal particles and if, furthermore, ThO₂ is promoting the CO hydrogenation just at these locations, then the 0.5 wt% Rh/ThO₂/SiO₂ catalyst should have an activity twice as large as the 1.5 wt% Rh/ThO₂/SiO₂ catalyst. This was not the case. Within the experimental error (10 %) the catalysts had the same activity. We therefore conclude

that the ThO_2 -promoted sites are not solely located at the perimeter of the rhodium particles, but must also be positioned on top of the rhodium metal particles.

We conclude that MoO and V_2O_3 are positioned on top of the rhodium metal particles, while only a small part of the ThO_2 -promoter is positioned on top of the rhodium particle.

The promoter oxides not only influenced the activity but also changed the selectivity pattern. As shown in the Results section, the selectivity differences between the catalysts tested mainly were a result of differences in methanol formation rate. Molybdenum oxide greatly enhanced the formation of methanol and therefore exhibited high oxo-selectivities. The increase of the methanol formation rate was only modest for the V_2O_3 - and ThO_2 -promoted catalysts and much lower than the increase of the formation rate of the other products, resulting in a relatively low methanol selectivity. In contrast to the other products of CO hydrogenation, methanol is thought to be formed non-dissociatively [25] over metal ions [22-24]. It is possible that the $\text{Rh}/\text{MoO}/\text{SiO}_2$ catalysts contain more Rh^+ ions, stabilized by the MoO , and in this way increase the methanol formation rate. We do not have any information about the amount of rhodium ions, but it is not likely that the increase of methanol formation by a factor 171 can be ascribed to a higher amount of Rh^+ ions. From TPR we can conclude that the reducibility of $\text{Rh}/\text{V}_2\text{O}_3/\text{SiO}_2$ and $\text{Rh}/\text{MoO}_3/\text{SiO}_2$ is comparable, while the factors of increase of the methanol formation rates were 7 and 171, respectively. The CO chemisorption measurements combined with IR spectroscopy showed that CO can be adsorbed on MoO and not on the other promoter oxides. Considering the results of Poels *et al.* [22-23] and Hindermann *et al.* [24] that methanol is formed over metal ions, we think that the CO adsorbed on $\text{Mo}^{\text{n+}}$ ions is hydrogenated to methanol by H atoms, formed over rhodium metal. Thus, in this case, the catalytic reaction is taking place on the promoter oxide.

Because the CO insertion reaction is thought to be responsible for oxygenate formation [29,50,51], this reaction needs closer attention. The increase of the formation of C_2 -oxygenates due to the addition of the promoter oxides was in all cases lower than the increase of the activity for all other products, except methanol (see Table 9.3, methanol is excluded because it is thought to be formed via another mechanism [25]). This suggests that the addition of promoter oxides does not increase the CO insertion reaction. Ethylene addition to a working catalyst at 0.15 MPa and 503 K clearly supports this suggestion. The increase of C_3 -oxygenates formed by CO

insertion into ethylene, was slightly lower for the promoted catalysts than for the unpromoted catalyst. Assuming first order kinetics in ethylene, the amount of CO inserted into ethylene when 0.30 vol% ethylene was added at 503 K to the synthesis gas mixture ($H_2/CO = 3.0$, $P = 0.15$ MPa), was 0.022, 0.017, 0.015 and 0.014 vol% for the unpromoted, MoO-, ThO₂- and V₂O₃-promoted Rh/SiO₂ catalysts, respectively. It is clear that the addition of the promoter oxides did not enhance the rate of CO insertion.

The formation rate of longer chain products (C_{2+} and C_3O^+) varied for the promoters studied and increased in the order unpromoted < ThO₂ < V₂O₃ << MoO. This points to a higher chain-growth probability for the MoO-promoted catalysts. Ethylene addition experiments pointed to the same conclusion. For the MoO-promoted catalyst, the amount of C₃-hydrocarbons increased, indicating the incorporation of ethylene into a C₁-fragment. For the ThO₂-promoted catalyst only a minor increase of C₃-hydrocarbons was observed, while for the V₂O₃-promoted catalyst no increase of C₃-hydrocarbons was found.

Ethylene addition was also used to study the hydrogenation rate of a working catalyst. Assuming first order kinetics, the amount of ethylene hydrogenated during CO hydrogenation at 503 K (0.30 vol% added ethylene) was found to be 0.13, 0.16, 0.20, and 0.27 vol% for the unpromoted, ThO₂-, V₂O₃- and MoO-promoted catalyst, respectively. Thus, the hydrogenation activity of the promoted catalysts was somewhat higher than that of the unpromoted catalyst. Nevertheless, from the ethylene addition experiments it can be concluded that the hydrogenation is not rate limiting. Although the hydrogenation of ethylene proceeds well over a Rh/SiO₂ catalyst at 503 K, its activity for CO hydrogenation at that temperature was low. The ethylene hydrogenation reaction rates for the promoted catalysts were in the same order of magnitude as that of the unpromoted catalysts, but the CO hydrogenation was enhanced by a factor of 30 to 170. This suggests that CO dissociation, instead of hydrogenation, is the rate limiting step in the hydrogenation of CO and that the main role of the promoter oxide is to enhance this dissociation reaction. Mori *et al.* [4] studied promotion of Ru/Al₂O₃ by oxides of V, Nb, Mo, W and Re using Pulse Surface Reaction Rate Analysis (PSRA). In this technique the rate of CO dissociation and subsequent hydrogenation to CH₄ can be determined separately, be it under non-steady-state conditions. Based on their experiments, they concluded that the role of the promoter is to enhance CO dissociation, while the influence of the promoter oxide on the hydrogenation was small.

Possible reasons for the enhancement of CO bond dissociation by adding a

promoter oxide are: an electronic effect of the promoter oxide on the rhodium particle, or a direct effect of the promoter on the CO bond strength, a participation of the promoter oxide in the dissociation of CO.

In the view of an electronic effect, the addition of the promoter will increase or decrease the electron density on the active metal and in this indirect way change the catalytic behaviour of the active metal. Especially in the case of alkali addition, this effect is invoked by numerous authors [52-58]. Addition of alkali is known to result in an increased electron density on the metal [58-59]. However, in our case, the shifts of the bands in the IR spectra were small and could be explained by the decrease of the dipole-dipole coupling due to a decreased CO coverage. For ThO_2 , the band of the linearly bonded CO did not shift at all. These results suggest that there is not an electronic effect of the promoter oxides on the metal particles.

Mori *et al.* [4,59] proposed a mechanism as shown in Figure 9.7A, in which the promoter oxide plays an active role in the CO dissociation. They postulated an hydroxycarbene (M-CHOH) intermediate for C-O bond dissociation, based on an observed inverse $\text{H}_2\text{-D}_2$ isotope effect for CO dissociation. A CO molecule is adsorbed on the metal, forming the M-CHOH intermediate. A V^{3+} -ion adjacent to the metal atom, to which the hydroxycarbene is attached, pulls the oxygen atom away from the M-CHOH fragment, and forms a transition state that promotes the dissociation of CO to $(\text{CH}_x)_{\text{ad}}$ and $(\text{OH})_{\text{ad}}$. Simultaneously V^{3+} is oxidized to V^{4+} . The $(\text{OH})_{\text{ad}}$ species on V^{4+} can be hydrogenated, forming H_2O and V^{3+} . In this way the vanadium oxide promoter catalyzes the CO dissociation by an oxidation/reduction cycle. A similar cycle is possible for the MoO-promoted catalysts.

For this model, it is necessary that the promoter oxide is positioned on top or at the perimeter of the rhodium metal particle and that a reduction/oxidation cycle is possible. For the ThO_2 -promoted catalysts, temperature programmed reduction studies did not provide any evidence for a reduction/oxidation cycle. Therefore the mechanism proposed by Mori *et al.* can not explain the promoter effect of ThO_2 .

The postulation of a hydroxycarbene fragment contrasts with conclusions drawn by Araki and Ponc [60]. They studied methanation over a Ni film. From ^{13}C measurements they concluded that CO methanation occurs by dissociation of CO via a C_1 -intermediate. Isotopic transient measurements of Biloen *et al.* [61] also suggested that the intermediates in hydrogenation of CO over Co, Ni and Ru catalysts have a carbidic character.

Burch *et al.* [62], Rieck and Bell [63] and Sachtler *et al.* [29,51,64] pro-

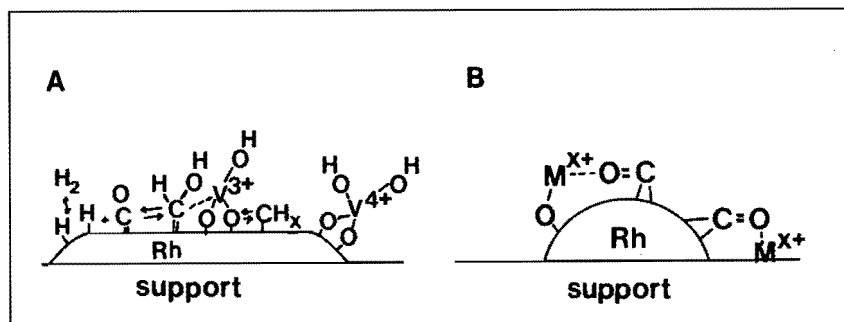


FIGURE 9.7: Model for the promotion mechanism for the C-O bond dissociation in the CO hydrogenation.

A. model according to Mori *et al.* [4] requiring a reduction/oxidation cycle of the promoter,

B. model according to Burch *et al.* [62], Bell *et al.* [63] and Sachtler *et al.* [51,64], in which CO is C bonded to the rhodium metal and O bonded to the promoter ion.

posed a model based on the activation of CO by the interaction of a promoter ion with the oxygen atom of a chemisorbed carbonyl (see Figure 9.7B). The ions of an electro-positive metal (the promoter ion) on the surface of a metal particle might provide sites at which CO may be bonded with its carbon atom to a metal atom and with its oxygen atom to the promoter ion. This results in a weakened C-O bond, which shows up as a lowering of the CO stretching frequency in IR spectroscopy. Frequency decreases in the order of 100 to 300 cm⁻¹ are common for C- and O-bonded carbonyl compounds and must be compared with frequencies at 1950-2130 cm⁻¹ (linearly bonded CO), 1850-1950 cm⁻¹ (bridge-bonded CO) and 1750-1900 cm⁻¹ (C-bridging three metal atoms). Ichikawa *et al.* [50] and Sachtler [29] reported a band around 1530 cm⁻¹ for CO adsorbed on Mn²⁺ promoted Rh catalysts, suggesting that C- and O-bonded carbon monoxide is present. Of course, the V and Mo ions can also pass through the reduction/oxidation cycle in this mechanism. The oxygen atom bonded to V or Mo ions can oxidize these promoter ion after the CO dissociation, and the oxidized promoter ion can be reduced by hydrogen atoms dissociated on the Rh metal. However, such an reduction/oxidation cycle is not necessary.

For the ThO₂-promoted catalysts a broad IR band between 1300 and 1750 cm⁻¹ and a shoulder around 1700 cm⁻¹ were seen, pointing to C- and O-bonded CO. Small amounts of ThO₂ positioned on the rhodium metal

particle will be responsible for this effect since the CO/Rh did not decrease with increasing ThO₂ content. Kiennemann *et al.* [11] reported an absorption band at 1725 cm⁻¹ for CeO₂-promoted Rh/SiO₂ catalysts and assigned it to side-on adsorbed CO.

No bands in the region below 1700 cm⁻¹ were found in the infrared spectra of the MoO- and V₂O₃-promoted catalysts used in this study. This does not fully exclude the model proposed by Sachtler *et al.* for this catalysts. The extinction coefficient for a C- and O- bonded CO molecule will be very small because such a CO molecule is positioned (almost) parallel to the metal surface. As discussed by Pearce and Sheppard [65], the vibrations of a dipole parallel to the metal surface will be annihilated by its mirror image in the surface and therefore will have a very small extinction coefficient. Furthermore, the IR spectra have been measured after admission of only 10 Torr CO at room temperature and therefore we do not have information of the side-on bonded CO under reaction conditions. Thirdly, Erley *et al.* [66] also observed the 1530 cm⁻¹ band for CO on a stepped Ni surface and showed that an increase in temperature to only 310 K resulted in a complete disappearance of the 1530 cm⁻¹ band, indicating the rapid dissociation of this form of adsorbed CO. The temperature in our FTIR apparatus is about 300-310 K and this might explain why we did not observe the side-bonded CO for the MoO- and V₂O₃-promoted catalysts.

9.5 CONCLUSIONS

Temperature programmed reduction studies showed that the molybdenum oxide and vanadium oxide promoters are co-reduced with rhodium oxide. The results suggest the formation of a mixed oxide for these promoter oxides (Rh₂MoO₆, RhVO₄). The TPR profiles of the ThO₂-promoted catalysts show that ThO₂ can not be reduced under the conditions used. No indication has been found for the formation of a mixed rhodium thorium oxide, nor for any interaction between ThO₂ and Rh₂O₃ or Rh.

Hydrogen and carbon monoxide chemisorption measurements indicated the coverage of the rhodium metal particles by patches of V₂O₃ and MoO. At higher promoter/rhodium ratios, H₂ is also adsorbed on V₂O₃ and MoO and CO is only adsorbed on MoO. For ThO₂-promoted catalysts, no indication of a covering of the rhodium metal particle by patches of promoter oxide is found from the chemisorption measurements.

IR spectroscopy measurements showed that V₂O₃ decreased the amount of bridge-bonded and linearly bonded CO, while MoO suppressed all forms of

CO adsorption. ThO₂ mainly decreased the amount of bridge-bonded CO. No indication of C- and O-bonded CO (C to metal and O to promoter ion) was found for the V₂O₃- and MoO-promoted catalysts. IR spectra of the ThO₂-promoted catalysts exhibited bands below 1750 cm⁻¹ pointing to the formation of side-on bonded CO.

All promoter oxides enhanced the CO hydrogenation rate. The methanol formation rate was increased by MoO to a greater extent, probably via an intermediate bonded on Mo-ions. Ethylene addition at 503 K and 0.15 MPa showed that the CO insertion rate into ethylene decreased in the order unpromoted > MoO > ThO₂ > V₂O₃, while hydrogenation decreased in the order MoO > ThO₂ > V₂O₃ > unpromoted. The results suggest that CO dissociation is rate limiting and that the main role of the promoter is to enhance the dissociation of CO.

9.6 REFERENCES

1. B.J. Kip, P.A.T. Smeets, J.H.M.C. van Wolput, H. Zandbergen, J. van Grondelle and R. Prins, accepted for publication in *Appl. Catal.*, chapter 7 of this thesis.
2. B.J. Kip, P.A.T. Smeets, J. van Grondelle and R. Prins, accepted for publication in *Appl. Catal.*, chapter 8 of this thesis.
3. T. Mori, A. Miyamoto, N. Takahashi, M. Fukagaya, N. Niizuma, T. Hattori and Y. Murakami, *J. Chem. Soc., Chem. Commun.*, (1984) 678.
4. T. Mori, A. Miyamoto, N. Takahashi, M. Fukagaya, T. Hattori and Y. Murakami, *J. Phys. Chem.*, 90 (1986) 5197.
5. P.C. Ellgen and M.M. Bhasin, US Patent 4096164 (1978).
6. T.P. Wilson, P.M. Kasai and P.C. Ellgen, *J. Catal.*, 93 (1981) 193.
7. F.G.A. van den Berg, J.H.E. Glezer and W.M.H. Sachtler, *J. Catal.*, 93 (1985) 340.
8. S.D. Jackson, B.J. Brandreth and D. Winstanley, *Appl. Catal.*, 27 (1986) 325.
9. M. Ichikawa, K. Shikakura and M. Kawai, in "Heterogeneous Catalysis Related to Energy Problems", *Proc. Symp. in Dalian, China*, (1982) A.08-I.
10. R.P. Underwood and A.T. Bell, *Appl. Catal.*, 21 (1986) 157.
11. A. Kiennemann, R. Breault, J.P. Hindermann and M. Laurin, *Far. Sym. Chem. Soc.*, 21 (1986) paper 14.
12. L. De Gueldre, L. Clerbols, Y. Gobillon and L. Bourgeois, *Solvay Cie., Ger. Offen.* 2200693 (1972).
13. *Gmelin Handbook of Inorganic Chemistry*, Rh supplement B1, compounds, (1982) Springer Verlag, Berlin.

14. B.J. Kip, J. van Grondelle, J.H.A. Martens and R. Prins, *Appl. Catal.*, 26 (1986) 353., chapter 5 of this thesis.
15. H. Boer, W.J. Boersma and N. Wagstaff, *Rev. Sci. Instr.*, 52 (1982) 439.
16. T. Huizinga, J. van Grondelle and R. Prins, *Appl. Catal.*, 10 (1984) 199.
17. J.C. Vis, H.F.J. van 't Blik, T. Huizinga, J. van Grondelle and R. Prins, *J. Catal.*, 95 (1985) 333.
18. J. Lamotte, J.C. Lavalley, E. Druet and E. Freund, *J. Chem. Soc., Far. Trans. I*, 79 (1983) 2219.
19. P. Arnoldy, J.C.M. de Jonge and J.A. Moulijn, *J. Phys. Chem.*, 89 (1985) 4517.
20. P. Arnoldy, J.C.M. de Jonge, O.J. Wimmers and J.A. Moulijn, to be published.
21. T.M. Duncan, J.T. Yates, Jr. and R.W. Vaughan, *J. Phys. Chem.*, 73(2) (1980) 975.
22. E.K. Poels, E.M. van Broekhoven, W.A.A. van Barneveld and V. Ponec, *React. Kinet. Catal. Lett.* 18 (1981) 223.
23. J.M. Driessen, E.K. Poels, J.P. Hindermann and V. Ponec, *J. Catal.*, 82 (1983) 20.
24. J.P. Hindermann, A. Kiennemann, A. Chakor-Alami and R. Kieffer, in "Proc. Int. Congr. Catal., 8th (Berlin, 1984)", II-163, Verlag Chemie, Weinheim, 1984.
25. A. Takeuchi and J.R. Katzer, *J. Phys. Chem.*, 85 (1981) 937.
26. S.C. Chuang, J.G. Goodwin, Jr. and I. Wender, *J. Catal.*, 92 (1985) 416; S.C. Chuang, Y.H. Tian, J.G. Goodwin, Jr. and I. Wender, *J. Catal.*, 96 (1985) 396.
27. D.S. Jordan and A.T. Bell, *J. Phys. Chem.*, 80 (1986) 4797.
28. M. Ichikawa, K. Sekizawam, K. Shikakura and M. Kawai, *J. Molec. Catal.*, 11 (1981) 167.
29. F.G.A. van den Berg, J.H.E. Glezer and W.M.H. Sachtler, *J. Catal.*, 93 (1985) 340; F.G.A. van den Berg and J.H.E. Glezer, *Proc. Kon. Ned. Akademie Wetensch. B86* (1983) 227; W.M.H. Sachtler, "Proc. Int. Congr. Catal., 8th (Berlin, 1984)", I-151, Verlag Chemie, Weinheim, 1984.
30. M. Pijolat and V. Perrichon, *Appl. Catal.*, 13 (1985) 321.
31. S.J. Tauster and S.C. Fung, *J. Catal.*, 55 (1978) 29.
32. S.J. Tauster, S.C. Fung and R.L. Garten, *J. Am. Chem. Soc.*, 100 (1978) 170.
33. S.J. Tauster, S.C. Fung, R.T.K. Baker and J.A. Horsley, *Science*, 211 (1981) 1121.
34. P. Meriaudeau, J.F. Dutel, M. Dufaux and C. Naccache, *Stud. Surf. Sci. Catal.*, 11 (1982) 95.
35. D.E. Resasco and G.L. Haller, *J. Catal.*, 82 (1983) 279.
36. B.R. Powell and S.E. Whittington, *J. Catal.*, 81 (1983) 382.
37. A.J. Simoens, R.T.K. Baker, D.J. Dwyer, C.F.R. Lund and R.J. Madon, *J. Catal.*, 86 (1984) 359.

38. G.L. Haller, V.E. Henrich, M. McMillan, D.E. Resasco, H.R. Sadeghi and S. Sakellson, "Proc. Int. Congr. on Catal., 8th (Berlin, 1984)", V-135, Verlag Chemie, Weinheim, 1984.
39. Y.W. Chung, G. Xiong and C.C. Kao, *J. Catal.*, 87 (1984) 279.
40. X.-Zh.Jing, T.F. Hayden and J.A. Domesic, *J. Catal.*, 83 (1983) 168.
41. J. Santos, J. Phillips and J.A. Domesic, *J. Catal.*, 81 (1983) 382.
42. R.F. Hicks, Q. Yen and A.T. Bell, *J. Catal.*, 89 (1984) 498.
43. T. Tatsumi, A. Muramatsu and H. Tominaga, *Chem. Lett.*, (1984) 685.
44. B.E. Concha, G.L. Bartholomew and C.H. Bartholomew, *J. Catal.*, 89 (1984) 536.
45. E.A. Lombardo, M.L. Jacono and W.K. Hall, *J. Catal.*, 64 (1980) 150.
46. R. Segawa and W.K. Hall, *J. Catal.*, 77 (1982) 221.
47. P. Hollins, *Ads. Science and Techn.*, 2 (1985) 177.
48. J.B.F. Anderson, R. Burch and J.A. Cairns, *Appl. Catal.*, 21 (1986) 179.
49. B.J. Kip, F.B.M. Duivenvoorden, D.C. Koningsberger and R. Prins, *J. Catal.*, to be published, chapter 4 of this thesis.
50. M. Ichikawa, T. Fukushima and K. Shikakura, in "Proc. Int. Congr. Catal., 8th (Berlin, 1984)", II-69, Verlag Chemie, Weinheim 1984.
51. W.M.H. Sachtler and M. Ichikawa, *J. Phys. Chem.*, 90 (1986) 4752.
52. M.M. McClory and R.D. Gonzalez, *J. Catal.*, 89 (1984) 392.
53. D.L. King and J.B. Peri, *J. Catal.*, 79 (1983) 164.
54. T. Okuhara, H. Tamaru and M. Misono, *J. Catal.*, 95 (1985) 41.
55. E.L. Garfunkel, J.E. Crowell and G.A. Somorjai, *J. Phys. Chem.*, 86 (1982) 310; J.E. Crowell, E.L. Garfunkel and G.A. Somorjai, *Surf. Sci.*, 121 (1982) 303.
56. M. Kiskinova, *Surf. Sci.*, 11 (1981) 584.
57. N.K. Ray and A.B. Anderson, *Surf. Sci.*, 125 (1983) 803.
58. R. van Santen, "Proc. Int. Congr. on Catal., 8th (Berlin, 1984)", IV-97, Verlag Chemie, Weinheim, 1984.; G.A. Martin, *Stud. Surf. Sci. Catal.*, 11 (1982) 315.
59. T. Mori, A. Miyamoto, N. Takahashi, H. Niizuma, T. Hattori and Y. Murakami, *J. Catal.*, 102 (1986) 199.
60. M. Araki and V. Ponec, *J. Catal.*, 44 (1976) 439; V. Ponec, *Catal. Rev.-Sci. Eng.*, 18 (1978) 151.
61. P. Biloen, J.N. Helle, F.G.A. van den Berg and W.M.H. Sachtler, *J. Catal.*, 81 (1983) 450.
62. J.D. Bracey and R. Burch, *J. Catal.*, 86 (1984) 384; J.B.F. Anderson, J.D. Bracey and R. Burch, "Proc. Int. Congr. Catal., 8th (Berlin, 1984)", vol V, p. 251, Verlag Chemie, Weinheim, 1984.

63. J.S. Rieck and A.T. Bell, *J. Catal.*, 96 (1985) 88 and 99 (1986) 262.
64. W.M.H. Sachtler, D.F. Shriver, W.B. Hollenberg and A.F. Lang, *J. Catal.*, 92 (1985) 429.
65. H.A. Pearce and N. Sheppard, *Surf. Sci.*, 59 (1976) 205.
66. W. Erley, H. Ibach, S. Lehwald and H. Wagner, *Surf. Sci.*, 83 (1979) 585.

Chapter 10

CO HYDROGENATION OVER ALKALI-PROMOTED Rh/Al₂O₃, Rh/V₂O₃/SiO₂ AND Rh/ThO₂/SiO₂

Addition of Li, Na, K and Cs to a 1.5 wt% Rh/Al₂O₃ catalyst resulted in a decrease of the hydrocarbon formation rate, while the methanol formation rate was almost unaffected. The overall result is an increased oxygenate selectivity at a decreased total activity. The oxo-selectivity increased in the order unpromoted < Li < Na < K < Cs. The results suggest that the main role of the alkali promoter is to decrease the CO dissociation reaction.

Rh/SiO₂ catalysts promoted with ThO₂ or V₂O₃ had higher C₂-oxygenate selectivities and a higher activity than a Rh/SiO₂ catalyst. Addition of Li, Na, K and Cs did not increase the oxo-selectivity of the ThO₂- and V₂O₃-promoted Rh/SiO₂ catalysts. Independent of the kind of alkali added, it mainly decreased the activity and lowered the hydrogenation rate, suggesting that the added alkali blocked the special perimeter sites which are held responsible for the ThO₂ and V₂O₃ promotion effect. Alkali ions, therefore, did not improve the catalytic behaviour of the ThO₂- and V₂O₃-promoted Rh/SiO₂ catalysts.

10.1 INTRODUCTION

The hydrogenation of carbon monoxide over supported rhodium catalysts produces both hydrocarbons and oxygenated compounds such as alcohols and aldehydes [1-9]. From an economic point of view, C₂-oxygenates are the favoured products [10]. Modification of the catalytic behaviour of rhodium catalysts by the support [1,2] or by a promoter [3-9] has been a topic of considerable interest and debate. Drastic changes in selectivity and activity have been observed with different supports and promoters, and high ethanol selectivities can be reached with rhodium catalysts containing transition metal oxides. Promoters can influence the CO hydrogenation at different steps, i.e. the adsorption of CO, the formation of C₁-intermediates by CO dissociation and subsequent hydrogenation, the C-C bond formation for chain-growth, and the CO insertion into a growing chain, forming oxygenates [3-5].

In previous studies, we investigated the influence of V_2O_3 - [11,12] and ThO_2 - and MoO -promotion [13] on the CO hydrogenation over Rh/SiO_2 at 4.0 MPa. The major influence of these promoters is to enhance the CO dissociation, thereby strongly increasing the total activity of the catalysts. Addition of ethylene to a working catalyst showed that the CO insertion reaction, which is thought to be responsible for C_2+ oxygenated products [3,5,14], is only slightly influenced by the promoter oxides. The selectivity to C_2 -oxygenates was relatively high for the ThO_2 - and V_2O_3 -promoted catalysts (40-50 %). However, further improvement of the selectivity to oxygenated products is necessary for industrial application.

Addition of alkali compounds is widely used in CO hydrogenation reactions to influence the activity and selectivity of the catalysts. For iron catalysts, it has been shown that alkali compounds increase the total activity and shift the selectivity to longer chain hydrocarbons [15]. McLaughlin McClory and Gonzalez [16] reported that alkali addition to Ru/SiO_2 catalysts suppressed the activity, mainly due to a suppressed hydrogenation activity because of site blocking by the alkali atoms. Mori *et al.* [17] studied the effect of addition of alkali carbonate to a Ru/Al_2O_3 catalyst using a microreactor in conjunction with an emissionless infrared diffuse-reflectance spectrometer. The alkali carbonate decreased the rate constant for C-O bond dissociation, but hardly affected the hydrogenation of the surface carbon species produced. Kikuzono *et al.* [18] reported that palladium catalysts prepared from M_2PdCl_4 complexes (M = alkali metal) selectively produced methanol even below atmospheric pressure, be it at a low conversion. The catalytic activity for methanol formation depended sharply on the alkali metal cation in the order: $Li > Na \gg$ unpromoted $> K$. The Cs- and Rb-promoted Pd catalysts did not produce methanol and had a low total activity.

Also for Rh catalysts, several authors reported that the catalytic behaviour is improved by the addition of alkali metals. Wilson *et al.* [19] reported that addition of alkali to a Mn-promoted Rh/SiO_2 catalyst resulted in an increased C_2 -oxygenate selectivity. Tamaru *et al.* [20,21] studied the syngas reaction over alkali metal-doped rhodium catalysts at pressures below 0.1 MPa. Addition of Na and K resulted in an increased selectivity and formation rate of C_2 -oxygenates for Rh/Al_2O_3 catalysts [20], Li- and Na-doped Rh/TiO_2 also exhibited an increased activity and selectivity to C_2 -oxygenates, while the addition of K and Cs resulted in a decreased formation rate [21]. Iwasawa *et al.* [22] reported that addition of alkali chlorides to Rh/SiO_2 resulted in an increased C_2 -oxygenate selectivity for

Li, Na and K, whereas Rb and Cs caused a decreased C₂-oxygenate selectivity compared with the unpromoted Rh/SiO₂. Chuang *et al.* [23,24] studied promotion of Rh/TiO₂ by Li, K and Cs. The CO conversion during syngas reaction at 573 K and 1.0 MPa decreased in the order unpromoted > Li > K > Cs. Although the formation rate of all products decreased by alkali promotion, the decrease was largest for the hydrocarbons (by a factor of 55) and small for methanol (by a factor of 4). The decrease for the C₂-oxygenates was intermediate (by a factor of 22). Van der Lee [25] studied the influence of alkali addition to a Rh/V₂O₃ catalyst. Alkali salts enhanced the activity of the Rh/V₂O₃ catalyst, but the C₂-oxygenate selectivity decreased.

In this paper the addition of alkali metals to V₂O₃- and ThO₂-promoted Rh/SiO₂ catalysts is studied in order to investigate the possibility of further improvement of activity and selectivity to C₂-oxygenates. For comparison, we examined the alkali addition to a Rh/Al₂O₃ catalyst under the same experimental condition because, as can be derived from the literature, the effect of alkali addition strongly depends on the metal, support and experimental conditions. We did not study the addition of alkali a to Rh/SiO₂ catalyst for comparison, because this catalyst has a low activity and should therefore be studied at high reaction temperatures (above 573 K), resulting in low oxygenate selectivities [12,13]. To make sure that metal particle size did not influence the results, alkali metal salts were added to the catalysts after calcination of the promoted rhodium-on-support catalysts. Since a preliminary study indicated that chlorine had a (positive) influence on catalyst activity, we used alkali metal nitrates throughout this investigation.

10.2 EXPERIMENTAL

10.2.1 Catalyst preparation

A 1.5 wt% Rh/Al₂O₃ catalyst was made by impregnating γ -Al₂O₃ (Ketjen, type 000-1.5E, surface area 200 m² g⁻¹, pore volume 0.6 ml g⁻¹) with an aqueous solution of Rh(NO₃)₃ (pH = 2.5, Drijfhout, Amsterdam). V₂O₃- and ThO₂-promoted 1.5 wt% Rh/SiO₂ catalysts were made by sequential impregnation of the SiO₂ support (Grace, type 113, surface area 360 m² g⁻¹, pore volume 1.1 ml g⁻¹) by a solution of NH₄VO₃ (Merck, p.a.) and Th(NO₃)₄·xH₂O (Merck, p.a.), respectively, and by a solution of Rh(NO₃)₃. After each impregnation step the catalysts were dried in air at

395 K for 16 h (heating rate 2 K min^{-1}) and subsequently calcined in air at 723 K for 3 h in order to remove nitrogeous residues from the precursor.

Li, Na, K and Cs were added to these catalysts by impregnation using solutions of LiNO_3 , NaNO_3 , KNO_3 (Merck) and CsNO_3 (Janssen). After drying at 395 K these catalysts were also calcined in air at 723 K for 3 h. An alkali/rhodium ratio of 1.0 was used for the $\text{Rh/Al}_2\text{O}_3$ catalyst and an alkali/rhodium ratio of 0.5 was used for the ThO_2 - and V_2O_3 -promoted 1.5 wt% Rh/SiO_2 catalysts.

10.2.2 CO chemisorption measurements

Volumetric CO chemisorption measurements were performed as described elsewhere [11-13,26]. Catalysts were reduced at 723 K (heating rate 8 K min^{-1}) for 1 h and evacuated for 0.5 h at 723 K before the chemisorption experiment. CO chemisorption was preferred over H_2 chemisorption, because H_2 chemisorption also takes place on V_2O_3 [11], preventing its use for the determination of the rhodium dispersion.

10.2.3 CO hydrogenation

The high pressure reactor and analysis system were described in detail elsewhere [11]. The catalysts were reduced *in situ* in pure H_2 at 0.1 MPa, using a temperature ramp of 5 K min^{-1} between 298 and 723 K and holding the final temperature for 1 h. All catalysts were measured under the same reaction conditions ($\text{GHSV} = 4000 \text{ l l}^{-1} \text{ h}^{-1}$, $\text{H}_2/\text{CO} = 3.0$, $P = 4.0 \text{ MPa}$ and $T_{\text{react}} = 528 \text{ K}$). The behaviour of the various catalysts were compared after 15 h time on stream.

10.3 RESULTS

10.3.1 $\text{Rh/Al}_2\text{O}_3$

The effect of alkali addition to the 1.5 wt% $\text{Rh/Al}_2\text{O}_3$ catalyst, using an alkali/Rh ratio of 1.0 is presented in Table 10.1. Clearly, the CO/Rh chemisorption values of the alkali-promoted catalysts are lower than that of the unpromoted $\text{Rh/Al}_2\text{O}_3$ catalyst. The alkali promoted and unpromoted 1.5 wt% $\text{Rh/Al}_2\text{O}_3$ catalysts were tested in the CO hydrogenation reaction at 723 K and 4.0 MPa. The total activity and hydrocarbon selectivity decreased in the order unpromoted > Li-promoted > Na-promoted > K-promoted > Cs-promoted, while the methanol selectivity increased in that order. The C_2 -oxygenate selectivity was not much influenced by the

TABLE 10.1: Hydrogenation of CO over 1.5 wt% Rh/Al₂O₃ catalysts promoted with alkali, using an alkali/Rh ratio of 1.0. *In situ* reduction at 723 K. Reaction conditions: 528 K, 4.0 MPa, GHSV = 4000 l l⁻¹ h⁻¹, H₂/CO = 3.0.

catalyst system	Rh/-	Rh/Li	Rh/Na	Rh/K	Rh/Cs
CO/Rh ^a	1.85	1.60	1.52	1.47	1.41
Act. ^b	4.1	3.3	2.7	2.1	1.9
Sel. (%) ^c					
C ₁ ^d	59.5	54.8	51.0	49.9	42.8
C ₂₊ ^e	8.3	5.3	6.2	4.2	4.6
C ₁ OH ^f	6.3	12.5	17.0	20.9	26.8
C ₂ oxy ^g	22.4	25.6	23.6	22.8	21.1
oxo sel. ^h	32.2	39.9	42.8	45.9	52.6
C ₄ =/C ₄ ⁱ	0.53	0.28	0.24	0.17	0.63
Formation rates ^j					
C ₁ OH	0.26	0.41	0.46	0.44	0.51
C ₂ oxy	0.93	0.83	0.64	0.48	0.40
C _x H _y	2.8	2.0	1.6	1.2	0.9
CO disso. ^k	3.4	2.4	2.0	1.4	1.2
CO non disso. ^l	0.76	0.87	0.69	0.72	0.71
ethers ^m	1.4	1.3	0.5	0.5	0.4
dehydration ⁿ	2.4	2.1	1.2	0.9	1.1

a) carbon monoxide chemisorption results, b) activity in mmol converted CO (mol Rh)⁻¹ s⁻¹ at 528 K, estimated uncertainty in the activity ± 5 %, c) selectivities expressed as %C efficiency, d) methane, e) hydrocarbons containing two or more C atoms, f) total amount of methanol, ethers and esters included, g) total amount of C₂-oxygenates, ethanol, acetaldehyde and acetic acid, ethers and esters included, h) total oxo-selectivity, i) amount of unsaturated hydrocarbons in C₄ fractions. j) in mmol CO converted (mol Rh)⁻¹ s⁻¹, estimated uncertainty ± 10%, k) formation rate of products or part of products formed via a dissociative mechanism (mmol converted CO (mol Rh)⁻¹ s⁻¹), uncertainty ± 10%, l) formation rate of products or part of products formed via a non-dissociative mechanism (mmol converted CO (mol Rh)⁻¹ s⁻¹), uncertainty ± 10%, m) dehydration of alcohols into corresponding ethers in mol H₂O (g Al₂O₃)⁻¹ s⁻¹, n) dehydration of alcohols into ethers or esters in mol H₂O (g Al₂O₃)⁻¹ s⁻¹.

addition of alkali metal, with the exception of lithium, which gave a slightly higher C_2 -oxygenate selectivity.

From the formation rates calculated for the various products (Table 10.1), one can conclude that the formation rates of methanol and hydrocarbons are higher, respectively lower, for the alkali-promoted catalysts than for the unpromoted catalyst. The suppression of the formation rate of C_2 -oxygenates by alkali was less than that of the hydrocarbons. Chuang *et al.* [23] reported that alkali addition to Rh/TiO_2 resulted in a small decrease in methanol formation rate, a huge decrease of the formation rate of hydrocarbons and an intermediate decrease of the formation rate of C_2 -oxygenates.

In order to distinguish between different mechanisms of CO conversion, we calculated the conversion of CO via a non-dissociative mechanism and via a dissociative mechanism. For the non-dissociative mechanism, we added together the formation rate of methanol, half of the formation rate of C_2 -oxygenates, one third of the C_3 -oxygenates etc., because methanol is thought to be formed via a non-dissociative hydrogenation of CO [27] and higher oxygenates are thought to be formed by CO insertion into a growing carbonaceous intermediate [3,5,14,28]. The conversion of CO via a dissociative mechanism is clearly suppressed by the presence of alkali and different suppression levels are observed for the several alkali metals. The following order is observed: unpromoted > Li > Na > K > Cs (see Figure 10.1). The conversion of CO via a non-dissociative mechanism is unaffected by the presence of alkali.

These results suggest that the main role of the alkali promoter in the Rh/Al_2O_3 catalysts is to suppress the CO dissociation reaction. Mori *et al.* [17] came to the same conclusion for alkali carbonate addition to Ru/Al_2O_3 catalysts. They used a pulse micro reactor in conjunction with an emissionless diffuse-reflectance infrared spectrometer, and in this way they could study the dynamics of adsorbed CO as well as produced CH_4 , be it under non steady-state conditions. Alkali carbonate added to the Ru catalyst decreased the rate constant for C-O bond dissociation, but hardly affected the hydrogenation of the surface carbon species produced. Also in our study the hydrogenation activity was not suppressed by the alkali metal. The amount of unsaturated hydrocarbons even slightly decreased by the addition of alkali. Furthermore, the results of Mori *et al.* show that the rate constant for the C-O bond dissociation was much smaller than that for the hydrogenation of the resulting formed CH_x species, suggesting that the C-O bond dissociation is rate limiting for the methanation reaction. Mori *et al.*

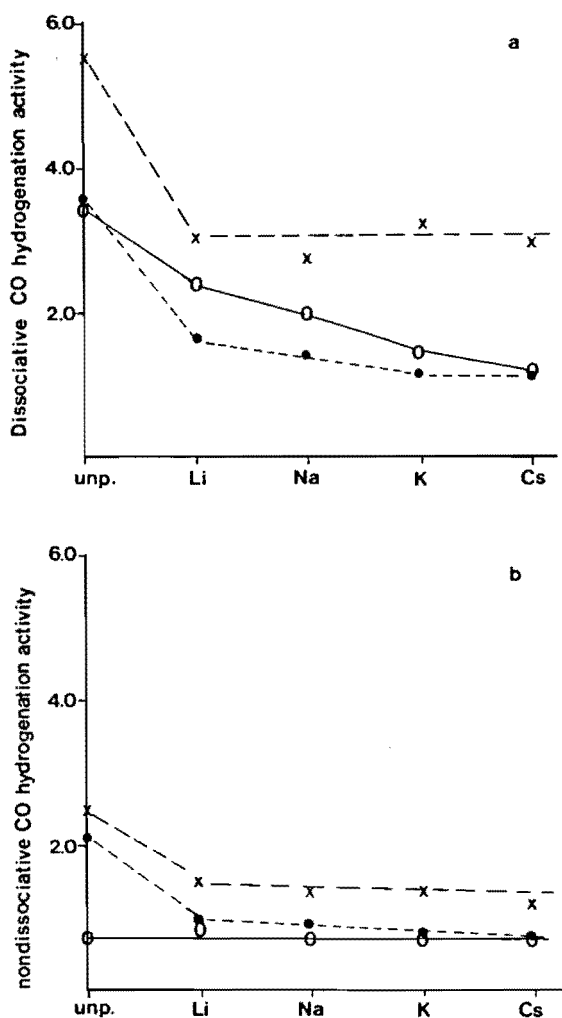


FIGURE 10.1: Influence of alkali promoters on the CO conversion rate via the dissociative mechanism (a) and via the non-dissociative mechanism (b) for Rh/Al₂O₃ (o), Rh/V₂O₃/SiO₂ (x) and Rh/ThO₂/SiO₂ (●).

postulated a hydroxy carbene [(CHOH)_{ad}] species as an intermediate in the CO dissociation and ascribed the suppressing effect of the alkali metal on the C-O bond dissociation to an increased electron density on the Ru metal, resulting in a stabilization of (CO)_{ad} and therefore a decrease in the equilibrium concentration of (CHOH)_{ad}. We think that the suppression of the CO dissociation reaction also can be a result of the blocking of the active

centers for CO dissociation, as the CO/Rh value decreased by the addition of alkali.

Comparing the results of alkali promotion of Rh/Al₂O₃ with studies of alkali promotion of Rh/TiO₂ [23,24] and Rh/SiO₂ [22], it becomes clear that for the same alkali/Rh ratios, the effect of alkali is much smaller for the Rh/Al₂O₃ than for the Rh/SiO₂ and Rh/TiO₂ catalysts. This suggests that the major part of the added alkali does not directly interact with the rhodium metal particle, but that a significant part is scavenged by the Al₂O₃ support. Using IR studies of adsorbed CO and H₂ desorption studies, Blackmond *et al.* [29] came to the same conclusion for Cs promotion of Rh/Al₂O₃.

In Table 10.1, two additional data sets are given for reactions which are thought to proceed over the Al₂O₃ support. The amount of ether, formed by dehydration of the corresponding alcohols over acidic sites on the Al₂O₃ support [30], decreased by addition of alkali. The formation of esters from alcohols and acetic acid is also thought to take place at sites on the Al₂O₃ support. The total dehydration of alcohols to ethers and esters also is presented in Table 10.1 for the unpromoted and alkali-promoted Rh/Al₂O₃ catalysts. Clearly, the dehydration is suppressed for the alkali-promoted Rh/Al₂O₃ catalysts, proving that the added alkali also changed the properties of the support, again indicating that part of the alkali is positioned on the support.

10.3.2 Rh/V₂O₃/SiO₂

In Table 10.2, the effect of alkali addition to 1.5 wt% Rh/V₂O₃/SiO₂ (V/Rh = 1) is presented. An alkali/Rh ratio of 0.5 was used and the catalysts were tested at 4.0 MPa and around 532 K. In order to compare activities at the same temperature, we calculated the activity at 528 K, using $E_{\text{act}} = 100 \text{ kJ mol}^{-1}$. This activation energy was measured for the Rh/V₂O₃/SiO₂ (V/Rh = 1) catalyst [12]. As is shown in Table 10.2, the Rh/V₂O₃/SiO₂ catalyst exhibited a relatively high total oxo-selectivity (56 %) and C₂-oxygenate selectivity (41 %).

Addition of alkali to this catalyst resulted in a decreased CO/Rh chemisorption ratio, pointing to the covering of adsorption sites. The catalytic activity of the Rh/V₂O₃/SiO₂ catalysts decreased by almost a factor of 2 by addition of alkali, but not much difference was observed between the different alkali metals. The C₂-oxygenate and total oxygenate selectivities were slightly influenced by alkali addition. Hydrogenation activity was suppressed by the presence of alkali, as judged from the fact that the

TABLE 10.2: Hydrogenation of CO over alkali-promoted 1.5 wt% Rh/V₂O₃/SiO₂, V/Rh = 1.0 catalysts, using an alkali/Rh ratio of 0.5. *In situ* reduction at 723 K. Reaction temperature around 533 K, P = 4.0 MPa, GHSV = 4000 l l⁻¹ h⁻¹, H₂/CO = 3.0. See Table 10.1 for the notation.

Catalyst system	Rh/V	Rh/V+Li	Rh/V+Na	Rh/V+K	Rh/V+Cs
CO/Rh ^a	0.29	0.20	0.18	0.17	0.18
React Temp (K)	530	533	533	534	533
Act.	8.6	5.7	5.1	5.9	5.1
Corr. Act. ^b	8.0	4.6	4.1	4.6	4.1
Sel. (%C)					
C ₁	28.6	26.3	25.3	26.9	24.3
C ₂ ⁺	15.6	12.4	14.4	16.4	16.7
C ₁ OH	8.9	9.7	10.1	8.2	7.6
C ₂ oxy	41.3	45.0	42.6	40.6	44.0
oxo sel.	55.9	61.3	60.3	56.7	59.0
C ₂ =/C ₂	0.2	0.3	0.4	0.5	1.0
C ₄ =/C ₄	1.2	1.5	2.0	2.0	2.1
Formation rates: ^b					
C ₁ OH	0.71	0.45	0.41	0.38	0.31
C ₂ oxy	3.3	2.1	1.9	1.9	1.8
C _x H _y	3.5	1.8	1.6	2.0	1.7
CO disso.	5.5	3.0	2.7	3.2	2.9
CO non disso.	2.5	1.5	1.4	1.4	1.2

a) reduction at 523 K and evacuation at 723 K. The reason for this special pre-treatment is discussed in Ref. [11]. b) calculated activity and formation rates at 528 K (in mmol converted CO (mol Rh)⁻¹ s⁻¹) using E_{act} = 100 kJ mol⁻¹, estimated uncertainty 10%.

amount of unsaturated hydrocarbons was higher for the alkali-promoted Rh/V₂O₃/SiO₂ catalysts. The fraction of unsaturated products in the C₂-oxygenates (acetic acid and acetaldehyde) increased due to alkali promotion, also suggesting a decreased hydrogenation reaction for these catalysts.

The conversion rate of CO via the non-dissociative and the dissociative route were both suppressed by the presence of alkali, and the extent of the suppression was independent on the kind of alkali (Figure 10.1). These

results are in contrast with the effect of alkali on Rh/Al₂O₃.

10.3.3 Rh/ThO₂/SiO₂

The results of alkali addition to ThO₂-promoted Rh/SiO₂ catalysts are presented in Table 10.3. The CO/Rh chemisorption ratio decreased by the addition of alkali. The activity decreased due to alkali promotion in the following order: unpromoted >> Li > Na > K, Cs. The hydrocarbon selectivity was almost unaffected by alkali addition, but the methanol selectivity increased and C₂-oxygenate selectivity decreased in the order unpromoted, Li, Na, Cs, K. The hydrogenation rate decreased by addition of the alkali of the alkali promoter, as can be concluded from the increase of the C₄=/C₄ ratio. The conversion rate of CO via the dissociative and via the non-dissociative route were both suppressed by the presence of alkali.

TABLE 10.3: Hydrogenation of CO over alkali-promoted 1.5 wt% Rh/ThO₂/SiO₂, Th/Rh = 1.0 catalysts, using an alkali/Rh ratio of 0.5. *In situ* reduction at 723 K. Reaction temperature 528 K, P = 4.0 MPa, GHSV = 4000 l l⁻¹ h⁻¹, H₂/CO = 3.0. See Table 10.1 for the notation.

Catalyst system	Rh/Th	Rh/Th+Li	Rh/Th+Na	Rh/Th+K	Rh/Th+Cs
CO/Rh	0.63	0.42	0.45	0.39	0.38
Act.	5.7	2.6	2.3	1.8	1.8
Sel. (%C)					
C ₁	32.3	28.9	30.6	30.9	32.4
C ₂ ⁺	5.8	3.4	4.9	4.9	5.2
C ₁ OH	7.7	13.0	17.9	19.6	18.5
C ₂ oxy	51.8	52.1	43.6	41.6	40.4
oxo sel.	61.9	67.7	64.7	64.2	62.5
C ₂ =/C ₂	0.2	0.2	0.2	0.3	0.4
C ₄ =/C ₄	0.7	1.0	0.9	0.9	1.0
Formation rates:					
C ₁ OH	0.44	0.34	0.41	0.35	0.33
C ₂ oxy	3.0	1.4	1.0	0.75	0.73
C _x H _y	2.2	0.84	0.81	0.64	0.68
CO disso.	3.6	1.6	1.4	1.1	1.1
CO non disso.	2.1	1.0	0.9	0.8	0.7

Our results indicate that the role of the alkali promoter in the ThO_2 - and V_2O_3 -promoted catalysts is different from that in the $\text{Rh}/\text{Al}_2\text{O}_3$ catalysts. For $\text{Rh}/\text{Al}_2\text{O}_3$ the rate of CO bond dissociation is decreased and the hydrogenation rate is unaffected. This of course only influenced the CO conversion via a dissociative mechanism. For the ThO_2 - and V_2O_3 -promoted catalysts we also observed a suppression of the hydrogenation reaction by the addition of alkali. This might explain why for these catalysts the CO conversion via a non-dissociative mechanism is also suppressed.

10.4 DISCUSSION

Several explanations might be given for the effect of alkali additives on the CO hydrogenation over ThO_2 - and V_2O_3 -promoted Rh/SiO_2 catalysts.

- An electronic effect has been suggested for the alkali promotion of group VIII metal catalysts by many authors [31-37]. We do not think that this effect can completely explain the results of alkali addition to the V_2O_3 - and ThO_2 -promoted Rh/SiO_2 catalysts. As can be seen in Tables 10.2 and 10.3 and in Figure 10.1, the effect of alkali addition was almost independent on the kind of alkali metal used. The electronic effect is expected to be different for Li, Na, K and Cs and therefore, an electronic influence of the alkali metal on the rhodium metal can not be the major reason for the lower activity. The electronic effect might explain the influence of alkali promotion of the $\text{Rh}/\text{Al}_2\text{O}_3$ catalysts because for these catalysts differences are observed between the several alkali promoters.

- It is known that alkali metals can react with both V_2O_3 and ThO_2 [38] and form mixed oxides. The mixed oxides of Na_2O and ThO_2 and of K_2O and ThO_2 can be made at temperatures of 823 - 1023 K. For Li_2O and ThO_2 no mixed oxides have been reported. Alkali oxides can form bronzes with vanadium oxide. For Li and Na, mixed oxides with V(III), V(IV) and V(V) oxides have been reported and for K, bronzes are known with V(IV) and V(V). The formation of mixed oxides could explain the decrease in activity, because by removing the promoter oxides one may decrease the promoter effect of V_2O_3 and ThO_2 . It is also possible that the alkali promoter only adsorbs on ThO_2 or V_2O_3 , not forming a new chemical compound, but still influencing the promoter role of ThO_2 or V_2O_3 .

- The CO/Rh ratio decreased by alkali addition. This suggests that (at least part of) the added alkali promoter is positioned on top of the rhodium metal. If the added alkali metal is situated at the perimeter of the ThO_2 or

V_2O_3 patches covering the rhodium metal, it blocks the special perimeter sites which have been hold responsible for the promoter effect [12,13,39]. In this way the effect of ThO_2 and V_2O_3 is counteracted, resulting in a decreased CO conversion via the dissociative and non-dissociative route and a decreased hydrogenation activity. This also explains that the results for all alkali promoters are the same, the alkali only physically blocks the active centers.

From our measurements, it is not possible to distinguish between the second and third explanation, the formation of mixed oxides and the physically blocking of active centers, respectively. A combination of these explanations cannot be ruled out either.

10.5 CONCLUSIONS

Addition of Li, Na, K and Cs to Rh/Al_2O_3 decreased the activity, but increased the total oxo-selectivity due to an increased methanol selectivity. The results suggest that alkali addition decreased the C-O bond dissociation without affecting the hydrogenation activity. Most of the alkali is positioned on the support, only a small part of the added alkali is positioned on top of the rhodium metal particles.

Addition of Li, Na, K and Cs to $Rh/V_2O_3/SiO_2$ and $Rh/ThO_2/SiO_2$ also decreased the activity, but the oxo-selectivity was hardly affected. The results suggest that in this case the alkali addition reversed the promoter function of V_2O_3 and ThO_2 by the physical blocking of the active sites at the perimeter of the promoter oxide patches covering the rhodium metal particle, or by the formation of a mixed oxide of alkali and promoter oxide. The alkali addition decreased the CO dissociation as well as hydrogenation. Thus, the alkali addition to the $Rh/V_2O_3/SiO_2$ and $Rh/ThO_2/SiO_2$ did not result in a higher C_2 -oxygenate selectivity.

10.6 REFERENCES

1. M. Ichikawa, Bull. Chem. Soc. Jap., 51 (1978) 2268; Bull. Chem. Soc. Jap., 51 (1978) 2273; J. Chem. Soc., Chem. Commun., (1978) 566.
2. J.R. Katzer, A.W. Sleight, P. Gajardo, J.B. Mitchel, E.F. Gleason and S. McMillan, Far. Disc. Chem. Soc., 72 (1981) 121.
3. F.G.A. Van den Berg, J.H.E. Glezer and W.M.H. Sachtler, J. Catal., 93 (1985) 340.
4. H. Orita, S. Naito and K. Tamaru, J. Catal., 90 (1984) 183.

5. M. Ichikawa, T. Fukushima and K. Shikakura, in "Proc. Int. Congr. Catal., 8th., (Berlin, 1984)" I-69, Verlag Chemie, Weinheim, 1984.
6. P.R. Watson and G.A. Somorjai, *J. Catal.*, 72 (1981) 347.
7. P.R. Watson and G.A. Somorjai, *J. Catal.*, 74 (1982) 282.
8. M. Ichikawa, K. Shikakura and M. Kawai, in "Heterogeneous Catalysis Related to Energy Problems", Proc. Symp. in Dalian, China, 1982, A.08-I.
9. T.P. Wilson, P.M. Kasai and P.C. Ellgen, *J. Catal.*, 93 (1981) 193.
10. A. Aquilo, J.S. Alder, D.N. Freeman and R.J.H. Voorhoeve, *Hydrocarbon Process*, 62 (1983) 57.
11. B.J. Kip, P.A.T. Smeets, J.H.M.C. van Wolput, H. Zandbergen, J. van Grondelle and R. Prins, *Appl. Catal.*, submitted for publication, chapter 7 of this thesis.
12. B.J. Kip, P.A.T. Smeets, J. van Grondelle and R. Prins, *Appl. Catal.*, submitted for publication, chapter 8 of this thesis.
13. B.J. Kip, E.G.F. Hermans, J.H.M.C. van Wolput, N.M.A. Hermans, J. van Grondelle and R. Prins, *Appl. Catal.*, submitted for publication, chapter 9 of this thesis.
14. W.M.H. Sachtler, in "Proc. Int. Congr. Catal., 8th., (Berlin, 1984)" I-151, Verlag Chemie, Weinheim, 1984.
15. R.B. Anderson, in "Catalysis" vol. IV (P.H. Emmett, Ed.) New York, Reinhold, 1956, p. 123.
16. M. McLaughlin McClory and R.D. Gonzalez, *J. Catal.*, 89 (1984) 392.
17. T. Mori, A. Miyamoto, N. Takahashi, H. Niizuma, T. Hattori and Y. Murakami, *J. Catal.*, 102 (1986) 199.
18. Y. Kikuzono, S. Kagami, S. Naito, T. Onishi and K. Tamaru, *Far. Disc. Chem. Soc.*, 72 (1981) 135.
19. T.P. Wilson, W.J. Bartley and P.C. Ellgen, in "Heterogeneous Catalysis Related to Energy Problems", Proc. Symp. in Dalian, China, 1982, A.27-U.
20. S. Kagami, S. Naito, Y. Kikuzono and K. Tamaru, *J. Chem. Soc., Chem. Commun.*, (1983) 256.
21. H. Orita, S. Naito and K. Tamaru, *Chem. Lett.*, (1983) 1161.
22. Y. Iwasawa, T. Hayasaka, N. Ito and S. Ogasawara, in "Heterogeneous Catalysis Related to Energy Problems", Proc. Symp. in Dalian, China, 1982, A.11-J.
23. S.C. Chuang, J.G. Goodwin, Jr. and I. Wender, *J. Catal.*, 92 (1985) 416.
24. S.C. Chuang, J.G. Goodwin, Jr. and I. Wender, *J. Catal.*, 95 (1985) 435.
25. G. Van der Lee, Thesis, Leiden (1986), p. 131-150.
26. B.J. Kip, J. van Grondelle, J.H.A. Martens and R. Prins, *Appl. Catal.*, 26 (1986) 353, chapter 3 of this thesis.
27. A. Takeuchi and J.R. Katzer, *J. Phys. Chem.*, 85 (1981) 937.

28. F.G.A. van den Berg and J.H.E. Glezer, Proc. Kon. Ned. Akademie Wetensch. B86 (1983) 227.
29. D.G. Blackmond, J.A. Williams, S. Kesraoui and D.S. Blazewick, J. Catal., 101 (1986) 496.
30. B.J. Kip, F.W.A. Dirne, J. van Grondelle and R. Prins, Appl. Catal., 25 (1986) 43, chapter 5 of this thesis.
31. D.L. King and J.B. Peri, J. Catal., 79 (1983) 164.
32. T. Okuhara, H. Tamaru and M. Misono, J. Catal., 95 (1985) 41.
33. E.L. Garfunkel, J.E. Crowell and G.A. Somorjai, J. Phys. Chem., 86 (1982) 310; J.E. Crowell, E.L. Garfunkel and G.A. Somorjai, Surf. Sci., 121 (1982) 303.
34. M. Kiskinova, Surf. Sci., 11 (1981) 584.
35. E.L. Ray and A.B. Anderson, Surf. Sci., 125 (1983) 803.
36. R. van Santen, "Proc. Int. Congr. Catal., 8th., (Berlin, 1984)" IV-97, Verlag Chemie, Weinheim, 1984; G.A. Martin, Stud. Surf. Sci. Catal., 11 (1982) 315.
37. T. Mori, H. Masuda, H. Imai, A. Miyamoto, H. Niizuma, T. Hattori and Y. Murakami, J. Mol. Catal., 25 (1984) 263.
38. Gmelins Handbuch der Anorganischen Chemie, 8. Auflage, Vanadium B-2, p. 369-424, Verlag Chemie, Weinheim, 1967; Thorium C-2, p. 1-2, Springer Verlag, Berlin, 1976.
39. M.E. Levin, M. Salmeron, A.T. Bell and G.A. Somorjai, Faraday Symp. Chem. Soc., 21 (1986) paper 10.

Chapter 11

CONCLUDING REMARKS

Although the results of the studies described in this dissertation have already been extensively discussed in chapters 3-10, in this chapter we will discuss the general conclusions arrived at in this thesis and relate them to new experimental data and theoretical studies recently reported in the literature.

In this thesis the results of studies on the hydrogenation of CO over supported rhodium and iridium catalysts are described. The influence of the support, the promoter and the active metal was investigated. The supports can be divided into two groups. The supports of the first group, e.g. V_2O_5 , TiO_2 , MoO_3 , La_2O_3 and ThO_2 , cover the metal particles under our conditions, whereas the supports of the second group, Al_2O_3 and SiO_2 , do not do that. The covering can be a result of two different processes. First, during a high temperature reduction ($T > 773$ K), mobile suboxides can be formed. These mobile suboxides can migrate onto the metal surface and in this way cover the metal particles. It is also possible that during the wet steps of the catalyst preparation, part of the support dissolves in the presence of acids (the metal precursor solutions used had a pH of around 2) and can subsequently precipitate on the metal particles upon drying, as was proposed by Hicks et al. [1] for La_2O_3 -supported Pd catalysts and by Bastein et al. [2] for Rh/ V_2O_3 systems. For the metal precursor solutions used (pH around 2), SiO_2 and Al_2O_3 are not soluble.

The patches of support oxide present on the metal particles are thought to be responsible for the modification of the catalytic behaviour of the active metal. For instance, TiO_2 -, MoO_3 - and Nb_2O_5 -supported rhodium catalysts exhibited high activities, ThO_2 - and V_2O_3 -supported catalysts exhibited high C_2 -oxygenate selectivities, and MgO -, ZnO -, and La_2O_3 -supported catalysts showed high methanol selectivities (chapter 6). The support itself can also influence the behaviour of the catalyst. For instance, the acidic sites of Al_2O_3 are responsible for consecutive reactions of initially formed oxygenates resulting in a lower total oxo-selectivity for these catalysts. Especially when a chlorine-containing rhodium precursor is used, this effect is observed (chlorine increases the acidity of the alumina surface), as is shown in chapter 5.

As is shown in chapters 7-9, also in the case of V_2O_3 , MoO_3 and ThO_2 promotion of rhodium catalysts, part of the metal surface is covered by the

promoter oxides. The main effect of the promoter oxides is to increase the activity in CO hydrogenation. The activity increased by a factor of 170, 99 and 79 in the presence of molybdenum oxide, vanadium oxide and thorium oxide, respectively, at a promoter/Rh ratio of one. These results and data in the literature [3] strongly suggest that highly active sites for CO hydrogenation are positioned at the perimeter of the promoter oxide patches on the metal particles. At low coverage, an increasing amount of promoter oxide results in an increase of the activity. At higher coverage, however, the activity decreases with increasing covering because the effect of blocking of active sites is larger than the creation of new highly active sites. Levin et al. [3] reported an optimum coverage of 15 % for the Rh/TiO₂ systems. We could not determine the coverage in our systems during reaction. Although coverage after reduction of the catalyst system (but before reaction) as determined by chemisorption techniques (chapter 7 and 9), can be different from coverage during reaction (water, formed during reaction, can reverse the covering), it is clear from our results that in the case of ThO₂-promoted catalysts only a limited covering is present. This limited covering dramatically increases the CO hydrogenation activity. This suggests that only a limited covering is necessary for a sharp increase in activity.

Although Rh/V₂O₃ exhibits a high C₂-oxygenate selectivity (45 %) after a high temperature reduction (873 K), the activity is very low because of the dominance of the creation of new highly active sites over blocking. The covering of the rhodium surface by V₂O₃ is too high. For the alumina-supported V₂O₃-promoted rhodium catalysts another complication arises. Due to the strong interaction between RhCl₃/Rh₂O₃ and the alumina support and between NH₃VO₃/V₂O₅ and the alumina support, an interaction between vanadium oxide and rhodium can only occur at high V/Rh ratios (7.0 and 8.4). Therefore, only at high V/Rh ratios an influence of V₂O₃ on the Rh/Al₂O₃ catalyst is observed. Thus, due to the strong interaction between vanadium oxide and alumina, most of the vanadium oxide promoter is scavenged by the support. However, if the relatively inert support SiO₂ is used, small amounts of vanadium oxide already cause a dramatic increase in activity without loss of selectivity.

For the vanadium oxide- and thorium oxide-promoted Rh/SiO₂ catalysts an increase in the promoter/Rh ratio causes an increase in the activity even up to a promoter/Rh ratio of 4.0. In these cases the effect of creating active sites dominates the blocking effect. For the MoO₃-promoted Rh/SiO₂ system, the activity as a function of the promoter/Rh ratio showed a maximum at Mo/Rh = 1.0. Apparently, for Mo/Rh > 1.0, the blocking effect is

larger than the effect of creating sites.

Temperature programmed reduction and diffuse reflectance infrared spectroscopy showed that in the case of V_2O_5 - and MoO_3 -promoted Rh/SiO₂ catalysts the intimate contact between rhodium and promoter was already present in the calcined samples in the form of mixed oxides, RhVO₄ and Rh₂MoO₆, respectively. Already after reduction of this oxidic phase at low temperature (523 K) the promotor oxide patches cover the metal particles. Thus, reduction at relatively high temperatures is not needed. No indication for mixed oxide formation was found for the ThO₂-promoted Rh/SiO₂ catalysts.

Besides influencing the activity, the promoter oxides also affected the selectivity. The thorium oxide- and vanadium oxide-promoted Rh/SiO₂ catalysts had a high selectivity to C₂-oxygenates, while molybdenum oxide-promoted Rh/SiO₂ exhibited high methanol selectivities. This high methanol selectivities for Rh/MoO₃/SiO₂ catalysts originated from the fact that the non-dissociative reaction towards methanol was only enhanced by a factor of 3 and of 7 by ThO₂, and V₂O₅, respectively, but was greatly enhanced by MoO₃ by a factor of 171. This high factor of increase of the methanol formation rate due to MoO₃ addition was attributed to the reaction of CO to methanol over molybdenum ions. Thus, in the Rh/MoO₃/SiO₂ catalysts at least two types of active sites were present: Rh metal sites for CO dissociation and subsequent reactions to hydrocarbons and higher oxygenates and molybdenum ions for methanol formation.

An unanswered question is, what the role of the promoter oxides is in enhancing the CO hydrogenation. The catalytic studies and the results of addition of ethylene under reaction conditions strongly suggested that their main role is to enhance the CO dissociation reaction. The models mentioned in chapter 8 and 9 are: an electronic effect of the promoter oxide on the rhodium particle, or a direct effect of the promoter on the CO bond strength, a participation of the promoter oxide in the dissociation of CO. In the electronic model, the C-O bond weakening has been ascribed to promoter-induced charge transfer to the antibonding CO 2 π orbital (see, e.g., the review in [4]). Mori et al. [5] proposed a mechanism in which the promoter oxide plays an active role in the CO dissociation. They postulated a hydroxycarbene intermediate for C-O bond dissociation. A Pⁿ⁺-ion adjacent to the metal atom, to which the hydroxycarbene is attached, pulls the oxygen atom away from the M-CHOH intermediate. In this step the promoter ion is oxidized. However, for the ThO₂-promoted catalysts in our study, the C-O bond dissociation was greatly enhanced by ThO₂, while temperature

programmed reduction studies did not provide any evidence for a reduction/oxidation cycle of the thorium ion. Therefore, the mechanism proposed by Mori et al. can not explain the observed promoter effects.

Burch et al. [6], Rieck and Bell [7] and Sachtler et al. [8] proposed a model based on the activation of CO by the interaction of a promoter ion with the oxygen atom of CO. In this way, CO may be adsorbed parallel to the metal surface with the C-atom attached to a metal atom and the O-atom attached to the promoter ion. This results in a weakened C-O bond, which shows up as a lowering of the C-O stretching frequency in infrared spectroscopy.

In the past year, a large number of papers concerning the effect of positive ions in the activation of the C-O bond have been published. Especially, model studies of CO and alkali (mainly potassium) coadsorption on single crystal metal surfaces using sophisticated surface analysis techniques and theoretical calculations were used to answer questions like: is the effect of the promoter a short range or a long range effect, does the promoter cause tilting or even completely side-on bonding of the chemisorbed CO, is the promoter ion influencing the metal electronically and in this indirect way influencing the C-O bond, or is a direct interaction between the promoter and CO present? Although we will not review these studies completely (for an excellent review we refer to Bonzel [9]) and although these studies did not result in a new consensus about the role of the promoter, we wish to summarize the most relevant results here.

Several techniques were used to study the orientation of CO on the surface in the promoted systems. Angle resolved Auger spectroscopy was used by Wurth et al. [10] to study coadsorption of CO and K on Ru(001) and they came to the conclusion that CO is vertically bound to the surface. NEXAFS studies of Sette et al. [11] for CO and Na on Pt(111) pointed to the same conclusion. Heskett et al. [12], studying CO+K/Ru(001) with angle-resolved photoemission spectroscopy, and Wessner et al. [13], studying CO+K/Pt(111) with X-ray photoelectron diffraction, also concluded that the CO molecules adsorb vertically on the metal surface in the presence of an electropositive promoter. An upper limit of 10° as the maximum possible tilt angle is mentioned. Of course these measurements do not fully exclude that a small part of the adsorbed CO is side-on adsorbed. They, however, deliver serious doubts about the suggestions that the main promoter action is to cause the double bonded CO in the side-on mode. In contrast to these experimental techniques, an atom superposition and electron delocalization molecular orbital study by Anderson and Dowd [14] showed that the oxygen end of CO adsorbed on a cluster model of the Pt(111)

surface is attracted by π donation to empty d orbitals in Ti and Fe cations, causing tilting from the normal and leading to a decrease in the CO vibrational frequency of 300–400 cm^{-1} .

Interesting information about the interaction between CO and the promoter can be obtained from vibrational spectroscopy studies like high resolution electron energy loss spectroscopy (HREELS) or infrared spectroscopy in reflection mode (IRS). Uram et al. [15] used IRS to study the adsorption of CO and K on Ni(111). Depending on the CO/K ratio and the amount of K present on the Ni(111) surface, several low frequency bands were observed.

Two absorption bands, at 1434 and 1750 cm^{-1} , were insensitive to coverage (did not shift to higher wavenumbers if the coverage is increased), suggesting a strongly perturbed CO which does not couple dynamically to other CO species which are not so strongly perturbed. Lackey et al. [16] suggest that such short range K ... CO interactions on Cu(110) result in the formation of polymeric CO anion complexes in the form $\text{K}_x^{\delta+}(\text{CO})_y^{\delta-}$. Schultz et al. [17] recently showed by theoretical calculations that a transfer of electrons from surface K to surface CO is energetically plausible and that this mechanism leads to a weakened C–O bond and to dramatically lowered C–O frequencies of around 1500 cm^{-1} . Heskett et al. [18] proposed a modified back-donation model. In this model the 1π orbitals of CO become involved in the bonding of CO not to the metal but to the modifier atom, in this case potassium. Finally, the suggestion of a rehybridized CO in the presence of alkalis has been made [10,19] to account for the dramatic shift in the CO vibrational frequency.

Uram et al. [15] also observed bands between 1500 and 1900 cm^{-1} , whose positions were coverage dependent. The total coverage dependent frequency shift for CO on clean Ni(111) was 103 cm^{-1} for bridging CO. The adsorption of even a small amount of potassium caused a shift of 169 cm^{-1} . Furthermore, an increasing potassium coverage greatly increased the magnitude of this shift. Uram et al. attributed these bands to long range potassium interaction with CO and from their results calculated a range of potassium–CO interaction of about 25 CO molecules per potassium atom, suggesting that the potassium has an observable radius of influence of 8–9 Å. Uram et al. explained the long range potassium–CO interaction in terms of electrostatic interactions. Holloway and Norskov [20] have attributed the observed decrease in CO frequency in an applied potential to an increase in the antibonding 2π orbital occupation. Recently, Müller and Bagus [21] have suggested, based on theoretical calculations, that direct dipole–electric

field interactions dominate the observed frequency shift (Stark effect) and that the field induced charge distributions described by Holloway and Norskov are quite small.

Other authors also attribute the shifting bands to short range electronic interactions between CO and K and propose that the electronic effect on CO mediated by the K species is shared by several CO molecules in the immediate vicinity of the K [9]. Hence the C-O stretch frequencies will also vary with the number of CO neighbours to the K species, i.e. in a quantized fashion.

Although the above cited results all concern promotion of single crystal metals by potassium, they can be very relevant for promotion by electropositive metals in general. Of course, these studies were all performed in the absence of hydrogen. The activation process of CO in the presence of hydrogen might be different. The relation between the fundamental studies described above and the activation under reaction conditions might be complicated by this. Thus, based on an inverse H_2 - D_2 isotope effect for C-O bond dissociation, Mori et al. suggested a hydrogen assisted C-O bond dissociation over Ru/ Al_2O_3 catalysts [5]. Shustorovich and Bell [22] concluded from theoretical calculations (the bond order conservation method) that cleavage of the C-O bond over Ni can occur either by direct dissociation or by hydrogen assisted dissociation, the activation barriers for both processes being identical. But, the activation energy for direct dissociation of CO on Pd and Pt is significantly larger than that for hydrogen assisted dissociation, and hence the latter process is more significant.

A topic which has not yet been discussed in this final discussion is the difference between rhodium and iridium. If SiO_2 or Al_2O_3 is used as a support, the iridium catalysts have a very low activity and mainly produce methane and methanol (chapter 5 and 6). If supports like V_2O_3 and ThO_2 are used, activities are higher and iridium is also capable to catalyze the CO insertion reaction forming C_2 -oxygenates. However, in all cases the activity and oxo-selectivity are higher for the rhodium catalysts than for the iridium catalysts.

REFERENCES

1. R.F. Hicks, W. Yen and A.T. Bell, *J. Catal.*, 89 (1984) 498.
2. A.G.T.M. Bastein, W.J. van der Boogert, G. van der Lee, H. Luo, B. Schuller and V. Ponc, *Appl. Catal.*, 29 (1987) 243.

3. M.E. Levin, M. Salmeron, A.T. Bell and G.A. Somorjai, *Far. Symp. Chem. Soc.*, 21 (1986) paper 10.
4. H.P. Bonzel, *J. Vacuum Sci. Technol.*, A2 (1984) 866.
5. T. Mori, A. Miyamoto, N. Takahashi, M. Fukagaya, T. Hattori and Y. Morakami, *J. Phys. Chem.*, 90 (1986) 5197; T. Mori, A. Miyamoto, N. Takahashi, N. Niizuma, T. Hattori and Y. Morakami, *J. Catal.*, 102 (1986) 199.
6. J.D. Bracey and R. Burch, *J. Catal.*, 86 (1984) 384; J.B.F. Anderson, J.D. Bracey and R. Burch, "Proc. Int. Congr. Catal., 8th (Berlin, 1984)", vol V, p. 251, Verlag Chemie, Weinheim, 1984.
7. J.S. Rieck and A.T. Bell, *J. Catal.*, 96 (1985) 88 and 99 (1986) 262.
8. W.M.H. Sachtler, D.F. Shriver, W.B. Hollenberg and A.F. Lang, *J. Catal.*, 92 (1985) 429; W.H.M. Sachtler and M. Ichikawa, *J. Phys. Chem.*, 90 (1986) 4752.
9. H.P. Bonzel, *Alkali-Metal-Affected Adsorption of Molecules on Metal Surfaces*, to be published.
10. W. Wurth, J.J. Weimer, E. Hudeczek and E. Umbach, *Surf. Sci.* 173 (1986) L619.
11. F. Sette, J. Stöhr, E.B. Kollin, D.J. Dwyer, J.L. Gland, J.L. Robbins and A.L. Johnson, *Phys. Rev. Letters*, 54 (1985) 935.
12. D. Heskett, E.W. Plummer and R.A. DePaola, *Phys. Rev.*, B33 (1986) 5171.
13. D.A. Wesner, G. Pirug, F.P. Coenen and H.P. Bonzel, *Surf. Sci.*, 178 (1986) 608.
14. A.B. Anderson and D.Q. Dowd, *J. Phys. Chem.*, 91 (1987) 869.
15. K.J. Uram, L. Ng and Y.T. Yates, Jr., *Surf. Sci.*, 177 (1986) 253.
16. D. Lackey, M. Surman, S. Jacobs, D. Grinder and D.A. King, *Surf. Sci.*, 152/153 (1985) 513.
17. P.E. Schultz, C.H. Patterson and R.P. Messner, to be published.
18. D. Heskett, I. Strathy, E.W. Plummer and R.A. DePaola, *Phys. Rev.*, B32 (1985) 6222; W. Eberhardt, F.M. Hoffmann, R.A. DePaola, D. Heskett, E.W. Plummer and H.R. Moser, *Chem. Phys. Lett.*, 124 (1986) 2327.
19. J.J. Weimer, E. Umbach and D. Menzel, *Surf. Sci.*, 155 (1985) 132; J.J. Weimer and E. Umbach, *Phys. Rev.*, B30 (1984) 4863.
20. S. Holloway and J.K. Norskov, *J. Electroanal. Chem.*, 161 (1984) 193; S. Holloway, J.K. Norskov and N.D. Lang, *Far. Symp. Chem. Soc.*, 21 (1986) .
21. W. Müller and P.S. Bagus, *J. Electr. Spectrosc. Related Phenomena*, 38 (1986) 103.
22. E. Shustorovich and A.T. Bell, submitted to *J. Catal.*

SUMMARY

Reliable sources of fuels and chemicals are of vital importance for our society. After the first and second oil crises other energy sources than oil, like coal, natural gas and wind and solar energy, gained interest. From these, coal is undoubtedly the most promising one, since coal reserves are very large. Coal can be converted into synthesis gas, a mixture of CO and H₂ which in turn can be converted into products like methane, longer hydrocarbons, methanol and longer oxygen containing molecules (oxygenates), the last product group being most interesting from an economic point of view. The mentioned reactions are catalyzed by metals like rhodium, iridium, platinum, iron, ruthenium and cobalt. The higher oxygenates are made if a rhodium catalyst is used.

To use the, often expensive, metals as efficient as possible, they are dispersed on porous oxides (support) with a high surface area (100-300 m²/g). This procedure results in very small metal particles (10-100 Å) with a very high fraction of exposed metal atoms. The catalytic properties of these small metal particles can be influenced by the support or by special additives (promoters). In this way the performance of the catalyst can be improved.

In this thesis, we tried to answer the following questions concerning the catalysts in CO hydrogenation: what is the size of the metal particles in supported Rh and Ir catalysts and what is the place of the promoter oxides in promoted Rh/SiO₂ catalysts. For this, we used a combination of techniques like H₂ and CO chemisorption, IR spectroscopy, EXAFS, TEM and temperature programmed reduction and oxidation. Furthermore the influence of promoter oxides like V₂O₅, MoO₃, ThO₂ and alkali (hydr)oxides on the catalytic behaviour of Rh/SiO₂ in synthesis gas reactions has been studied. Finally, attention has been paid to the effect of the catalyst precursor choice on the catalytic behaviour of Rh/Al₂O₃ catalysts.

The preparation and characterization of alumina- and silica-supported iridium catalysts is described in chapter 3. Two different preparation techniques, the incipient wetness impregnation method and the urea technique, were used. Hydrogen and carbon monoxide chemisorption clearly showed that on γ -Al₂O₃ the incipient wetness method resulted in catalysts with a very high dispersion, in contrast with the catalysts made by this technique on SiO₂. Reduction behaviour of the dried systems, oxidation behaviour of

the reduced systems and the loss of dispersity as a function of the oxidation temperature support this conclusion. The difference in dispersion is caused by the absence of adsorption sites on the SiO_2 support during the incipient wetness impregnation. The urea method proved successful for both supports. During the decomposition of the urea, the pH of the solution increased slowly and small metal hydroxide particles were deposited on the support. Thus, with these two methods, we were able to prepare highly dispersed Ir/ Al_2O_3 and Ir/ SiO_2 systems.

As H/Ir ratio's exceeding unity were measured, the hydrogen chemisorption measurements cannot be used directly to determine particle size of highly dispersed metals, because of the uncertainty in the hydrogen-to-surface metal stoichiometry. Therefore EXAFS (Extended X-ray Absorption Fine Structure) measurements were performed to determine the metal particle size and thereby calibrate hydrogen chemisorption results for Ir, Rh and Pt catalysts (chapter 4). The H/M ratio determined by hydrogen chemisorption is a linear function of the average metal coordination number determined by EXAFS. This linear relationship is independent of the support but varies with the metal with the H/M ratio increasing in the order Pt < Rh < Ir. Differences in H/M values cannot be explained by hydrogen spillover on the support or by subsurface hydrogen, but are due to multiple adsorption of hydrogen on metal surface atoms. The $\text{H}/\text{M}_{\text{surface}}$ stoichiometry differs among Pt, Rh and Ir in the order H/Pt < H/Rh < H/Ir, analogous to the order of stability of corresponding metal polyhydride complexes and of theoretical expectation. This is not surprising, since these very small particles are not truly metallic, because they consist of too few atoms. Using the model calculations presented in chapter 4, the H/M values can be quantitatively related to the percentage of exposed metal atoms.

The catalytic behaviour of SiO_2 - and Al_2O_3 -supported rhodium and iridium catalysts in CO hydrogenation at elevated pressure is presented in chapter 5. The iridium catalysts had a very low activity and mainly produced methanol, dimethylether and methane. Rhodium catalysts were superior to iridium catalysts, they exhibited a higher activity and a better selectivity to higher hydrocarbons and C_2 -oxygenates (ethanol, acetaldehyde and acetic acid). For rhodium-on-silica high oxo-selectivities were obtained (40%), while on chlorine-containing alumina this selectivity was rather low. When a chlorine-free metal precursor was used or when special pre-treatments were applied to a $\text{RhCl}_3/\text{Al}_2\text{O}_3$ catalyst, oxo-selectivities of rhodium-on-alumina were also rather high (30%). The observed effects were ascribed to chlorine, trapped by vacancies on the alumina surface, formed

by dehydroxylation of OH-groups. On SiO_2 this was not observed. A likely explanation for the detrimental effect of chlorine is based on the assumption that oxo-products such as methanol and ethanol are formed in primary reactions of synthesis gas over rhodium and are subsequently transformed in secondary reaction into hydrocarbons over acidic sites.

In order to improve the behaviour of rhodium and iridium catalysts, the influence of promoters and supports has been studied. In chapter 6, possible effects of promoters in synthesis gas reactions are reviewed and an explorative study of promotion of Rh and Ir catalysts is described. In all cases, Rh catalysts were superior to Ir catalysts with respect to the activity and C_2 -oxygenate selectivity. The promotion by additives was more effective than the promotion by the support. Based on the results presented in chapter 6, we decided to study the promotion of Rh/ SiO_2 by V_2O_5 , MoO_3 and ThO_2 in more detail (chapters 7-9).

The location of the promoter (V_2O_5 , MoO_3 and ThO_2) in supported rhodium catalysts was studied using various techniques. Temperature programmed reduction experiments and diffuse reflectance infrared spectroscopy showed that in the case of V_2O_5 - and MoO_3 -promoted Rh/ SiO_2 catalysts, a mixed oxide, RhVO_4 and Rh_2MoO_6 , respectively, is formed during calcination at 723 K, while no evidence was found for the formation of a mixed oxide in the ThO_2 -promoted Rh/ SiO_2 catalysts.

Reduction of Rh/ V_2O_5 / SiO_2 and Rh/ MoO_3 / SiO_2 catalysts resulted in a promoter oxide layer on top of the metal particle, as could be concluded from carbon monoxide chemisorption. CO chemisorption was suppressed by the presence of V_2O_5 and MoO_3 , while transmission electron microscopy showed that the rhodium particle size was not influenced by the addition of the promoter oxides. This indicates that the suppression of the CO chemisorption is not due to an increase of the metal particle size, but is due to covering of the metal particle. For Rh/ MoO_3 / SiO_2 , the hydrogen chemisorption was also suppressed, while for the Rh/ V_2O_5 / SiO_2 catalysts, no suppression of hydrogen chemisorption was observed, pointing to the formation of hydrogen bronzes in the latter case. For the ThO_2 -promoted Rh/ SiO_2 catalysts, no indication of a covering of the rhodium metal particle by patches of promoter oxide is found from the chemisorption experiments.

IR spectroscopy measurements showed that V_2O_5 decreased the amount of bridge-bonded and linearly bonded CO, while MoO_3 suppressed all forms of CO adsorption. ThO_2 mainly decreased the amount of bridge-bonded CO. Only for the ThO_2 -promoted Rh/ SiO_2 catalysts, a broad adsorption band between 1300 and 1750 cm^{-1} was observed, which is thought to be due to

CO bonded with the carbon atom to the metal and the oxygen atom to the promoter ion. From this observation and TEM experiments we conclude that the major part of the ThO_2 is positioned between the Rh particle and the SiO_2 support, while only a very limited covering of the Rh surface by ThO_2 patches will occur.

For the $\text{Rh}/\text{V}_2\text{O}_5/\text{Al}_2\text{O}_3$ catalysts, the major part of the V_2O_5 promoter was scavenged by the support. Only for high V/Rh values (7.0 and 8.4) the formation of RhVO_4 was observed. For these catalysts, Rh_2O_3 is believed to be partially positioned on top of a V_2O_5 (mono)layer.

CO hydrogenation was greatly enhanced by the presence of both MoO , V_2O_5 and ThO_2 (increase of activity by a factor of 170, 99 and 79, respectively, for a promoter/Rh ratio of 1.0). ThO_2 - and V_2O_5 -promoted Rh/SiO_2 catalysts had a high selectivity to C_2 -oxygenates, while MoO_3 -promoted Rh/SiO_2 catalysts exhibited high methanol selectivities. For the MoO_3 -promoted Rh/SiO_2 systems, the activity as a function of the promoter/Rh ratio showed a maximum at $\text{Mo}/\text{Rh} = 1.0$, pointing to covering by molybdenum oxide even during synthesis gas reactions. Thus, although the promoter oxides block part of the active metal surface, it also enhances the rate of CO hydrogenation at the metal-promoter oxide interface, that is at the perimeter of the promoter oxide patches on the rhodium particles.

These results and results of experiments in which ethylene was added to a working catalyst provide indications that the main promoter action of the ThO_2 , MoO_3 and V_2O_5 promoter is to increase the CO dissociation reaction, thereby increasing the activity of the Rh/SiO_2 catalyst. This can be understood by assuming that side-bonded CO, with its weakened C-O bond, is responsible for the higher CO dissociation activity. The non-dissociative reaction of CO towards methanol is only enhanced by a factor of 3 and of 7 for ThO_2 and V_2O_5 promotion, respectively, but is greatly enhanced by MoO_3 by a factor of 171, explaining the high methanol selectivity for the $\text{Rh}/\text{MoO}_3/\text{SiO}_2$ catalysts. This high factor of increase of the methanol formation rate due to MoO_3 addition is attributed to the reaction of CO to methanol over Mo-ions. Thus, in the $\text{Rh}/\text{MoO}_3/\text{SiO}_2$ catalysts at least two types of active species are present: Rh metal sites for CO dissociation and subsequent reactions to hydrocarbons and higher oxygenates and Mo-ions for methanol formation.

In order to further improve the ThO_2 - and V_2O_5 -promoted Rh/SiO_2 catalysts, the influence of alkali addition was studied (chapter 10). Addition of Li, Na, K and Cs did not increase the oxo-selectivity of ThO_2 - and V_2O_5 -promoted Rh/SiO_2 catalysts. Independent of the alkali added, it

mainly decreased the activity and lowered the hydrogenation rate, suggesting that the added alkali blocked the special perimeter sites which are held responsible for the ThO_2 and V_2O_5 promotion effect.

SAMENVATTING

Betrouwbare bronnen voor de energievoorziening en voor basisstoffen voor de chemische industrie zijn van wezenlijk belang voor de samenleving. De afhankelijkheid van ruwe olie werd duidelijk in de eerste en tweede oliecrisis in 1973 en 1979. Olie is nog steeds de belangrijkste bron voor energie en voor chemicaliën, maar om politieke, economische en strategische redenen wordt er veel (onderzoeks)aandacht gericht op alternatieve bronnen zoals steenkool, aardgas, kernenergie en water-, wind- en zonne-energie. Van deze bronnen is steenkool de meest belovende vanwege de grote voorraden aanwezig op aarde. Steenkool vertegenwoordigt ongeveer 75% van de fossiele brandstofvoorraad.

Via de gasfase kan steenkool worden omgezet in synthesegas, een mengsel van koolmonoxide (CO) en waterstof (H₂). Dit synthesegas kan met behulp van metaalkatalysatoren worden omgezet in methaan, hogere koolwaterstoffen, methanol en/of hogere zuurstofhoudende producten. Vooral de laatstgenoemde groep producten is economisch gezien interessant om te produceren. Overgangsmetalen zoals rhodium, iridium, platina, ijzer, ruthen en kobalt kunnen de genoemde reacties katalyseren. De hogere zuurstofhoudende producten worden vooral gemaakt wanneer een rhodium-katalysator wordt toegepast.

Om de, vaak dure, metalen zo efficiënt mogelijk te gebruiken, worden ze aangebracht op poreuze oxiden (dragers) met een groot inwendig oppervlak (100 - 300 m²/g). Op deze manier kunnen zeer kleine metaaldeeltjes worden gemaakt (10-50 Å) met een zeer hoge fractie geëxposeerde metaal-atomen.

De katalytische eigenschappen van deze zeer kleine metaaldeeltjes kunnen worden beïnvloed door de drager of door extra toevoegingen, promotoren. Op deze wijze kunnen we de reactie van koolmonoxide en waterstof sturen in een door ons gewenste richting, de zuurstofhoudende producten met twee of meer koolstofatomen.

De volgende belangrijke onderwerpen met betrekking tot de hydrogenering van koolmonoxide komen aan bod in dit proefschrift. Getracht werd om antwoord te vinden op de vraag hoe groot de metaaldeeltjes in gedragen rhodium- en iridiumkatalysatoren zijn en wat de plaats is van de promotoroxydes in de gepromoteerde Rh/SiO₂ katalysatoren. Hiervoor werd gebruik gemaakt van verschillende karakteriseringstechnieken, zoals waterstof- en koolmonoxide-chemisorptie, infrarood spectroscopie, EXAFS en temperatuur geprogrammeerde reductie, oxidatie en waterstof desorptie.

Vervolgens werd de invloed van promotoren zoals V_2O_5 , ThO_2 , MoO_3 en alkali metalen op het katalytisch gedrag van Rh/SiO_2 katalysatoren in de hydrogenering van koolmonoxide onderzocht. Tenslotte werd aandacht geschonken aan de invloed van de precursor van het actief materiaal, het metaal, op het katalytisch gedrag van Rh/Al_2O_3 katalysatoren.

De bereiding en karakterisering van alumina- en silica-gedragen iridium-katalysatoren is beschreven in hoofdstuk 3. Twee verschillende bereidingstechnieken werden gebruikt: de porievolumeiïmpregnatie-methode en de ureum-techniek. Waterstof- en koolmonoxide-chemisorptie-experimenten laten zien dat de porievolumeiïmpregnatie-methode resulteerde in hoog gedispergeerde alumina-gedragen iridiumkatalysatoren. Voor silica-gedragen iridiumkatalysatoren waren de dispersies een stuk lager. Temperatuur geprogrammeerde reductie van de gedroogde systemen, oxidatiegedrag van de gereduceerde systemen, en het verlies van dispersie tijdens een oxidatieve behandeling ondersteunen bovenstaande conclusies. Het verschil in dispersie tussen de alumina- en silica-gedragen systemen wordt veroorzaakt door de afwezigheid van adsorptie-sites op de SiO_2 drager gedurende de porievolumeiïmpregnatie-methode. De ureum-methode blijkt geschikt voor beide dragers. De pH van de oplossing stijgt langzaam gedurende de ontleding van ureum en kleine iridiumhydroxide kristalletjes worden afgezet op de dragers. Concluderend kunnen we zeggen dat met behulp van de genoemde bereidingsmethoden hoog gedispergeerde Ir/Al_2O_3 en Ir/SiO_2 systemen kunnen worden gemaakt.

Kennis van de waterstof-metaal-stoichiometrie is nodig om uit de waterstof-chemisorptiemetingen de metaaldeeltjesgrootte te bepalen. Omdat H/Ir -waarden groter dan één werden gevonden en in de literatuur steeds vaker H/M -waarden groter dan één worden gerapporteerd voor Rh , Pt en Ir katalysatoren is deze $H/M_{\text{oppervlak}}$ -stoichiometrie echter niet bekend. Daarom hebben we met behulp van de EXAFS (Extended X-ray Absorption Fine Structure) techniek een calibratie uitgevoerd voor drie metalen: Rh , Ir en Pt (hoofdstuk 4). Met behulp van deze techniek is het mogelijk het metaal-metaal coördinatiegetal (N) te bepalen. Nogal verrassend blijkt het H/M versus N gedrag niet afhankelijk te zijn van het gebruikte dragermateriaal, maar af te hangen van het chemisorberend metaal: bij gelijke N is $H/Ir > H/Rh > H/Pt$. Met behulp van modelberekeningen kan N worden omgerekend naar de dispersie en dus kan in het vervolg met behulp van de calibratie de gemeten H/M -waarde omgerekend worden naar een reële dispersie. Op grond van de gevonden relaties tussen H/M en N voor Rh , Ir

en Pt kunnen we enkele van de in de literatuur beschreven verklaringen voor de hoge H/M-waarden uitsluiten. De hoge H/M-waarden kunnen niet veroorzaakt worden door waterstofspillover, omdat die met name bepaald wordt door de drager. Wij constateren juist een grote invloed van het type metaal. Ook subsurface-waterstof kunnen we uitsluiten als verklaring voor de hoge H/M-waarden. Wij denken dat de $H/M_{\text{oppervlak}}$ -stoichiometrie verschilt voor Pt, Rh en Ir in de volgorde $H/Pt < H/Rh < H/Ir$, analoog aan de volgorde van de stabiliteit van de polyhydride-complexen H_nML_x (L = ander ligand).

Hoofdstuk 5 handelt over het katalytisch gedrag van SiO_2 - en Al_2O_3 -gedragen rhodium- en iridiumkatalysatoren in de hydrogenering van koolmonoxide bij hoge druk (40 atm). De iridiumkatalysatoren hebben een lage activiteit en produceren voornamelijk methaan, dimethylether en methanol, terwijl de rhodiumkatalysatoren een veel hogere activiteit hebben en een relatief hoge selectiviteit naar C_2 -oxoprodukten vertonen. Voor silica-gedragen rhodiumkatalysatoren worden hoge oxo-selectiviteiten gemeten (40 %), terwijl chloor-houdende alumina-gedragen rhodiumkatalysatoren een relatief lage oxo-selectiviteit hebben. Wanneer $RhCl_3/Al_2O_3$ echter op een speciale manier wordt voorbehandeld (calcinatie, "natte reductie") of wanneer een chloor-vrije metaalprecursor wordt gebruikt, dan worden relatief hoge oxo-selectiviteiten gemeten voor Rh/Al_2O_3 katalysatoren (30 %). De geobserveerde effecten schrijven we toe aan chloor, dat gelocaliseerd is op vacatures aan het alumina-oppervlak, gevormd door dehydroxylatie van OH-groepen. Dit effect treedt niet op voor de SiO_2 drager. Het negatieve effect van chloor op de oxo-selectiviteit kan verklaard worden door aan te nemen dat oxoprodukten zoals methanol en ethanol wel gevormd worden in primaire reacties maar vervolgens over zure sites op het alumina-oppervlak (chloor verhoogt de zuurgraad) door volgreacties worden omgezet in koolwaterstoffen.

In hoofdstuk 6 wordt een exploratieve studie naar de invloed van promotoren en dragers op het katalytisch gedrag van rhodium- en iridiumkatalysatoren beschreven. Rhodiumkatalysatoren zijn in alle gevallen beter dan iridiumkatalysatoren: ze hebben een hogere activiteit en C_2 -oxoselectiviteit. Additieven zijn effectiever dan dragers in het beïnvloeden van de katalytische eigenschappen. Op grond van de resultaten uit hoofdstuk 6 besloten we het promoterend effect van V_2O_5 , MoO_3 en ThO_2 op Rh/SiO_2 verder te bestuderen (hoofdstukken 7-9).

Verschillende technieken zijn toegepast om de plaats van het promotoroxide (V_2O_5 , MoO_3 en ThO_2) in gedragen rhodiumkatalysatoren te

bestuderen. Temperatuur geprogrammeerde reductie en diffuse reflectie infrarood spectroscopie tonen aan dat er in het geval van MoO_3 - en V_2O_5 -gepromoteerde Rh/SiO_2 gemengde oxides, respectievelijk RhVO_4 en Rh_2MoO_6 , worden gevormd tijdens de calcinerings. Voor de ThO_2 -gepromoteerde Rh/SiO_2 katalysatoren zijn geen aanwijzingen gevonden voor de vorming van een gemengd oxide.

Reductie van $\text{Rh}/\text{V}_2\text{O}_5/\text{SiO}_2$ en $\text{Rh}/\text{MoO}_3/\text{SiO}_2$ katalysatoren resulteert in een laagje promotoroxide bovenop het rhodiummetaaldeeltje, zoals kan worden geconcludeerd uit de CO-chemisorptiemetingen. De CO-chemisorptie wordt onderdrukt, terwijl uit transmissie electronen microscopie blijkt dat de rhodiumdeeltjesgrootte niet wordt beïnvloed door de toevoeging van de promotoroxides. Dit suggereert dat de afname van de CO chemisorptiecapaciteit niet wordt veroorzaakt door een toename van de metaaldeeltjesgrootte maar door een bedekking van de metaaldeeltjes. Voor het $\text{Rh}/\text{MoO}_3/\text{SiO}_2$ systeem wordt ook een onderdrukking van de waterstofchemisorptie gevonden, terwijl voor de $\text{Rh}/\text{V}_2\text{O}_5/\text{SiO}_2$ systemen geen onderdrukking van de waterstofchemisorptie is waargenomen. Dit laatste wijst op de adsorptie van waterstof aan de V_2O_5 promotor en de vorming van waterstofbronzen. Chemisorptiemetingen geven geen aanwijzingen voor het optreden van bedekking van het metaal in de $\text{Rh}/\text{ThO}_2/\text{SiO}_2$ katalysatoren.

Infraroodspectroscopie aan geadsorbeerde CO laat zien dat de V_2O_5 promotor de gebrugd- en lineair-gebonden CO onderdrukt, maar niet de gemdicarbonyl vorm. De MoO_3 promotor onderdrukt alle vormen geadsorbeerde CO. ThO_2 onderdrukt vooral de gebrugd-gebonden CO. Voor de door ThO_2 gepromoteerde katalysatoren wordt tevens een brede absorptie band in het infraroodspectrum waargenomen tussen 1300 en 1750 cm^{-1} . Voor de andere promotoren is deze band niet gezien. De band bij laag golfgetal wordt toegeschreven aan CO met de C-zijde geadsorbeerd aan het rhodiummetaal en met de O-zijde aan het promotoroxide. Uit deze metingen en uit TEM-opnamen kunnen we concluderen dat het merendeel van het ThO_2 tussen het rhodiumdeeltje en de SiO_2 drager zit. Tevens is een klein gedeelte van het rhodiumoppervlak afgedekt door ThO_2 .

Bij de $\text{Rh}/\text{V}_2\text{O}_5/\text{Al}_2\text{O}_3$ katalysatoren wordt het merendeel van de toegevoegde vanadiumoxide weggevangen door de Al_2O_3 drager. Alleen voor hoge V/Rh-verhoudingen (7.0 en 8.4) vinden we aanwijzingen voor een beïnvloeding van het rhodium door de V_2O_3 promotor.

De toevoeging van MoO_3 , V_2O_5 en ThO_2 aan een Rh/SiO_2 katalysator resulteert in een zeer sterke stijging van de activiteit van deze katalysator in de koolmonoxidehydrogenering. Bij een promotor/rhodium-verhouding van

1.0 zijn de verhogingen van de activiteiten respectievelijk 170, 99 en 79. De door ThO_2 en V_2O_5 gepromoteerde katalysatoren vertonen een hoge selectiviteit naar C_2 -oxoprodukten (50 %), terwijl de door MoO_3 gepromoteerde katalysator vooral methanol produceert (methanol selectiviteit 50 %). Het feit dat de activiteit met toenemende promotor/rhodium-verhouding voor het door MoO_3 gepromoteerde systeem een maximum bereikt bij $\text{Mo/Rh} = 1.0$, wijst op bedekking van het rhodiumoppervlak met eilandjes MoO_3 , ook tijdens de synthesegasreactie. Alhoewel de promotoroxides dus een gedeelte van het actieve metaaloppervlak bedekken, neemt de snelheid van CO hydrogenering toch toe. Deze toename schrijven we toe aan een versnelde CO hydrogenering op zeer actieve plaatsen op het grensvlak tussen het promotoroxide en het rhodiumdeeltje.

De beschreven metingen en resultaten van de etheentoevoeging aan een werkende katalysator suggereren, dat de belangrijkste rol van de promotoren bestaat uit het versnellen van de dissociatie van koolmonoxide. Dit kan verklaard worden door aan te nemen dat de "side-on" gebonden CO, met z'n verzwakte C-O band, verantwoordelijk is voor de versnelde CO-dissociatie. De niet-dissociatieve reactie van koolmonoxide naar methanol wordt slechts met een factor 3 en 7 door ThO_2 en V_2O_5 versneld. MoO_3 versnelt de vorming van methanol veel meer (factor 171). De hoge versnelingsfactor voor de vorming van methanol voor molybdeenoxide schrijven we toe aan de reactie van CO over Mo-ionen. In de $\text{Rh/MoO}_3/\text{SiO}_2$ katalysatoren zijn er dus tenminste twee actieve centra: het rhodiummetaal voor de dissociatie van CO en verdere reacties (eventueel gepromoteerd met molybdeenoxide) en de molybdeen-ionen voor de vorming van methanol.

Toevoeging van alkali aan de ThO_2 - en V_2O_5 -gepromoteerde Rh/SiO_2 katalysatoren is onderzocht om deze katalysatoren verder te verbeteren (hoofdstuk 10). De toevoeging van Li, Na, K en Cs verhoogt echter niet de oxo-selectiviteit van deze door ThO_2 en V_2O_5 gepromoteerde Rh/SiO_2 katalysatoren. Onafhankelijk van het toegevoegde alkalimetaal, vinden we een afname van de activiteit en hydrogeneringscapaciteit ten gevolge van de toevoeging van alkali. Dit suggereert dat het alkali juist die plaatsen blokkeert, die verantwoordelijk zijn voor het promoterend effect van de ThO_2 - en V_2O_5 -promotor.

DANKWOORD

Hartelijk dank aan al diegenen die me gesteund hebben bij het tot stand komen van dit proefschrift.

Mijn vrouw Anne dank ik voor het creëren van een vast rustpunt, voor alle zorg en begrip tijdens de promotieperiode en voor de opoffering die zij zich met name in de laatste maanden heeft moeten getroosten. Mijn ouders dank ik voor de stimulans die ze mij tijdens de school- en studiejaren gaven. De andere familieleden dank ik voor hun ondersteunende belangstelling.

Natuurlijk wil ik alle leden van de vakgroep Anorganische Chemie aan de Technische Universiteit Eindhoven dank zeggen voor de prettige wijze waarop ik met hen heb kunnen samenwerken. Dat geldt vooral voor mijn kamergenoten Joop van Grondelle, voor de vele discussies, het "poolen" en het aanleren van het "hoge druk vak", en Jan Martens voor de vele kritische kanttekeningen, voor het uitvoeren van de modelberekeningen beschreven in hoofdstuk 4 en 5, voor de vele discussies, het aanleren van de bridge-kunst en het uitdagen voor een partijtje badminton. Ik zal echter wel nooit een echte bridger en/of sportman worden. Frank Dirne en Eveline Hermans (afstudeerders TU Eindhoven) en Paul Smeets (afstudeerder HTS Eindhoven) ben ik zeer erkentelijk voor hun niet aflatende inzet en hun kritisch meedenken, hetgeen geresulteerd heeft in een aantal hoofdstukken van dit proefschrift. Mijn promotor Roel Prins dank ik voor het in mij gestelde vertrouwen, voor zijn kritische opmerkingen die de manuscripten zeer ten goede zijn gekomen, voor het feit dat hij mij op tijd "uit de rekken" heeft gehaald en voor zijn meeleven in het laatste promotiejaar vanuit Amerika tijdens zijn sabbatical leave. Rutger van Santen, mijn tweede promotor, ben ik erkentelijk voor het overnemen van de geregelde begeleiding van Roel in het laatste jaar van mijn promotie en voor de stimulerende discussies.

De overige leden van de "koffieclub", Fanny van Zon, Ad de Koster, Peter Wijnen, Frans Kampers, Diek Koningsberger, Dick van Langeveld en Hans Niemantsverdriet ben ik dankbaar voor de kollegialiteit, de wetenschappelijke discussies, het aanleren van de computertaal en de vele gezellige koffie (half)uurtjes.

In het kader van hun tweede jaars praktikum, S8, P3, stage HTS en afstudeerwerk HTS hebben de studenten Saeys, Couwenberg, Sagis, Mommers, Theelen, de Leeuw, Hermans, Stuyvenberg, Stroeks, van Amelsfoort, den Engel en van Evert bijgedragen aan het in dit proefschrift

beschreven onderzoek.

Jos van Wolput dank ik voor het vele infraroodwerk, Henny Zandbergen (Rijksuniversiteit Leiden) voor de TEM-opnamen, Dick van Langeveld en Hans Niemantsverdriet voor de XPS metingen, Adelheid Elemans-Mehring voor het verrichten van analyses, Wout van Herpen voor het ontwikkelen van de *in situ* infrarood-cel en de technische ondersteuning en Henk van Lieshout voor de snelle afwikkeling van de administratieve zaken. De medewerkers van de glasblazerij ben ik dank verschuldigd voor het vervaardigen van de infrarood-cel.

Mijn "wetenschappelijke broertjes" Hans Lansink Rotgerink en Leon Lefferts wil ik dankzeggen voor het meeleven en de vele wetenschappelijke discussies zowel tijdens lange telefoongesprekken als gedurende de meerdaagse dienstreizen.

The co-workers of the Centre for Electron Microscopy of Antwerp (RUCA) are thanked for the use of the JEOL 200 CX.

The EXAFS measurements described in chapter 4 were done at SSRL (Stanford University, USA), which is supported by the National Science Foundation (NSF) through the Division of Materials Research and the National Institute of Health through the Biotechnology Resource Program in the Division of Research Resources in cooperation with the U.S. Department of Energy, and at SRS (Daresbury Laboratories, UK). We gratefully acknowledge the assistance of SSRL and SRS staff.

This dissertation has been supported by the Netherlands Foundation for Chemical Research (SON) with financial aid from the Netherlands Organization for the Advancement of Pure Research (ZWO).

CURRICULUM VITAE

Berend Jan Kip is geboren op 5 juli 1960 te Dinxperlo. Na het behalen van het eindexamen Atheneum aan de Christelijke Scholengemeenschap te Aalten begon hij in augustus 1978 met de studie Chemische Technologie aan de Technische Hogeschool Twente. Zijn afstudeeronderzoek betrof de karakterisering van oxidatiekatalysatoren met behulp van temperatuur geprogrammeerde reductie uitgevoerd onder leiding van prof. dr. P.J. Gellings in de vakgroep Anorganische Chemie en Katalysator Materialen. Op 18 januari 1984 werd het doctoraalexamen met lof afgelegd.

Op 1 januari 1984 trad hij in dienst van SON/ZWO en startte met een promotieonderzoek onder leiding van prof. dr. R. Prins in de vakgroep Anorganische Chemie en Katalyse aan de Technische Universiteit Eindhoven. De resultaten hiervan zijn beschreven in dit proefschrift.

Op 3 februari 1984 trad hij in het huwelijk met Anne Veltman en op 27 juni 1987 werd hun dochter, Anke, geboren.

Vanaf 1 november 1987 hoopt hij werkzaam te zijn op het Centraal Research Laboratorium van de DSM Limburg B.V. te Geleen.

PUBLICATIONS

Several chapter or parts of chapters have been or will be published:

Chapter 3:

- Preparation and characterization of very highly dispersed iridium on Al_2O_3 and SiO_2 , B.J. Kip, J. van Grondelle, J.H.A. Martens and R. Prins, *Appl. Catal.*, 26 (1986) 353-373.

Chapter 4:

- Determination of metal particle size of highly dispersed Rh, Ir and Pt catalysts by hydrogen chemisorption and EXAFS, B.J. Kip, F.B.M. Duivenvoorden, D.C. Koningsberger and R. Prins, *J. Catal.*, 105 (1987) 26.
- Determination of metal particle size of highly dispersed Rh, Ir and Pt catalysts by hydrogen chemisorption and EXAFS, B.J. Kip, F.B.M. Duivenvoorden, D.C. Koningsberger and R. Prins, *J. Am. Chem. Soc.*, 108 (1986) 5633.
- Determination of the metal particle size of supported Pt, Rh and Ir catalysts. A calibration of hydrogen chemisorption by EXAFS, F.B.M. Duivenvoorden, B.J. Kip, D.C. Koningsberger and R. Prins, *J. de Phys.*, 47 (1986) C8-227.

Chapter 5:

- The effect of chlorine on the formation of oxygenates in synthesis gas reaction over Rh on SiO_2 and Al_2O_3 , B.J. Kip, F.W.A. Dirne, J. van Grondelle and R. Prins, *Am. Chem. Soc., Div. Petr. Chem., Mechanisms of Fischer Tropsch Chemistry* (1986) 163.
- The effect of chlorine in the hydrogenation of carbon monoxide to oxygenated products at elevated pressure on Rh and Ir on SiO_2 and Al_2O_3 , B.J. Kip, F.W.A. Dirne, J. van Grondelle and R. Prins, *Appl. Catal.*, 25 (1986) 43.

Chapter 7:

- Preparation and characterization of vanadium oxide-promoted rhodium catalysts, B.J. Kip, P.A.T. Smeets, J.H.M.C. van Wolput, H. Zandbergen, J. van Grondelle and R. Prins, *Appl. Catal.*, ... (1987)

Chapter 8:

- Hydrogenation of carbon monoxide over vanadium oxide-promoted rhodium catalysts, B.J. Kip, P.A.T. Smeets, J. van Grondelle and R. Prins, *Appl. Catal.*, ... (1987)

Chapter 9:

- Hydrogenation of carbon monoxide over molybdenum oxide- and thorium oxide-promoted rhodium catalysts, B.J. Kip, E.G.F. Hermans, J.H.M.C. van Wolput, N.M.A. Hermans, J. van Grondelle and R. Prins, *Appl. Catal.*, ... (1987)

Chapter 10:

- CO hydrogenation over alkali-promoted Rh/Al₂O₃, Rh/V₂O₃/SiO₂ and Rh/ThO₂/SiO₂, B.J. Kip, E.G.F. Hermans and R. Prins, *Appl. Catal.*, ... (1987)

Other publications of the author of this thesis are:

- The effect of gas environment (H₂, O₂) on the structural properties of small iridium metal particles supported on Al₂O₃ as determined by EXAFS, D.C. Koningsberger, F.B.M. Duivenvoorden, B.J. Kip and D.E. Sayers, *J. de Phys.*, 47 (1986) C8-255.
- Methanol from synthesis gas over iron-rich FeIr/SiO₂ catalysts, D.C. Koningsberger, C.P.J.H. Borgmans, A.M.J. van Elderen, B.J. Kip and J.W. Niemantsverdriet, *J. Chem. Soc., Chem. Com.*, (1987)

"To realize the relative validity of one's convictions and yet stand for them unflinchingly is what distinguishes a civilized man from a barbarian."

Schumpeter in "Capitalism, Socialism and Democracy"

stellingen

behorende bij het proefschrift

**OXYGENATED PRODUCTS FROM CARBON MONOXIDE
HYDROGENATION OVER SUPPORTED
RHODIUM AND IRIIDIUM CATALYSTS**

van

Berend Jan Kip

1. Beard en Ross schrijven het voorkomen van een piek beneden 1 Å in hun Fourier getransformeerde EXAFS spectra voor TiO₂-geïmpregneerde Pt/C katalysatoren ten onrechte toe aan het afkappen van de CHI-spectra bij eindige k-waarden.
B.C. Beard en P.N. Ross, J. Phys. Chem., 90 (1986) 6811.
2. De conclusie van Lazarov *et al.*, dat het gebruik van verschillende dragermaterialen voor een zilverkatalysator de activiteit voor de methanoloxidatie niet beïnvloedt, kan op grond van hun metingen niet worden getrokken.
D. Lazarov, K. Ivanov en S. Manev, Comm. Dep. Chem. Bulg. Acad. Sci., 17 (1984) 439.
L. Lefferts, J.G. van Ommen en J.R.H. Ross, Appl. Catal., 23 (1986) 385.
3. Klose en Baerns laten ten onrechte na de door hun met modelstudies bepaalde dissociatieve adsorptie warmte van waterstof op nikkel van 32 kJ/mol te vergelijken met de in de literatuur gerapporteerde waarden van 85-125 kJ/mol.
J. Klose en M. Baerns, J. Catal., 85 (1984) 105.
I. Toyashima en G.A. Somorjai, Catal. Rev. 19 (1979) 105.
4. In een MO-studie van CO geadsorbeerd op een Pt₃Ti legering brengen Mehandru *et al.* een correctie in de C-parameter aan om binding van CO met de O-kant aan Pt₃Ti te voorkomen. Gezien het feit, dat de door hen gebruikte berekeningsmethode ook problemen oplevert bij adsorptie van zuurstofatomen aan rhodium, is dit aan bedenking onderhevig.
S.P. Mehandru, A.B. Anderson en P.N. Ross, J. Catal., 100 (1986) 210.
5. De piek bij 1 Å die Kunoff *et al.* vinden in het Fourier getransformeerde EXAFS spectrum van arseen als implantaat in bismuth, kan beter worden toegeschreven aan multiëlectron excitaties dan aan het voorkomen van bismuth naburen op die afstand.
E.M. Kunoff, M.S. Dresselhaus en Y.H. Kao, Phys. Rev., B34 (1986) 8460.
A.G. Kochur, A.M. Nadolinski en V.F. Demekhin, J. de Phys., C8 (1986) 83.
6. In hun studie naar het gedrag van verschillende Fe-Ir/SiO₂ systemen in de hoge druk synthegasreactie maken Fukushima *et al.* twee essentiële fouten:
 - a. ze vergelijken het katalytisch gedrag van verschillende Fe-Ir/SiO₂ systemen na 4 uur reactie, terwijl uit werk van Koningsberger *et al.* blijkt, dat pas na ± 40 uur een steady-state toestand is bereikt;

- b. op grond van hun selectiviteitsresultaten concluderen ze dat de vorming van methaan en C₂-oxoprodukten wordt onderdrukt, hetgeen een aanwijzing is voor de verkleining van de ensemblegrootte van de iridiumdeeltjes, terwijl uit hun activiteitsresultaten het tegengestelde blijkt.
- F. Fukushima, Y. Ishii, Y. Onda en M. Ichikawa, J. Chem. Soc., Chem. Commun., (1985) 1752.
- D.C. Koningsberger, C.P.J.H. Borgmans, A.M.J. van Elderen, B.J. Kip en J.W. Niemantsverdriet, J. Chem. Soc., Chem. Commun., (1987) 892.
7. De opmerking van Tamaru *et al.* dat de ethanol/aceetaldehyde verhouding een maat is voor de hydrogeneringsactiviteit van rhodiumkatalysatoren in synthesegasreacties is in tegenspraak met metingen van dezelfde onderzoekers op grond waarvan ze suggereren, dat de route voor de vorming van ethanol en aceetaldehyde verschillend is.
- S. Kagami, S. Naito, Y. Kikuzono en K. Tamaru, J. Chem. Soc., Chem. Commun. (1983) 256.
- H. Orita, S. Naito en K. Tamaru, Chem. Lett., (1983) 1161, J. Catal., 90 (1984) 183.
8. Het bewijs van B.H. Chin *et al.* dat de tinconcentratie in indiumfosfide gegroeid met behulp van liquid phase epitaxy als functie van het tingehalte in de smelt verzadigt, is gebaseerd op metingen in een te klein concentratiegebied en moet gezien de grote spreiding verworpen worden.
- B.H. Chin, R.E. Frahm, T.T. Sheng en W.A. Bonner, J. Electronchem. Soc., 131 (1984) 1373.
- M.G. Astles, F.G.H. Smith en E.W. Williams, J. Electronchem. Soc., 120 (1973) 1750.
9. De veel gehoorde aansporing om met minimale inspanning maximale resultaten te bereiken leidt veelal niet tot een gedetermineerde oplossing.
10. Het veelvuldig spreken over maatschappelijke voor- en achteruitgang is gezien de afwezigheid van een communis opinio over het einddoel van die maatschappij niet gerechtvaardigd. Voor- en achteruitgang zijn immers alleen bepaald, indien een einddoel bekend is.